Thése

Pour l'obtention du Grade de

DOCTEUR DE L'UNIVERSITE DE POITIERS

(Faculté des Sciences Fondamentales et Appliquées)
(Diplôme National - Arrêté du 25 mai 2016)

Ecole Doctorale : SIMME
École nationale supérieure d'ingénieurs de Poitiers (ENSI Poitiers)

Présentée par :

Kush CHADHA

Secteur de Recherche : Mécanique et Energétique

Improvement of water management in PEM fuel cells using water balance and electrochemical noise analysis

---

Directeur de Thèse : Serguei Martemianov
****
Soutenue le : 07 Jan 2021
****

devant la Commission d'Examen

****

JURY

Rapporteur	Professeur MARANZANA Gaël	Université de Lorraine - LEMTA
Rapporteur	Professeur ALOUI Fethi	Université Polytechnique Hauts de-France - LAMIH
Examinateur	Professeur émérite HUET François	Sorbonne Université
Examinateur	Professeur MARTEMIANOV Sergueï	Université de Poitiers – Institut P'
Examinateur	Maitre de conferences THOMAS Anthony	Université de Poitiers – Institut P'

Acknowledgements

First and foremost I will thank to Lord Hanuman, the unseen powers who have been holding me tight during the course of PhD and throughout my life.

I would like to thanks my director of thesis, Dr. Serguei Martemianov under whose guidance and directions, I am able to give my best and able to complete things in a much easy manner. I am thankful to all the facilities provided considering the equipment's and permission to travel for conferences.

I would also thankful to my supervisor Dr. Thomas Anthony who stayed as a friend with me, who had supported, encouraged and motivated me during tough times. From his decisions on development of bipolar plates to timely completion of experiments and modelling, all helped me to complete my thesis with improved results.

Not far, I would also like to thanks my friends in the lab who created an environment of great enthusiasm mainly, Melissa, Armande, Andres, Lorena, Julien, Rafet, Sirajuddin, Raveto, Ivan, Abhishek. Also professors who always helped me for research and other activities - Karl, Jose, Younas. For all my computer and software's help, I will thank to Jean and a big thanks to administration - Helene and Bouba.

I would like to thanks the french government for trusting the project of Fuel cells and powering that trust on our team.

At the end, respect to my family, for whom I dedicate this work, my Father, my Mother, my brother Deepesh who were the main source of motivation, letting me far away from them and understanding my decisions. To all my relatives - Rachita, Harsh, Sahej, Mayank who motivated me and supported me whenever needed with their stories, sense of humor, motivation and energy.

Preamble

In today's era where the demand of energy is heavily vested on hydrocarbons and with the increase in population the need to extract more of these, pose a serious problem to the nature. With already a strong dependency on conventional source of energy, there is a need for non conventional sources and hydrogen can play an important role. Hydrogen is a clean, sustainable energy solution and can be stored efficiently in gaseous, liquid or solid form however the cost still posses a major challenge. Hydrogen (H_2) is the most abundant element in the universe and is mainly in water and organic compounds [Gielen et al., 2019, Kötter et al., 2016]. Currently grey hydrogen accounts to maximum production of hydrogen and there is a shift to green hydrogen using sunlight, biomass fuels and other conventional sources of energy.

Fuel cells have gain importance as an electrochemical device in recent years, using hydrogen as a fuel. In the fuel cell hydrogen combines with oxygen to produce water, electricity and heat. Some of the advantages such as low operating range of temperature makes it as a lucrative choice. Again cost of platinum loading, weights of bipolar plate stack, gaskets to avoid leakage, cost of noble metals for coating all plays a major role. The efficiency highly depends on choice of material for bipolar plate, design of flow fields[Wilberforce et al., 2019], removal of water, platinum loading, diffusion mechanism [Zawodzinski Jr et al., 1991] , robustness and diagnosis [Martemianov and Danaila, 2003, Maizia et al., 2017] of the fuel cell.

A typical fuel cell stack can weigh up to 135 kW with weight up to 44 kg having 450 cells in total [Hemmer et al., 2019]. Serpentine flow field design is the most used in commercial fuel cell stacks. However these traditional plates suffer from high pressure head losses and slug formation at the bends. More the slug formation, higher will be the power required by the compressor in order to run fuel cell stack. Thereby there is research and development required in more efficient flow field designs which can help in more ease in removal of water. Moreover materials of bipolar plates can also play a big role in reducing the overall weight of stack. Graphite has been used since long as a preferred material for stack [Sundén and Faghri, 2005, Scholta et al., 1999]. Stainless steel bipolar plates are one of the most favourable choice [Hung and Lin, 2012,] because of the ease in manufacturing.

In order to commercialize the fuel cells, after ease in production of hydrogen, diagnosis and fault analysis plays an important role. There are many techniques used such as pressure drop measurements for irregularities in channels/ gas diffusion layer [Mortazavi et al., 2018], water distribution by x-ray, optical photography [Cochet et al., 2018, Meyer et al., 2016]. These techniques can be costly or requires the use of prototypes for measurement. Electrochemical noise analysis techniques can be more favourable compared to robustness of information recorded. ENA has been used to understand coating analysis and degradation [Huet, 1998, Huet et al.,

2004], for application in fuel cells [Martemianov and Danaila, 2003, Maizia et al., 2018, Lee and Bae, 2012]. ENA can be used to analyse un-interrupted signals over long duration and these results can be interpreted through visualization in time domain, characterization in frequency domain (Power spectral density) or analysis in time frequency domain. Tools developed for diagnosis or prognosis of fuel cells should be aimed at more robustness, ease of application and reduced costs.

Experiments always provides a clear way for examining performance but development of a fuel cell stack is a costly process. Moreover, it is not always possible to deploy sensor and capture in-situ diagnosis. In order to predict this information modelling [Chevalier et al., 2018, Morin et al., 2017] can play an important role. Models developed analytically or numerically can give much insights and can help for ease in development process for a fuel cell stack. Apart from analytical modelling, there can be data driven modelling approach using complete black box and utilizing experimental data for predicting performance. In any case modeling approach with experimental results can ease up development and commercialization of fuel cells.

With the decreasing cost, more green hydrogen availability, advanced research, fault diagnosis, development of innovative flow field designs can make better fuel cells and less dependency on natural or conventional sources of energy. In this research more focus is on water management techniques and use of diagnosis tools to improve overall power density of stack so that polymer electrolyte membrane fuel cells can be improved for existing limitations.

This research is primarily focused on developing new flow field bipolar designs and improving water management. The main objective is to study different flow field designs with electrochemical techniques, analysing the compressor power, modelisation for water management by diffusion.

Contents

List of Figures

List of Tables

Nomenclature

Subscripts

- atm : Atmospheric pressure
- sat: Saturated conditions
- ha: Humidifier temperature at anode
- hc: Humidifier temperature at cathode
- m: Membrane
- co: Condenser cooling
- a: Anode
- c: Cathode
- λ:Water content
- w: Water
- in: Inlet
- o : Outlet
- $comp$: Compressor
- sys : System

Parameters

- D:Diffusion coefficient $cm.s^{-1}$
- F:Faraday constant $96485 C.mol^{-1}$
- k:Transfer coefficient $m.s^{-1}$
- M:Molecular weight $g.mol^{-1}$
- N:Molar flux density $mol.m^{-2}s^{-1}$
- n:Molar flux $mol.s^{-1}$
- P:Pressure $N.m^{-1}$
- RH:Relative humidity

- T:Temperature K
- ρ:Density $kg.m^{-3}$
- μ:Chemical potential $Nm.kg^{-1}$
- fv:Volume fraction of water in the membrane
- EW:Equivalent weight $gpolymer.(molionic\text{-}group)^{-1}$
- R:Gas constant $J.kg^{-1}K^{-1}$

Abbrevations

- PSD :Power spectral density
- $PEMFC$:Polymer electrolyte fuel cells
- CVD :Chemical vapor deposition
- ICR :Interficial contact resistance
- OCV :Open circuit voltage
- CNC :Computer numerical controlled
- EDM :Electrode discharge machining
- BPP :Bipolar plates
- ENA :Electrochemical noise analysis
- MEA :Membrane electrode assembly
- STD :Standard deviation
- AC :Alternating current
- DC :Direct current
- MEA :Membrane electrode assembly
- A :Ampere
- FFT :Fast Fourier Transform
- f :Frequency
- T :Temperature
- RH :Relative humidity

Chapter 1

Fuel cell's principle and development

1.1 History of fuel cells

The history of fuel cells can be traced back to 180 years old, where the first few innovations in fuel cell belong to Sir William Grove's invention approximately in 1839. From polymer electrolyte membrane fuel cell (PEMFC) to alkaline fuel cell (AFC), phosphoric acid fuel cell (PAFC),the molten carbonate fuel cell (MCFC) and solid oxide fuel cell(SOFC) all have been worked upon [Perry and Fuller, 2002,]. Fuel cells have been quite attractive in earlier times because of other technologies that have poor efficiency. Slowly and slowly as research progressed and there was an improvement in the efficiency of other technologies, fuel cells got less attention. Ludwig Mond and Dr.Charles Langer after certain research, came up with advancements to increase the power density of fuel cell. [Mond and Langer, 1890,] employed a porous matrix to contain their liquid electrolytes and they introduced the use of powdered electrocatalysts like platinum black.

Later contributions came from Baur and Tobler, in 1933 in an comprehensive review which shows promise in commercialisation of fuel cells. They can be made to work at ordinary temperatures, with alkaline electrolyte and hydrogen as a fuel. Figure 1.1 shows example of ancient fuel cell powered vehicle.

Figure 1.1: A Allis-Chalmers fuel cell powered tractor driven by Dr Harry Karl [photo produced from W. Mitchell (Ed). Fuel cells, academic press, New york, 1963]

From Ballard stationary product [Prater, 1996,] application to other PEMFC

developers which took fuel cell into development such as Siemens, De Nora and Plug Power [Stone and Morrison, 2002,] have played a role in strengthening consumer awareness and acceptance of PEMFC technology.

1.2 Types of fuel cells

There have been various types of fuel cells in history which have been in verge of development. Few are discussed here -

1. **Molten carbonate fuel cells (MCFC)** [Andújar and Segura, 2009,]

   (a) Electrolyte- Mixture of lithium carbonate and potassium

   (b) Temperature - 65° C

   (c) Pressure- 1-10 atm

   (d) Output - 0.7V- 1V

   (e) H_2 after reforming

   Molten carbonate fuel cells (Figure 1.2) have been used because of their spontaneous internal reforming fuel. Since they use liquid electrolyte it possess problems of handling. These cells requires preheating. Anode does not tolerate more than 1.5 ppm of sulphur as there can be fuel cell deterioration issues. Recent developments in porous and non porous materials have been done which lead to increase in stack lifetime [Dicks, 2004,].

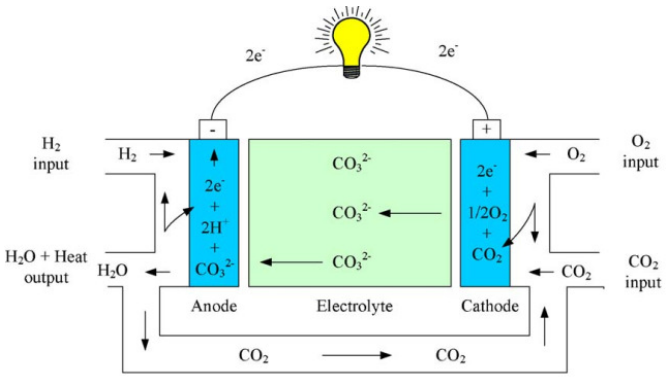

Figure 1.2: Molten carbonate fuel cells principle

2. **Solid oxide fuel cells (SOFC)**

   (a) Electrolyte- Solid oxide , zirconioum. Electrode material - Nickel or cobalt.

   (b) Temperature - 1000° C (Very high temperature)

   (c) Pressure- 1 atm

   (d) Output - 0.8V- 1V

   (e) Fuel - H_2 after reforming

Solid oxide fuel cells (Figure 1.3) allows spontaneous internal reforming fuel and generates a lot of heat. With fast chemical reactions they also have high efficiency. Moreover SOFC can be worked at higher current densities then molten carbonate fuel cells. No use of any noble metal catalysts and solid electrolyte makes it a favourable choice for working. Since the SOFC works at high temperatures hence materials are needed which are chemically stable, have sufficient conductivity at high temperature and chemically compatible with other components of fuel cell. [Andújar and Segura, 2009, Park et al., 2000,]

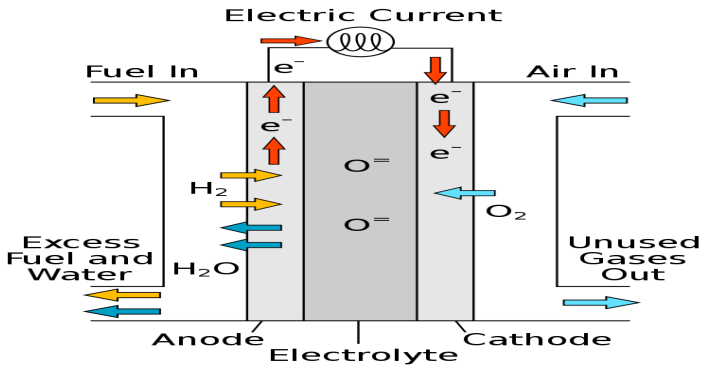

Figure 1.3: Solid oxide fuel cell principle, adopted from [Diakite et al., 2014]

3. **Alkaline fuel cells(AFC)**

   (a) Electrolyte- Molten alkaline mixture of potassium hydro oxide (KOH)

   (b) Temperature - (65-220)° C

   (c) Pressure- 1 atm

   (d) Output - 1.1 V- 1.2V

   (e) Fuel - H_2

Being able to work at low temperatures, fast start, high efficiency, no corrosion, low weight and volume made alkaline fuel cells a suitable choice for Shuttle program manufactured by UTC Fuel cells. However these cells (Figure(1.4)) are tolerant to CO_2 and also on CO hence oxidant must be pure oxygen and fuel must be pure hydrogen. It is always beneficial to use natural oxygen then pure oxygen. One drawback is that, they possess short lifetime. These fuel cells tend to lack the R and D support required to refine the technology into successful market offerings. [McLean et al., 2002,] provides a detailed assessment in the Alkaline fuel cell technology .

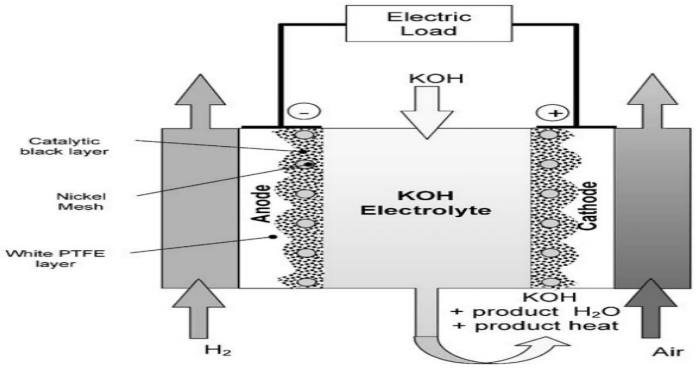

Figure 1.4: Alkaline fuel cells principle, adopted from [McLean et al., 2002,]

4. **Phosphoric acid fuel cell (PAFC)**

   (a) Electrolyte- Liquid phosphoric acid within matrix of silicon carbide.

   (b) Temperature - (150-200)° C

   (c) Pressure- 1 atm

   (d) Output - around 1.1 V

   (e) Fuel - H_2

   Phosphoric acid fuel cells were developed for terrestrial applications, unlike Alkaline fuel cells (Figure 1.5) were targeted for spacecraft. The advantage of these cells lie in fact that they can tolerate 30 % CO_2. Since they can work with medium temperature , they can utilize the waste heat for regeneration. Another advantage is with the electrolyte, which has stable characteristics. However, they suffer certain drawbacks such as maximum tolerance of 2% CO, require liquid state of electrolyte, they are big and heavy and cannot auto reform, moreover they need to be maintained at certain temperature before starting.

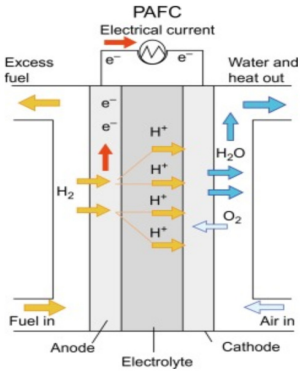

Figure 1.5: Phosphoric acid fuel cells principle, adopted from the [Sudhakar et al., 2018,]

5. **Direct methanol fuel cells (DMFC)**

   (a) Electrolyte- Proton exchange membrane

(b) Temperature - (130)° C

(c) Pressure- 1 atm

(d) Output - around 1.1 V

(e) Fuel - Liquid methanol

In 1990's, NASA's first collaboration with University of South Carolina, developed direct methanol fuel cells. [Wasmus and Küver, 1999,] provided insight regarding the trends and application in methanol fuel cells. The use of reforming process and having solid electrolyte as proton exchange membrane makes it a favourable choice. However there efficiency is lower compared to hydrogen fuel cells and require large amount of nobel materials or catalysts for the oxidation of methanol at the anode. Figure 1.6 represents a direct methanol fuel cell.

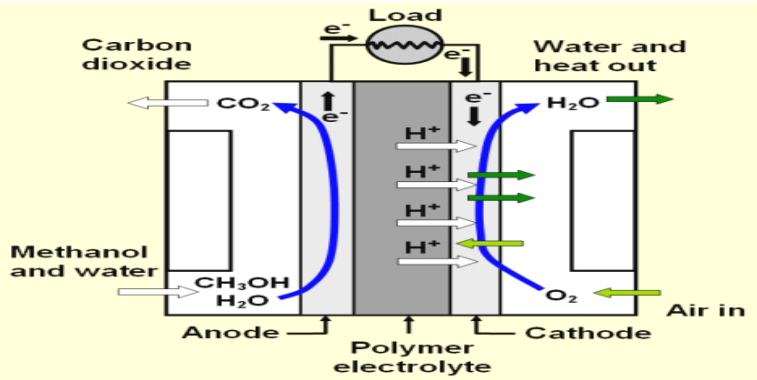

Figure 1.6: Direct methanol fuel cells principle, adopted from [Long et al., 2011]

6. **Polymer electrolyte membrane fuel cells (PEMFC)**

Polymeric membrane technology was first invented by General electric (GE) company with the work of T.Grubb and L.Niedrach. This small fuel cell which was first developed around mid sixties was fed with hydrogen generated by mixture of water and lithium hydoroxide and was stored in bottles. Due to this, it became important to use this fuel cell in isolated areas.

(a) Electrolyte- Proton exchange membrane

(b) Temperature - (60-80)° C

(c) Pressure- 1 -2 atm

(d) Output - around 0.9- 1 V

(e) Fuel - Hydrogen

PEMFC (Figure 1.7) is one of the preferred choice for automobile and aviation industry. Some of the advantages such as low operating range of temperature makes it a lucrative choice. Non corrosive electrolyte, separator between anode and cathode, usage of atmospheric air, compact, robust and simple design, working at low pressures all makes it a favourable choice for commercialization. However PEMFC, suffer some disadvantages such as they are very sensitive

to impurities in hydrogen. Humidification is required in certain cases for the reactive gases. Use of catalyst(platinum) makes it expensive to work with.

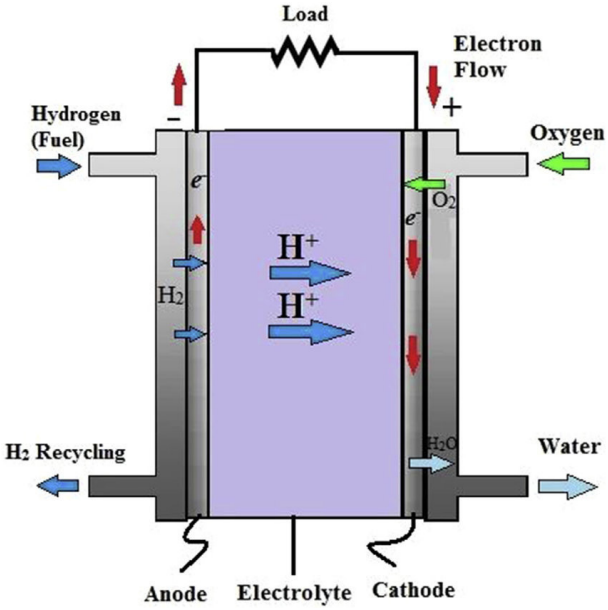

Figure 1.7: Polymer electrolyte fuel cell adopted from [Gurz et al., 2017,]

Figure 1.8 represents and graphically shows the historical evolution of cost of PEMFC, using DMFA and Bottom up estimation [Moreno et al., 2015,].DFMA is a methodology of design and cost estimation. In bottom up estimation, the cost of larger components is split in to smaller components. As one look in to the cost analysis there is always a similar cost for some consecutive years. The reason can be due to the assumptions used in the analysis of the system. On the other hand bottom up approach cost estimation technique, uses the concept of splitting cost of all major components into sub components and this results in greater and more transparent cost analysis of big components. It can be seen that cost of PEMFC, has reduced drastically from 2001-2005.

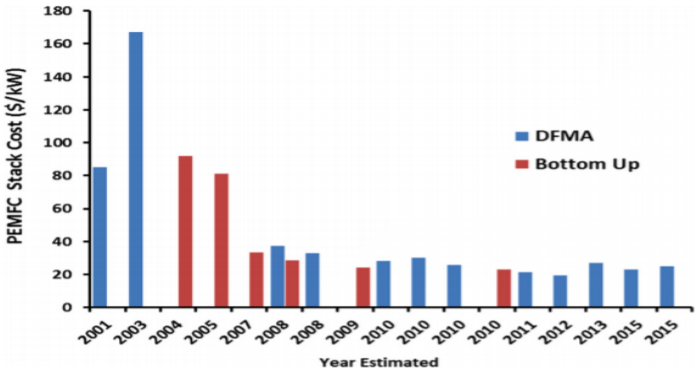

Figure 1.8: Evolution of PEMFC stack cost [Moreno et al., 2015,]

1.3 Principle of PEMFC

A polymer electrolyte membrane fuel cell is an electrochemical device that directly converts chemical energy of fuel to electricity via an electrochemical reaction taking place in the cell. It consist of two electrodes, namely anode and cathode, two bipolar plates, an electrolyte and gas diffusion layers. On the anode side hydrogen is fed and on the cathode side is oxygen. The two electrodes are in contact with membrane which acts as a medium for transfer of protons and separates gases from mixing. The hydrogen is oxidized at anode and $2H^+$ ions are liberated with 2 electrons (e^-). Now the H^+ are basically the protons which pass through the membrane and electrons are the one which conduct electricity and passes through the external circuit. Hydrogen is oxidised and the reaction is known as hydrogen oxidation reaction(HOR).

$$H_2 \rightarrow 2H^+ + 2e^- \tag{1.1}$$

At cathode, oxygen reacts with electrons and protons (passing through the membrane) to produce water.Heat is produced as a by product. Oxygen is reduced in this reaction and it is called as oxidation reduction reaction (ORR)

$$2H^+ + 2e^- + 1/2O_2 \rightarrow H_2O + Heat \tag{1.2}$$

Global reaction can be written as –

$$H_2 + 1/2O_2 \rightarrow H_2O + Electricity + Heat \tag{1.3}$$

1.4 Heat of reaction

Combustion is an exothermic process, which means that energy is released out in the process of combustion. This is in the form of heat, and requires water circulation in opposite side of bipolar plate (fuel cell stack) to maintain the same cell working temperature. The reaction is given as -

$$H_2 + 1/2O_2 = H_2O + Heat \tag{1.4}$$

This heat is actually difference of heat of formation of reactants and products. Heat of formation of liquid water in the reaction is given by $\Delta H = -286kJ/mol$. Negative sign indicates that heat is given out in the reaction and reaction can now be written as

$$H_2 + 1/2O_2 = H_2O + Heat + 286kJ/mol \tag{1.5}$$

1.5 Electrical work, theoretical and thermodynamics of fuel cell

There is maximum amount of energy that can always be extracted from fuel cell, it is impossible to convert all the energy to electricity because of generation of entropy and irreversibly in the system and hence only a portion of energy can be converted and is given by Gibbs free energy by equation 1.6

$$\Delta G = \Delta H - T\Delta S \tag{1.6}$$

In order to calculate the theoretical fuel cell potential it is important to understand the charge and entropy and their working. Electrical work is given by-

$$W_{el} = q \times E \tag{1.7}$$

where W_{el} is the electrical work in J/mol , q is the charge in Coulomb and E is the potential in Volts. The theoretical fuel cell potential is given by

$$E = -\Delta G/(n \times F) \tag{1.8}$$

and the theoretical fuel cell potential calculated at 25° C is 1.23 volts. Nernst equation provides a relation between standard potential for the cell reaction and open circuit voltage, given by equation 1.9

$$E = E^{\circ} + \frac{RT}{nF} \ln\left(\frac{P_{H_2} \times P_{O_2}^{0.5}}{P_{H_20}}\right) \tag{1.9}$$

If the standard potential is known for desired temperature (T), then based on the partial pressures of the reactants and the products open circuit voltage can be determined. It is important to understand, the above equations is only represented for gaseous products and reactants. Consider the case of liquid water production in the fuel cell, $P_{H_20} = 1$. Again considering equation 1.9, it can be observed that at higher reactant pressures the cell potential will be higher. If reactants are diluted or not in pure form (air in place of oxygen), the cell potential decreases. [Barbir, 2012,]

Fuel cell polarisation curve is an important tool [Zhang, 2008,] and in general displays the voltage output of the fuel cell for a given current density.

Figure 1.9 represent a general fuel cell polarization curve showing the various losses occurring which can give insights in the working of the cell. There can be three types of losses displayed depending upon the current loading.

1. **Activation polarization** Part (a to b) in Figure(1.9) represent the activation losses , or activation polarization. In order to make an electrochemical reaction going some voltage difference from the equilibrium is needed. This is activation polarization. These losses occur at both anode side and the cathode side. In the cathode side a higher over potential is required, as oxygen reduction requires much more over-potentials and it is much slower reaction then hydrogen oxidation.

$$\Delta V_{actual,c} = \frac{RT}{\alpha_c F} \ln \frac{i}{i_o, c} \tag{1.10}$$

$$\Delta V_{actual,a} = \frac{RT}{\alpha_a F} \ln \frac{i}{i_o, a} \tag{1.11}$$

The activation losses can be expressed by Tafel equation given by equation 1.12

$$\Delta V_{activation} = a + b \ln i \tag{1.12}$$

where a = $-\frac{RT}{\alpha F} \ln i_o$ and b = $\frac{RT}{\alpha F}$

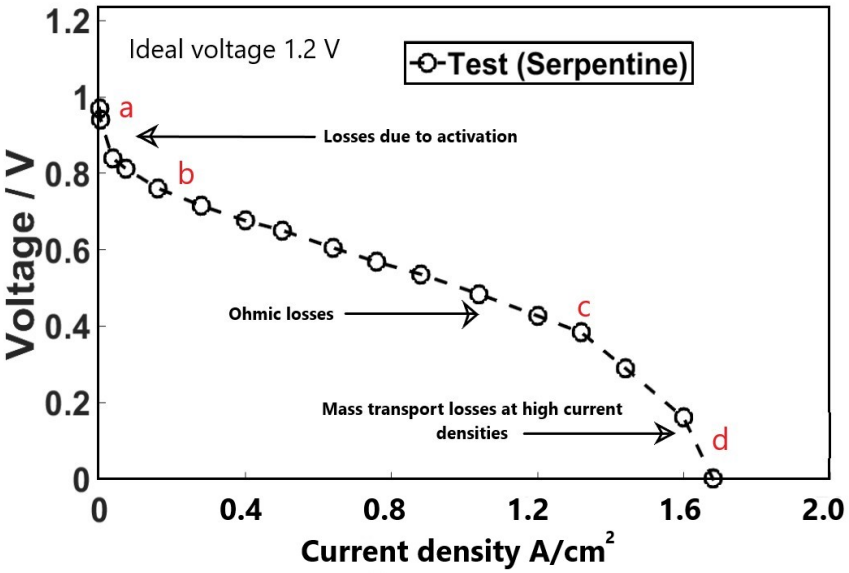

Figure 1.9: Example of a PEMFC polarization curve

2. **Ohmic losses**

   Ohmic losses occur because of resistance to flow of ions in the electrolyte and resistance to flow of electrons. Ohm's law can be used to express these losses in the fuel cell polarization curve. Region from (b to c) in Figure (1.9) shows the voltage losses due to resistance or ohmic loss. Ohmic losses can be due to electronic resistance in the fuel cell, contact resistance, resistance due to coating or due to compression effects.

$$\Delta V_{ohm} = i \times R_i \tag{1.13}$$

   where i is the current in Ampere, R_i is the total internal resistance of the cell in Ω.

3. **Concentration losses** Concentration losses mainly occur at higher current densities and departs from linear relationship mainly due to concentration polarization. Concentration loss is indicated by part (c-d) in the Figure(1.9). These losses are dominant when there is a high consumption of the reactant at electrode by electrochemical reactions. At high current densities, it gives an idea for the mass transport losses in the system. Concentration losses are followed by equation-

$$\Delta V = \frac{RT}{nF} \ln \frac{C_b}{C_s} \tag{1.14}$$

   where C_b is the bulk concentration of reactant in mol/m^3 and C_s is the concentration of reactant at the surface of the catalyst in mol/m^3.

   When the rate of consumption equals to the diffusion rate at catalyst surface at a particular current density, this current density is termed as limiting current density. It means the reactant gets consumed at the same rate as it is reaching

the surface. Limiting current density can be given by

$$I_l = \frac{nFDC_b}{\delta} \tag{1.15}$$

and the final equation of limiting current density can be expressed as -

$$\Delta V_{conc} = \frac{RT}{nF} \ln \frac{I_l}{I_l - i} \tag{1.16}$$

where I_l is the limiting current density.

A relation between fuel cell potential and current density (fuel cell polarization curve) can be summarised in equation 1.17

$$E_{cell} = E_r - \frac{RT}{\alpha_c F} \ln \frac{i}{i_o, c} - \frac{RT}{\alpha_a F} \ln \frac{i}{i_o, a} - \frac{RT}{nF} \ln \frac{I_{lc}}{I_{lc} - i} - \frac{RT}{nF} \ln \frac{I_{la}}{I_{la} - i} - iR_i \tag{1.17}$$

1.6 Composition of PEM fuel cell

Easier to manufacture and assemble, compared to internal combustion engine, PEMFC should be mechanically, thermally and electrically stable. This will result in better efficiency of fuel cell.

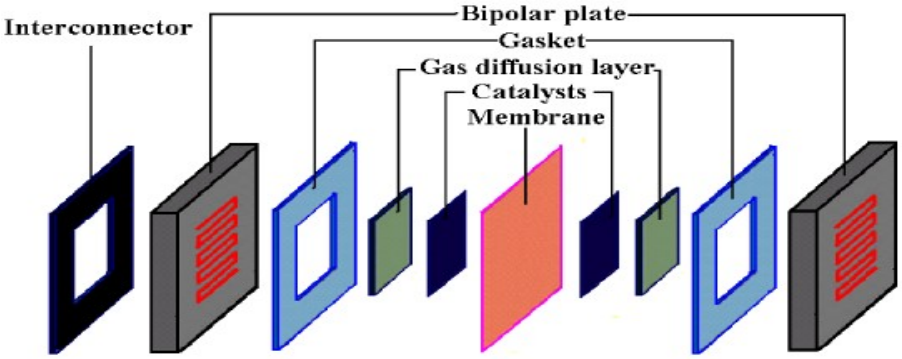

Figure 1.10: Construction of PEMFC

The elements which constitute the fuel cell (Figure 1.18) are bi-polar plates, followed by a gasket, which completely covers the cell in such a way that it avoids any gas leak. Directly attached with this is a gas diffusion layer (GDL) or porous transport layer (PTL) to uniformly diffuse the gas. GDL ($200 - 400\ \mu m$ thick) is then connected to catalyst layer, which performs an important function in breakdown of platinum to H^+ ions and e^-. Centered is the membrane which is approximately 50 microns thick. It should be very effective to create a strong barrier with no electrons passing and making the way only for positively charge ions.

1.6.1 Membrane

Membrane has one of the most important role in the working of fuel cell. On one hand it helps to separate the anode and cathode compartments thereby restricting the transfer of electrons and on the other hand helps in transfer of protons. These composite membranes with platinum particles embedded in perfluorosulphonate acid resin has shown to possess good properties of self-humidifying. Conductivity of proton exchange membrane is highly related to proton conductivity. They are made to withstand a temperature of 100°C [Kerres, 2001,] and shows good proton conduction at such temperatures also. Conductivity of proton exchange membrane is directly related to water content. Aim of the membrane is to keep the membrane in good hydrated conditions without the need of reactant humidification [Zhang et al., 2006, Bouchet and Siebert, 1999,]. Figure 1.11 shows the chemical structure of PFSA.

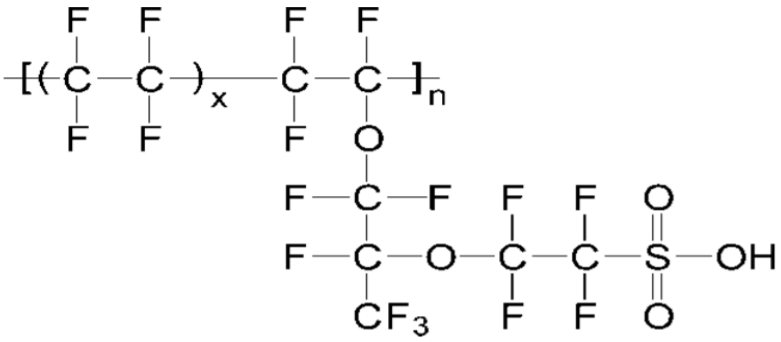

Figure 1.11: Chemical structure of PFSA adopted from [Healy et al., 2005,]

Nafion derivatives were first synthesized by the co-polymerization of tetrafluoroethylene and derivative of perfluoro with sulphonyl acid fluoride. Due to the presense of perfluoroalkyl backbones in Nafion, it has high hydrophobicity properties. The high quantity of Nafion ionomer in the CL may lead to mass transport limitations, while low amount of Nafion ionomer reduces proton conductivity and the triple phase boundary area in the catalyst layer. Water in catalyst layer is important to maximize the Pt utilization because it facilitates the proton conduction and form electrochemically active substances. Thickness of Nafion membrane can explain a lot number of things considering the swelling of membrane, degradation, transfer mechanism as they are directly related to the water uptake, proton conductivity, oxygen permeability.

1.6.2 Electrodes

Electrodes are active layers or the active sites for the electrochemical reaction to take place. For an efficient functioning of cell, the main function of electrode is to transport the protons to the membrane and the electrons to current collectors via gas diffusion layer and the metallic bipolar plates. Electrodes can vary between (5 -30) μm. Electrode is made up of carbon powder, particles size ranging from (20 – 50) nm of diameter on which particles of platinum are dispersed [Litster and McLean, 2004,]. These particles are bonded by means of the polymer providing the proton conductivity [Lundblad, 2004,]. This is where much of the multi physics

play part and it is a zone of three materials, composing of three materials: platinum supported by carbon, the polymer and the porosity, which allow the passage of gas. The Figure 1.12 shows schema of electrode and surface of electrode, the large view and platinum particles attached to the surface of carbon.

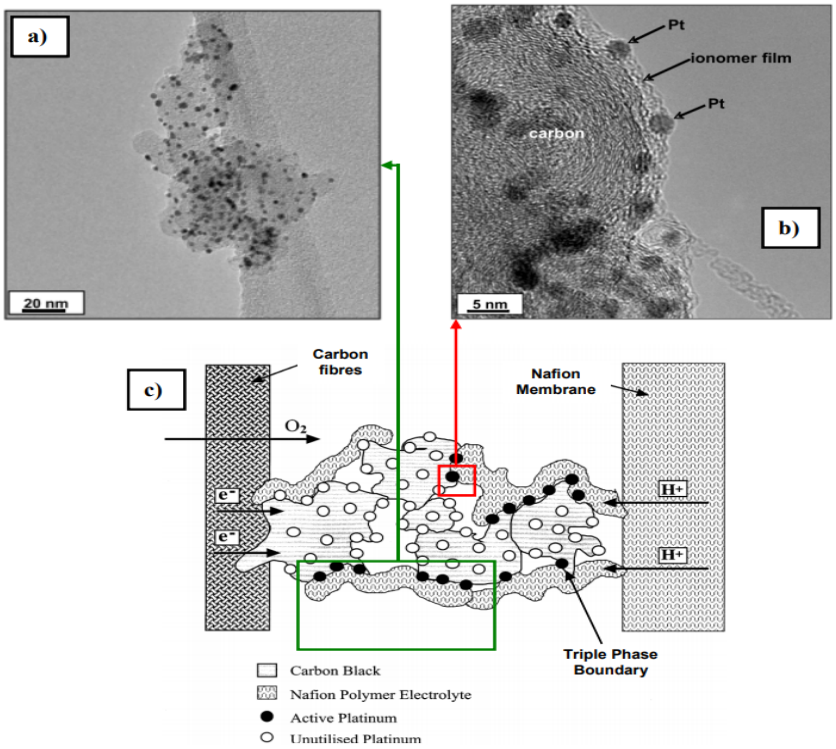

Figure 1.12: (a) Carbon support with uniform Platinum dispersion , (b) Close up on individual platinum particles of sphere of carbon and (c) electrode overview [Lamibrac, 2013,]

Diameter of the platinum particles play a key role in order to increase the performance and reduce cost as the material is very costly. More the reaction surface and less platinum loading is very beneficial for a cost effective coating. Compared to 1960's where 28 mg of platinum [Larminie et al., 2003,] per cm^2 was required is exceptionally reduced to 0.3 mg today [Ren et al., 2020,]. An important structural change to electrode is the use of oriented carbon nanofibers to increase the electrochemical surfaces with increase in stability and decrease in platinum loading. (< 0.03 mgPt cm^{-2}) [Álvarez et al., 2012,] . Poisoning by CO catalyst is another phenomenon which can harm the electrodes or damaging the sites of gas diffusion layer, however poisoning phenomenon is observed during metallic uncoated plates more compared to graphite [Li et al., 2010, Sulek et al., 2011,]

1.6.3 Gas diffusion layer

Commonly known as porous transport layers (PTL) or gas diffusion layer (GDL), figure 1.13, have several function in a PEMFC. When the gas flows through the channel it is very important that the gas is distributed uniformly. Gas diffusion layer plays an important role in order to distribute gases homogeneously from channels to the electrodes, evacuation of water and the heat produced. Gas diffusion layer is also

responsible for transport of electrons to the current collectors. Ability to permeate the reactants and products and to maintain good electrical and thermal contact with the plate is one of the main function of gas diffusion layer [Swamy et al., 2011,]. On general, the gas diffusion layer is composed of paper or carbon felt having an average pore size ranging from (10 - 50)μm. The porosity of these layers varies between $(60 - 90)\%$ and thickness can be varied in the range of (200- 450) μm. Gas diffusion layer is placed between the two bipolar plates and tightened to ensure no leaks of reactants and products is observed. Based on the amount of pressure applied they can undergo a decrease in thickness by $(10 - 40)\%$ which can effect results in polarization curve [Chen et al., 2008,] . Since the main aim is to redistribute reactants and products, it is very important that the gas diffusion layers is treated with PTFE to increase the hydrophobicity and facilitate the removal of water. Spray technique is generally used which involves surface deposition in macroporous layer compared to micropores. In order to increase the performance, a micro porous layer is inserted between the electrodes and the gas diffusion layer. The porous layer compose of carbon size varying in the range of (10 -100) nm between which PTFE is also inserted by spray or ink[Chen et al., 2008,]. Addition of MPL brings the performance improvement [Owejan et al., 2010, Karan et al., 2006, Malevich et al., 2008, Atiyeh et al., 2007,] and the result can be due to better electrical and thermal behavior[Thomas et al., 2014,] . Since the gas diffusion layer and the micro porous layer involves carbon particles so there are degradations related issues too, due to oxidation of carbon. Improper use of the system subjecting to adverse current, or temperature can lead to carbon oxidation and removal of PTFE. This can further impact the water management thereby reducing the mechanical strength and other properties. [Yan et al., 2010,] showed that importance of addition of PTFE produces crack and also leads to appearance of crack in MPLs [Yan et al., 2010,], [Fishman and Bazylak, 2011,] and [Hizir et al., 2010,].

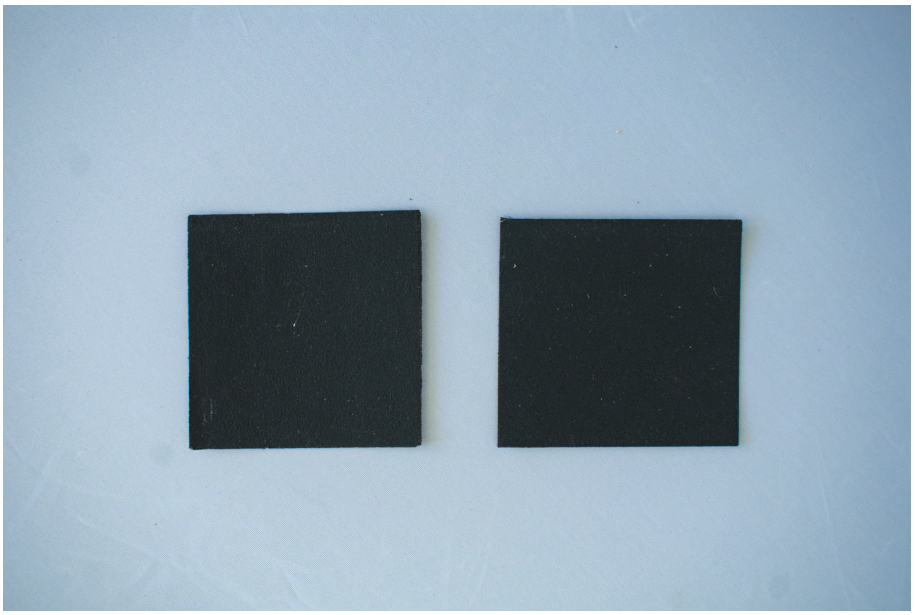

Figure 1.13: Gas diffusion layer

1.6.4 Gasket

Gasket (Figure 1.14a, 1.14b)is one of the most important component of fuel cell used mainly to prevent leaks in fuel cell or fuel cell stack and to provide correct compression. An improper management or problems concerning gasket can lead to sealing problem of stack which can ultimately lead to efficiency related issues considering the supply of reactants to the cell [Lee et al., 2015,]. Not only this maintenance cost of the system will rise and durability and reliability can also be affected in the long run. Silicon, EPDM rubber and PTFE are few commonly used gaskets for low temperature fuel cells. A gasket is usually 200 μm in thickness and can further depend based on the application if low temperature fuel cells or high temperature fuel cells.

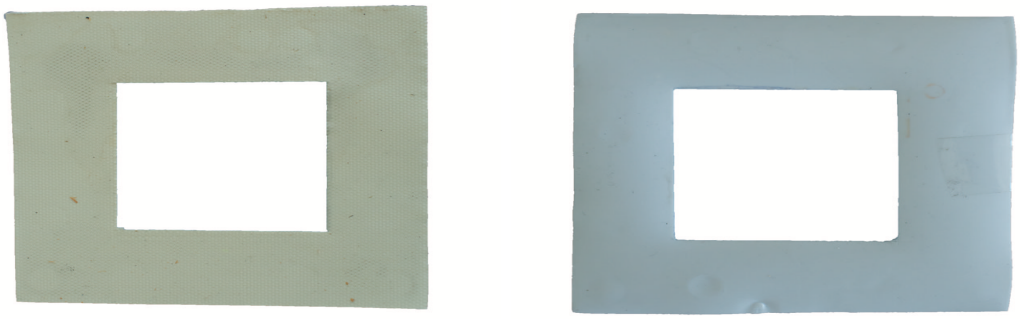

(a) Silicon gasket (b) Teflon gasket

Figure 1.14: Types of gasket

A gasket should serve some important functions -

1. Chemical stability
2. Prevent mixing of fuel and oxidant
3. No leakage to outside environment and inside
4. Stability over required temperature range
5. Prevent mechanical bonding of components
6. Electrical insulation between components

1.6.5 Bipolar plates

Bipolar plates are used for distribution of gases, evacuation of water and excess reagents using millimetre channels. They can be of different materials such as graphite, which is most used material so far, apart from that active research is going on for stainless steel, titanium, aluminium . One of the most important property of these bipolar plates is good mechanical strength and to withstand corrosion. Graphite possess good corrosion resistance but bipolar plates made of stainless steel, aluminium needs to be coated . The material used for plates should be non impermeable to gases thereby avoiding any leaks in the system. Stack usually consist of

many plates combined together to supply energy, therefore it is very important that the plates are of least weight and with less machining cost. Being good conductor of electricity and chemical stable graphite is the choice of bipolar plates from long time but machining of this material is difficult and expensive. However carbon composite materials are proposed which are more compact, possess better machining properties and chemically stable [Yuan et al., 2005,] . Figure 1.15 represents a metallic bipolar plate, circular design used in the application of fuel cell.

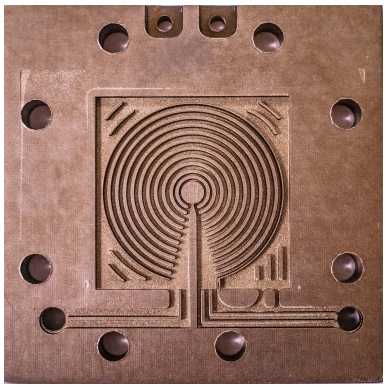

Figure 1.15: Metallic bipolar plate

Some important functions of bipolar plates are listed below -

1.6.6 Distribution

Bipolar plates used have channels, inlet and outlet. The gas entering from the inlet is then distributed over the entire length to flow evenly across the active gas diffusion layer or electrode area. Since distribution is directly related to homogeneity of flow hence it becomes very important for an efficient channel design.

1.6.7 Water and heat management

Bipolar plates are not only limited towards distribution of gases but also serves a purpose to efficiently remove the water produced during the fuel cell reaction. This is very important for the fuel cell to work efficiently as an improper water removal can lead to flooding behavior of the cell and thereby would result in the stop of fuel cell. After water management, fuel cell bipolar plates serve a dual purpose to heat management also. Most of the bipolar plates have channels in and out of the plate. Inner channels are used for distribution of gases and outer are mainly used to control heat, as they are equipped with channels distributing water. It serves to maintain the temperature inside the fuel cell stack. Apart from flooding there are problems related to drying of the fuel cell and hence heat management is important.[Ilie et al., 2016, Thomas et al., 2012,] investigated local temperature and overheat inside membrane electrode assembly. There can be two types of cooling or water cooling of air cooled PEMFC [Shahsavari et al., 2012,]

1.6.8 Electrical circuit between individual cells

Since electrons produced during the reaction needs to be transported and hence bipolar plates serves an important function to conduct or to maintain an electrical

circuit.

1.6.9 Mechanical support

Bipolar plates also serves some important function in providing mechanical support to MEA. [Karimi et al., 2012,]. It acts as a rigid structure and supporting every element in the mechanism.

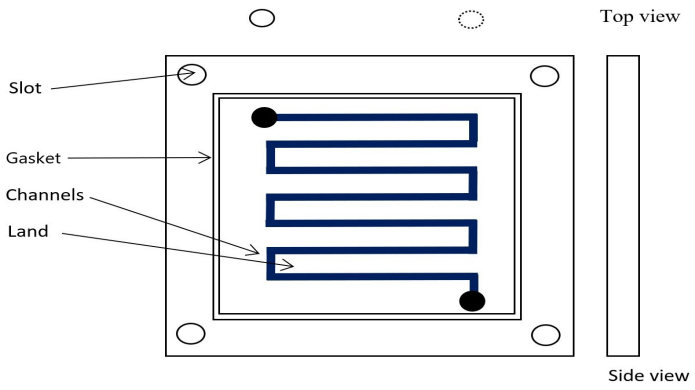

Figure 1.16: A general representation of bipolar plate with traditional serpentine design

1.7 Water distribution in PEM fuel cells

There are four important ways of water distribution during fuel cell operation. All the processes plays a key role. There should always be sufficient amount of water to avoid the condition of drying as it can affect the protonic conductivity of membrane and increase degradation in GDL and membrane. Similarly excess of water (often in cathode side) can result in flooding of fuel cell. This can be due to more water production than water removal. Due to flooding condition the active catalyst surface reaction would stop. Since it is important to address water management, hence the mode by which this process of water transfer takes place needs to be understood. And of all the modes of transfer, diffusion and electro-osmosis [Sellin et al., 2019] plays an important role.

1. **Electro-osmotic drag**

   It can be defined as movement of water or other solvents across the membrane, capillary tube, micro channel etc. associated with movement of ions under influence of electric field [Pivovar, 2006, Sellin et al., 2019,]. Considering the fuel cell applications water is also transported by electro osmotic drag of water by protons from anode to cathode side. Electro osmosis can only occur if there are charged species in the fluid that can respond to electric field.

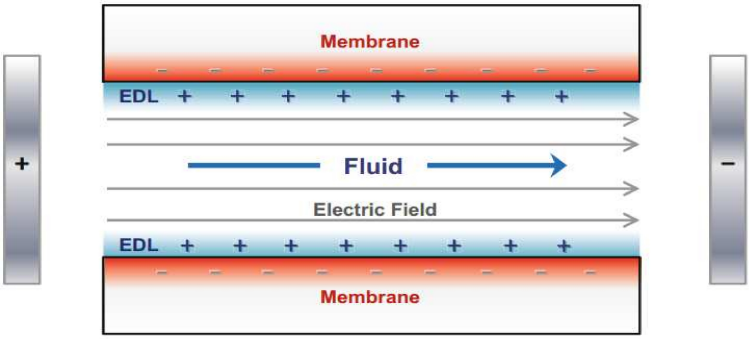

Figure 1.17: Representation of electro osmosis in membrane pore, with effect of electric field.[Wiley and Weihs, 2016,]

2. **Back diffusion**

   When the two sides across the MEA are subjected under different concentration gradients there is always a possibility to achieve equilibrium. This is achieved through back diffusion. In most of the cases, back diffusion can be dominant at higher currents when at anode side there is less water compared to cathode and could result in back diffusion of water in the anode side.

3. **Convection**

   There can also be possibility for water transport due to convection of the liquid in the channels [Jung and Nguyen, 1998,].

4. **Thermo osmosis**

   Thermo osmosis can be defined as a flow due to temperature gradient. The flow due to this process occurs due to the entropy difference. The flow from cold to hot side results in an increase of entropy of the system, which is thermodynamically favored [Tasaka et al., 1990,]. In the fuel cell applications, temperature difference can occur, if the two sides are maintained at different temperatures and at higher currents [Mench, 2008,]. Cases related to thermo osmosis are performed but the results were not observed as the flow was dominated by concentration gradient. [Zaffou et al., 2006,] have observed no flow in their experiments, but [Mench, 2008, Tasaka et al., 1992, Villaluenga et al., 2006,] have observed the thermo osmosis phenomenon through the membrane.

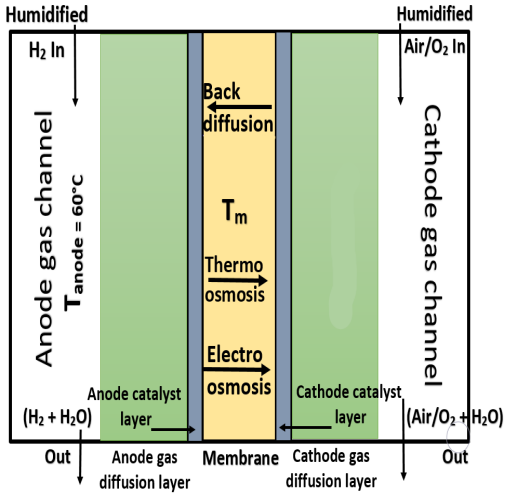

Figure 1.18: General water distribution in PEMFC (If $T_m > 60°C$)

Fig 1.18 shows a general distribution of water in a polymer electrolyte fuel cell. There can be many cases possible. If it is considered that temperature of membrane to be higher as in [Thomas et al., 2012,], thermo-osmosis is from colder to hot side. During working of cell, the distribution of water may vary too.

1.8 Electrochemical tools and diagnosis

A new flow field design in PEMFC should satisfy condition of homogeneous distribution of reactants, temperature and most importantly water removal. Water monitoring inside is a complicated procedure and there has been extensive research considering the different aspects of water distribution. The water produced during fuel cell operation results in two phase flow - liquid and gas. This water needs to be distributed evenly across the gas diffusion layer and monitoring can give insightful results on the characteristics of new flow field design plate. [Dillet et al., 2010] worked on prototype of single channel fuel cell with the objective of monitoring the appearance and transport of water droplets in the gas channels There are many direct methods of monitoring the water produced in the fuel cell such as neutron imaging [Owejan et al., 2007, Hickner et al., 2008,] ,gas chromatography [Mench et al., 2003,], [Yang et al., 2005,], monitoring through transparent fuel cell [Tüber et al., 2003,] . The problem with direct methods is that they are expensive and may require the use of special design or equipment in order to analyze the fuel cell performance with respect to water. Hence there is a need of indirect methods which can help in quickly analysing the water distribution in the fuel cell. One of the concept used can be using parameters that can directly effect the output results such as pressure drop. It can give in-situ results regarding the present condition of water in the fuel cell. Voltage drops to zero can indicate severe water accumulation and ultimately blocking of channels for further reactants[Maizia et al., 2018,]. A list of methods to analyse the water management are given below-

1. **Neutron imaging** Neutron imaging is a direct and non destructive experimental tool which can be used to evaluate water management in the fuel cell.

Neutron imaging has principle similar to X ray radiography where a beam of neutrons passes through a sample and is attenuated in accordance with sample's composition. The concept involves passing neutrons through the objects to be imaged, then a scintillation screen converts the neutrons into visible light. It is a complex technique and requires cost and expertise to work with the setup. [Hussey et al., 2007,], [Satija et al., 2004, **?**,] explored the method of neutron imaging as an experimental tool to evaluate water management system of fuel cells. It gave insights related to water in cell flow channels and gas diffusion layer. Since many new designs of flow field are coming up hence, [Wu et al., 2020,] utilised neutron imaging for application in foam flow fields as foam flow field is susceptible to flooding at low current density.

2. **Impedance spectroscopy** Impedance spectroscopy is a powerful diagnostic testing method. It is non destructive and used in order to diagnose faults in fuel cell system and can give results considering the resistance of various components of fuel cell. [Wu et al., 2019,] analysed the water distribution with hydro-electrochemical impedance imaging by giving small AC sinusoidal perturbation to the cell. The utility of combining with imaging technique helped to collect information on the source and history of water in the system. With this tool it is possible to detect the water management within the cell but has certain limitations such as interruption of the system. With higher frequency, results are obtained quickly but in order to analyze the lower frequency the time is higher.[Meyer et al., 2019,] use this technique to analyse the catalyst and carbon degradation in the fuel cells.

3. **Current interruption technique** Current interruption method can also be used to diagnose and estimate fuel cell performance. The concept consist of interrupting the current for a very short period of time especially a few milli seconds and recording the resulting voltage. By doing so the ohmic losses will immediately reduce to zero followed by activation losses which will take time to disappear [Vachtsevanos and Vachtsevanos, 2006,]. This voltage profile then can give valuable information regarding the ohmic and activation losses. Also, the difference between cell voltage before and after the current interrupt can give information regarding the current resistance.

4. **X ray tomography** X ray tomography can be used to get water distribution in a running fuel cell. It can give information regarding the compression of gas diffusion layer fibres and hence for new flow field design this can be an insightful tool to understand. [Hack et al., 2020, Meyer et al., 2016,] used X-ray computed tomography for local degradation of membrane electrode assembly (MEA) at various locations of channels of serpentine flow field. This led to understand in depth analysis of catalyst layers with order of degradation and was found to be outlet > middle > inlet. [Banerjee et al., 2016,] analysed the structure of bi-layered gas diffusion layer with X ray computed tomography in PEMFC. Samples with and without MPL's are studied for impact of rib-channel compression on porosity profiles. Porosity results shows that under the channel, the porosity channel is nearly identical to uncompressed profile. However under land region there is a decrease in GDL thickness.

5. **Pressure drop** Pressure is yet again a non destructive,in-situ diagnostic tool which can give insightful information considering the flooding and drying of the cell, the amount of liquid water accumulated within the gas channel. Lower pressure drop is always preferred as it requires lower compressor power. [Mortazavi and Tajiri, 2015,] worked on reviewing two phase flow patterns which is achieved by reviewing the two phase flow patterns followed by the two phase flow pressure drop.

6. **Electrochemical noise analysis** Electrochemical noise analysis can be a powerful tool to analyse in-situ results considering the water management of fuel cell systems. Spontaneous fluctuation of potential or current is recorded which is generated by electrochemical systems. Electrochemical noise have been earlier used to analyse corrosion studies [Bernard et al., 2005,], batteries [Huet et al., 2006, Martinet et al., 1999,] , evaluation of gas [Boinet et al., 2007,]. The concept involves recording the stochastically evolving electrochemical noise generated due to the reactions going on in the setup. There can be long recorded signals for more than 2 hours in order to understand the variation of voltage or pressure over time [Maizia et al., 2017, Martemianov et al., 2020,]. This method to analyse the faults in fuel cell diagnosis is better over other non destructive methods as it can be easily used in laboratory setups without interrupting the system. This quality helps to analyse the signal over a set of current values and record the variation which can then be use to interrupt the results of health of fuel cell. The setup consist of a pressure sensors to measure pressure, electronic load to impose current, National instruments data acquisition card to record the signals of pressure and fuel cell voltage fluctuation. In the present research noise analysis as a tool is used to understand water issues, working of different design of fuel cell bipolar plates.

   Again electrochemical noise can be subdivided in to temporal and frequency domain. Both can have their own advantages of decoding the information from the signal which is explained in chapter 4 of this thesis.

1.9 Faults and importance of prognosis in proton exchange membrane fuel cell

Fuel cell is a complex system which involves a complex number of phenomenon and it is important to minimize losses and increase performance. Making a stack work in optimal conditions can help to avoid possible performance degradation. Some of the most important faults which can be found in the system are -

1. Faults inside fuel cells
2. Faults on reactant supply
   - Contamination
   - Improper pressures
   - Improper gas flow rates
3. Faults in heat management

4. Faults on water management

    - Membrane drying
    - Flooding

5. Faults in electrical circuits

For the scope of this study faults with respect to water distribution will only be analysed through techniques as discussed. In order to work on this issues, diagnosis and prognosis can also be a reliable tool which can be dedicated to access the current state of health and to work on future predictions of failure and risk which may lead to shut down of system.

Diagnostic methods can be further divide in to two or more sub category

1. Model based diagnostic methods

2. Data driven diagnostic models

Model based on diagnostics do not rely on experimental data but starts by residual procedure with an aim to create estimates by process outputs and to build difference between process output and their estimates [Li et al., 2010,] thereby to extract diagnosis based information and make diagnostic decisions. [Petrone et al., 2013, Mohammadi et al., 2015,] worked on model based diagnostic tools to give a detailed review for various models and to give diagnosis related to temperature and current diagnosis.

For the scope of this research it is limited to data driven diagnostic models which uses an experimental data in order to analyse and produce the results. [Li et al., 2014,] , [Li et al., 2015,] worked with water related faults (flooding and membrane drying) by using pattern classification methodology,[Ma et al., 2018,] used deep learning method is order to predict fuel cell degradation. Again [Mao et al., 2017,] [Mao et al., 2017,] used the concept of signal processing through sensors and data driven approaches to understand the effects of prognosis and detect faults in the system.

1.10 Identify the scope of this work and objective

From the various important information discussed in section 1.7, 1.6.5, 1.8 and 1.9, it brings into water distribution and management into account and how it effects the fuel cell performance. Section 1.7 explains various types of water distribution. Water through diffusion and electro-osmosis accounts for the maximum amount of transfer in PEMFC. Section 1.6.5 highlights importance of bipolar plates to develop new flow field designs in order to address the water removal or effective distribution of reactants. Section 1.8 shows different diagnosis methods used in order to detect the faults in fuel cells. Now in order to understand water distribution in PEMFC can these diagnostics tools be reliable and robust for various parameters and operating conditions ? Finally in section 1.9, it highlights the importance of predicting the faults in the running fuel cell setup. A fuel cell is prone to several faults and in such case prognosis can play an important role in order to minimize the effect.

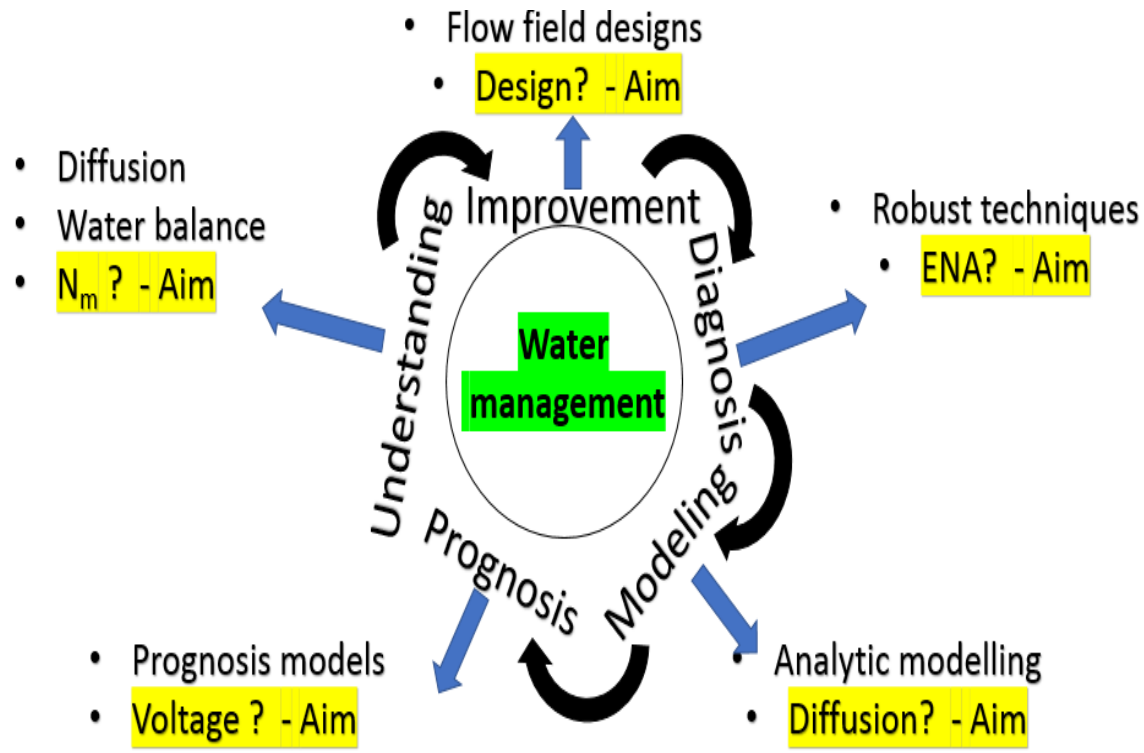

Figure 1.19: Importance of understanding, improvement, diagnosis and prognosis of water management in PEMFC

The above Figure 1.19 sets the main idea of this research work and how the layout of this thesis is presented in order to answer the research questions.

1.10.1 Research question

1. Is it possible to identify specific methods which can estimate the diffusion coefficient (important method for water distribution) resembling fuel cell setup over varying operating conditions?

2. Can water management and distribution be improved by developing new flow field designs ?

3. Can the new developed flow field designs be diagnosed with robust and effective methods in order to check the water distribution?

4. Tools and methods available for prognosis of PEMFC performance.

   These all above points can help to answer if water management and diagnostics can be improved in PEMFC ? How this is carried out in this thesis is discussed in next section.

1.10.2 Layout of the thesis

In order to better understand the thesis and answer the questions, this thesis is divided in to 5 chapters which are as follows-

1. CHAPTER 2 -

   Since there are many ways of water distribution as described in section 1.7, hence this chapter deals with estimation of effective diffusion coefficient through water balance method. There is summary of work by authors in order to estimate diffusion coefficient through the membrane. The value of diffusion varies by 4 orders with respect to water content. Also how parameters such as density, water content and equivalent weight can effect diffusion is discussed here.

2. CHAPTER 3 -

   Having understood one form of water distribution by diffusion, the next idea is in improvement of water distribution in PEMFC. This is done by introduction of new flow field designs in PEMFC using stainless steel plates. For characterisation, polarization test and pressure head loss test are used. This chapter tries to answer the second research question.

3. CHAPTER 4 -

   Once the flow field designs are developed, the next is diagnosis. There have been many methods to see water distribution in literature such as X-ray, neutron imaging which requires use of prototype cells, expertise, cost and quality. In this chapter, electrochemical noise analysis is introduced and it tries to answer if ENA is a reliable tool to understand water distribution with respect to different flow field designs and its effect on operating conditions of current and relative humidity.

4. CHAPTER 5 -

   After having understanding of water distribution by diffusion, improvement, diagnostics, the final question is with respect to modelling? How can modelling of water fluxes reduce the dependence on experiments and improve the understanding of water distribution? Finally this chapter ends with prognosis. Prognosis can be important to predict the faults in the fuel cell system. Here machine learning and deep learning approach is used to understand the prediction of voltage based on data used, where voltage is varied with respect to different water concentrations.

Finally, this research concludes with the need of new designs of bipolar plates and choice of tools to diagnose the fuel cell health.

Chapter 2

In-situ estimation of effective diffusion coefficient and effect of membrane swelling with respect to water content, density and equivalent weight.

2.1 Introduction

This chapter deals with the measurement of effective water diffusion coefficient in a setup which resembles a fuel cell setup. In the beginning of this chapter main idea is to estimate effective diffusion coefficient using "water balance method" as an easy and quick procedure. In the literature there is huge variation of values of diffusion coefficient based on various point of interests of different authors and hence to model an effective value is required. The research is further expanded to understand how water balance method is an effective tool to understand variations of imposed gradient in relative humidity, variations of results with respect to change in temperature in the cell. It is further described how water balance method is prone to errors and what steps are necessary to keep the results in permissible limits of error.

Later half of this chapter deals with the variation of parameters on the diffusion coefficient which is mostly not touched and can explain how these factors of density, equivalent weight and water content λ can produce large difference in the estimation of diffusion coefficient.

2.1.1 Diffusion mechanism

Diffusion is movement of molecules from region of higher concentration to region of lower concentration. Hence, it becomes very imperative to understand what are the factors responsible directly or indirectly which can influence the transfer process in fuel cell applications. Effective ways which can help to measure in-situ value of diffusion coefficient and role of diffusion coefficient in water management.

Earliest works in diffusion, dates back to 1855, when Adolf Fick [Fick, 1855,] gave Fick's law of diffusion.This law expresses a relation between the diffusion flux

and concentration gradient under assumption of steady state. The law explains the nature of flux going from region of higher concentration to lower concentration in order to achieve equilibrium which can be mathematically expressed by equation (5.26) as -

$$J = -D \times \frac{\mathrm{d}\phi}{\mathrm{d}x} \tag{2.1}$$

Where,

1. J is the diffusion flux, expressed in dimension of amount of substance per unit area per unit time. $(mol/m^2/s)$

2. D is the diffusion coefficient defined in dimensions of area per unit time. (m^2/s)

3. ϕ is the concentration expressed in amount of substance per unit volume. (mol/m^3)

The process of diffusion can also be extended to second law of diffusion which predicts how the concentration can change with respect to time given by

$$\frac{\mathrm{d}\phi}{\mathrm{d}t} = D \times \frac{\mathrm{d}^2\phi}{\mathrm{d}x^2} \tag{2.2}$$

Based on the assumptions and modelling any of the above can be helpful to understand the dynamics of physics in fuel cell applications.

There are numerous approaches, methods in the history of literature of polymer membrane in order to understand the diffusion through polymer electrolyte membranes [Zawodzinski Jr et al., 1991, Hietala et al., 2000, Majsztrik et al., 2007,], as the values obtained have a key role to play in numerical models which can accurately capture the physics. The physics involved is to understand the much-complicated model of actual working of fuel cell. Out of which a few are listed. In the subsequent parts of chapter more focused will be on water transfer coefficient, how concentration effect this parameter? The need to understand Fick's water diffusion(D_f) and it's comparison with diffusion taking water sorption into account(D_λ).

2.1.2 Cation exchange membranes

These membranes (Figure 2.1) are proton conductive and only allow the cross over of protons. This serves the key purpose of these membranes in PEMFC. These membranes include negative charges (example PO^{3-} ,COO^-, C_6H4O^-, SO_3^-) [Bhunia and Dutta, 2018] in the backbone of membrane which restricts the passing of anions (negative charge ions) and only allows cation (positive charge ions H^+) to pass through. Cation exchange membranes has properties of low internal resistance and superior conductivity. Also, the most common type of membrane in this category of cation exchange is Nafion®, developed by Dupont Inc in 1970.

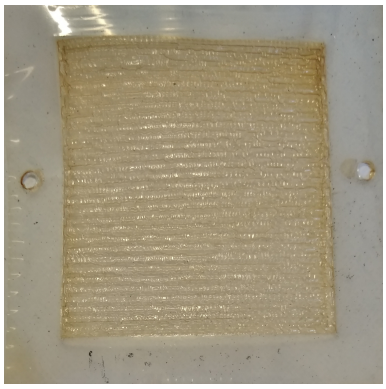

Figure 2.1: Nafion (Cation) membrane - NRE-211

2.1.3 Anion exchange membrane

These membranes have positive charges such as PR^{3+}, SR^{2+}, and NH^{3+} attached to the membranes and are responsible for the transfer of anions [Rahimnejad et al., 2015,]. In order to improve the proton conductivity, Anion exchange membranes (Figure 2.2) serves a special purpose as they utilize carbonate and phosphate and hence directly target to improve the proton transport efficiency [Zhuang et al., 2012,]. However, diffusion coefficients and mobilities of (OH^-) are less dissociated than typical sulphonic acid groups and the nucleophilic property of (OH^-) anion can result in poor chemical stability for fuel cell [Merle et al., 2011].

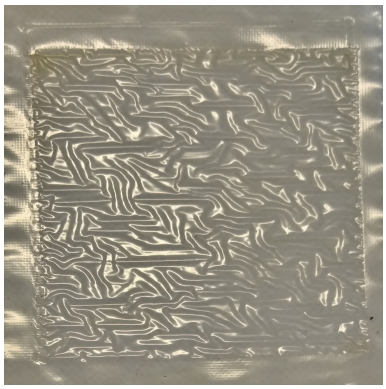

Figure 2.2: Tokuyama (Anion) membrane- A 201

2.1.4 Dual exchange membranes

Dual exchange membranes use both anionic and cationic properties. They are arranged sequentially with MEA's aligned which consist of an anion exchange membrane and cation exchange membrane. [Lee et al., 2020,] used this for cases of non-humidified PEFC operation, in order to improve the humidification conditions.

Since the membranes have their own utility and all have been used in fuel cell operations so it would be insightful to understand the diffusion process through these membranes. In this chapter water balance method is employed to Nafion® and Anion membranes in order to understand the diffusion.

2.1.5 Nafion and transport mechanism

One of the most important and promising candidate for fuel cell operations is the solid-state polymer electrolytes Nafion® membrane[Pivovar, 2006, Mauritz and Moore, 2004,] and the key characteristic which makes it so are its resistance to chemical environments, good strength and ability to withstand with different operating temperatures of fuel cell. What makes the Nafion® membrane more utile is the diffusion across membrane under varied conditions of different fuel cell temperature, relative humidity and thickness.

There can be multiple transport mechanism through the membrane at various length and time scales and it is not easy to define or monitor any single process at any time. In a normal working of fuel cell, fluid can transfer by (1) Hydraulic mechanism (Darcy law) (2) Thermo-osmosis (flow due to gradient in temperature) (3) Electro-osmosis [Pivovar, 2006,] (due to current) (4) Mass transfer (Fick's law). Mass transfer by Fick's law can further be divided by (interface + bulk) [Kusoglu and Weber, 2017,] transfer and pre evaporation. Since in our experimental setup there is no chance for condensation of liquid water from humidified air so we do not consider the effect of pre evaporation. Thermo-osmosis [Zaffou et al., 2006,] is possible but thermo-osmosis lies 1or 2 order of magnitude less than bulk diffusion[Kim and Mench, 2009,].

2.1.6 Water transport and sorption

Water sorption in general, considering Nafion membranes can be defined as amount of water absorbed by the membrane in equilibrium with vapor or liquid water at a known temperature. Although we can use the concept and modelling approaches for other solvents, but for the scope of this research the focus will be limited to water only. This amount of water contained in hydrated membrane can be expressed as number of water molecules per sulphonic acid sites.

$$\lambda = \frac{n[H_2O]}{n[SO_{3-}]} \tag{2.3}$$

an also be expresses as -

$$c = \frac{mH_2O}{m_{dryNafion}} \tag{2.4}$$

There can be different behaviours of sorption isotherms of Nafion membranes as presented in Figure 2.3. Different types of sorption mechanism can be attributed to different shapes of sorption isotherm.

1. Langmuir contribution : The dissociation of the acid group SO_3H $(\lambda - (2-3))$

2. Henry's law : Adsorption to tightly bound water $(4 < \lambda < 10)$

3. Flory Huggins theory : Aggregation of water molecules (clustering $\lambda > 10$)

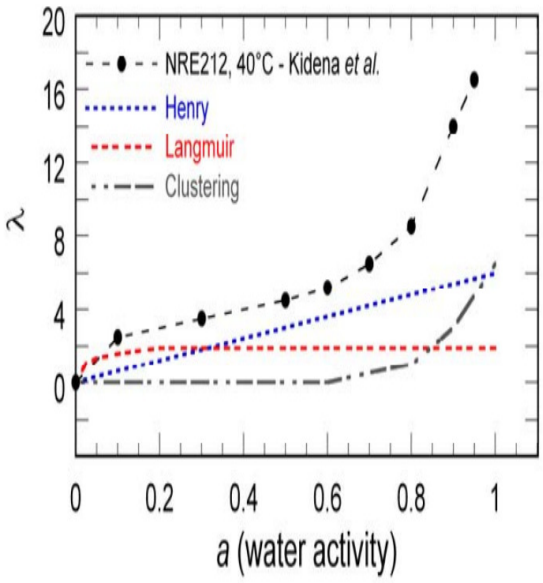

Figure 2.3: Sorption isotherm of Nafion NRE212 at 40°C, adapted from [Kidena, 2008,] The curve can be decomposed into three contributions: Henry, Langmuir and Clustering.

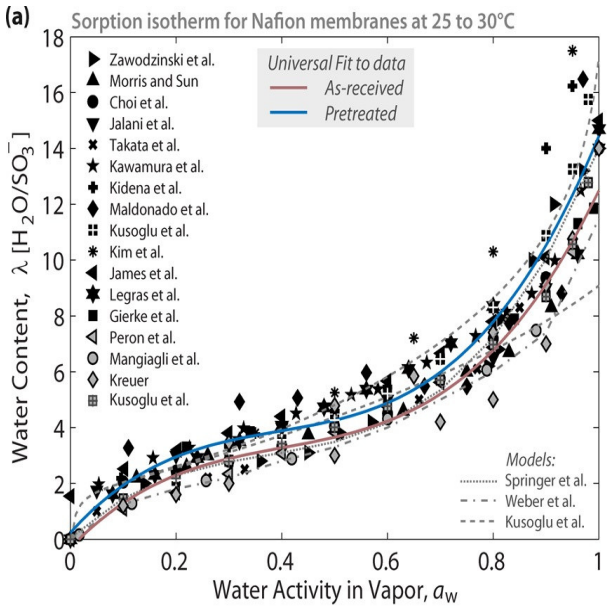

Figure 2.4: Sorption curves for Nafion membranes $(25-30)°C$ adapted from [Kusoglu and Weber, 2017,]

One of the key process for efficient working of fuel cells is the sorption and transport of water in polymer membranes and water content stands out to be an important variable to characterise the state of art of polymer electrolyte membrane. Figure 2.4 shows sorption curve for Nafion membrane at $(25-30)°C$ for different studies. Structural properties, followed by transport properties leading to overall durability of fuel cell performance can be highly affected by water content leading to effects on proton conductivity, degradation, homogeneity, swelling, under various

fuel cell operations [Barbir and Yazici, 2008, Ge et al., 2005, Thampan et al., 2000, Weber and Newman, 2004, Zawodzinski Jr et al., 1993,].

There are various models in literature to understand the water sorption behaviour in polymer electrolyte membranes. The isotherms of water sorption of these membranes have sigmoid shape. At low relative humidity it is concave to water activity and convex at high relative humidity. These models can be further categorised in (1) Dual mode sorption mode (2) The Sigmoid Sorption model (3) The new dual mode sorption model . Isotherms, sigmoid shape for water sorption in membranes were analysed with Feng's new dual mode model to analyse Nafion® membranes with different counter ions and protonated Nafion® membranes, under different degrees of humidity. Feng's model was then used to analyse membrane structure/property relationships [Li et al., 2013,]

2.2 Experimental techniques to understand diffusion

In order to estimate the diffusion coefficient, different approaches and methods are used to understand water sorption and transport in Nafion® thereby calculating diffusion coefficient. [Majsztrik et al., 2007,] gave a description of various methods used to understand and analyse transport and water sorption, which are as follows-

2.2.1 Water sorption and desorption technique

In these techniques usually experiments are carried out with a balance, a membrane, humidity controller sensors. In order to carry out the sorption measurements, the membrane is fully dried and based on the requirements of experiments can be pre-treated. The drying temperature may vary with respect to the experimental conditions. In sorption experiments [Majsztrik et al., 2007,] usually a membrane is hanged in container which is filled partially with water. The whole system is kept on weight balance. Relative humidity based on the interest of experiments is maintained periodically and can be equipped with humidity sensors for better or optimized results.

On the other hand, in order to carry out water desorption experiments the water in the container is replaced by a new container containing desiccant.

2.2.2 NMR studies

Nuclear Magnetic Resonance (NMR) spectroscopy is again a very useful technique which is used to understand the diffusion coefficient. In domain of chemistry it is mainly used in quality control and research to understand the molecular structure. Further use of this method can help to understand the diffusion of water in the fuel cell channels. This technique is difficult to use and is not easily available considering inputs required. Also, nuclear magnetic resonance techniques are costly to carry out and require specialization in order to carry out experiments. But these methods have certain benefits as they can probe the movement of water, which can avoid the problems of interficial and boundary conditions. They consider the size

and shape of molecules into account in order to understand the diffusion process and estimate the values [Perrin et al., 2016, Klein et al., 2013,].

2.2.3 Mass uptake measurements

Mass uptake measurement takes place as a function of time. In order to determine the water diffusivity, rate constant is multiplied by square of characteristic dimension of the given polymer. Water sorption is governed by Fickian diffusion or Non Fickian diffusion. If controlled by Fickian, the sorption water diffusivity (D_{sorp}) can be given by equation 2.5 and 2.6

$$D_{sorption} = k_{absorption} \times (Lm)^2 \tag{2.5}$$

And similarly, for desorption it can be given as

$$D_{dsorp} = k_{desorption} \times (Lm)^2 \tag{2.6}$$

As can be seen in above equations, rate constant holds the key to determine the diffusivity for both the process. Out of all the experiments carried out, diffusion coefficient found by NMR experiments (10^{-5} cm^2/s) have the highest values, followed by permeation measurements and the least are with water uptake and water desorption measurements (up-to 10^{-7} cm^2/s) [Hietala et al., 2000, Majsztrik et al., 2007, Suresh et al., 2006, Tsushima et al., 2005, Zawodzinski Jr et al., 1991, Verhagen et al., 2019,]

2.2.4 Water balance measurements

Up to now, the methods described require a different setup in order to estimate diffusion. Water balance method, use the same fuel cell setup in order to calculate diffusion coefficient and is not much used technique [Thomas et al., 2012, Zaffou et al., 2006] . The idea involves working on same fuel cell setup and utilising condensing tubes (for water condensation) with weight balance (to measure exit water flux). With time, the water collected at the exit of cathode and anode section is then used to calculate the diffusion occurring through the membrane. For the scope of this research water balance method is employed to measure the diffusion coefficient and is restricted to membrane with effect on various parameters such as relative humidity gradient and temperature.

2.3 Diffusion coefficient estimated through membranes

2.3.1 Nafion membranes

Importance of calculation of diffusion coefficient by water balance method is important because of varsity of values in literature. A wide range of values for diffusion coefficient is the output of research from the several years ranging from (10^{-9} to 10^{-5}) cm^2/s as evident by [Kusoglu and Weber, 2017,] (Figure 2.5). Not all the approaches are specifically targeted to understand diffusion in PEMFC and thus there is a dynamic range of values. There are many reasons which can explain this

variation however few of them is discussed here. Firstly, ex -situ and in -situ approach, secondly most of the data published rely on industrial data for estimation of equivalent weight and density of membrane or literature review to estimate the value of λ at each side of the membrane by sorption curve. Thirdly and most important is different experimental setups and objectives. Moreover, diffusion of water plays a very important role for understanding and initialization for computational models related to fuel cell. [Majsztrik et al., 2007,] gave a good description of diffusivity by various methods and used Nafion® 112, 115, 1110 and 1123 and examined them experimentally in temperature controlled stainless container. According to results, water desorption measurements give intermediate diffusion coefficients. Neutron magnetic resonance (NMR) self-diffusion measurements give the highest value of diffusivity[Meresi et al., 1998, Tsushima et al., 2005,] in range of (10^{-5} - 10^{-6}) cm^2 /s , on the other hand permeation measurements [Villaluenga et al., 2006, Ye and LeVan, 2003,] gave diffusivity values in range of 10^{-7} cm^2/s slightly lower than NMR self-diffusion measurements.

Water distribution can help to explain the diffusion process. Efforts are put to understand time resolved water distribution inside and outside the membrane [Martinez et al., 2017,] when current load is changed. Results shows response of membrane to change in outside water content is instantaneous, proving existence of complex diphasic flows. Quasi elastic neutron scattering (QENS) [Martinez et al., 2018,] experiments was performed to understand measurement of water dynamics, resulting in diffusion coefficient of D= $0.20 \pm 0.03 \times 10^{-5} cm^2$/s.

In – situ measurement of water was analyzed and measured with other ex-situ measurement. [Peng et al., 2017,] analyzed operando μ - raman spectroscopy to understand water distribution across membrane is produced. Schroeder's paradox is verified by in situ water content measurements. [Zawodzinski Jr et al., 1993,] work has been mainly infield of determination of water diffusion coefficients with diffusivity of $2.5 \times 10^{-6} cm^2$/s at $25°C$. There NMR experiments are carried out using spectrometer and imaging probe. The dependence of self-diffusion coefficient on membrane water content was the central part of his work. In this research, it took into effect of membrane swelling to the equivalent water concentration in the dry membrane and the reported diffusion coefficient included the water concentration in the membrane. Non fickian diffusion of water is also reported by [Hallinan Jr and Elabd, 2009,] in which dynamics of water in Nafion® and is investigated both at low and high humidity with time resolved Fourier transform infrared – attenuated total reflectance (FTIR-ATR) spectroscopy. The test successfully demonstrates the measurement of water diffusion. [Shiau et al., 2017, Kusoglu and Weber, 2017,] also demonstrated water management a serious concern and demonstrated that low performance is mostly caused by non-uniform distribution of water and how this can affect the diffusion coefficient. [Ge et al., 2005,] highlighted transport mechanism considering the absorption, water transport and desorption of water diffusion coefficient considering the interfacial resistance into account. Interfacial mass transfer coefficient for absorption of water is equal to 3.53×10^{-5} fv m /s and that of desorption was 1.42×10^{-4}fv m/s. In this a pseudo 2D model is presented and it is explained how mass transfer coefficient for water desorption and absorption were dependent on water content of membrane.

Diffusion coefficient is not only limited to PEMFC but different other techniques and areas are also explored to understand it. [Schoo and Knoll, 2015,] presented a

new electrochemical method for measuring diffusion coefficient, permeability coefficient which is based on electrical conductivity of an electrolyte layer, which depends on water content inside the layer. Measurement of diffusion coefficient is also applied in areas to monitor chemicals in water, as [Verhagen et al., 2019,] estimated the values for calibration parameters for passive sampling of organic UV filters. [Kravanja et al., 2018,] used pendant drop tensiometry to understand diffusion coefficient in binary systems. Measuring of diffusion coefficient is also applied in areas of degradation for example [Kessentini et al., 2019,] used gravimetric and hygroscopic method to understand degradation behavior of conveyor belts, to investigate water ingression behavior in a composite polyester/ polyamide textile reinforced conveyor belt.

2.3.2 Anion membranes

Alkaline anion exchange membrane fuel cell has gained more attention, they have been widely used before 1980's but after introduction of Nafion® saw a reduction in utility. Many tests related to polarization, diffusion, water permeation have been used to understand the behaviour of anion exchange membranes. [Luo et al., 2018,] gave results related to water permeation behaviour of anion exchange membrane fuel cell and gave interesting results related to internal and interficial water permeation resistances.[Lee et al., 2020,] developed a dual exchange membrane fuel cell for non-humidified condition.[Eriksson et al., 2019,] studied water transport in Tokuyama A201 membrane using humidity sensors at inlet and outlet of both sides of MEA. Results related to water fluxes were presented for both vapour and liquid phase.[Saebea et al., 2019,] did a model-based study to evaluate the alkaline anion exchange membrane fuel cell with water management. The cell performance at unbalanced pressure operation is analysed, as thin membrane and unbalanced pressure operation are preferred to facilitate water transport. Water balance method is a comparatively fast method to find the effective diffusion coefficient and it was important to check the performance of diffusion results with other commercial membranes. In the work, water balance method is used to test diffusion due to Anion membranes and the results of diffusion are almost same compared to Nafion® membranes. [Li et al., 2010,] has found the similar behavior and they report almost similar diffusivity of Anion and Nafion® membranes.

The objective of this research is to use a method which is easier to set up, can generate results of diffusion values with respect to the conditions needed. As seen from the Figure 2.5 there can be many wide range of values depending upon the aim of the researcher. Water balance method used is a different approach as it uses same fuel cell setup and the results obtained can be directly used. In the next domain of this chapter water balance method is explained , procedure and results related to diffusion are analysed.

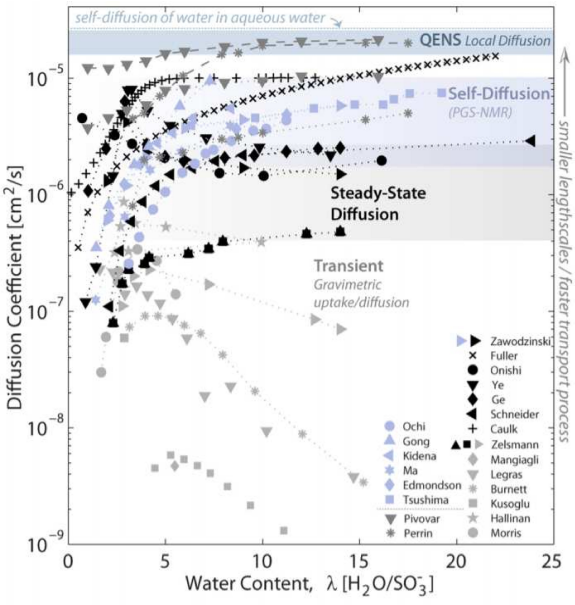

Figure 2.5: Water diffusion in Nafion membranes adopted from [Kusoglu and Weber, 2017,]

2.4 Water balance test bench

Water balance method has been discussed in section 2.2.4. Now in subsequent section, more details considering the experimental setup, the experimental conditions and methodology will be discussed. The main idea to used water balance method is to calculate N_m which can later be used to calculate water diffusion coefficient.

2.4.1 Experimental setup

Figure 2.6 shows the schematic representation of experimental setup in order to calculate the effective water diffusion coefficient. The method used is based on water balance measurements obtained by collection of water at outlets. Air is used as a medium to calculate the effective water diffusion coefficient. Mass flow meters, by Brooks instruments® is used in order to supply air from the flow meters to mass flow controller (Figure 2.7). A mass flow controller is used in order to supply the air at desired flow rate. Borosilicate glass tubes figure (2.12) is used to condense the water. In order to measure the condensed liquid two separate mass balance, manufactured by Kern® is used. They are sensitive to measure smaller changes in mass. When the air is passed through humidifier to cell the entire path between humidifier and cell is heated at temperature of 70° C (preheated) to avoid condensation in the connections connecting various devices.

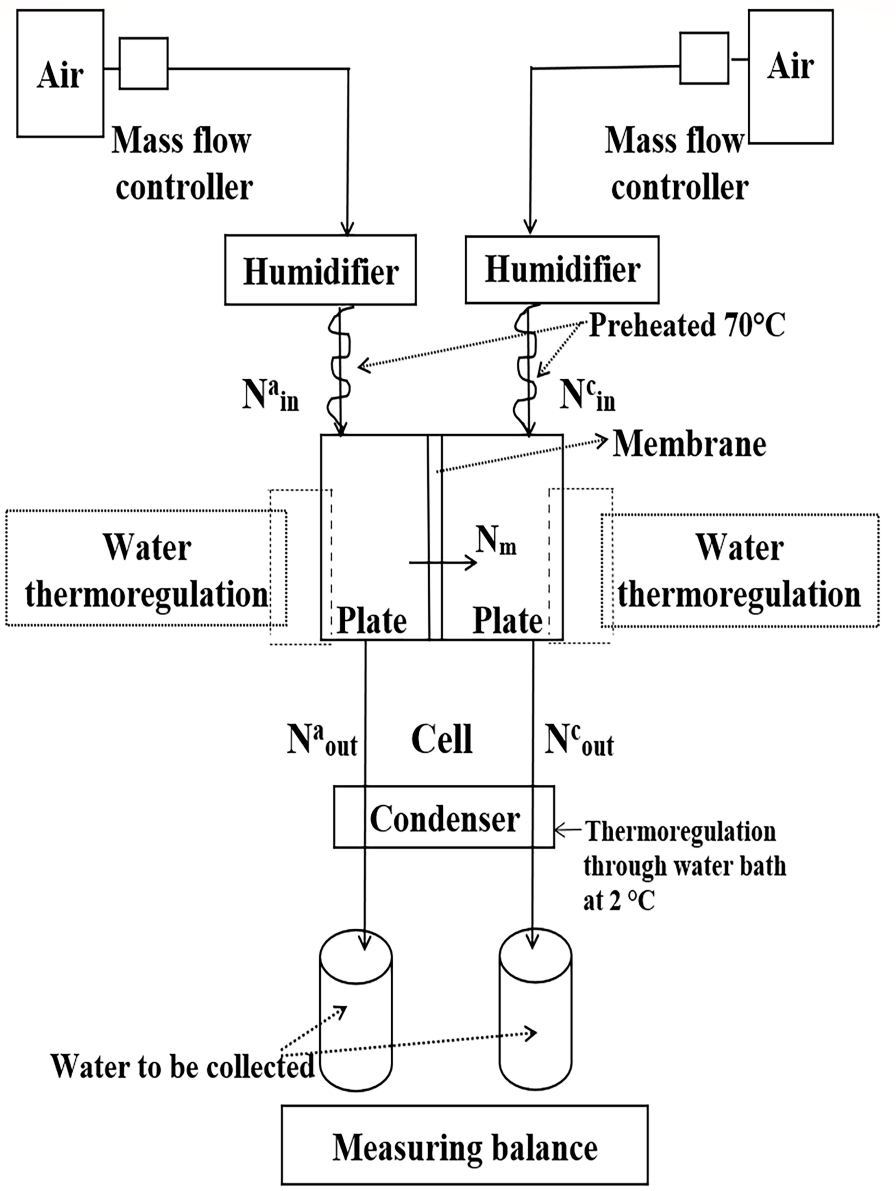

Figure 2.6: Fuel cell setup

Figure 2.8, presents humidifier controller used, in order to maintain the temperature as required. Humidifiers (Figure (2.9a, 2.9b) are used in order to heat the air flowing into the cell, in order to maintain the relative humidity, connected to humidifier temperature controllers. Material used for the bipolar plates is graphite and is assembled using two brass plates in order to clamp the system. Special aluminium blocks Figure (2.10) are attached to the end of brass plates which maintains the temperature on both the sides of the graphite plates and hence two seperate water thermo regulation is used for this purpose.

2.4.2 Experimental conditions

Fuel cell is maintained at temperature of 60°C or 70°C throughout the calculations. In order to change the relative humidity, the temperature of humidifiers is changed and relative humidity is varied from $(20 - 100)\%$. A thermal cooler is used

Figure 2.7: Mass flow controller

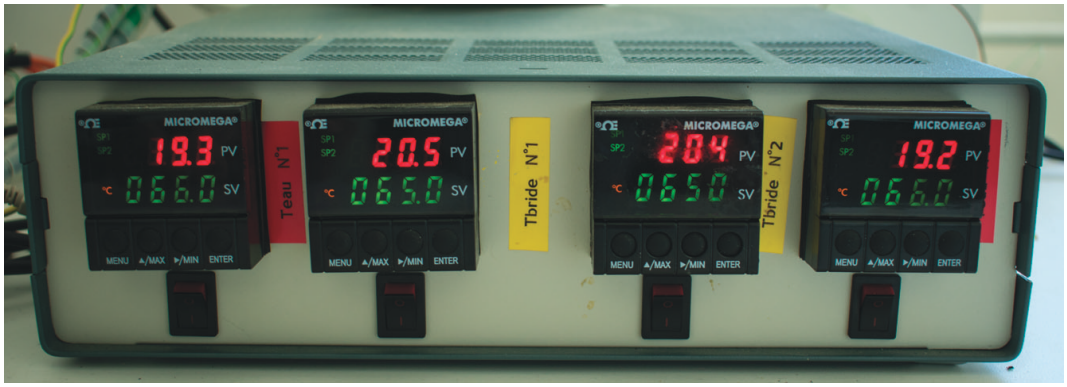

Figure 2.8: Humidifier temperature controller

to maintain the temperature at 2°C in order to condense air in condensing spiral tubes. For the experiments, membrane used is NRE-211(thickness - 29μm) provided by *Ionpower*@ and Anion membrane provided by *Tokuyama*@ A-201.

2.4.3 Experimental methodology

Effective steady state water diffusion coefficient measurements with water balance method are carried out by using the Nafion® membrane NRE 211 (29μmthick) with or without GDL, sandwiched between two graphite plates (Geometry type – serpentine). Before start of any experiment-humidified air is passed through the membrane for 2 hours to make sure, it is fully saturated. It is presented by [Didierjean et al., 2015,] by using Neutron magnetic resonance (NMR) experiments to measure the time required for the membrane to get humidified. For thickness of 50μm it requires up to 2 hours to attain a relative humidity of 86 %. Since our membrane has a thickness of 29 μm so 2 hours is sufficient to humidify the entire membrane. Gas used to carry out the experiments is air and the flow rate is set to 310 ml / min. For each side, lower value of flow rate is preferred because at higher values gas was not getting fully humidified resulting in less weight collection at the mass balance. Two separate humidifiers on each side are used to humidify the air passing and the aim is to see what effect gradient of relative humidity has on the diffusion rate.

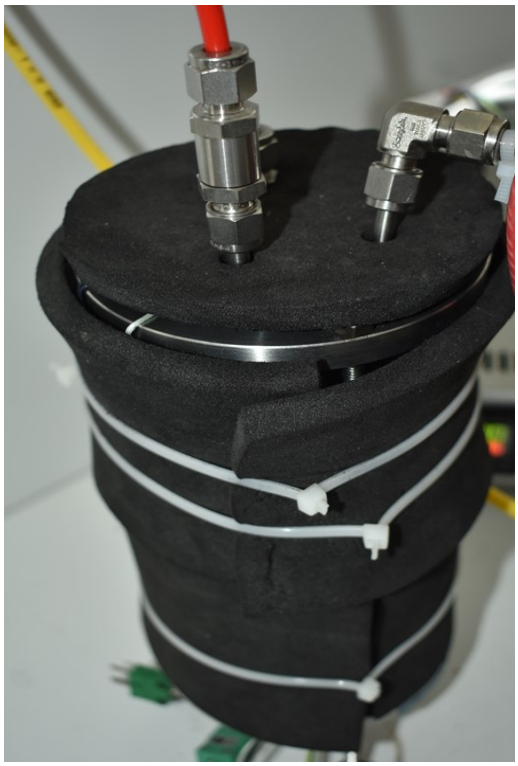

(a) Anode side humidifier

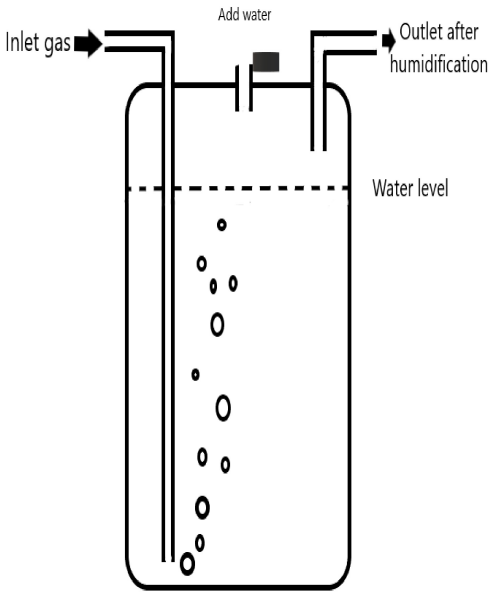

(b) Schema of humidifier

Figure 2.9: Humidifier

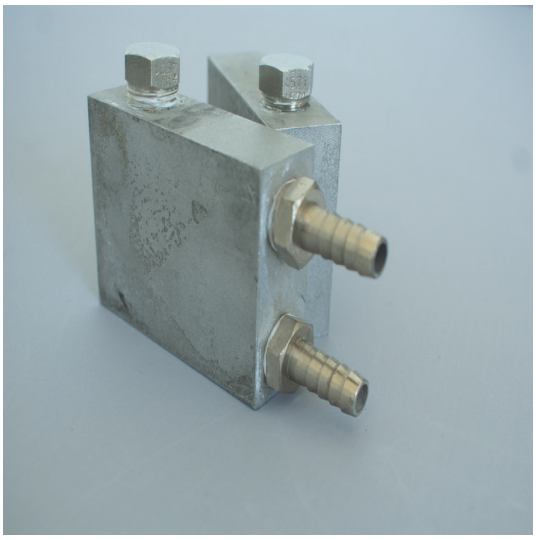

Figure 2.10: water blocks

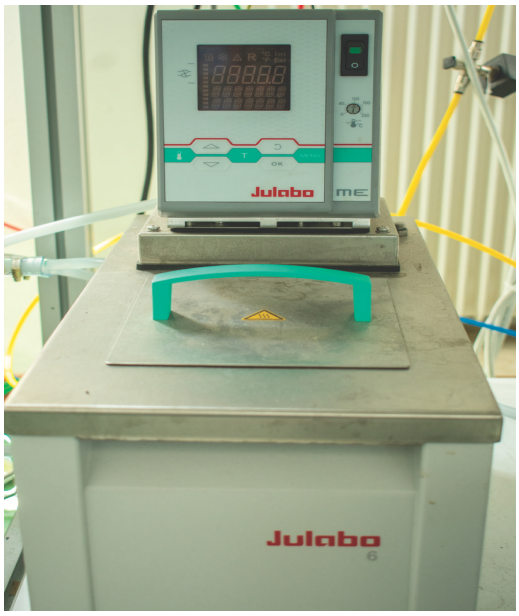

(a) Water temperature regulators

(b) Water temperature regulators

Figure 2.11: Water regulators used in experiment

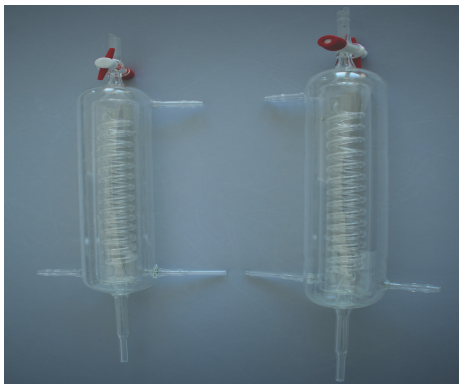

(a) Condensing tube 1

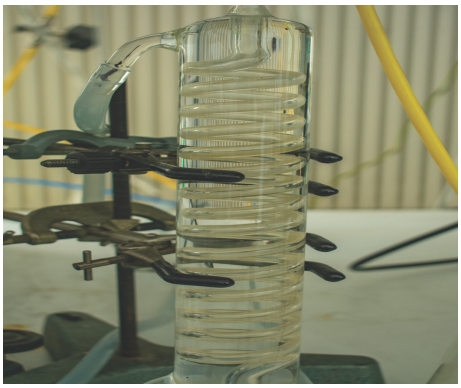

(b) Condensing tube under setup

Figure 2.12: Condensing tubes used in water balance setup

2.5 Calculations

In the following text, calculations with respect to vapour pressure of water and redistribution of water flux through membrane will be discussed.

2.5.1 Vapor pressure calculations

The vapor pressure of water is the pressure at which water vapor is in the state of thermodynamic equilibrium with its condensed state and hence it is very important property in order to understand the physics involved for water balance method. The simplest equation is the Clausius- Clapeyron [Piringer, 2020,] equation with assumption of constant molar enthalpy of vaporization. It is not accurate for general applications and hence various other correlations has been proposed to understand with different empirical constants based upon certain set of experiments.

1. Antoine formula-

   In order to calculate vapor pressure over a wide range of temperature one of the widely used correlation is Antoine equation [Piringer, 2020,] ,given by $\log(P_{vp}) = A - B/(T + C)$ which uses three empirical constants. This correlation is more accurate at higher temperatures but perform poorly at freezing temperatures above 0°C.

2. Magnus formula-

$$P = 0.61094(e^{17.625\times T})/(T + 243.03) \tag{2.7}$$

   [Alduchov and Eskridge, 1996,] described algorithms based on Magnus's form equation to minimize the difference between several relationship between temperature and water pressure at saturation.

3. Teten formula-

   Teten's formula is another such method to calculate the saturation vapor pressure given by

$$P_s = 0.611(e^{17.27\times T}/(T + 273)) \tag{2.8}$$

4. Buck's equation

$$P_s = 0.61121(e^{18.67-(T/234.5)}/(257.4 + T))), if T > 0°Celsius. \tag{2.9}$$

   [Junzeng et al., 2012] evaluated saturation vapor pressure by different formula and found Buck formula result in acceptable saturation vapour pressure under all temperature conditions from $-50°C$to $+50°C$, on the other hand Teten formula shows an increase of error as calculated when the temperature is below $0°C$.

5. Rankine's formula

   Rankine's formula can also be used in order to calculate the saturation vapor pressure as used by [Thomas et al., 2012] given by equation , where T is the temperature for which P_{sat} is to be calculated and it is the temperature of fuel cell. Similarly, to calculate the P_{sat} of humidifier it is obtained from equation 2.11, fixing the relative humidity.

$$P_{sat} = P_{atm} \times \exp\left\{(13.669 - \left(\frac{5096.23}{T}\right))\right\} \tag{2.10}$$

   Rankine formula provides more flexibility over calculations. Antoine formula suffers from many constants. It requires the use of A, B and C in order to calculate and hence is prone to more errors. Buck'a formula has temperature limiting conditions from $-50°C$to $+50°C$ and Teten formula shows error while calculations below $0°C$. The experiments deal with relative humidity variation so it was ensured to maintain a right amount of relative humidity, analytical expression for the same is given below $0°C$.

$$RH = \frac{P_{sat}\,(Humidifier)}{P_{sat}\,(Cell)} \tag{2.11}$$

In all the experiments carried out the cell is at fixed temperature, which means relative humidity was maintained by changing the temperature of water within humidifiers where air flow through. Vice versa is also possible and it makes no difference in the calculations.

2.5.2 Water fluxes calculations

The water molar rates fed to the cell n^a_{in} and n^c_{in} can be calculated by the humidifier temperatures T_{ha} and T_{hc}. In order to make sure that gases are fully saturated at exit of humidifier, lower flow rate of the incoming gas in humidifier was used and with water balance the inlet and outlet was measured accordingly.

$$n^a_{in} = n^{air}_{in} \times \frac{RH_a \times P_{sat}\,(T_{ha})}{(P - RH_a \times P_{sat}\,(T_{ha})} \tag{2.12}$$

where,

$$n^{air}_{in} = 310\ ml/min = \ 9.25 \times 10^{-4}\ \ mol/s \tag{2.13}$$

This flow rate was in accordance with the flow rate which would have been here if there was a current density of $0.5A/cm^2$ used in fuel cell experiments.

Similarly, for cathode

$$n^c_{in} = n^{air}_{in} \times \frac{RH_c \times P_{sat}\,(T_{hc})}{(P - RH_c \times P_{sat}\,(T_{hc})} \tag{2.14}$$

$$n^{air}_{in} = 310\ ml/min = 9.25 \times 10^{-4} mol/s \tag{2.15}$$

Water molar rate at the outlet can be obtained via two balance by weighing the mass of water condensed and collected at the outlet, divided by time and water molar mass equation 2.16 and 2.17.

At anode

$$n^a_{out} = \frac{(Wt\ of\ water\ collected\ by\ time\ (g)\ )}{\Delta \mathrm{t} \times (M_{H2O})} \tag{2.16}$$

$$n^c_{out} = \frac{(Wt\ of\ water\ collected\ by\ time\ (g)\ )}{\Delta \mathrm{t} \times (M_{H2O})} \tag{2.17}$$

The water molar flux through the membrane n_m is obtained by making a balance between water flow rate at the inlet and outlet on each side corrected of losses ,

At anode

$$n^a_{in} \ - \ n^a_{out} - \ n^a_{in_{leak}out} - \ n^a_{out_{condense}} = n_m \tag{2.18}$$

At cathode

$$n^c_{in} \ - \ n^c_{out} - \ n^c_{in_{leak}out} - \ n^c_{out_{condense}} = -n_m \tag{2.19}$$

Both equation 2.18 and 2.19 are used for the calculations. Consider equation 2.18, the humidified air is prone to two losses which are condensation and leak and this effect is taken into consideration. Equation 2.19 can be used in a similar way but the sign of flux through membrane is reversed. In this convention, the water flux through the membrane is account positive from anode to cathode.

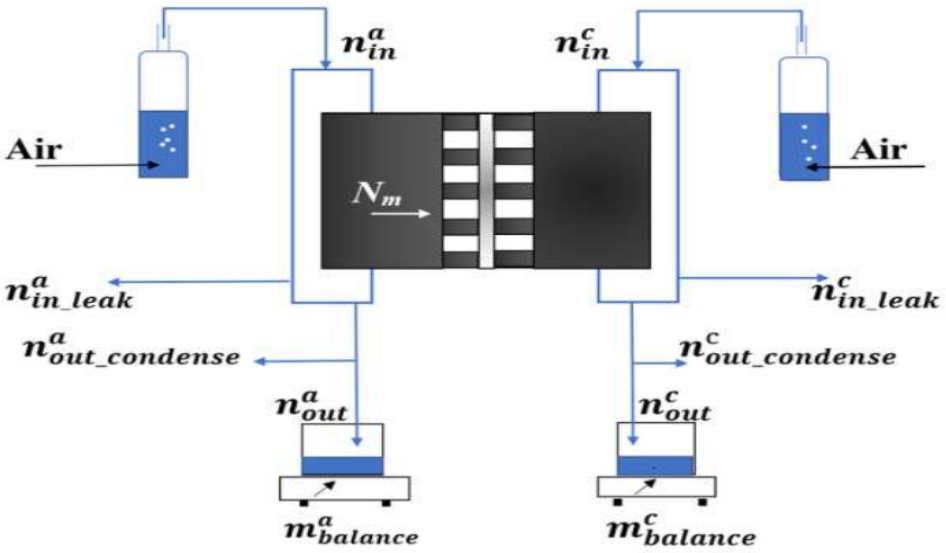

Figure 2.13: Experimental setup with losses

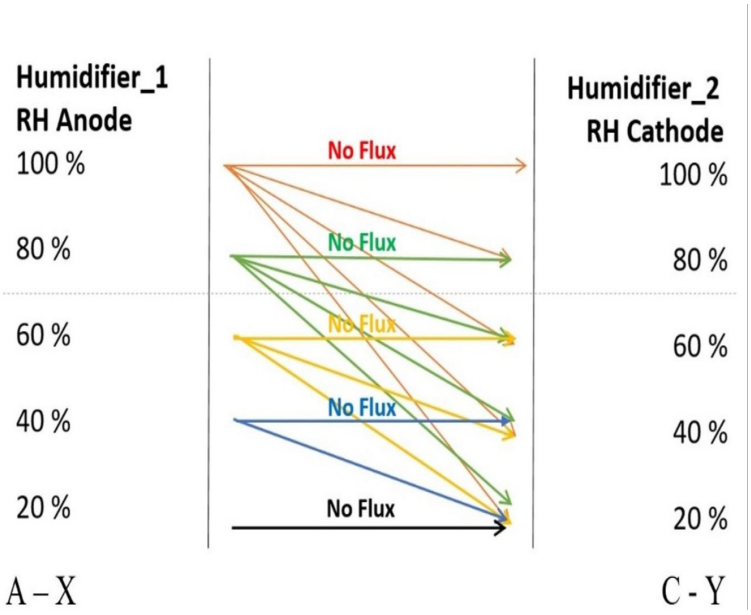

Figure 2.14: Relative humidity cases

2.6 Imposing gradient of relative humidity

Several experiments with relative humidity gradient are performed, fixed at a particular cell temperature and are presented here. Figure 2.14 explains the respective humidity at cathode and at anode. A-X means anode – relative humidity, where X = 100, 80, 60, 40, 20, similarly, C-Y means cathode – relative humidity where Y = 100, 80, 60, 40, 20. Cases of (A-X, C-Y) are discussed here. For an example (A-20, C-80) means the anode section is maintained at relative humidity of 20% and the cathode section is maintained at 80%. Figure 2.14 explains the number of cases possible for example, lines generating from anode at 100% to cathode (100, 80, 60, 40, and 20) are for cases where anode is fixed to 100% relative humidity and at the

cathode side relative humidity is varied. Lines generating from anode at 40% to cathode (40 and 20), where cathode side relative humidity can have only two cases possible, first with 40% on each side to verify there is no flux and second at 20% relative humidity.

Considering the case at anode with 100% relative humidity and at cathode 80% there will be a concentration gradient established, due to which there would be a flow from anode to cathode. Similarly, for the opposite case there will be a flow from cathode to anode. Now the excess flow of humidified air in anode will be diffused only by diffusion to cathode side through the membrane in order to redistribute. This is N_m. This flux plays a very important role and hence this value is used to calculate diffusion coefficient in the membrane.

2.7 Error's estimation

Water balance method is a very sensitive method as the flux value obtained depends upon the water condensed and hence accuracy lies in measuring accurately the droplet formed which can then have results that are more appropriate. There are several factors which can contribute to error for example the sensitivity of mass balance used, the outside conditions of temperature, the slip angle on boro-silicate glass tube to allow the condense water to move down, leakage of air passing through the connections, pre condensation. For most of the cases, appropriate steps are taken to avoid any such error but there are three types of error which is considered in experiment of water balance measurement which are freezing losses, gas leak and evaporative losses.

In order to check if water balance method works correctly, initial experiments are carried out with same relative humidity on both the sides of fuel cell setup, in this case it was ensured no flux is passing through membrane as both sides of membrane are maintained on same concentration. Results will be shown in Table 2.1. Anode and cathode are used in general (representation) to represent the two sides of cell.

2.7.1 Gas leaks

There is always possibility of gas leak from the system and it can be due to many connections being assembled together, leaks from fuel cell or leaks from condenser, which is used to cool the humidified air passing. Table 2.2 presents the total losses in the system, which is obtained by averaging the error produced over 5-hour duration. Since the anode and cathode side are on the same side of relative humidity so the net flux passing is zero and hence, we obtain the losses. Losses due to the liquid not able to condense are calculated and in equation 2.20. Considering overall losses, we take an average of 15% of error into our calculations which is added in Table 2.3 .

2.7.2 Freezing losses

Freezing losses mainly occur when it is difficult to condense entire humidified air passing after exit from outlet of cathode and anode section to condensing tubes. In our case, the cold water for condensation of humidified air is set to 2° C so it is possible that a very small amount of gas goes without condensation, which is defined

by an expression. T_{co} is temperature of condenser at 2°C. Losses due to non-freezing (condensed) water are shown in Table 2.2 and compared to leak losses.

$$n^{a}_{out_{condense}} = n^{air}_{in} \times \frac{RH_a \times P_{sat} \times (T_{co})}{(P - RH_a \times P_{sat} \times (T_{co}))} \tag{2.20}$$

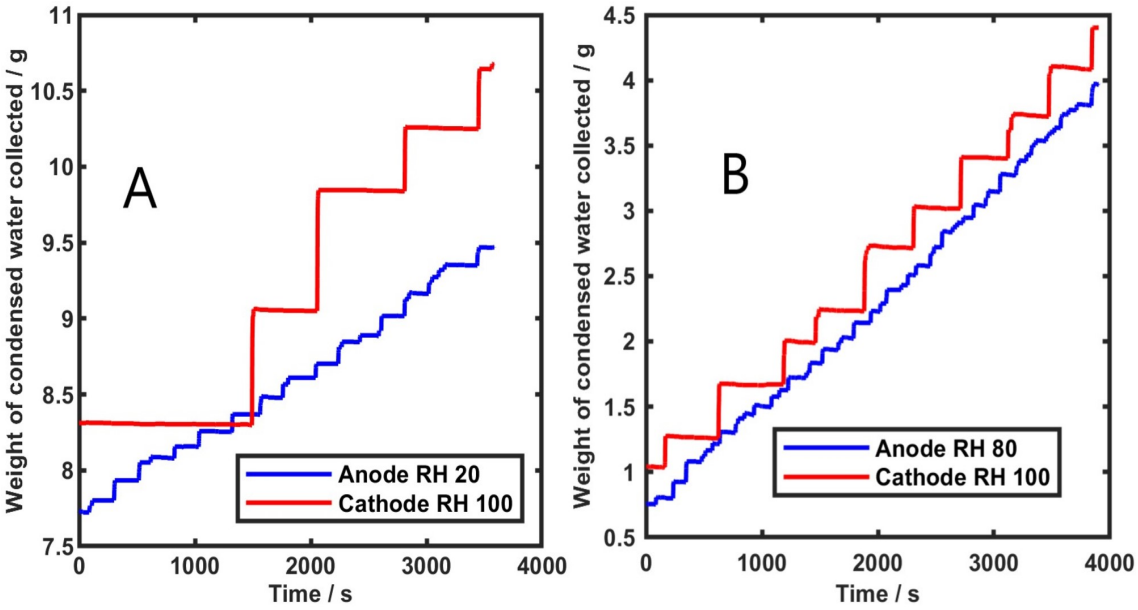

Figure 2.15: Figure (12-a) Relative humidity case of A-80, C-100 Figure (12-b) Relative humidity cases of A -20, C -100

2.7.3 Evaporative losses

These losses are dominant when the outside conditions of atmosphere are more humid and at high temperature. In our case as it can be seen that in Figure 2.15 there is no negative slope in the system or any trend of slope of weight of water condensed going down so there is no leak due to evaporation in the system.

2.8 Interfacial resistance

In order to understand diffusion process, interfacial resistance can play an important role. Biot number can be a useful tool to understand weather considering interfacial resistance is important or not, which is defined by ratio of characteristic time for bulk diffusion of water to mass transport through the membrane surface [Kusoglu and Weber, 2017,]. Biot number is defined as

$$Bi = (k_m \times L)/D \tag{2.21}$$

Where k_m is the mass transfer coefficient, L is the normalized distance in thickness direction and D represent the diffusion. [Didierjean et al., 2015,] gave result related to effective mass transfer coefficient (cm /s) with respect to the relative humidity and temperature and also explain the absorption and desorption of the water

Time sample-RH	Wt inlet anode (g)	Wt inlet Cathode (g)	Wt outlet anode (g)	Wt outlet cathode (g)	Loss in g (Inlet outlet) anode	Loss in g (Inlet - outlet) cathode	Loss in water molar flux (Inlet -outlet) anode (mol /s)	Loss in water molar flux (Inlet -outlet) cathode (mol /s)	Percentage error averaged over 5 hours
A20%-C20%	0.61	0.61	0.60	0.50	0.01	0.10	3.85×10^{-8}	1.62×10^{-6}	Anode-3% Cathode-17%
A40%-C40%	1.26	1.26	1.05	1.02	0.20	0.23	3.21×10^{-6}	3.58×10^{-6}	Anode-16% Cathode-20%
A60%-C60%	1.97	1.97	1.76	1.69	0.20	0.27	3.20×10^{-6}	4.25×10^{-6}	Anode-11% Cathode-14%
A80%-C80%	2.76	2.76	2.40	2.31	0.35	0.44	5.49×10^{-6}	6.88×10^{-6}	Anode-13% Cathode-16%
A100%-C100%	3.66	3.66	3.03	3.03	0.63	0.63	9.79×10^{-6}	9.72×10^{-6}	Anode-16% Cathode-16%

Table 2.1: Total losses during the experiments

Relative humidity	Total losses (anode) (g)	Total losses (cathode) (g)	Anode freezing losses (g)	Cathode freezing losses (g)	Losses due to leak in anode (g)	Losses due to leak at cathode (g)
A20%-C20%	0.01	0.10	0.02	0.02	0.0	0.08
A40%-C40%	0.20	0.23	0.04	0.04	0.16	0.19
A60%-C60%	0.20	0.27	0.07	0.07	0.13	0.20
A80%-C80%	0.35	0.44	0.09	0.09	0.26	0.35
A100%-C100%	0.63	0.63	0.11	0.11	0.52	0.52

Table 2.2: Losses separated from total losses - freezing and leak during the experiments

content in membrane. Most of the results lies in this range of $1.25 \times 10^{-4}(cm/s)$ to $35.3 \times 10^{-4}(cm/s)$ [Ge et al., 2005, Okada, 1999,]

An average value of mass transport coefficient 4.0×10^{-4}cm /s is used in calculations with L = 29 μm and $D = 1.16 \times 10^{-7} cm^2/s$(this value is calculated from this experiments and are reported in Table 2.3 for case of 70 °C. Biot number calculated is 10.24 and hence the hypothesis in our calculations is that mostly the effective diffusion coefficient is measured and interficial resistance can be neglected.

2.9 Results and discussion for Nafion-211 effective diffusion coefficient

In this section, results related for variation of diffusion coefficient on relative humidity difference and temperature are discussed. Water content λ is defined as the number of water molecules to number of sulphonic sites present. It is an important parameter, which brings into effect the degree of humidification in the fuel cell and hence sorption behaviour becomes more important as they can redefine overall transport and structural properties. Figure 2.16 shows the membrane water content λ as a function of relative humidity. It provides data on water uptake of Nafion® membranes (replot sorption curve from [Maldonado et al., 2012,]). [Maldonado et al., 2012,]) gave results regarding the pre-treatment of membrane and present the influence of drying temperature on sorption isotherm on Nafion® in range of $30°C < T < 80°C$. The λ_{sat} value change greatly based upon the pre drying conditions.

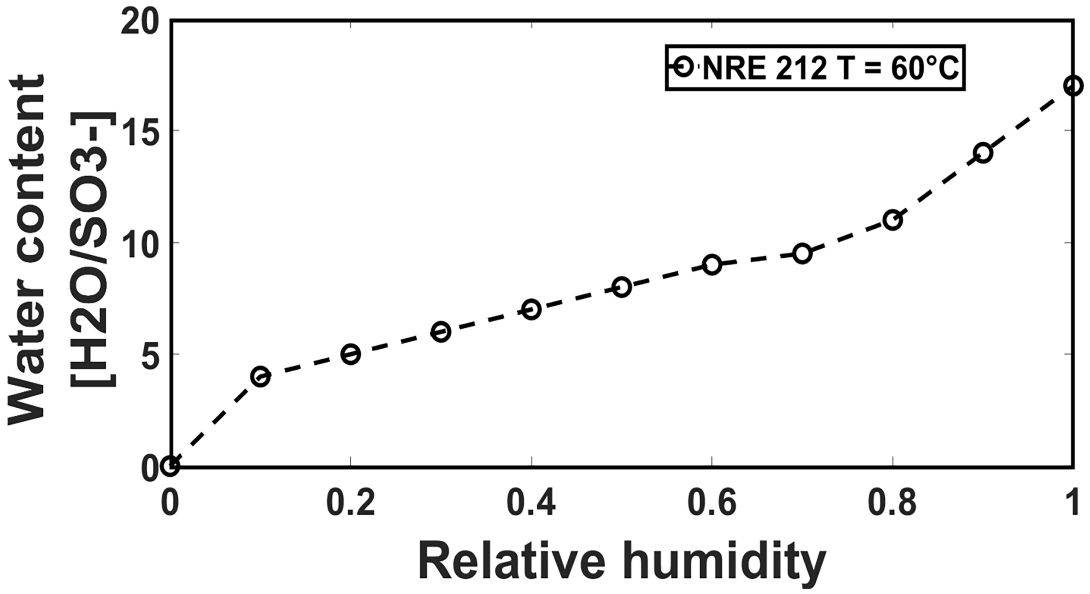

Figure 2.16: Absorption curve Nafion® NRE 212 at T= 60°C, replot [Maldonado et al., 2012,]

A well-known expression given by [Springer et al., 1991] which takes into the effect of density, equivalent weight, flux, absorption is depicted in equation 2.22 which gives a relation to connect flux through membrane with diffusion coefficient.

$$N_m = \frac{\rho}{EW} \times D_\lambda \times \frac{\Delta\lambda}{e_m} \tag{2.22}$$

It is seen that N_m depends on 5 factors ρ, EW, D_λ, $\Delta\lambda$ and e_m. In our experiments N_m will be measured and D_λ is calculated. For $\Delta\lambda = \lambda_a – \lambda_c$ sorption curve is used from Figure 2.16. In reality the thickness of membrane is dependent of relative humidity and temperature $e_m(RH, T)$ and this, can affect the results of diffusion to great extent where both swelling and shrinking of membrane can be affected by aging phenomenon [Naudy et al., 2014,]. Density of membrane changes and if found to have different values at different operating conditions [Zook and Leddy, 1996,] and aging can affect density. Equivalent weight can have a huge impact too on diffusion coefficient [Jalani and Datta, 2005,]. Here value of ρ, EW and e_m is fixed because aim of this research is to present a simple method to deduce D_λ for experimental conditions and to implement into models.The value taken for calculation, for ρ is 1250 kg/m^3 and for EW is 1100 g-polymer molionic /group and e_m is 29μm. It can be noted that water flux density ($mol/m^2/s$) through the membrane is calculated by dividing the measured water flux by water balance by the active diffusion area of cell. To be sure that the entire surface of membrane is involved, measurements with porous transport layer between flow field plate and membrane, have been done and results , in overall, give same values. So, it can be concluded that the total surface of the membrane is involved in the water transport.

$$N_m = \ n_m \times \frac{10^4}{S} \ mol/m^2/s \tag{2.23}$$

For all the calculations 1-D hypothesis is used for the water flux passing to the entire area for distribution. In most of the case this hypothesis is not too strong. The total length of the serpentine is 1250 mm involved in redistribution before the outlet of the cell. It will have an impact on the effective surface of membrane involve in the water transfer that will be smaller if there is an equilibrium before the outlet of the cell. It means that 1D hypothesis underestimated a little bit the values of diffusion coefficient (because the total surface of 25 cm^2 is used (equation 2.23). Especially, for the cases with 20% relative humidity, the 1D hypothesis become less pertinent and it can be extended to 2-D hypothesis. Primary calculations have been made and it is assumed in a first order that 2D effect is taken in our error calculations and results at a relative humidity of 20% are prone to more dissimilarity due to very low amount of water content.

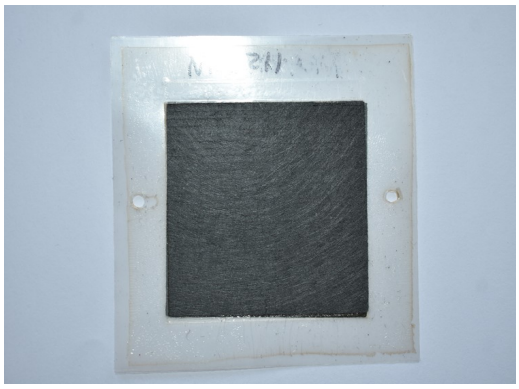

(a) Membrane with GDL

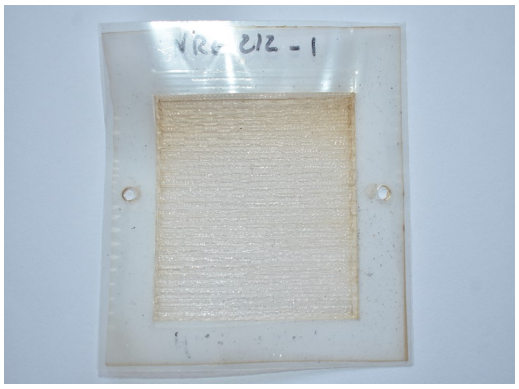

(b) Membrane without GDL

Figure 2.17: Cationic membranes

The error due to $n^a_{in_{leak}}$, $n^a_{out\_condense}$ are considered in final diffusion coefficient as presented in Table 2.3 for the sake of simplicity in calculations. Based on results of Table 2.1, 2.2, a final averaged error limit of 15% is imposed on the final calculated values.

2.9.1 Effect of difference of relative humidity

Anode section and cathode section relative humidity	Cell temperature – 70°C - Diffusion coefficient $(D_\lambda) cm^2/s$	(N_m) $mol/m^2/s$
A20%-C40%	$1.58 \pm 0.40 \times 10^{-7}$	0.0006
A20%-C80%	$2.35 \pm 0.40 \times 10^{-7}$	0.0051
A20%-C100%	$1.60 \pm 0.33 \times 10^{-7}$	0.0081
A40%-C60%	$4.31 \pm 0.71 \times 10^{-7}$	0.0025
A40%-C80%	$1.79 \pm 0.26 \times 10^{-7}$	0.0031
A40%-C100%	$1.26 \pm 0.22 \times 10^{-7}$	0.0059
A60%-C80%	$3.78 \pm 0.64 \times 10^{-7}$	0.0044

Table 2.3: Diffusion coefficient with varying relative humidity

In Table 2.3, for most of the cases an increase in diffusion coefficient is observed with the increase of relative humidity and is in accordance with work of other researchers [Gallagher et al., 2009, Gong et al., 2001, Kidena, 2008, Ochi et al., 2009, Okada, 1999, Zelsmann et al., 1990,]. In some cases, there is a decrease and the reason can be attributed to the error in measurement. For all the cases, the values obtained are in same order of $10^{-7} cm^2/s$ so Table 2.3 provides here a general idea of diffusion coefficient values by water balance method.Figure 2.18 shows

the water flux density evolution with average relative humidity for temperature at 70°C. It can be noticed that water flux density increases with the increase of average relative humidity and at fixed value of average relative humidity water flux density is higher when the difference of relative humidity is higher (due to a higher mass gradient).

Figure (2.19) shows the plot of water membrane diffusion coefficient as calculated with the average water content and the results are in line with the steady state water diffusion coefficient in Nafion® membrane [Kusoglu and Weber, 2017,] work. Values are in the range of steady-state diffusion coefficient between $1 \times 10^{-7} cm^2/s$ and $4 \times 10^{-7} cm^2/s$. The evolution of D_m with λ are seems to follow Hallinan results obtain using time-resolved Fourier transform infrared-attenuated total reflectance spectroscopy [Hallinan Jr and Elabd, 2009,]

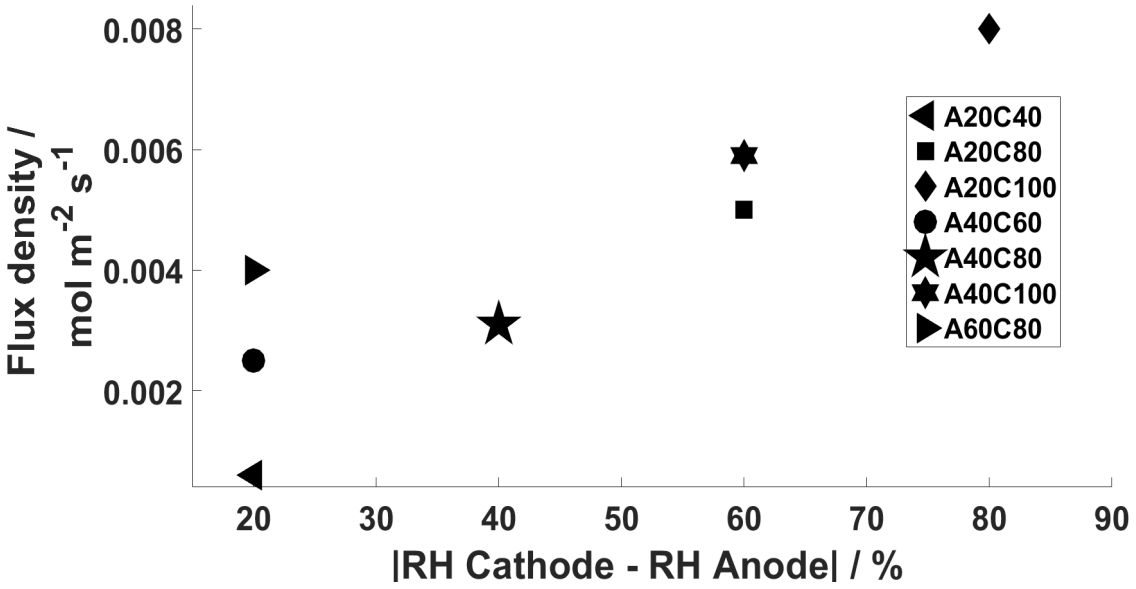

Figure 2.18: Plot of water flux density through the membrane in function of the average relative humidity at 70°C

2.9.2 Effect of temperature on Nafion® 211 membranes

To study the temperature effect, experiments with 60°C and 70°C are conducted, as they have produced faster condensation of water with moderate step size of humidified gas during condensation. Working above 80°C was avoided for safety reasons, similarly working below 60°C was avoided as the condensation of water would be difficult and large step sizes would be produced as shown and explained in Figure 2.15 (a and b).

Table 2.4 presents results for variation of diffusion coefficient at a fuel cell temperature of 60°C and 70°C. Based on the results an increase of diffusion coefficient is observed with increase of temperature [Majsztrik et al., 2007,] found a similar increase in water diffusivity with increase in temperature.

Anode section and cathode section relative humidity	Cell Temperature temperature – 60°C Diffusion diffusion coefficient $(D_\lambda)cm^2/s$	Cell Temperature temperature – 70°C Diffusion diffusion coefficient $(D_\lambda)cm^2/s$
A20%-C40%	$1.42 \pm 0.21 \times 10^{-7}$	$1.58 \pm 0.40 \times 10^{-7}$
A20%-C60%	$1.26 \pm 1.34 \times 10^{-8}$	$3.28 \pm 0.52 \times 10^{-7}$
A20%-C80%	$2.92 \pm 0.43 \times 10^{-7}$	$2.35 \pm 0.40 \times 10^{-7}$
A20%-C100%	$1.37 \pm 0.20 \times 10^{-7}$	$1.60 \pm 0.33 \times 10^{-7}$
A40%-C60%	$9.45 \pm 1.41 \times 10^{-7}$	$4.31 \pm 0.71 \times 10^{-7}$
A40%-C80%	$2.56 \pm 0.38 \times 10^{-7}$	$1.79 \pm 0.26 \times 10^{-7}$
A40%-C100%	$1.17 \pm 0.17 \times 10^{-7}$	$1.26 \pm 0.22 \times 10^{-7}$
A60%-C80%	$1.16 \pm 0.17 \times 10^{-7}$	$3.78 \pm 0.64 \times 10^{-7}$
A80%-C100%	$4.41 \pm 0.73 \times 10^{-8}$	$8.62 \pm 1.24 \times 10^{-8}$

Table 2.4: Comparison of diffusion coefficient based on cell temperature.

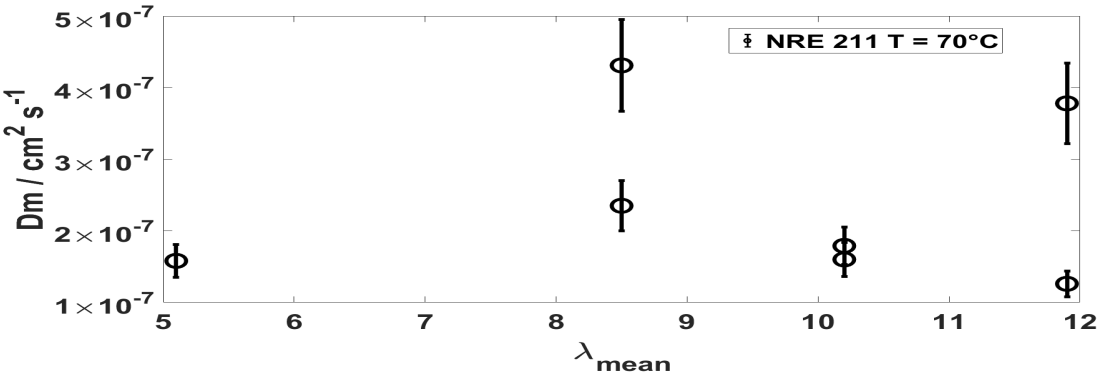

Figure 2.19: Plot of membrane diffusion coefficient with water content and error bar

2.10 Water diffusion coefficient with Anion membrane (Tokuyama A201)

Figure 2.20 represents the water uptake absorption curve as evident from experiments of [Li et al., 2010,] for wide range of temperatures. Table 2.5 presents the diffusion coefficient. For most of the cases, we see an increase of diffusion coefficient values with increase in water content. The values are calculated to get an overall idea of diffusion through Anion membranes and the values lies in range with Nafion® membranes. No further analysis is made for this membrane.

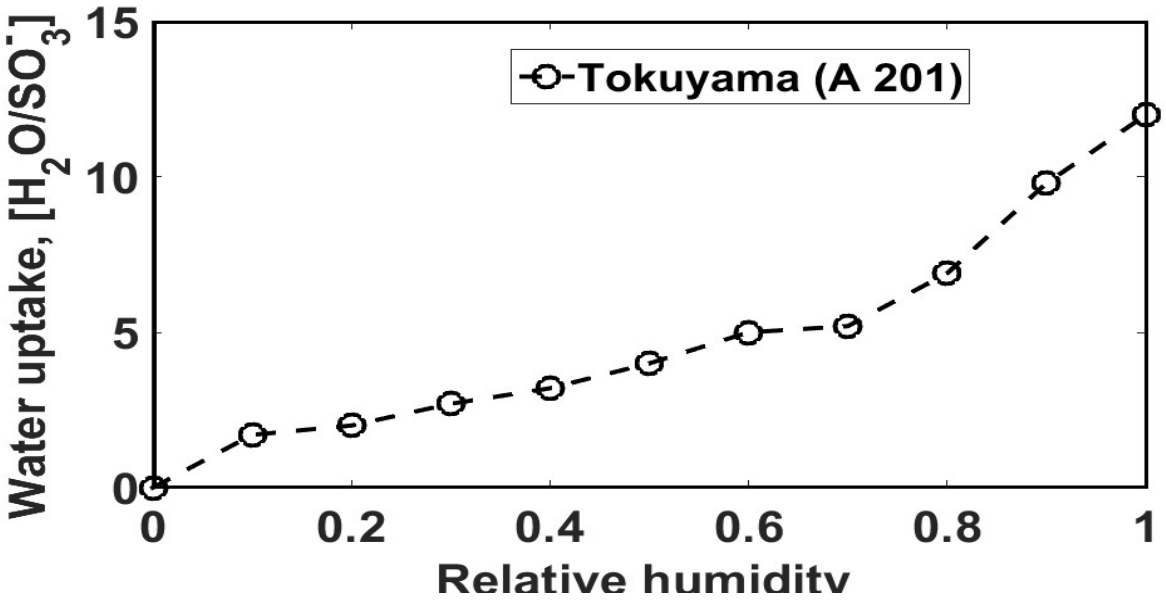

Figure 2.20: Represents the water uptake measurements at 60 °C replot from [Li et al., 2010,], Fig (5)

Relative humidity cases	Diffusion coefficient Anion Tokuyama A201 $D_\lambda(cm^2/s)$
A20%-C40%	$1.63 \pm 0.24 \times 10^{-7}$
A20%-C60%	$6.30 \pm 0.94 \times 10^{-8}$
A20%-C80%	$2.29 \pm 0.34 \times 10^{-7}$
A40%-C100%	$1.17 \pm 0.17 \times 10^{-7}$
A40%-C60%	$7.07 \pm 1.06 \times 10^{-8}$
A60%-C80%	$5.05 \pm 0.75 \times 10^{-7}$

Table 2.5: Results related to Anion membrane diffusion coefficient

2.11 Conclusion with respect to diffusion coefficient for Nafion® and Anion membranes

To sum up the results it can be seen that for the Nafion or Anion diffusion coefficient are in the range of 6×10^{-8} to $5 \times 10^{-7} cm^2/s$. However, in this scope of research, for anion membranes only diffusion coefficient information is mentioned.Considering the results in Table 2.3 and Table 2.5 both the results of water diffusion coefficient are in the same order considering similar thickness, temperature and absorption curves for $\Delta(RH)$. A full detailed comparison of results considering several parameters such as relative humidity, equivalent weight is not possible due to limitations of time of experiments considering Anion membranes.

In the subsequent parts of this chapter diffusion parameter will be further explored based on the water content inside and hence swelling of membrane plays an important role. An relation between Fick's diffusion (D_f) and effective membrane diffusion coefficient D_λ will be explored and how they can be an important factor considering the effect of diffusion will be studied.

2.12 Introduction to D_f and D_λ

After having calculated diffusion by various membranes it is important to understand how the diffusion due to Fick and diffusion considering water effect into account can be important, what are the variations possible? One of the easy way to solve diffusion problems is by Fick's law which assumes flow passing through membrane without considering any swelling of the membrane due to vapor or water. Given by

$$N_m = \left(\frac{D_f}{e_m}\right) \times \ \triangle C \tag{2.24}$$

Where D_f is the diffusion coefficient obtained by Fick's. ΔC is the concentration of humidified gas in the fuel cell which is given by $\frac{P_{sat}}{R \times T} \times RH$. Here it is considered that humidified gases are passing through the membrane and water passes through membrane in form of vapour. e_m is the thickness of membrane used to understand diffusion. N_m is the flux across the membrane as discussed above.

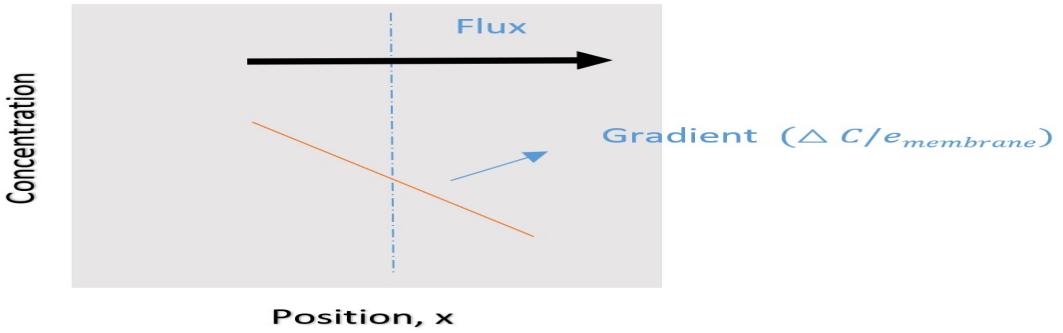

Figure 2.21: Shows a simple case of 1D flow though the membrane, given by Fick's, Governed only by concentration potential

In order to move further, effect of swelling of membrane needs to be evaluated to understand the diffusion coefficient and performance of properties of membrane. Swelling behavior can affect various properties of Nafion® membrane from mechanical to electrical and hence this study becomes imperative to explore.[Gebel et al., 1993, Li et al., 2010,] performed studies related to swelling understanding the solvent, counter ion and temperature effect on membrane. Swelling behavior of PFSA membrane is also attributed to its structure response to hydration effects at multiple length scales which can be varied from nano to meso.[Gebel et al., 1993,] studied the morphology of ionomer resin of Nafion® with wide angle and small angle diffraction. [Elfring and Struchtrup, 2008,] developed a model to understand thermodynamics of pore setting and swelling of Nafion® membrane. Swelling of membrane is also responsible for varied result in the fuel cell as [Zawodzinski Jr et al.,

1991,] gave a numerical formulation of diffusion considering both swelling and non-swelling behavior of the fuel cell. This concept of membrane swelling is beneficial to understand the effect of $\Delta\lambda, \rho_{mem}$ and equivalent weight (EW) of membrane on diffusion coefficient.

Since 1991, when [Zawodzinski Jr et al., 1991,] first published results of the diffusion coefficient taking into the effect of membrane swelling in the model, the equivalent water concentration in dry membrane $\frac{\lambda \times \rho_{dry}}{M_m}$, , to a new coordinate considering the water activity in to account where the final expression was given by equation 2.25. Chemical potential was considered related to water diffusion flux and in turn the logarithmic of activity into account.

$$N_m = \frac{\rho}{EW} \times D_\lambda \times \frac{\Delta\lambda}{e_m} \tag{2.25}$$

Where e_m is the thickness of the membrane and $\Delta\lambda$ is the water content in the membrane.

$$RH = \frac{C}{C_{sat}} \tag{2.26}$$

Where C_{sat} is the concentration at saturated condition in the system. Also,

$$C_{sat} = \frac{P_{sat}}{R \times T} \tag{2.27}$$

Considering equation 2.26 and 2.27 we get

$$C = RH \times \frac{P_{sat}}{RT} \tag{2.28}$$

Where equation 2.28 describes the relation between relative humidity and concentration in system.

If we consider Henry's law for sorption curve from ,

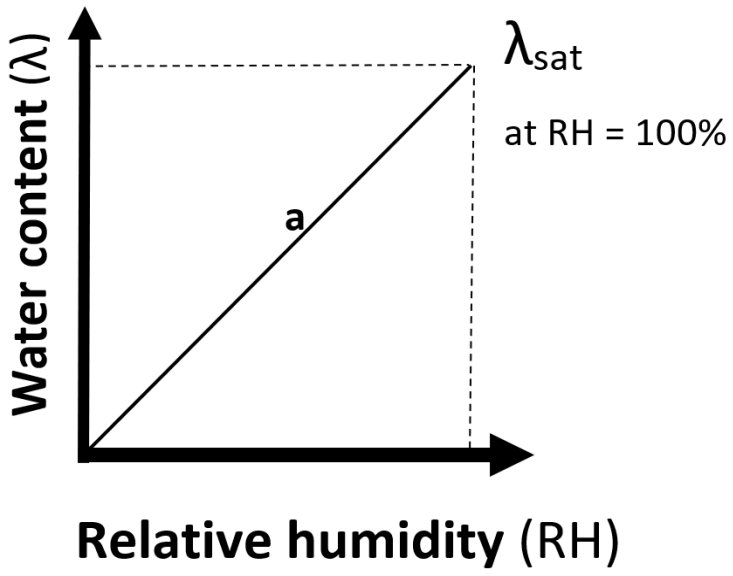

Figure 2.22: Henry's law

$$\lambda = a \times RH \tag{2.29}$$

$$\lambda = \lambda_{sat} \times RH \tag{2.30}$$

$$\Delta\lambda = \lambda_{sat}(\Delta RH) \tag{2.31}$$

Where λ_{sat} is the value at saturated condition for the membrane, C_{sat} is the saturated concentration of water in the membrane and ΔC is the net change in concentration in the system due to change of relative humidity values at both sides of the membrane and this possess a gradient in terms of relative humidity.

$$\Delta C = \frac{\Delta(RH)}{R \times T} \times P \tag{2.32}$$

$$\Delta\lambda = \frac{\lambda_{sat}}{C_{sat}} \times \Delta C \tag{2.33}$$

Considering equation 2.25 and 2.33, the final expression becomes

$$N_m = \frac{\rho}{EW} \times D_\lambda \times \frac{\lambda_{sat} \times \Delta C}{C_{sat} \times e_m} \tag{2.34}$$

If we analyse equation 2.34, the flux N_m depends on density, Equivalent weight and λ_{sat} which can be changed for various conditions. Since then most of the research have the same value of the density, EW and λ, which is not true because the value of density is reported at certain condition and in the actual working condition of the fuel cell the value change continuously. Equivalent weight is varied from chain and the type of condition in fuel cell. λ which is defined as the ratio of number of water molecules to number of sulphonic sites present at saturation has an effect especially with temperature.

2.12.1 Relation between D_f andD_λ

By equation 2.24 and 2.34, we get a relation between D_f and D_λ,

$$D_f = \frac{\rho}{EW} \times D_\lambda \times \frac{\lambda_{sat}}{C_{sat}} \tag{2.35}$$

2.13 Variation of $\Delta\lambda, \rho$ and equivalent weight of membrane on diffusion coefficient.

2.13.1 Density of membrane (ρ)

Variation of density of membranes play a key role in understanding the effect of diffusion. There are many studies performed on Nafion® membranes which are mainly in commercial membranes, film recast from solution at room temperature and annealed recast films which are processed by heat. [Ye and LeVan, 2003, Dorenbos and Suga, 2009,]. Not much extensive work considering the density of membrane is reported in literature. [Zook and Leddy, 1996,] studied density of Nafion® films in water and acetonitrile and the maximum and minimum density was varied from

between $(1.40 \pm 0.15$and $2.03 \pm 0.13)$ kg/m^3. In this research, hydrostatic weighing method was used to understand and find the densities of wetted Nafion® films in water and acetonitrile. The need to understand this is important as density of Nafion® is changed. Density is a direct function of temperature and also relative humidity as the amount of water in the membrane can affect the proton conductivity. In the actual working of fuel cell temperature and density dynamically changes. More over most of the research used standard industrial data of density as reported by industries which can directly change with temperature, water saturation and also the degradation over ageing phenomenon.

2.13.2 Equivalent weight (EW)

Nafion® is a copolymer composed of hydrophobic Teflon ([–$CF2$–$CF2$–]) to which short side chains are attached. Equivalent weight is average distance between the side chains or number of grams of dry polymer per mole SO_3.[Dorenbos and Suga, 2009,] performed dissipative particle dynamics to understand micro phase separation within hydrated Nafion® membranes. There are various preparation methods for membrane to enhance the EW and one such is one-step solvent evaporation method [Joseph et al., 2016,] with EW 1100 using Ortho-dichlorobenzene as porogne. EW is a critical parameter influencing ionomer behaviour and its transport relation thereby maintaining stability and transport. [Kreuer et al., 2008,] compared Dow membranes with different EW and then compared the data to Nafion® and characterised with respect to water sorption, transport (water diffusion, water drag, proton conductivity). [Hensley et al., 2007,] explained the effects of thermal annealing on commercial Nafion®. As depicted by [Maalouf et al., 2009,] the increase in equivalent weight increases the stability and the conductivity decreases. Data regarding the effect of EW and its effect on the change in properties of membrane as reported by [Jalani and Datta, 2005,] is reported in Table 2.6 and shows that EW can change from 750 to 1100 and hence much results are not experimented considering the effect of equivalent weight of Nafion® membranes.

Properties 90°C - 30% RH	EW -750	EW- 950	EW -1100
Degradation	Medium	Highest	Least
Chain type	Shorter side	Long side	Long side
Durability	Medium	Least	Highest
Chemical stability		Least	Highest
Fluoride emission		Highest	Minimum
Water absorption	High		Least
Membrane swelling	Highest		Least

Table 2.6: Effect on equivalent weight on properties

2.13.3 Effect of $\Delta\lambda$

The water content or λ can be defined as the number of water molecule to number of sulphonic sites present, the very first introduced in a paper of [Zawodzinski Jr et al., 1993,]. It is an important parameter, which brings into effect the degree of humidification in the fuel cell and hence sorption behaviour becomes more important as they can redefine overall transport and structural properties. An important phenomenon effecting the overall transport and structural properties is the sorption phenomenon of PFSA ionomers. Figure 2.23 shows the mean of membrane water content λ as a function of water activity measured, provides data on water uptake of Nafion® membranes. This is obtained from chemical review, [Kusoglu and Weber, 2017,] and it has plots from various sources.[Gierke et al., 1981,] studied the effect of water content by small angle X ray measurement.

$$\lambda = \frac{n(H_20)}{N(SO_3)} = \Delta \frac{M_{H_20}}{M_p} \times \frac{EW}{M'_{H_20}} \tag{2.36}$$

where M_{H_20} and $M\prime_{H_20}$ are the mass and molar mass of water (dry polymer).

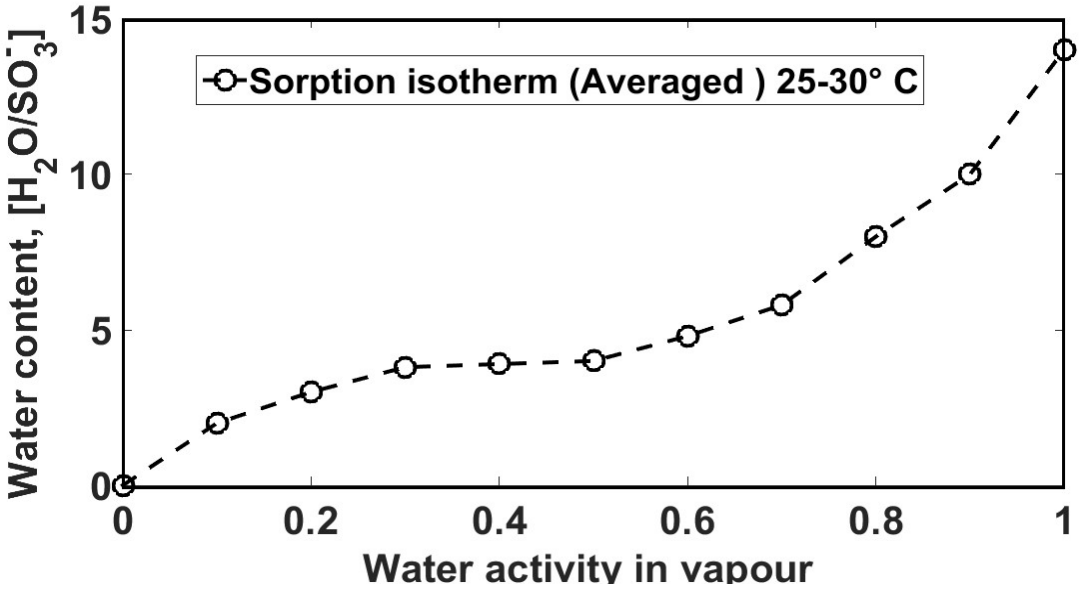

Figure 2.23: Replot [Kusoglu and Weber, 2017,] , Sorption isotherm for Nafion®

2.14 Magnitude of uncertainty of density, EW and $\Delta\lambda$ on calculations

Considering the above three parameters and multi physics involved during fuel cell operation it is observed that (D_λ) can be varied based upon these parameters.

It will be insightful to explore how individual parameter is responsible for the variation in outcome for the diffusion coefficient. Below three cases represent the outcome of diffusion coefficient and shows the variation in the values. All the values of individual parameter have already been discussed under respective topics.

Case 1. ($\Delta\lambda = 4$, EW = 1.1 kg/mol, $\rho = variable$)

$$\rho_{min} = 1250\ kg\ /m^3$$

$$\rho_{max} = 2160\ kg\ /m^3$$

Based in the density variation we obtain a following variation in the product of $(\frac{\rho}{EW} \times \lambda)$

$$(\frac{\rho}{EW} \times \Delta\lambda)_{minimum} = 4545 \tag{2.37}$$

$$(\frac{\rho}{EW} \times \Delta\lambda)_{maximum} = 7854 \tag{2.38}$$

Case 2. ($\Delta\lambda = 4$, EW = variable, $\rho = 1250\ kg/m^3$)

$$EW_{min} = 0.75\ kg\ /mol$$

$$EW_{max} = 1.1\ kg\ /mol$$

Based in the equivalent weight variation we obtain a following variation in the product of $(\frac{\rho}{EW} \times \Delta\lambda)$

$$(\frac{\rho}{EW} \times \Delta\lambda)_{minimum} = 4545 \tag{2.39}$$

$$(\frac{\rho}{EW} \times \Delta\lambda)_{maximum} = 6666 \tag{2.40}$$

Case 3. ($\Delta\lambda = variable$, EW = 1.1 kg/mol, $\rho = 1250\ kg/m^3$)

$$\Delta\lambda_{min} = 1$$

$$\Delta\lambda_{max} = 17$$

Based in the $\Delta\lambda$ variation we obtain a following variation in the product of $(\frac{\rho}{EW} \times \Delta_\lambda)$. In equation 2.41 and 2.42, we report the maximum and minimum value of the factor $\frac{\rho}{EW} \times \Delta_\lambda$. These values reported here is just to explain the variation in diffusion coefficient which is mostly overlooked but if taken into consideration, there can be a 10-15 times change in the results obtained.

$$(\frac{\rho}{EW} \times \Delta\lambda)_{minimum} = 1136 \tag{2.41}$$

$$(\frac{\rho}{EW} \times \Delta\lambda)_{maximum} = 20454 \tag{2.42}$$

2.15 Diffusion results as evaluated through water balance method

All the values plotted are listed on Table 2.4. Figure 2.24 shows the diffusion values at both $70°C$ and $60°C$. Few points can be noted , first considering the temperatures, as in [Majsztrik et al., 2007,] with increase in temperature , diffusitivity increases , hence in this for most of the cases a similar trend is observed. Again the diffusion values as evaluated, lies in intersection region of transient and steady state. With an increase in λ a clear trend is not observed. Most of the values form lies or are restricted in a particular region. However if more accuracy is observed in combating the errors then there can be chance to see a trend with an increase or decrease in values. For the moment water balance method can estimate the values defined in region of transient and steady state. The two red lines marked shows the value at maximum product of $(\frac{\rho}{EW} \times \Delta\lambda)_{maximum}$ and similarly minimum product of $(\frac{\rho}{EW} \times \Delta\lambda)_{minimum}$

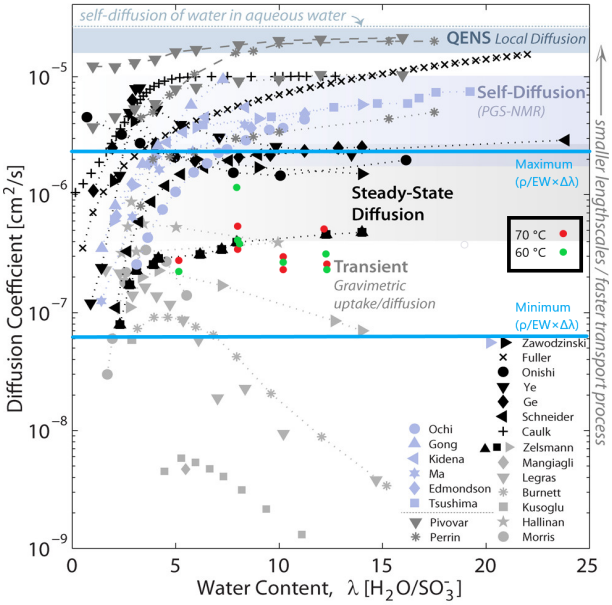

Figure 2.24: Plot of diffusion values ($70°C$ and $60°C$)as listed in table 2.4

2.16 Conclusion

In this work, we have calculated effective diffusion coefficient with water balance method. Diffusion coefficient can have large number of values based on viewpoint of authors and method used and it becomes difficult to fix a value based on a given operating conditions. In literature, there are methods such as gravimetric that cannot provide in-situ results, or in-situ methods such as neutron imaging, but are costly. In this we choose a cheap, effective in-situ method. Water balance method can be a very useful to provide value of in-situ diffusion coefficient based on the operating condition and uses same working setup as of fuel cell. This can be done within any fuel cell setup with nitrogen or air feed gases (when fuel cell is no running). This method is used to see an effect on relative humidity, temperature. For temperature, it is observed, an increase in diffusion coefficient with the cell

temperature. Results of diffusion coefficient are also calculated for Anion membranes providing nearly same values as Nafion. These results show that water balance method, not only give information on water production and distribution in a fuel cell in operation, but can also be applied easily to measure an effective membrane water diffusion coefficient based on our desired operating conditions. Moreover, at the end of this chapter, results considering the effect of density, equivalent weight and ($\delta\lambda$) on effect of diffusion are reported. ($\delta\lambda$) shows the maximum effect on diffusion results followed by density and minimum for equivalent weight. equivalent weight.

Chapter 3

Influence of flow field designs on the performance of fuel cells

3.1 Introduction

This chapter deals with new development of bipolar plates flow field design and its input on overall performance. At the beginning of this chapter, the main idea is to give an explanation for innovative flow field geometry. Why there is a need to improve flow field designs ? How it can impact the durability in the long term, overall performance, pressure head losses and materials.

As things become clear, this chapter advances about the electrochemical characteristics of new geometry of flow field designs and pressure drop measurements. Here 5 designs are introduced based upon the use and necessity. Various techniques for bipolar plates manufacturing are discussed based on the use, production, to develop plates based on the complexly involved in the designs. Coating plays a major role in increasing the overall performance in the plates design considering mainly stainless steel. What are types of coatings, cost-wise analysis of coatings and other materials. Overall the elements which contribute to the effective design and performance of bipolar plates are discussed in this chapter.

3.2 Materials for bipolar plates

With the interests in fuel cell's development many materials have been a favourable choice. However, in the recent years many new researches have led to use of metallic bipolar plates. Bipolar plates contribute $(60-70)\%$ of the total mass of components of PEMFC stack. Research is needed in this area to explore more feasibility in designs with improvement in conductivity, heat management, vibration tolerant, flexural strength, impact strength, and overall weight of bipolar plates based on DOE targets in Table 3.1. Graphite plates can have certain advantages compared to metallic, considering mainly the corrosion aspect as metallic plates needs coatings. Life of coatings further depends on method used to apply coating, the thickness, the base material, cost. Carbon polymer composites on the other hand are also used but suffer certain disadvantages considering mainly the low electrical conductivity.

1. **Graphite and polymer composites** Graphite has been a favorable choice as a material for bipolar plate mainly because of its good corrosion resistance

properties leading to better chemical stability. Apart from chemical stability graphite plates are better in showing good electrical and thermal conductivity [Sundén and Faghri, 2005,]. Graphite bipolar plates have problems related to machining and are brittle in nature. Research is needed to improve the properties further. [Scholta et al., 1999,] have shown improvements regarding the electrical conductivity, corrosion, chemical compatibility, gas tightness and mechanical strength. [Yan et al., 2006,] worked on cost and weight of bipolar plates and extended the work further for the stack. Graphite cannot be directly used for mass production because of its brittle nature. Stamping operation performed on the plates can simply result in the failure. Moreover, machining graphite is costly. Mostly the bipolar plates are made up of polymer resin impregnated graphite however there is search for better alternatives considering cost and production. This has led to open doors for carbon composites or carbon-carbon composites. These types of carbon polymer composites have thermosetting or thermoplastic polymer matrix loaded with conductive carbon fillers for example graphite, carbon black ([Brett and Brandon, 2007,], [Antunes et al., 2011,],[Yang et al., 2010,]). This leads to increase in electrical conductivity and an optimum balance to achieve an equilibrium between mechanical and electrical properties ([Taherian, 2014,], [Planes et al., 2012,]).

2. **Metals** Metallic bipolar plates (Figure 3.1) have been in use for commercial vehicles because of their excellent physical and mechanical properties, competitive cost compared with non-porous graphite and composite materials. However, despite having such properties many metallic plates fail in the area of corrosion. Based on the grade of material too, fabrication costs can be varied. Considering metallic plates, it is possible to achieve the thickness of 1.5 mm. This can also help in proper heat management. [Wang et al., 2006,] worked on BPP's made of titanium, due to its lightweight and corrosion resistance properties. Coating used is gold and weight for BPP's reported is 175 g. [Lin and Tsai, 2012,] used aluminium bipolar plate as base material with Ni-P coating and thereby understanding the hydrophobicity and corrosion resistance properties. [Song et al., 2019,] gave a detailed description of various materials with their advantages and disadvantages, considering into account the composite material, graphite and metals. Not only materials are discussed but also details regarding the manufacturing was provided out of which stamping and hydro-forming [Hung and Lin, 2012,] are mainly used for stainless steel plates.

   Problems associated with metallic bipolar plates is related to corrosion in the humid and acid environment. Also, the ions present in the metals may poison the membrane leading to membrane poisoning, degradation, which can affect the durability of the polymer electrolyte fuel cells using metallic plates as end to end plates. [Pozio et al., 2003,] experimented with SS361L and found Nafion degradation by contamination. Procedure involves checking of fluorides at the exit of outlet. Test was conducted to check the water collected at cathode and anode outlet and was analysed for metal concentration, conductivity and fluoride. Based on the results, stainless steel was unsuitable material for end plates in PEM fuel cell applications which led to degrada-

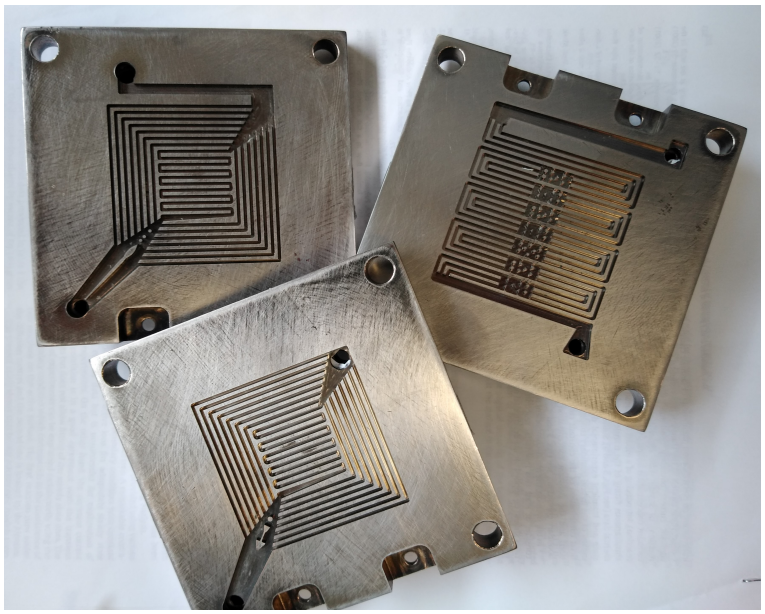

Figure 3.1: Metallic bipolar plates with different flow field designs developed in this research

tion of polymer and fluoride loss. [Wu et al., 2008,] performed similar tests to understand the performance and degradation of Nafion and tested several stainless-steel plates in environment carried for bipolar plate working. Based on the results, chromium content in the steel alloys has an important part in anodic behaviour. Based upon the interficial resistance evaluated for carbon-stainless steel interface and test conducted on 316L, 317L and 349TM, it was found that 349TM performed better because of its high chromium content.

3.3 Coatings

Since metallic bipolar plates offer advantages compared to graphite, the corrosion aspect should be worked upon. In order to protect the metal used in bipolar plate applications and to enhance the durability of the membrane it is very important that the plates be protected by corrosion and the best alternative is to apply coating on the surface of the metal. Controlling corrosion is not only important to protect the plates but the DOI targets recommends certain level and limit of corrosion as evident from Table 3.1.

3.3.1 Techniques and methods of applying coatings

Application of coating is a complicated process and it should be understood that the coating applied should fulfil all conditions of temperature, acidic environment and humidity. The coating should be able to bear the harsh chemical environment and compression effects due to coupling of plates together. There are various methods to apply coatings. [Asri et al., 2017] gave a detailed description of various methods used for coating which includes cyclic voltammetry (CV), physical vapor deposition (PVD), electroplating, air brushing, plasma surfacing alloy and chemical vapor deposition (CVD) Plasma specifically for SS304. For SS 316, PVD, nano

Parameter	Unit	DOE Target
Plate cost	Dollar K/W	5
Plate rate	kg /kW	< 0.4
H2 permeation rate	$m^3/s/cm^2$	$< 2 \times 10^{-6}$
Corrosion	$\mu A/cm^3$	< 1
Resistivity	Ohm cm	< 0.01
Flexural strength	Mpa	> 25
Flexibility	Percent	3-5

Table 3.1: DOE Targets limiting to corrosion

particle implantation, Magnetron sputtering ion plating, cathode arc ion plating, Active screen plasma nitriding (ASPN) and thermal spraying. Electrodeposition and multi arc ion plating are some of the suitable techniques for coating plates with titanium. These techniques can be further classified as spraying, Ion implantation, vapor deposition, heat treatment.

[Wind et al., 2002,] gave results regarding the stainless-steel performance considering coated and uncoated plates.[Jannat et al., 2019,] used PVD technique by depositing (Ti/TiN) multi-layer coating on 316L SS plate. Based on their research, coated (Bipolar plates) BPP's has interficial contact resistance (ICR) of (11 and 18) $m\Omega/cm^2$ before and after potentiostatic polarization. Since a lot of metallic plates require plating hence it becomes very important to understand the corrosion effect and its durability. How much time a coating can be used until a replacement is required is an important question. Potentiodynamic voltammetry can be used as a method to understand the corrosion resistance of the material and can be applied on stainless steels. [Richards et al., 2012,] studied the effect of coating on SS 316L, 316Ti, Al276, AI265, AI6XN for delivered state and after electrochemical surface treatment by potentio-dynamic voltammetry and microscopic analysis. It is seen that only 316L and 316Ti have met target for corrosion in their untreated state. After electrochemical treatment the corrosion current for AI6XN and AI265 decreased by more than 50 %. [Yi et al., 2013,] developed a multi-layered Cr-C/a-C:Cr coating on SS316L sheet as bipolar plates where the thickness of film is about 1.4 μm and is mainly composed of amorphous carbon. Method used is closed field unbalanced magnetron sputter ion plating and contact resistance reported is 2.89 mΩ/ cm^2 at 1.5 MPa, research shows good water management as static water contact angle of the film is 89.1° . [Wang et al., 2019,] used electrodeposition method where Nb doped TiO2 nanopowders modified polyaniline (TNO-PANI) and polyaniline (PANI) are electrodeposited galvanostatically on 316 stainless steel BPP's.

Gold coated plates have been used in many areas ([Yun, 2010,], [Thomas et al., 2012,]). In order to apply coating it is very essential to apply a base. A base coating possess the capabilities to bind the metallic coating and base properly in

order to give the best performance. As presented in Figure 3.2, it represents the thickness of base layer required to efficiently coat layer of gold on it. [Yun, 2010,] used 2μm thick gold layer with an interlayer of 0.1-μm thick titanium or nickel. Considering an equivalent comparison to graphite, nobel metal coatings are 3-4 times costly as reported by [Tawfik et al., 2007,], the gold coated aluminum plates are 4 times costly than graphite bipolar plates. However, reducing the thickness of gold coatings can reduce the cost and is evident from the recent work of [Kumar et al., 2010,] which optimized the thickness to nanometer. Reducing the thickness helped to retain the properties of noble metals and also reducing the cost. In the above study conducted, stainless steel material was used and a uniform coating of 10nm was applied to understand the electrochemical behavior of these plates. Operating temperature conditions was 80°C with a solution of 0.5mM $H_2SO_4(PH3)$. The results shows excellent corrosion resistance with current density less than $1\mu A/cm^2$ at 0.8 V .

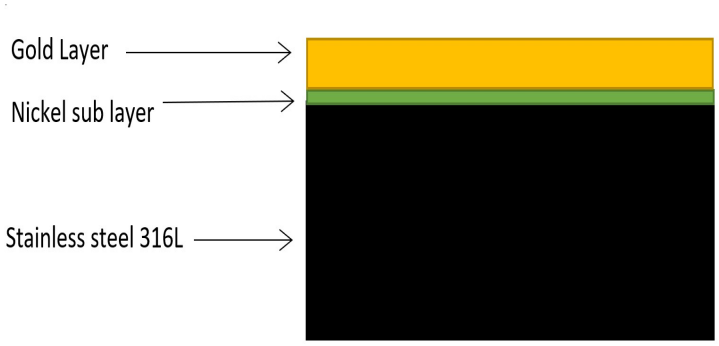

Figure 3.2: Coating on metal with sub layer

3.4 Bipolar plates flow field design

Flow field design plays a very important role in understanding of transport of reactive substances into the fuel cell. Not only mass transport is affected with a poorly designed flow field but can also lead to improper water management in the cell. A well formulated area wise distribution of land and channels can help for a effective and efficient current distribution and homogeneous load distribution on membrane electrode assembly (MEA). [Wilberforce et al., 2019,] gave a detailed review considering distribution of various flow field designs and performance of proton exchange membrane fuel cells (PEMFC).

3.4.1 Parallel and serpentine flow field

Parallel flow field (Figure: 3.3(a)) and serpentine geometry(Figure: 3.3(b)) are two mostly used for the fuel cell operations mainly because of the ease in designing and simplicity. Out of the two, parallel flow field geometry is the easiest. With multiple channels for the reactants distribution, it allows uniform distribution and water removal. However this design suffers certain disadvantages, if the pressure is not maintained equally in all the channels, it can result in non-uniform reactant

distribution and hence unequal flow of gas along the channels. In order to overcome this shortcoming, serpentine design which is also commercially favoured has reactants flow directed along specific channels using the entire area of channels, thereby uniform distribution. Due to larger channel lengths, serpentine geometry suffer higher pressure head losses.

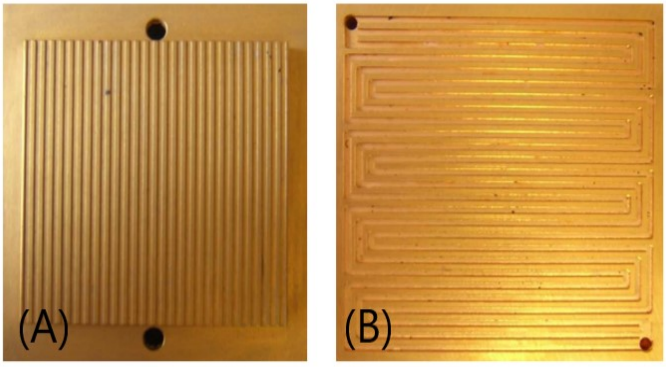

Figure 3.3: (a)Parallel and (b)serpentine flow field geometry adopted from [Thomas et al., 2012,]

3.4.2 Interdigitated design

These designs have been into analysis but not fully explored. They use the concept of flow under ribs. The traditional serpentine design can transport the gases via diffusion but interdigit(Figure 3.4) designs can transport with two processes of diffusion and forced convection. This method can increase the mass transfer of reactant gases.

[Nguyen, 1996,] worked on gas distribution design to improve mass transport of reactants from flow channels to inner catalyst layers. They presented study comparing parallel straight channel design with interdigit, which shows later having better performance in polarization curve (mass transfer region) compared to parallel design. [Wang and Liu, 2004,] made performance studies with interdigitated flow fields and understood the effect of cell temperature, gas humidification, cell operating pressure and reactant gas flow rate on these designs. Based on the experimental conditions these designs work with good humidification and increase in operation pressure. One of the advantages of interdigitated design is that it avoids flooding. Since it utilises the concept of forced convection so it results in forcefully removal of water. However interdigitated designs can suffer some disadvantages as forced convection can result in uneven distribution of reactants on gas diffusion. Interdigitated designs can also result in increase in pressure based upon the gas diffusion layer thickness. More the thickness of gas diffusion layer more is the pressure required by the gases to flow through the GDL. For designing the interdigitated plates, thickness and porosity of gas diffusion layer play an important role [Wilberforce et al., 2019,].

3.4.3 Bio inspired

Nature has inspired in many areas to incorporate and advance the innovation, fuel cells is one such area. It is not new that the veins in the leaves Figure 3.5b are

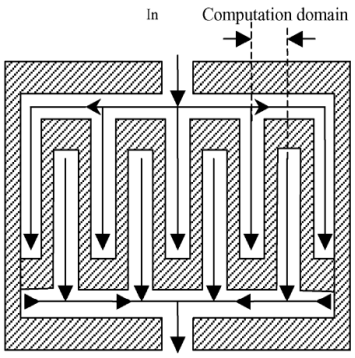

Figure 3.4: An interdigitated flow field design adopted from [Hu et al., 2004,]

able to transfer and distribute water much evenly. Similar case can be observed for lungs, Figure 3.5a, with main function in effective distribution of air and removal of CO_2. Inspired by nature to develop the novel flow field designs, [Kloess et al., 2009,] (Figure 3.5) worked on bio inspired channel designs inspired from nature a hybridization of serpentine and interdigitated. Results were observed with an increase in power density at T = 75°C and relative humidity (RH) from (100% to 30%). [Cho et al., 2020,] further extended the work in the region of lung inspired fuel cells by developing a finite element fuel cell model of lung inspired flow field. Based on results, the lung inspired flow fields perform an effective task of reducing velocity and homogenizing of reactants concentration, before entering in the catalyst layer. Key to efficiency is good flow without dead zones in channels, effective distribution of reactants and lower pressure drops.

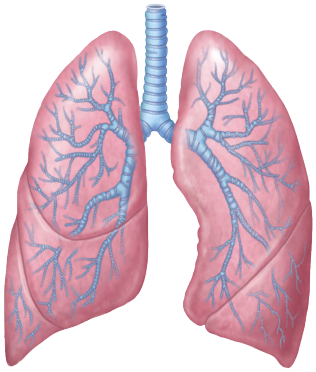

(a) Lung

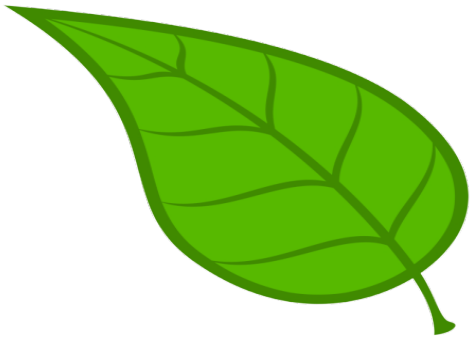

(b) Leaf

Figure 3.5: Bio inspired designs

3.4.4 Other designs in literature

Apart from traditional designs, bio inspired, interdigited, there have been other which have been worked upon, circular and spiral geometries are one of them. [Ibrahimoglu et al., 2017,] investigated flow field design considering spiral geometry (Figure 3.7) with less area considering the standard area of serpentine plates ($25cm^2$). Ansys (Fluent PEMFC) module was used to study the performance of

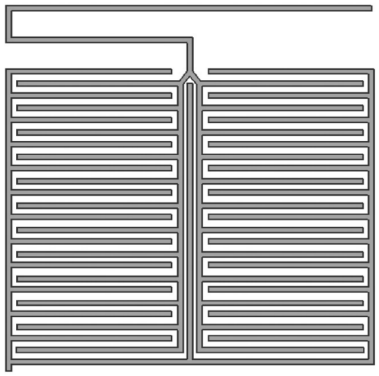

Figure 3.6: A lung inspired flow field design adopted from [Kloess et al., 2009,]

spiral design. The motivation behind this study is to identify the feasibility of circular shape PEMFC with a spiral flow-field design. The 3-D model developed aims to understand the electrochemical transport phenomenon such as gases, temperature and pressure distribution. Based on the results, pressure head losses are less compared to the serpentine geometry and more compared to parallel plate geometry. [Cano-Andrade et al., 2010,] gave a numerical solution using spiral geometry of flow channel. Using computational fluid dynamics code, finite volume scheme, various flow configurations were modelled ranging from 4 to 12 channels in multiples of 4, with 12 channel design showing the maximum efficiency and higher pressure drop. Increase in inlet hydrogen velocity can increase the output performance of the cell. Comparing current density at the entrance of fuel cell at same position shows highest for radial in comparison to spiral and serpentine. [Juarez-Robles et al., 2011,] (Figure 3.7) investigated the effect of spiral flow channel geometry in shape of 1, 2,3,4,6 and 8 concentric spirals. Results were simulated by a three dimensional non isothermal model, predicting water content and entropy generated in all zones inside the cell. Channel with 4 spirals shows maximum efficiency with lower entropy drop. Developing numerical models is a time-consuming process and working on actual fuel cell plate is costly, which further depends on the type of metal used, the method for manufacturing hence there is need to explore other alternatives for flow geometry which can be optimised. [Behrou et al., 2019,] developed a method using topology optimization to design flow field of PEMFC resulting in non-trivial optimised geometries. The objective function is to optimize both homogeneity of current density distribution and output power permitting reduced cost and increase in durability. The objective of this work or the objective function was to maximize both the current density distribution and homogeneity.

Research is not only limited to rectangular plate type fuel cell geometry but is extended to circular based geometry also. [Suseendiran et al., 2017,] developed cylindrical fuel cells, thereby removing the use of bipolar plates. This cylindrical design has certain advantages such as machining cost for bipolar plates is removed, overall reduction in dead weight. They offer more easy and efficient water management compared to the traditional fuel cell in practise. However, the design of cylindrical fuel cell may be simple but the fabrication is complex. Few important results considering the cylindrical fuel cell performance are reduction in contact resistance from 75 milliohms to 50 milliohms. Increase in open circuit voltage (OCV) from 0.85V to 0.95V. Increase in OCV can have one indication of low activation

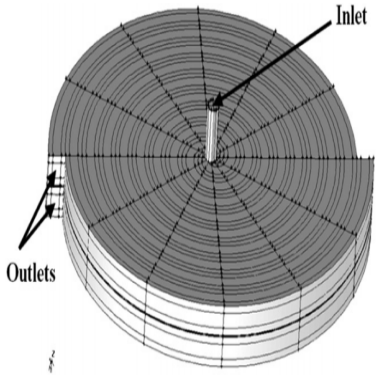

Figure 3.7: A lung inspired flow field design adopted from [Juarez-Robles et al., 2011,]

losses. Also, a 40% increase in peak power was observed from optimization of hydrogen flow rate and cathode rib width. There is always a need to optimize the design of fuel cell stack and hence new designs and methods are indeed helpful to understand the feasibility and explore new solutions. Optimising hydrogen flow rate with properly designed channel is one such priority as it will directly result is lower costs.

Apart from the designs there had been much work in order to optimize the geometrical parameter for the serpentine design. For example, there have been research carried out in order to optimize serpentine flow field design. One of the most important is to reduce the pressure head losses. Now, one of the possible solutions is to use multiple channels (Figure 3.8). Using multiple channels does not imply using parallel flow field geometry but using multiple channels with the already existing serpentine design. [Shimpalee et al., 2006,] showed that fuel cells with shorter path length, gave more uniform current distribution. The paper investigates how 200 cm^2 serpentine flow-fields with different number of gas paths, and thus different gas path lengths, affect performance and distribution. This variation in gas path and length also resulted in more efficient water removal compared to a long single geometry. They performed their calculations over flow field from -

(a) 3-channel multiple serpentine flow-field

(b) 6-channel multiple serpentine flow-field

(c) 13-channel multiple serpentine flow-field

(d) 26-channel multiple serpentine flow-field

(e) 26-channel multiple symmetric serpentine flow-field

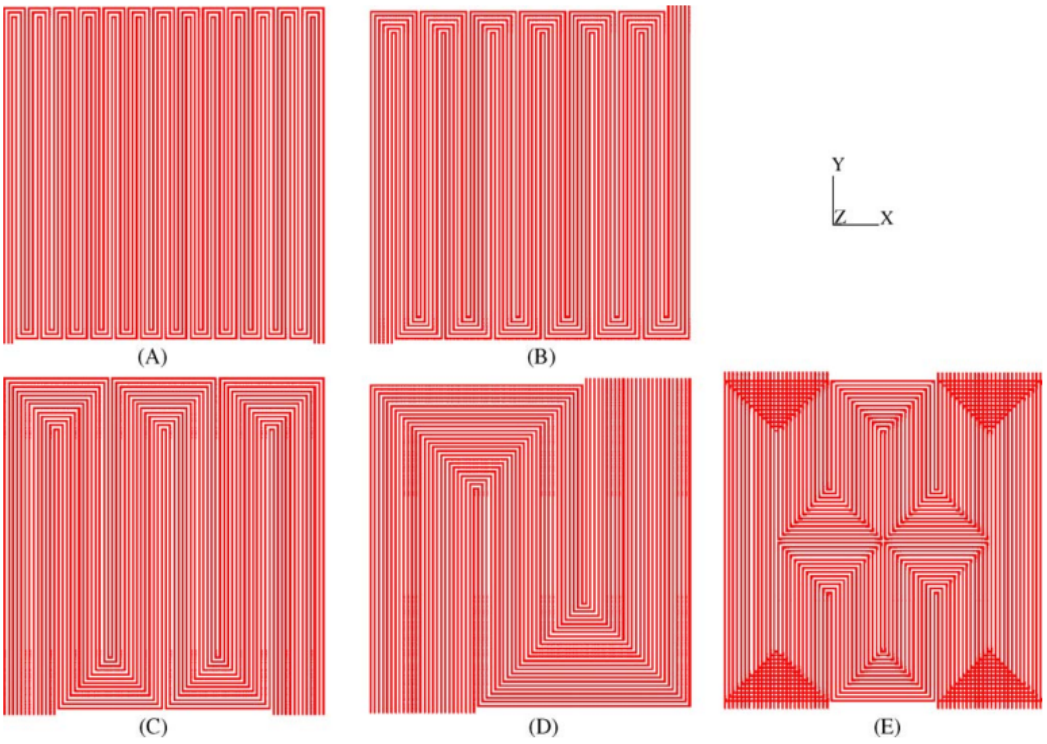

Figure 3.8: A multi serpentine design with (a) 3-channel (b) 6 channel (c) 13 channel (d) 26-channel and (e) 26-channel complex flow field adopted from [Shimpalee et al., 2006,]

All the calculations were made on cell of active area of 200 cm^2. It was further concluded that a 13-channel flow path performed better compared to 26 channel path. Present commercial fuel cells mostly use multiple channel serpentine plates in order to increase the performance. [Karthikeyan et al., 2015,] experimental investigated zigzag positioned porous inserts on rib surface of cathode flow channel for performance enhancement. In Figure 3.9, they experimented BPP designs varying the porosity of carbon inserts in the range of $(60-70)\%$, $(70-80)\%$, $(80-90)\%$ respectively These porous inserts which have $(80-90)\%$ porosity has improved the power density and current density by 11.5% and 7%respectively compared to conventional serpentine channel. The concept and idea involved here is to enhance water removal with the capillary action. The porous inserts on the rib helps to remove the stagnated water and hence improving the efficiency of the fuel cell.

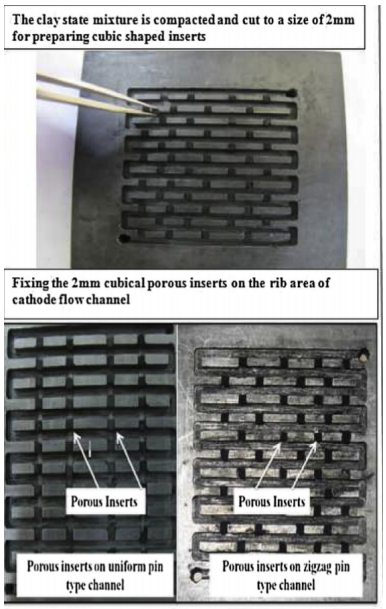

Figure 3.9: Carbon zigzag inserts as adopted from [Karthikeyan et al., 2015,]

3.5 Geometrical parameters

Geometric parameters for flow channel design plays an important role for effective distribution and removal of reactants. [Manso et al., 2012,] reviewed the influence of geometric parameters of flow fields and its performance on PEMFC. Following their work, flow field, flow direction, channel length and number of channels, use of baffles, cross sectional dimensions, rib width, channel depth, height to width ratio can have huge effect on performance of fuel cell.

Considering parallel flow fields, limiting current density and the raw power can be affected by the channel/land width. [Cooper et al., 2016,] did the study on parallel and interdigitated flow fields and found stoichiometry an important parameter for interdigitated flows, and channel/land width for parallel flows. This can be very important study to understand the design consideration while developing the fuel cell plates, in order to optimize the results. Dimensions of cathode plate tested ranges from channel depth/height ranging from 1 mm – 0.25 mm, similarly width ranging from 1 mm – 0.25 mm. Some of the important conclusions considering the channel height – width ratio and their effects are discussed in table 3.2 -

1. Statistical results examined showed maximum net power occurs for most of the design at a hydraulic diameter of 0.4 – 0.45. Smaller the diameters, introduce pumping losses. Larger the hydraulic diameter suffers transport issues.

2. Stoichiometry increase is found to be non-beneficial at lower hydraulic diameters.

3. Interdigitated designs are more beneficial at large hydraulic diameters, increase in reactants supply and pumping power.

4. Insights considering effect of geometrical parameters was highlighted [Cooper et al., 2016,] and it was resulted that both the geometry (parallel and inter-

digitated) requires different design procedures to understand the working of plates.

Bipolar plates channel design was not only limited to rectangular dimensions as [Khazaee and Ghazikhani, 2011,] worked on annular shaped geometries. The results shows that the cell performance increase as the number of connections between gas diffusion layer and bipolar plate increases. [Carton and Olabi, 2017,] worked on three-dimensional proton exchange membrane fuel cell model thereby providing a 3-D CFD model for open pore cellular foam material. Results indicated that open pore cellular foam material plates distribute both hydrogen and oxygen more evenly from inlet to outlet, compared to double channel fuel cell.

Characteristics	**Case 1**	**Case 2**
Channel length and number of channels	Flow field designs with shorter path lengths or with higher number of channels are better in reactant distribution and overall power consumption.	On the other hand, gas channels with higher channel lengths produces more uneven pressure distribution over the adjacent channel length and can introduce convection flow or under rib movement of reactants
Baffles	Baffles have been used from long time in heat ex-changers in order to improve the heat exchange. Similarly, baffles used here can constrict the path of the gas flow and improve the force convection, thereby better mass transfer, increase in effective area	Although introduction of baffle has benefits but with baffles pressure drop increases and hence overall performance decrease in the long run. Also, introduction of baffles resulted in decrease of transient response of fuel cell operations.
Cross section shapes	Rectangular cross section is used mostly.	Circular, spiral are also researched
Channel rib width	Channel rib width can find its importance based on the type of conditions used. For effective water removal thinner ribs are preferred but if higher current conditions are imposed favourable. With air thinner ribs are preferred.	Large widths can reduce the efficiency of the cell, can increase the water stagnation because of inability to remove.

Channel height	Reduction in the channel height can offer certain advantages such as - 1. On cathode side less channel heights can increase the water elimination 2. Increase in mass transfer across the gas diffusion layer 3. Increase in fuel cell efficiency	Reduction in channel height can also increase the overall pressure drop and hence can result in more power from the compressor in order to drive the fuel cell.

Table 3.2: Fuel cell bipolar plate geometrical characteristics

3.6 Machining techniques for fabrication of bipolar plates

Bipolar plates are made up of stainless steel 316L. The designs have been developed on solidworks and fabricated by two machining process –

1. Computer numerical control (CNC)
2. Electro discharge machining (EDM)

3.6.1 Computer numerical control (CNC)

There are various methods for bipolar plate production [Cunningham et al., 2007,] out of which moulding is considered to be a feasible alternative for batch production. CNC machining [Smith et al., 2014,] comes to use when intricate shapes are required to be machined, which cannot be stamped. Moreover, it depends upon need too. For example, in order to test a new flow field design, it is better to opt for a CNC than a injection moulding or stamping. The problem with stamping is use of dies. Stamping requires a die, developing die for 1-2 sets of bipolar plates is not only costly but time consuming too. Hence in this research for the new flow field designs two manufacturing processes are preferred considering the speed and accuracy.

Diamond tool cutter with tip length measuring from (0.5 mm – 2.0 mm), Mitsubishi® were used for machining. The plates were buffed initially to remove any impurities, inclination and roughness. All the designs have depth of 2 mm and have been carved out starting with feed of 0.5mm. Doing this it removes the excessive impact load on the tool and tool wear out much later resulting in less chances for tool breakage.

A tolerance of 5% is taken on the channels and 10% on the edges. In order to develop threads for the connections of the outlets and inlets, taper drill was used. Taper drill of M10 was used and the material was carbon tool steel.

CNC stands for computer numerical control and it a subtractive manufacturing process which involves the concept of computerised control and machine tools to remove materials or layers of materials from a sample work piece required to be turned in to specific work piece materials. Depending upon the axis of machine chosen, more complicated shapes and geometries can be worked out from the work piece. Based on the geometry required, tools related to specific method can be used for example grinding, boring, milling, cutting or simple drilling operation. Now in order to operate CNC, it requires a set of instruction which are usually in the form of codes.

Type of metal plays a important role in using CNC because softer materials for example graphite are easier to cut and machined but stainless steel are difficult, hence feed rates come into play. A higher feed rate can decrease the time for machining the metal but can result in poor surface finish. Moreover a lower feed rate can increase time for machining but can result in a blunt tool without any chip formation. And hence, deciding an appropriate feed rate is important in working with CNC machining, which ensures speed and accuracy in the work piece. Lubricant also plays an important role in overall performance for the tools and work piece resulting in lower tool breakage loss and better finishing.

3.6.2 Electrode discharge machining (EDM)

Electrode discharge machining (EDM) is also known as die sinking, wire eroding or spark erosion process as it utilise the concept of spark produce to remove the material and generate the required end results. EDM have been used in literature [Bai et al., 2010, Dong-Hui et al., 2017,] for manufacturing of bipolar plates for PEMFC. [Hung et al., 2011,] used EDM procedure to fabricate micro channels in metallic bipolar plates. For this research EDM was used to create complicate flow field geometry where cutting was difficult compared to this procedure. Work piece, made up of stainless steel 316L is clamped at both sides. The main energy conversion in EDM is electrical to heat energy. Electrical current and time of current controls the heat energy required as electrical energy is proportional to current flowing. With an increase in current the material removal rate increases, wear of material increases and results in decrease in finishing, hence in our case the applied current density was 0.4 A/ cm^2. For copper electrodes the maximum current density is (5-7) A/ cm^2. Electrode used is copper with negative polarity. Flushing is again an important procedure to quickly remove the eroded part so that the finishing is not compromised. Flushing can be of various types such as motion flushing, pressure flushing, vaccum flushing or a combination of later all. For the present designs pressure flushing is used.

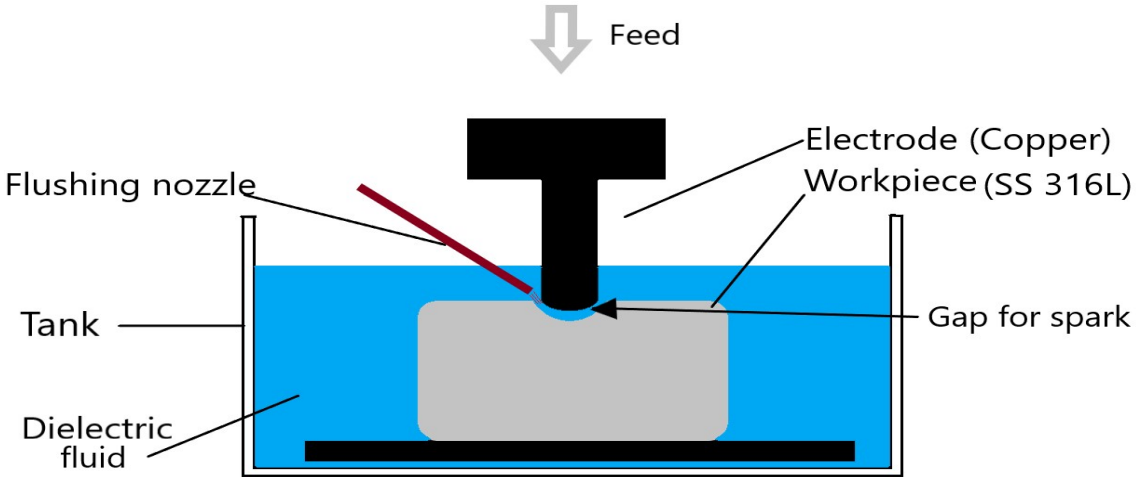

Figure 3.10: Setup for electrode discharge machining

3.7 Choice of flow field design of bipolar plates

In this research two new designs of bipolar plate are compared with traditional serpentine (Figure 3.11(a)). The plates have been named in order to highlight the use. Figure 3.11(b) represents the traditional serpentine geometry, Figure 3.11(c) multiple serpentine (multi-serpentine) geometry with additional slots and Figure 3.11(c) hybrid (serpentine + parallel) design. The choice of this design are explained below.

Traditional serpentine (Figure 3.11(a)) design suffers from various flooding and drying of membrane issues. [Le et al., 2010,] presented results regarding the liquid water behaviours in proton exchange membrane fuel cell cathode with serpentine channels. [Lee et al., 2011, Lee et al., 2013,] gave radiographic investigations of liquid water transport behaviour in PEMFC. [Aslam et al., 2018,] simulated similarly for direct visualization of liquid water in PEMFC's. Extensive research has been published so far regarding the use of this plates with both performance, modification and drawbacks ([Choi et al., 2011,], [Kahveci and Taymaz, 2018,], [Shimpalee et al., 2006,]).

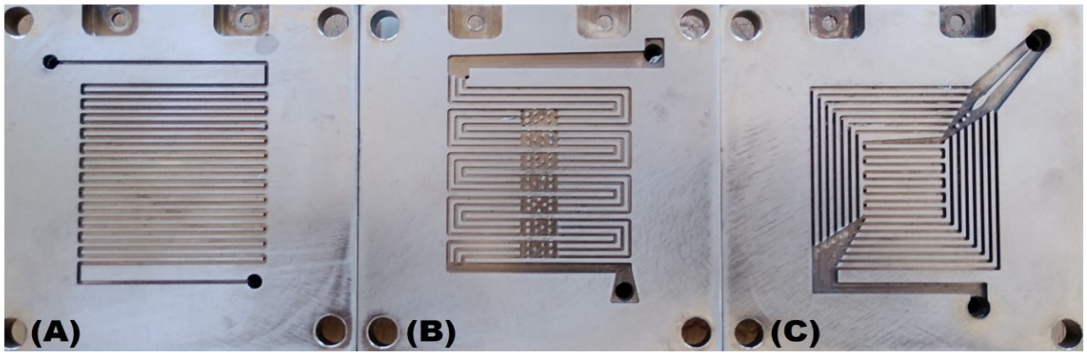

Figure 3.11: (a) traditional serpentine design (b) multi-serpentine design (with slots) and (c) hybrid design. Active area = 25 cm^2. Depth of channel is 2 mm.

Multiple serpentine geometry with additional slots (figure 3.11(b)) are developed to enable homogeneous water distribution. Multi-serpentine designs (Figure 3.8) have already analyzed in literature [Shimpalee et al., 2006,] by analyzing the optimum channel length for flow but not with slots addition. There is no accurate way to understand the water distribution in the bipolar plate accurately and precisely. A typical multi-serpentine channel has 4-8 channels in parallel to avoid long channel lengths and hence reduced pressure head losses, however if any one channel in multi-serpentine channel is blocked, there will be different possible cases : Reactants will be forced to move from the gas diffusion layer, inducing more pressure head and non-uniformity of pressure on the gas diffusion layer. Also, due to blockage by water, there is a possibility that the entire length which was supposed to carry the reactants will be without any reactants and hence again a non-uniform distribution on the gas diffusion layer.

Fuel cell working at higher relative humidity or at higher currents results in more water. This water needs to be flushed out to avoid flooding. For example, in multi-serpentine plates with size of 10 cm $\times$ 10 cm if a channel is blocked with slug or plug it will block the entire channel to further carry the reactants and decrease the reaction surface of electrodes that will impact the performance. In the present work slots are added to the multi-serpentine design to avoid slug formation. Indeed, if a channel is blocked, the slug thanks to the added slots, can redistribute into smaller droplets and can make a way forward for further reactants to distribute homogeneously.

Hybrid design (figure 3.11(c)), to take into the effect of the pressure losses, promote homogeneity, and ease in water removal. The idea behind using this design is to reduce the serpentine long lengths and equally replacing by exterior parallel channels to promote faster water removal and gas distribution and decrease pressure head losses. The next part of this chapter deals with electrochemical characterization through polarization curve and pressure drop measurements.

3.8 Circular and spot design

Two additional designs have been started in this research namely spot design (Figure 3.12) which have been already in literature studies and circular design (Figure 3.13). For both of these designs the data available is measured at 4A for 2 hour signals and pressure head losses are calculated. Due to time limitations for the scope of this research only pressure head losses are calculated.

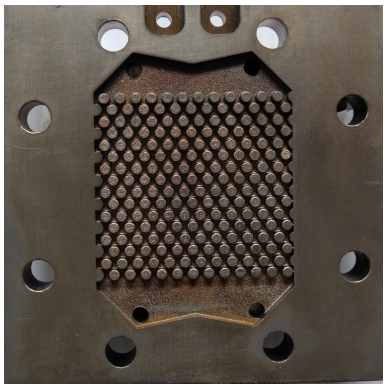

Figure 3.12: Spot type geometry

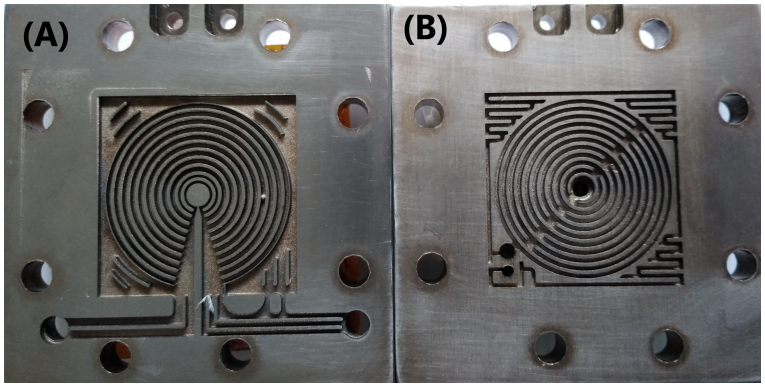

Figure 3.13: Circular type geometry

Starting with the spot design (Figure 3.12), the aim is to check for pressure head losses as it has the potential for better distribution of the reactants and products, as it does not restrict the flow in one direction but provides multiple passages for fluid flow. The aim of this design is also to provide better heat and water management. The present pressure drop as observed in this design was 3 mbar at the anode and 2.5 mbar at the cathode side.

The main aim to use circular design is to provide uniform homogeneity at the anode side (Figure 3.13(b)) and removal of water at cathode side. Considering the Figure (3.13(b)) it can be observed that the design performs better at high flow rate conditions as the water stagnated can have two directions to flush out. But since in this experiments operating condition of 4A was used, so flow rate was comparatively less to use this design and hence (Figure 3.14(b)) was used with one inlet at the left side and one outlet at center. This resulted in lesser effective area for distribution of reactants and gases and the left out effective area of 25 cm^2 was blocked. The same procedure was done in (Figure 3.14(a)) part which resulted in lesser area. Unfortunately the present operating conditions are not sufficient enough to arrive at the understanding of performance of these two designs.

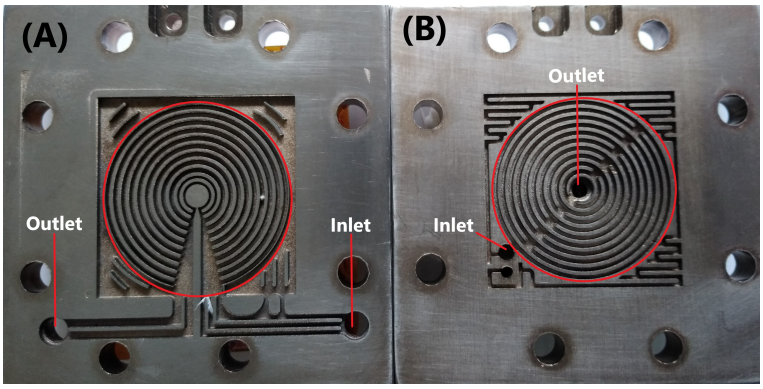

Figure 3.14: Circular type geometry

3.9 Experimental test bench

Figure 3.15: Fuel cell experimental setup

Figure 3.15 shows the experimental setup in order to carry out the diagnostic and polarization tests on the plates. Figure 3.17 presents the experimental setup used for our experiments. For the fuel cell assembly, metallic stainless steel 316L flow field plates are used. A carbon-based coating material developed by Precors® is used on the plates. Thickness used for the coating is 100 nm. Tests are carried out using Nafion® NRE-211 membrane, GDL Sigracet® 39 BC, for a fuel cell temperature of 60°C and relative humidity at the inlet set to 50%. Each bipolar plate has an area of 100 cm^2 (10 cm x 10 cm) and effective reaction area of 25 cm^2 (5 cm $\times$ 5 cm). Lands and channels are divided in ratio of 50%. Depth of channel is 2 mm. Gas used at anode is hydrogen and at the cathode side is pure oxygen, connected by flow meters

to regulate the amount of flow based upon the current applied. Stoichiometry for hydrogen is set to 1.4 and for pure oxygen is set to 1.2. Two separate humidifiers are used to maintain the right amount of humidity for effective working of fuel cell. A temperature controller was used to maintain the required amount of relative humidity in the fuel cell. The connection between humidifiers and fuel cell are preheated to avoid the condensation of water present within humidified gases which can result in flooding issues at the inlet of the cell. Temperature of preheating is set to 65°C. Thermo-regulation is used to maintain the fuel cell at 60°C on both the sides of stainless steel BPP's thanks to water circulation. Special C-clamps are used to hold the two plates together. It is made sure that equal compression is given to all the three sets of bipolar plates. Isoflon® gasket, thickness 0.25 mm is used to avoid gas leakage and insulation. Pressure sensors JUMO MIDAS® are connected both at hydrogen and oxygen inlet of PEMFC to measure the inlet pressure. The outlets are open to the atmosphere. Pressure sensors have range of 250 kPa and accuracy of 0.25 kPa. To impose current in galvanostatic mode an electronic load, Kikusui® PLZ664WA 0-150 V 0-132 A is used. Electrochemical data, except polarization curve, is collected at two operating current value of 4A and 19A (corresponding to 0.16 A/cm^2 and 0.76 A/cm^2 respectively) during 2 hours for each point. In order to record the signals of pressure and fuel cell voltage fluctuation for ENA, a National Instruments data acquisition card NI DAQ 9234 is used which has a 24-bit resolution for good accuracy and sensitivity of measurement with anti-aliasing filter. All data of pressure and voltage are recorded with a 2048 Hz frequency and using LabView®. Matlab® and Python® are then used for further signal treatment.

Figure 3.16: C-clamps

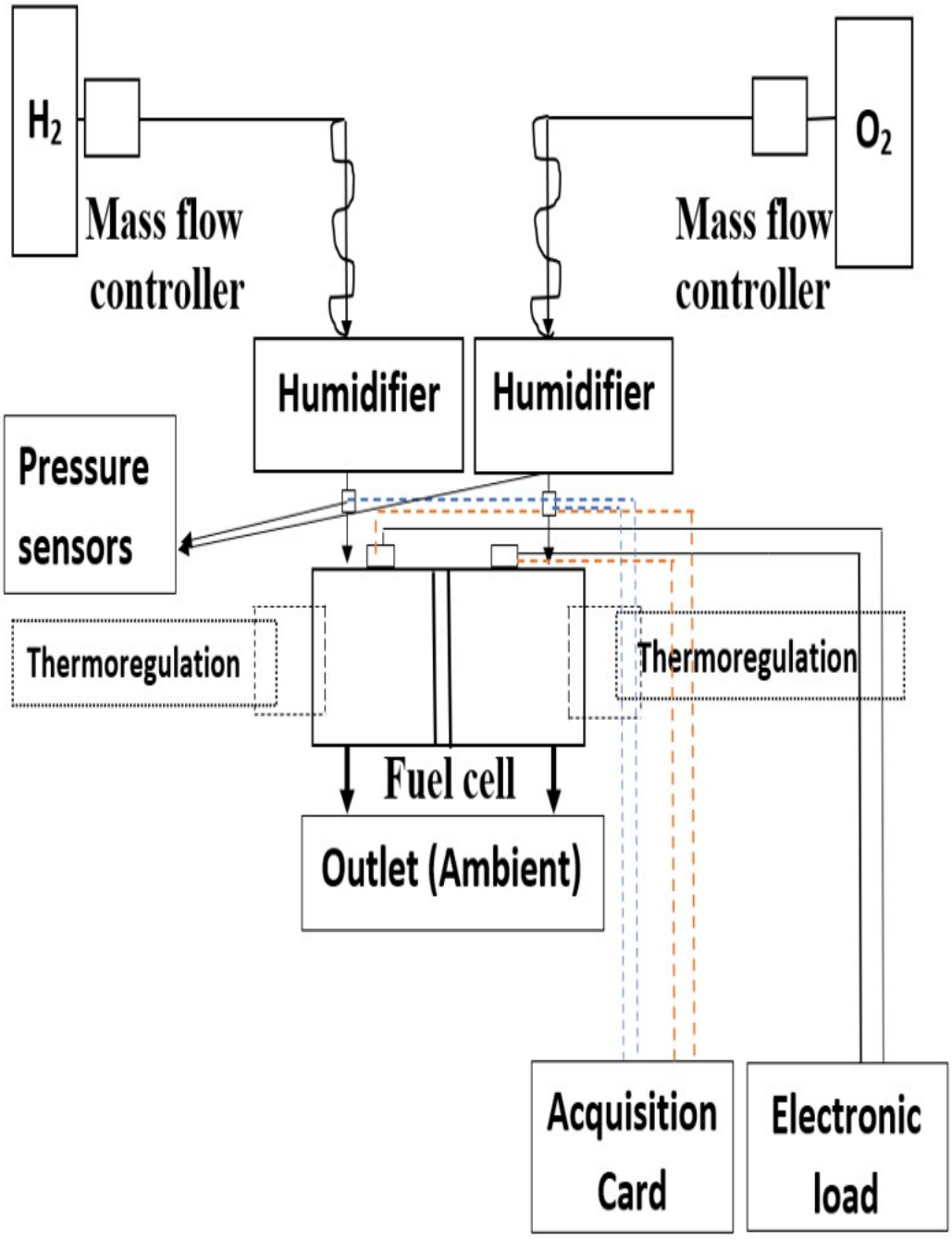

Figure 3.17: Schema of experimental setup

In order to clamp the plates, c-clamp (Figure 3.16) were used as the plates developed do not have same inlet and outlet openings and hence using clamps can ensure constant compression for all the designs. A variable compression to the gas diffusion layer can alter the results of the experiments and hence it is made sure that equal compression is applied by giving equal threads rotations to the c-clamp. All experimental conditions and material specification are listed in Table 3.3, Table 3.4.

Sr no	Property	Units
1	Relative humidity	50% and 100%
2	Temperature - Fuel cell	60 °C
3	Temperature of water heater	65°C
4	Current input range	(0-35) A
5	Humidifier temperature	46°C and 60°C
6	Insulation temperature	75°C
7	Outlet conditions	P_{atm}

Table 3.3: Material specifications

Sr no	Instrument/ Device	Mark / Brand
1	Humidifiers	
2	Gasket	Isoflon®
3	Membrane NRE- 211	Nafion®
4	Gas diffusion layer – 39 BC	Sigracet®
5	Mass flow meters	Brooks instruments®
6	Connecting tubes Ø 5mm, Thickness 1 mm	Legris®
7	Electrolyser	*Parker*
8	Thermal heater	
9	Pressure sensors	JUMO MIDAS®
10	Electronic load	Kikusui®
11	C clamps	HMT®
12	Data acquisition card	National instruments®
13	Hydrogen gas sensor	Sewerin
14	Coatings	Precors®
15	Software	Labview/ Solidworks/ Python/ Matlab

Table 3.4: Material specification

3.10 Results considering electrochemical tests

In order to analyse the designs based on the performance , water management for the scope of this research two tools are used-

1. Polarization test + pressure drop.
2. Electrochemical noise analysis (ENA).

In the subsequent part of this chapter results regarding the polarization and pressure drop will be discussed.

3.10.1 Polarization test

Polarization curves are generally used to describe the phenomenon of electrochemical reactions and to characterize the electrical performance of fuel cell. This can be an important tool to understand the kinetics, resistance and mass transfer of a fuel cell. Based upon this, important observations can be drawn, explaining global performances and losses in working of fuel cell. For the present research, the voltage is recorded for 10 minutes to get the point of stability. For stability point of view, repeatibility test are performed. The polarization curve of the three designs are presented in Figure 3.18. The activation losses, which occur at low current densities ($< 0.2 A/cm^2$), are similar for all three designs except multi-serpentine geometry shows less losses to begin the reaction. Major difference regarding fuel cell performance can be seen in ohmic part (linear part). Figure 3.18 highlights that multi-serpentine geometry, which gives the best electrical performance. The multi-serpentine design demonstrates a voltage of 0.65 V compared to 0.6 V to the hybrid and 0.58 V to the serpentine cell at 0.4 A/cm^2, and of 0.5 V compared to 0.3 V and 0.25 V at 0.9 A/cm^2, respectively. The ohmic loss is mostly significant for the case of serpentine geometry which is followed by hybrid in comparison of multi-serpentine mostly due to a higher membrane resistance.

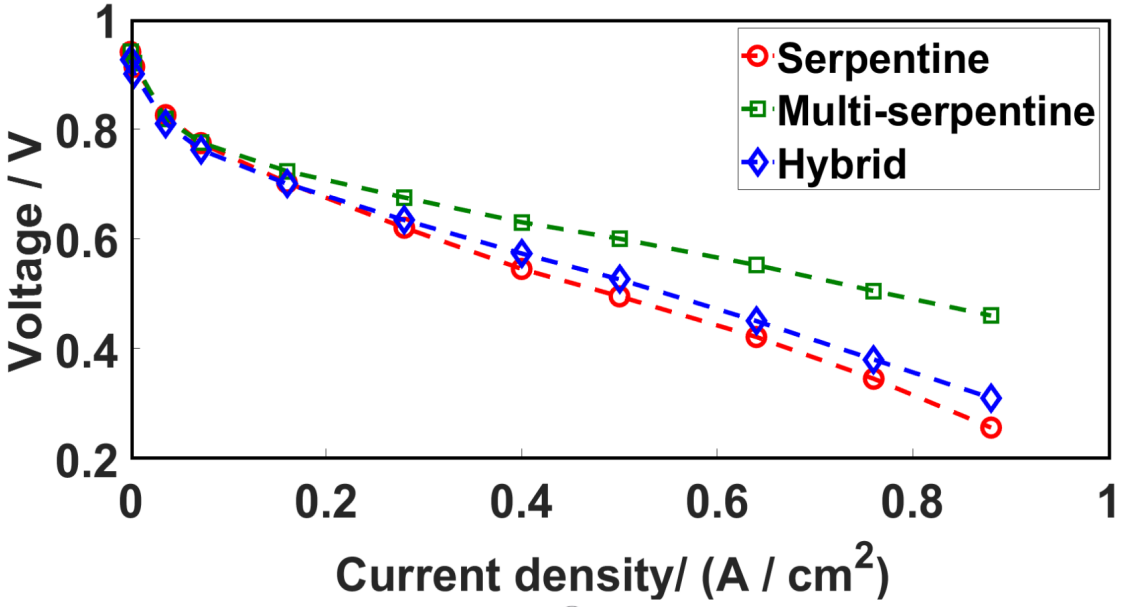

Figure 3.18: Polarization curve comparison for the three designs

3.11 Results considering pressure drop for different geometries

Pressure drop can provide various insights considering the functioning and water management in fuel cell. A stable signal with reduced pressure drops, signify better performance compared to higher pressure drops during operation. Moreover pressure sensors helps to collect the in-situ data with respect to monitoring the performance of the fuel cell. Figure 3.19 shows the mean pressure drop values over anode side (Figure 3.19a) and cathode side (Figure 3.19b). For all, an error limit is put to take in account the precision and sensitivity of the pressure sensor. For both side, serpentine shows the highest pressure head losses with a variation between 4.7 mbar to 5.7 mbar at anode side and variation between 2 to 2.4 mbar at cathode side. At higher currents (19A), a decrease in pressure head loss is observed at the anode side (Figure 3.19a). Multi-serpentine geometry gives stable and lower pressure head losses near 4.2 mbar at anode side and 1.2 mbar at cathode side. Hybrid geometry highlights the lowest pressure drop difference with stable value near 3.3 mbar at anode side. For cathode side, a value of 0.7 mbar at 4A and 0 mbar are measured. The value 0 at 19A is due to the error limit of ($\pm$ 0.7) mbar and offset precision of the pressure sensor. Hence it is assumed that with present sensor, accuracy limit it is not suitable to calculate the pressure drop limit for hybrid design at 19A. In overall, results shows that serpentine geometry has highest pressure head losses and minimum for hybrid design. Pressure head losses are lower at cathode side compared to anode side because pure oxygen (flow rate divided by two) is used. Pressure measurements here are mainly limited to single cell and a clearer picture can be provided by testing in stack considering the pressure head losses or cells having higher area.

It can be noted that serpentine although is the most traditional used geometry, suffers higher-pressure head losses and hence it directly effects the compressor power in the fuel cell stack. [Pei et al., 2016,] reviewed water fault diagnosis of PEMFC associated with pressure drop and gave useful descriptor regarding flooding or dehydration of fuel cell based upon the pressure drop information. [Grimm et al., 2012,] modelled gas flow in PEMFC channels and observed the flow pattern transitions and pressure drop through GDL.

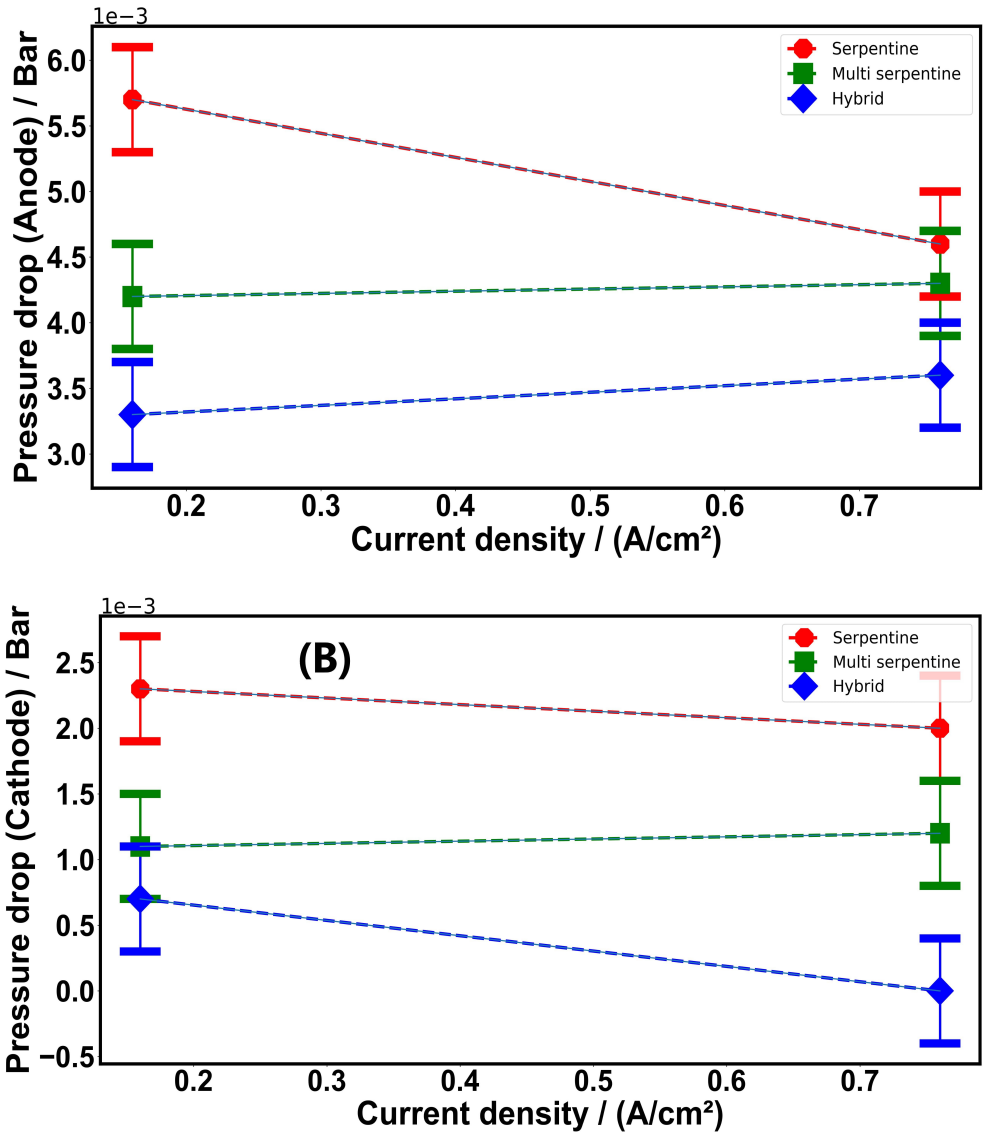

Figure 3.19: Pressure losses in the anode and cathode section of different geometries

3.12 Results considering total efficiency and power of compressor

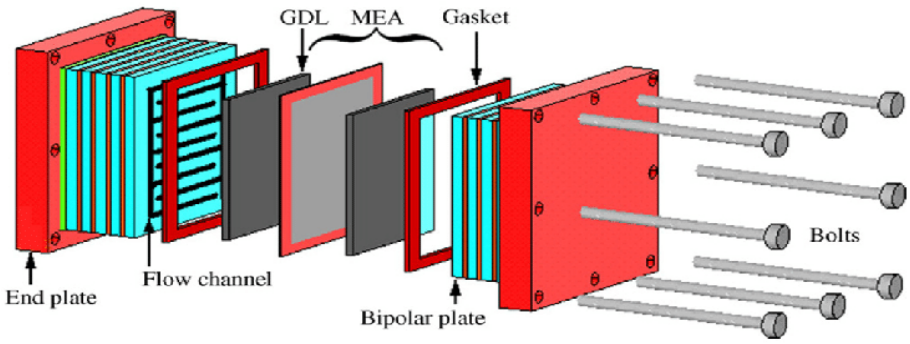

Figure 3.20: Representation of PEM fuel cell stack adopted from [Okel et al., 2008]

Figure 3.20 represents PEMFC stack which consists of bipolar plates, membrane electrode assemblies, electrodes, bolts and clamps to held the fuel cell compact. Connections for various reactants, gases and other control units are attached to make the cell work. The membrane electrode assembly helps in production of direct electricity. Bipolar plates play two important role in fuel cell stack-

1. Structural support to fuel cell

   Bipolar plates provide support to the MEA, thereby binding all the components together. A stack may consist on an average (100-200) bipolar plates stacked together depending upon the power produced in the cell.

2. Distribution of reactants

   Bipolar plates also serves the purpose to distribute the reactants in the cell, hydrogen in the anode side and oxygen/air in the cathode side. Cooling or heating water is used in the end to maintain the fuel cell temperature.

This basic unit of stack is repeated for many small cells. Maximum amount of electricity can be determined by the number of cells attached and the active area of surface producing electricity. Again current is determined by the active area of the cells and voltage is determined by number of cells it contains. For a fuel cell to perform better, there can be parameters in design part or operation. Considering the design part, it mainly consists of configuration of system and operating parameters consist of parameters required in the system[Lee and Lalk, 1998]. The various operating parameters which can effect the fuel cell performance are

1. Pressure : Pressure of fuel used in the stack
2. Temperature : Operating point of the stack
3. Humidity : The relative humidity of air or fuel entering in the stack.
4. Stoichiometry : The amount of air / oxygen or the excess fuel which can be given to the stack also determines the performance and load of the cell.

The various operating parameters which can effect the fuel cell performance [Lee and Lalk, 1998] are

1. Membrane : Type of membrane used in the system
2. Catalyst : Catalyst can severely effect the performance based on the amount or type used on each electrode.
3. Electrode : Material and type
4. MEA active area : Active area
5. Number of cells : The number of cells used in the system in order to maintain the performance.
6. Cooling fluid : Type of cooling fluid used.
7. Plate material : The material used for the plates again can effect the overall design which mainly consist of graphite bipolar plates and stainless steel bipolar plates.

3.12.1 Compressor pressure

There are many sub systems, which consumes the power of the fuel-cell. For example, a water pump may require a maximum of 8 W depending on the requirements of the stack. A stack equipped with heat exchanger may require 12 W of power, however the maximum losses can be attributed to the compressor which can go up to 65 W [Haubrock et al., 2006]. Hence, it is very important to work on compressor power efficiency. Figure 3.21 shows a general schema of various units connected with each other, motor and compressor is connected to supply manifold. After the gas is passed through supply manifold, it passes through the cooler and then to humidifier.

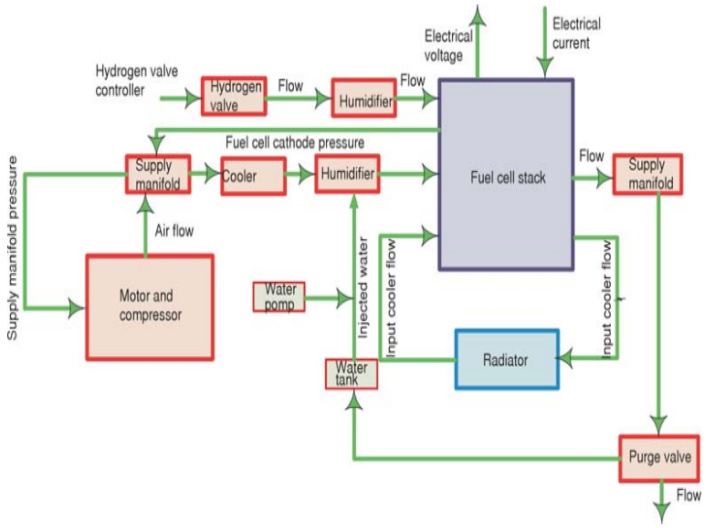

Figure 3.21: The PEM fuel cell system as adopted from [Malekbala et al., 2015]

Considering a fuel-cell system, the output power of fuel cell depends directly upon the air-mass or oxygen-mass flow of the system. Pressure and volume flow, are direct functions for air mass flow. Depending upon the operating conditions of the stack, there can be high pressure or low pressure in the system and this can effect the performance of fuel cell. Operating pressure of 300 kPa guage, increases the stack efficiency and minimizing the volume flow rate [Milburn et al., 1996]. Also high pressures are subjected to destruction of the membrane, therefore posing a risk for fuel leakage. In this present scenario, effective designs of bipolar plate with reduction in pressure drops are important as it reduces the overall pressure drop in the fuel cell system. At higher pressures, the fuel cell efficiency may decrease due to increased in energy consumption in the system.

There can be various methods to control stack pressure such as imposing back pressure at stack outlet. The pressure can be fixed with a pressure blow-off valve. Throttles can be used to achieve variable pressures resulting in low cost. However, some indirect systems can also lead to reduction in the compressor power such as improvement in flow field designs in the fuel cell system. As part of this research, to increase the overall performance in the cell, different pressure drops will be used to check the reduction in the power in the compressor. For the scope of this research, the flow rate is kept constant for all designs at specific operating conditions.

Membrane type or centrifugal type compressors can be used to supply pressurised air to fuel cell stack [Haubrock et al., 2006].The power of the compressor is given

by-

$$P_{comp} = \frac{Q_{oxygen} \times C_p \times T_c}{\eta_c \times \eta_m} \left[\frac{P_{sys}}{P_1}^{\frac{\gamma}{\gamma-1}} - 1 \right] \tag{3.1}$$

where,

1. γ is the isentropic path exponent.
2. Q_{oxygen} is the flow rate of gas input at particular current [kg/s].
3. P_1 is the suction pressure [Pa].
4. P_{sys} is the discharge pressure [Pa].
5. R is the universal gas constant $\mathrm{J}\overline{molK}$
6. M_w is the molecular weight of gas [k].
7. T_c is the temperature in Kelvin.
8. η_c is the efficiency of compressor
9. η_m is the efficiency of motor
10. P_{comp} is the power of compressor [W].

3.12.2 Calculations

Current	Serpentine	Multi-serpentine	Hybrid
4A	2.4 mbar	1.2 mbar	0.7 mbar
19A	2.1 mbar	1.3 mbar	0.7 mbar

Table 3.5: Pressure drop of different geometries at different currents from Figure 3.19 at cathode side

Temperature of the oxygen at inlet to the compressor is 20°C. Specific heat of oxygen is 918 J/Kg-K. Efficiency of compressor is 0.70 and the efficiency of motor is 0.90. Stochiometry of oxygen is fixed to 1.6. For calculation purpose, the P_{sys} of the stack is at atmospheric for single cell and is at 3 bar for 100 plates stack.

Considering the case of stack having multiple plates there is a need for a relation between the the flow rate and pressure drop. From Figure 3.22, the pressure drop is found to be in linear relation such that with increase in flow rate increases the pressure drop. Hence, for our case, considering equation (3.1) for 100 plates the flow rate will be multiplied by 100 and based on Figure 3.22, the pressure drop will be a factor of 0.77 as calculated from the slope.

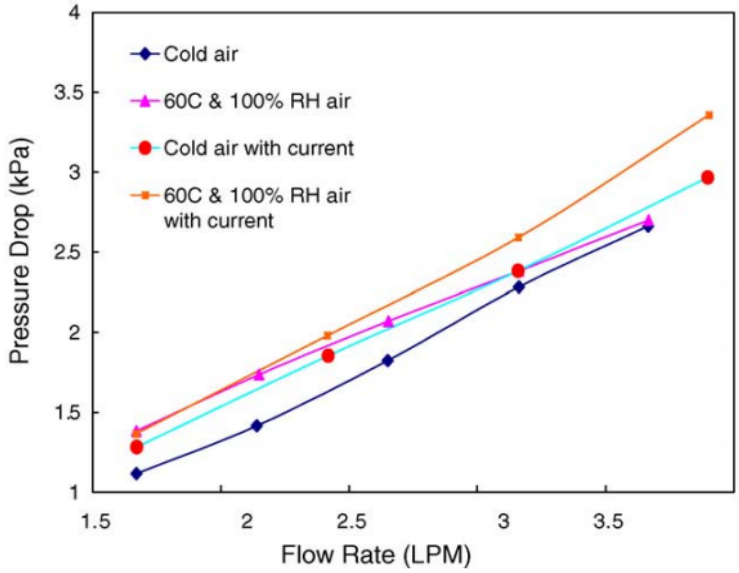

Figure 3.22: Pressure drop as a function of flow rate as adopted from [Barbir et al., 2005]

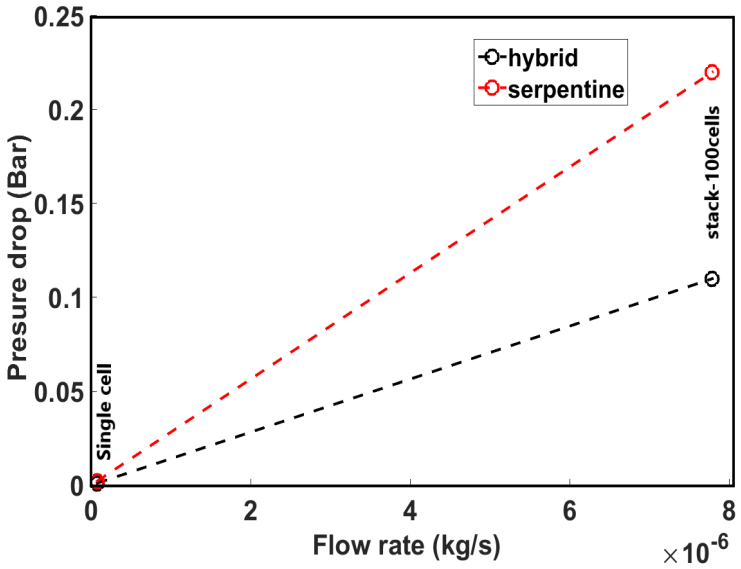

Figure 3.23: Pressure drop as a function of flow rate for hybrid and serpentine geometry

Based on the above parameters the power of the compressor is listed in Table 3.6

Power of compressor	**Serpentine**	**Multi-serpentine**	**Hybrid**
4A (Single cell)	0.091490 W	0.091455 W	0.091432 W
4A (100 plates stack)	9.71 W	9.45 W	9.28 W
19A (Single cell)	0.4345 W	0.4344 W	0.4343 W
19A (100 plates stack)	46.16 W	44.92 W	44.11 W

Table 3.6: Power develop in Watt for different designs

Considering the electrical power and the power liberated as heat, the total efficiency of the compressor is (1.82 - 2) %. However the power of compressor can vary depending upon the use of compressor and efficiency. With the different flow field designs, the total efficiency is effected as the electrical power is changed in the system. The total electrical efficiency of the stack is given in Table 3.7 based on polarization curve.

Efficiency of system (Electrical efficiency)	**Serpentine**	**Multi-serpentine**	**Hybrid**
4A (Single cell)	62.65%	63.43%	62.65%
4A (100 plates stack)	62.58%	63.39%	62.63%
19A (Single cell)	34.45%	43.07%	36.80%
19A (100 plates stack)	34.42%	43.04%	36.79%

Table 3.7: Efficiency of the entire system for various operations

3.12.3 Results and discussions

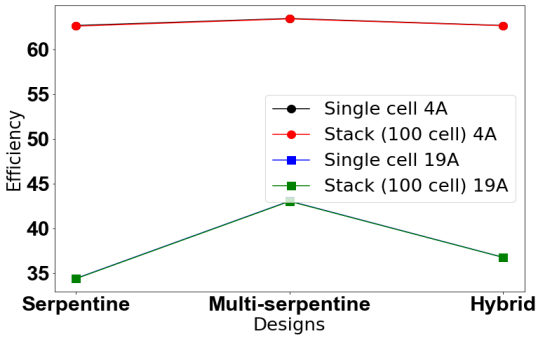

Figure 3.24: Total efficiency of the system

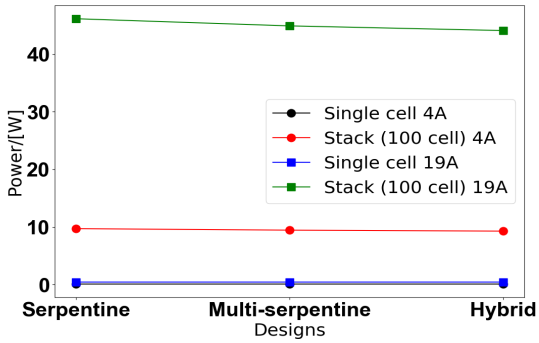

Figure 3.25: (a) Serpentine, (b) Multi-serpentine with slots, (c) Hybrid (d) Spot (e) Circular anode (f) Circular cathode

Considering Figure 3.24, where the results are plotted from Table 3.7, for single cell, the efficiency is higher for multi-serpentine, followed by similar efficiency for hybrid and serpentine design. Multi serpentine shows better performance with an increase of 1% for single cell configuration at current conditions of 4A. The compressor in this case accounts only for 2% of total power consumed and the calculations based here are on the assumption that the compressor compress the gas from atmospheric at 1.013 bar to operating conditions of the stack at 3.0 bar and to 1.0 bar for single cell. Again considering the overall power consumed by stack, 19A, multi serpentine shows superior performance then serpentine design by 8.62% and 6.25% by hybrid design. However considering conditions at lower current 4A, the results are more or less same with only 1% increase in total efficiency for multi-serpentine design.

Again considering Figure 3.25, the case of single cells not much noticeable difference can be observed in compressor power, however in a stack system, the power required by the compressor for hybrid design is the lowest at 1.86W and the highest if for serpentine design. The present calculations are only subjected to increasing the pressure of gas from atmospheric at 1.013 bar to 3 bar as required to be maintained on stacks. Hence from compressor point of view there is very little change in power savings , however from design point of view considering the electrical power there is an increase in efficiency by 6-8 %.

3.13 Conclusion

This chapter mainly deals with new designs of flow field bipolar plates and its diagnosis by polarisation tests and pressure head losses. Due to high-pressure head losses in traditional flow field design, there is always a need for new flow field geometry. Research related to flow field designs is limited mainly to numerical work with very less experiments. Hence there is a need to develop more based on reduce pressure head losses and improved performance. In this chapter, we have introduced four designs and compared 2 of them, serpentine and multi-serpentine, experimentally based on polarization curve and pressure head losses measurement. Out of all designs, multi serpentine shows superior electrical performance, Hybrid design shows improved water management compared to traditional serpentine design. Both the designs shows reduced pressure head losses compared to traditional serpentine design. In stack point of view with 100 plates our study estimates 8% of power saved compared to traditional serpentine. Overall, there is reduction in pressure head losses but for all 3 designs it does not create a big effect as compressor power accounts very less in comparison to total stack power. Designs of circular and spot are still under research and unfortunately not much analysis can be performed due to limitations in experimental results and time.

Chapter 4

Electrochemical noise analysis of PEM fuel cells with different flow field designs

4.1 Overview of electrochemical noise analysis

In this chapter, electrochemical noise analysis (ENA) and its application in the fuel cells signals will be discussed and analysed. The main aim is to understand ENA as a diagnosis tool for understanding of water management. In the upcoming sections results of ENA, are analysed with respect to the flow field designs, relative humidity and the current applied.

4.1.1 History and generality of electrochemical noise analysis

Traditionally the electrochemical studies in particular are oriented towards diagnosis or prognosis of fuel cells and use of conventional electrochemical techniques, such as polarization curve, current interruption technique and impedance measurements. These studies allows to characterize performance, durability and design impacts on fuel cells working. Noise measurements are becoming popular and have been used quiet long in corrosion studies[Bertocci et al., 1998, Hladky and Dawson, 1982,]. [Bertocci et al., 1998,] have used noise measurements on several corroding systems by simultaneously recording the current and voltage fluctuations. To analyse in-situ water distribution, methods such as neutron imaging, x-ray, electron microscopy or optical photography are often used ([Cochet et al., 2018,], [Meyer et al., 2016,], [Ge et al., 2019,]). These techniques gives detailed view to understand more clearly the physics within the system but are expensive to carry out in a practical point of view. In this study, in addition to polarization curve analysis and pressure losses measurements, an additional approach named Electrochemical Noise Analysis (ENA) is used. This approach is based on by recording and analysing fluctuations of fuel cell parameters as voltage and pressure. This approach do not require using of costly instruments, easy to set anywhere. This technique can be used upon any size of fuel cell and can give more faster results in varying conditions of fuel cell. ENA can be an important tool to understand the flooding and drying behaviour of fuel cell [Maizia et al., 2017,], [Dib et al., 2019,]. [Maizia et al., 2017,

] have used ENA for studying, flooding, to check accumulation or poor removal of water in the cell. [Mortazavi et al., 2018,] worked with similar approach to understand the liquid gas two-phase flow pressure drops in ex-situ fuel cell setup. The aim of the work was to understand pressure drop signatures with different flow rate within a flow channel. [Mishima and Hibiki, 1996,] developed a study to understand flow regime, void fraction, and velocity rise of slug bubbles in capillary tube with inner diameters ranging from 1 to 4 mm. [Mansfeld et al., 2001,] evaluated coating degradation with electrochemical impedance spectroscopy and electrochemical noise analysis on cold rolled steel. [Huet, 1998] worked on impedance measurements for determination of the state of charge or health of secondary batteries. [Martemianov et al., 2015,] worked on similar methodology of noise analysis and application for commercial Li-ion batteries. [Baert and Vervaet, 2003,] worked on noise voltage of batteries. [Gabrielli et al., 1986,] developed model of the stochastic behaviour of electrochemical interface governed by chemical or electrochemical reactions. [Rubio et al., 2016,] studied PEMFC failure mode of earlier diagnosis with wavelet analysis by electrochemical noise. In some cases, analysis of electrochemical noise, shows a drift in signal which can be due to low frequency components of signal. [Bertocci et al., 1998,] analysed and discussed various drift removal procedures. [Huet et al., 2004] worked on oxygen evolution on electrodes of different roughness with electrochemical noise analysis. Electrochemical noise analysis as a tool is used in many studies to explore the irregularities and possibilities of defects ([Lee and Bae, 2012,], [Searson and Dawson, 1988,], [Mansfeld and Lee, 1997,]).

The aim of the present work is to use ENA for study of new flow field design and water management of fuel cells. ENA will be performed by use of temporal descriptor as standard deviation (STD) as well as descriptors in frequency domain (Power spectral density). This will help, qualitatively and quantitatively, to understand the designs impacts with respect to water removal.

4.2 Signals and data treatment procedure

In order to use ENA, it is important to understand the type of signal recorded at the output. If the signals is deterministic, it solves the major problem, however if the signal is stochastic, suitable procedures for signal treatment and analysis should be used. The goal of these data treatment procedures is generation of statistical descriptors which can be used for characterization of statistical systems. In order to analyse the flow field designs, stochastic signals are discussed here. The physical origin of these fluctuations is related with mass transfer processes and water management in fuel cells. Study have been done earlier by [Maizia et al., 2018] who used similar technique to understand the drying and flooding behavior of fuel cell.

4.2.1 Different ways for generation of noise descriptors

There can be different methods in order to characterize signals for examples histograms, signal visualised in time domain, frequency domain or time-frequency domain.

1. **Histograms**- A histogram is a representation of distribution of numerical data. Considering the Figure 4.1, it explains about different range of voltage

values obtained. The histogram is obtained using matplotlib library in python.

A histogram is a graphical display of data using bars of different length where numbers represented in bar length represents minumum to maximum values. Histogram in signal processing, explains about the different range of voltage value obtained. For the present calculations, matplotlib library is used from Python. Figure 4.1 shows a normal distribution of the voltage signal at 19A. This histogram is plotted from signal in Figure 4.2.

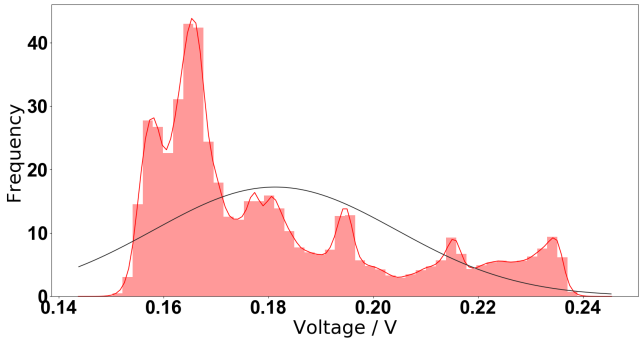

Figure 4.1: Normal distribution of voltage signal at 19A

2. **Statistical tools in time domain**

Visualising signals in time domain is another such method where the signal evolution is plotted with respect to time. Much useful information considering the nature of signal where stationary or non-stationary behavior can be visualised. Figure 4.2 shows a time domain signal.

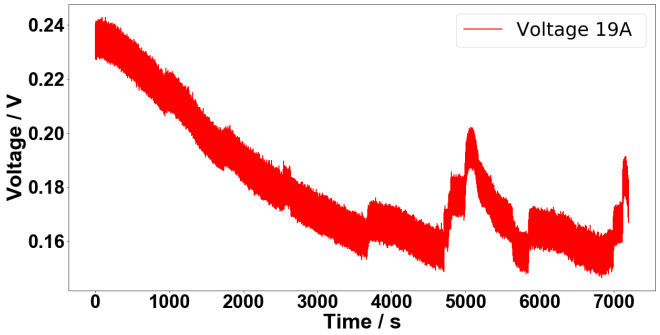

Figure 4.2: Time distribution of voltage signal at 19A

Traditional statistical descriptors in time domain are the following-

(a) **Mean value of signal**

Mean can be defined as the sum of the values divided by the length of values. A signal has fluctuation and it is important to understand a mean value to the signal.

$$\frac{\sum_X}{N} = \bar{x} \tag{4.1}$$

where n is the number of elements.

(b) **Standard deviation of signal**

Standard deviation can give an amount of variation or dispersion of values of a signal. Dispersion in other words can help to understand the appearance of signal, a low value means that values tends to be close to the mean of the signal and on the other hand a high value means the values are dispersed away from the mean.

$$\frac{\sum(X_i - \mu)^2}{N} = \sigma \tag{4.2}$$

(c) **Skewness of signal**

Skewness can be defined as measure of symmetry. This can give more characteristic about data, type of data, its distribution. For data considering $x_1, x_2, x_3 \ldots\ldots x_n$, skewness can be formulated as

$$\frac{\sum_{i=1}^{N}(x_i - \bar{x})^3}{N \times \sigma^3} \tag{4.3}$$

where $\bar{x}$ is the mean , N is the length of data points, σ is the standard deviation. The formula is referred as Fisher-Pearson coefficient of skewness.

Skewness can also be defined as

$$skewness = 3(\bar{x}) - \sigma(m) \tag{4.4}$$

where σ is the standard deviation and m is the median. For centred distribution, the median is the mean. And hence distributions have zero skewness. Considering the output, since skewness defines the measure of symmetry, for a data with normal distribution the skewness is 0. Any data symmetric about the values has zero skewness. A negative skewness shows the data is skewed to left and positive values of skewness shows data skewed to right.

(d) **Kurtosis of signal**

Kurtosis (Figure 4.3) can be defined as relation between centered moment of order 4 and order 2, precisely it can be defined as the peak of the distribution.

$$\frac{\sum_{i=1}^{N}(x_i - \bar{x})^4}{N \times \sigma^4} \tag{4.5}$$

Kurtosis can be further defined as –

i. Mesokurtic – It can be defined as a normal distribution with kurtosis value of 3 and they are more skewed outside.
ii. Leptokurtic – Distributions with kurtosis > 3 and they are more skewed inside.
iii. Platykurtic - Distributions with kurtosis < 3 are called platykurtic.

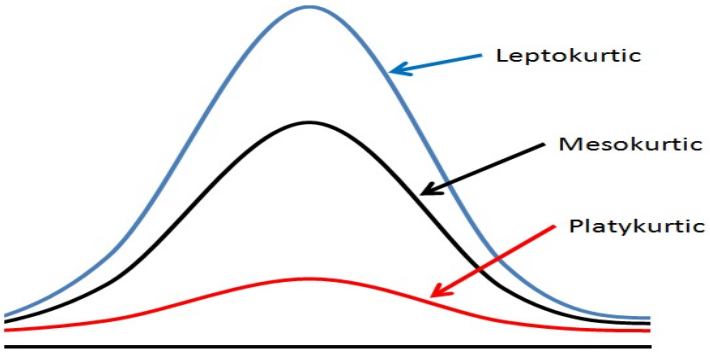

Figure 4.3: Types of kurtosis

3. **Frequency domain** Frequency domain is another such descriptor where the signal can be analysed through frequency components. Power spectral density can be estimated in order to know about the energy contained inside the signal. Figure 4.4 shows signal in frequency domain.

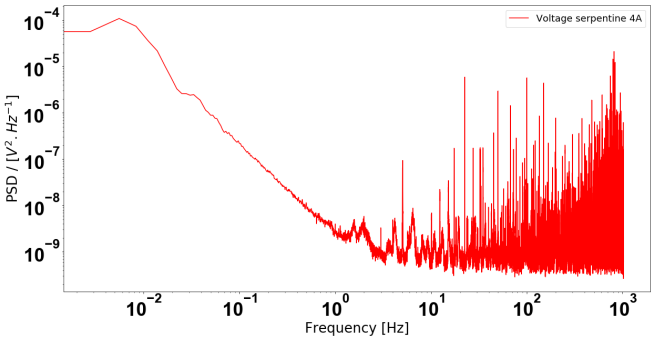

Figure 4.4: Voltage signal in frequency domain

4. **Time -frequency domain** Time frequency domain [Trebino et al., 1997, Gu and Bollen, 2000] is another category of signal visualization which comprises techniques to study signals in both time and frequency domain simultaneously. The main interest behind visualization of signals in time and frequency domain is to study the type and their transforms as they are tightly connected in both time and frequency. However for the scope of this research time frequency signals are not discussed.

4.2.2 Stationary property of signal

Visualization of the signals, as discussed in previous section can give details about stationarity of signals and hence it becomes important to understand the types of stationarity. Signals needs to be stationary which means statistical properties of signal do not change over time. With statistical properties being stationary means, it can show a trend which can be measured. For example, a constant slope or a linear slope of a signal. Stationary signals do not signify a straight line but a pattern or linearity in its structure.

1. **Strong stationarity** A signal is termed as strong stationarity if the distribution of any sub defined, finite sequence of number of points in random order shifted along time axis remains same. This can be done for any number for finite sequence of points and results remain same. This also implies that all the statistical properties are constant if there is modification or shift along the time. Considering the discrete stochastic process $X = (x_i; i \in Z)$ is stationary only if

   $F_X(x_{t_{1+\tau}}, ..., x_{t_{n+\tau}}) = F_X(x_{t_1}, ..., x_{t_n})$ for $T \subset Z$ with $n \in N$ and any $\tau \in Z$ [Maickel et al., 1968,]

2. **Weak stationarity** For a signal to show weak stationarity, it means the distribution of finite points in random location will not be same along the time axis.

4.3 Noise methodology

In order to proceed for the analysis of the signal it is very important to develop a methodology and remove any trends, outliers in the signal which may create a problem of poor results of less information. In this section two methodologies are initiated and discussed in subsequent section of this chapter both in time and frequency domain.

1. Noise methodology in time domain

   In order to analyse signals in time domain, it is important to remove trends, outliers which can change the nature of signals and may provide with poor analysis. Considering the time domain, detrending , window sizing is discussed in details in order to perform statistical analysis on the signal.

2. Noise methodology in frequency domain

   As the electrochemical noise is verified in time domain, it is also verified in frequency domain in section 4.8 to make sure that the bench noise is comparatively less then the electrochemical noise to proceed. All the information and procedures are discussed in section of 4.8.

Now in order to overcome this difficulty signal needs to be stationary and there is a solution proposed by mathematicians to incorporate stationary on short term basis. It goes by dividing the signal into small parts or time windows, where we can observe the desire stationarity. So, a signal is cut into n equal parts and different techniques are used to analyse the signal. Using n=1, makes no sense and by doing so, this not only decreases the speed to run the code but this method of linearity loses its prime aspect of making the signals stationary, no statistical analysis can be performed.

In order to proceed, the time window should not be too small as it can induce large calculation time and should not be too large, that again important information is missed out. In order to work with stationary signals, it is important to remove the trends in the signal. A trend can be in any direction and hence needed to be removed. Several techniques are discussed further to define detrending techniques in section 4.3.1 and specific time window in section 4.3.2

4.3.1 Signal detrending procedure

Time varying trends can contain useful information on the evaluation of signal which can show both slow (low-frequency) variations and fast (high frequency) variations. In order to understand the electrochemical signal, it is important to detrend signal function therefore isolating noise. Detrending as a tool in parts have been used to remove trends in electrochemical noise [Maes et al., 2017, Smulko et al., 2019, Mansfeld et al., 2001,].

There can be three types of fit depending upon the signal

1. **Constant fit**

   Figure 4.5, shows a random signal and its detrended signal with constant mode. This is an arbitrarily generated signal. As seen from the Figure 4.5 the signal is detrended by constant mode, which means only the mean is subtracted from the original signal. The mean reported from the calculations of original signal is 31 and the mean of detrended signal is 7.27×10^{-15} which is approaching to 0.

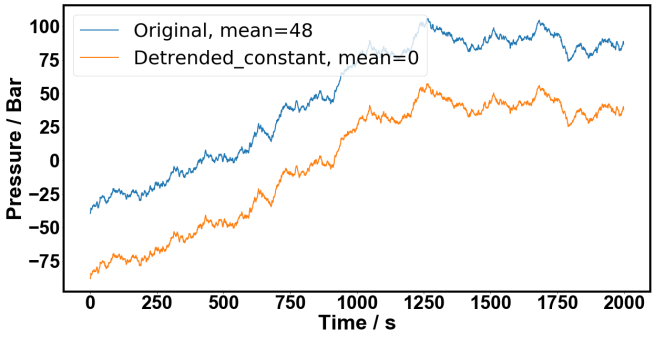

Figure 4.5: Constant fitting

2. **Linear fit**

   Figure 4.6, shows a random signal and detrended signal with linear mode. This is an arbitrarily generated signal.The idea is to fit a line in the data series and subtract that line from the original signal. As seen from the Figure 4.6 the signal is detrended by linear mode, and only the fluctuations are left. All local fluctuations are same exactly but the global trend is now removed. The mean reported from the calculations of original signal is -8 and the mean of detrended signal is -1.13×10^{-14} which is approaching to 0.

3. **Polynomial fit (Higher order)**

   Polynomial fit comes into play when the artifacts or the drifts cannot be removed by linear mode. When higher orders are required to completely remove noise from the signal. Consider the Figure 4.7, a polynomial generated signal with order of 3. Linear fit cannot remove these trends, hence polynomial fit of various order is chosen and and applied to remove trends 4.8.

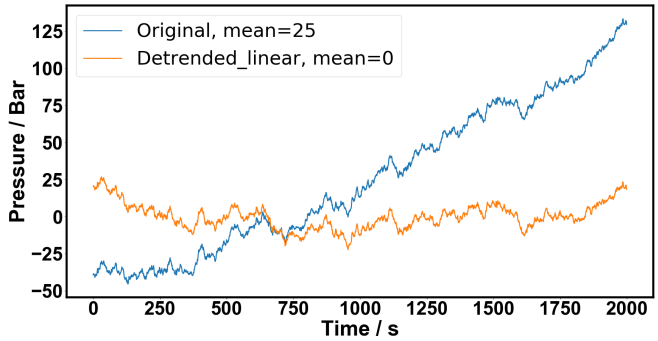

Figure 4.6: Linear fitting

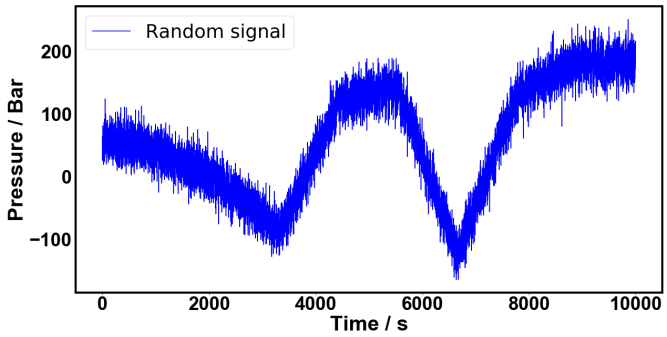

Figure 4.7: Polynomial fitting

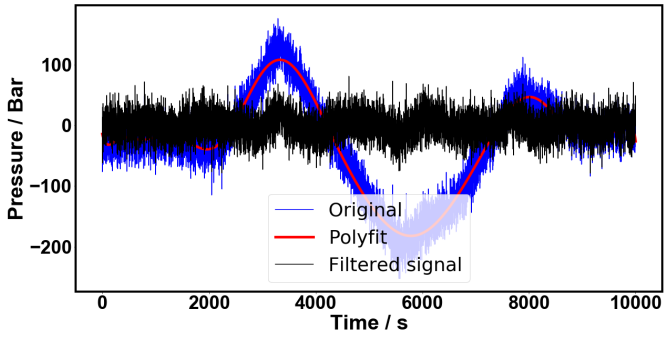

Figure 4.8: Sample signal with polynomial fit

Up to now, there has been no problem in detrending signals as the above signal created are with a defined polynomial order, but what happens when the signal order is unknown ? or the signal is highly non- stationary? At this point, it is advisable to break the signals in to small time windows if the sole purpose is to analyse the standard deviation(STD) or power spectral density(PSD).

In order to study and apply stationary methods, in the present work, signal is detrended with a linear polynomial in python SciPy module. For that, the 2 hours signal (7200 seconds) is broken down to 200 seconds windows (36 parts) and then an individual linear fit is performed for each part of data between two break points.

Linear mode calculates the linear least-squares fit to data and subtracts from data in the given time window. Figure 4.9 shows the evolution of voltage signal at 19 A (0.76 A/cm^2) and detrended signal for serpentine design. The voltage decreases from 0.25V to 0.15 V for the first 4800 seconds, some peaks until 0.20 V appears for a period of about 1000 s. From Figure 4.9, after applying linear detrend procedure, it removes certain trend, however some form of fluctuations especially for the peaks remains. Sure, the number of parts and the order of polynomial impact the detrend procedure [Smulko et al., 2019,]. To see the impact of detrend procedure some comparison has been made in the next section.

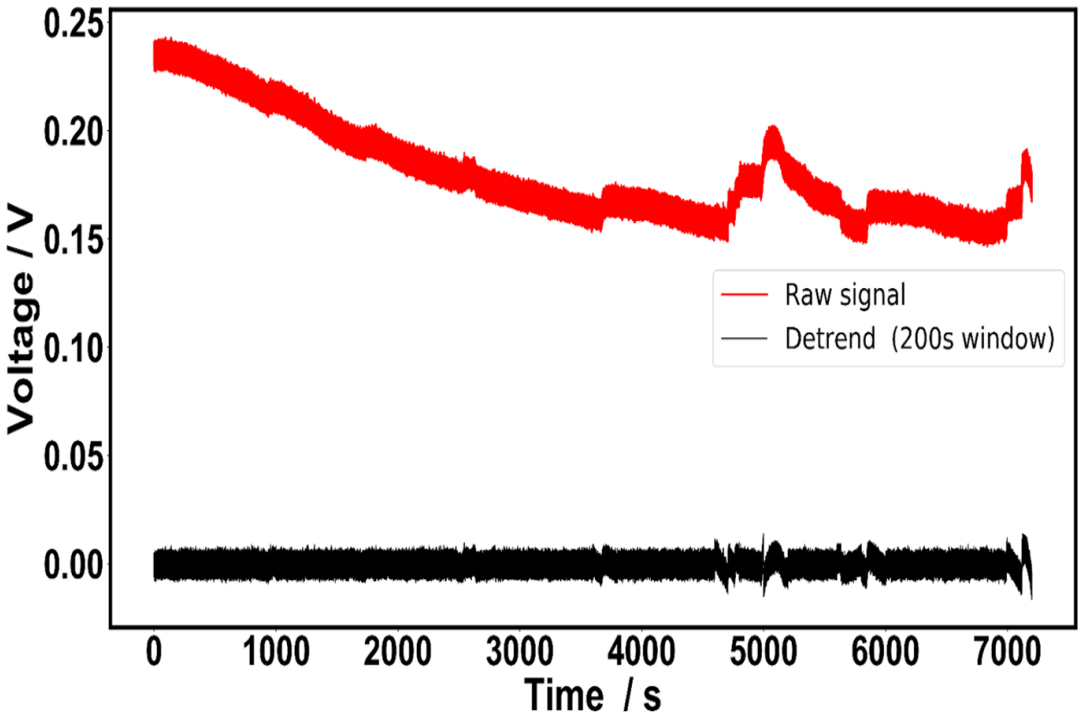

Figure 4.9: Evolution of voltage signal at 19A and detrend signal of serpentine design

After trends have been removed from the signal, it is important to work on the time window chosen, in order to apply statistical tools on the signal and this has been explained in section 4.3.2.

4.3.2 Time window comparison

Working with electrochemical noise is mainly working with stochastic signals, which have no preferred outcome, or which cannot be determined. It becomes important to analyse the signal while breaking into stationary points and choosing an appropriate time window. Indeed, electrochemical noise has a problem related to the non-stationary character of the signal [Xia and Behnamian, 2015, Bahrami et al., 2014,]. One of the possibilities to solve this problem is using short-time analysis [Maizia et al., 2018, Aballe et al., 1999,].

The same procedure of short-time analysis in previous work [Maizia et al., 2018,] is followed in this work, to guarantee the stability and relevance of the signal

detrending. Four size of time windows have been tested (18, 72, 200 and 400s) that are divided respectively in 400, 100, 36 and 18 parts. As an adapted filter, the choice of the size of windows can allow to filter the low frequency or high frequency part of the signal, depending of your time constant length. The more smaller the time windows, the more you cut your low frequency (as an high-pass filter). If your system has a long time constant it is preferable to use large time windows.

Figure 4.10 highlights the effect of the size of time window on the detrending of the signal. The same signal of voltage fluctuations at 19A, for serpentine design recorded during 7200s as Figure 4.9 is used for the comparison. It can be seen Figure 4.10(a) that when a 400s time window is used, some large fluctuations is always apparent near 5000 and 7000 seconds, corresponding to the large peaks on the raw signal figure 4.9. When the size of the time window is reduced to 200s the peaks influence decreases, but large fluctuation remains on the detrended signal. From the time window size of 36s and after 18s, no large fluctuations are noticeable on the detrended signal, due to higher filtering of the signal when smaller windows are used. Figure 4.10(b) shows the comparison of the four detrend signals with time windows of 400s, 200s, 72s and 18s. It is clear that all the signals are centred at 0V. STD evaluation (Figure 4.10(c)) highlights this behaviour and reveals large peaks between 4mV and 5 mV near 5000s, 5700s and 7200s. For the time windows of 72s, STD peaks are lower except at 7200s. For the time windows of 18s, this time windows size is small and a flat evolution of STD is obtained. Because in this research, ENA will be evaluated, thanks to the evolution of STD with time for the three different design and the aim is to track the effect of the design on water management. 200s tie window is chosen to detrend the signal, to not eliminate completely the presence of low frequency peaks information on the signals.

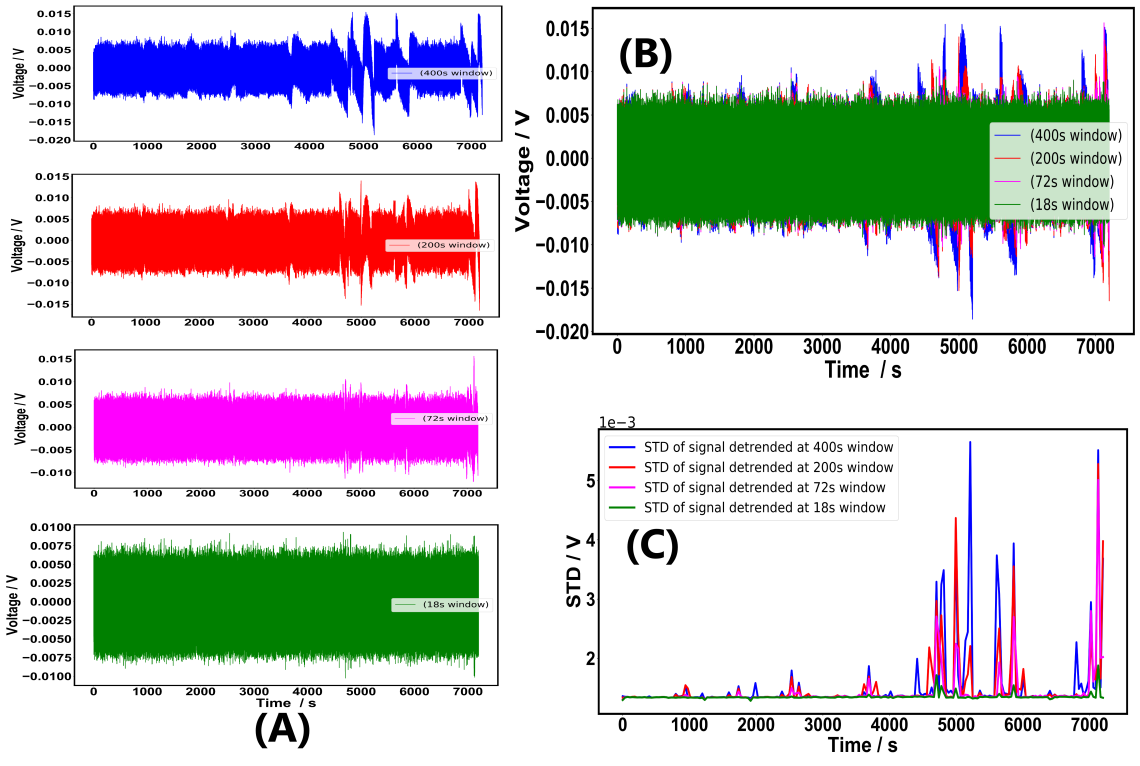

Figure 4.10: Time window comparison

It can be precised that for all STD calculations presented in Figure 4.10(c), a window of 36s seconds was chosen. There are two steps to calculate STD in our procedure. First, the signal is detrended by choosing size of time window and applying a linear polynomial to subtract the mean value from the raw signal. And secondly, the STD is calculated on the detrended signal choosing an appropriate window.

Figure 4.11 highlights the influence of the window on STD estimation for the 200s. Four value of windows is chosen to calculate STD, 18s, 36s, 72s and 200s. It can be noted that when a window of 200s is chosen, only few values (36 exactly) of STD are calculated. If the time of the windows is decreased to 72, 36, 18 richer information and more peaks with higher values appear, especially where low-frequency peaks are present within the raw signal (near 5000, 6000 and 7200 s – Figure 4.10(a)). The choice of the size of the time windows to calculate the STD must be done on a stability criterion (can be relative). Regarding Figure 4.11, a windows size of 36s is chosen to calculate the STD evolution with time for all results presented in upcoming section. The time windows of 36 seconds provided, in our point of view, the most relevant information on standard deviation (STD) of the measured signals that linked to the intensity of the signals.

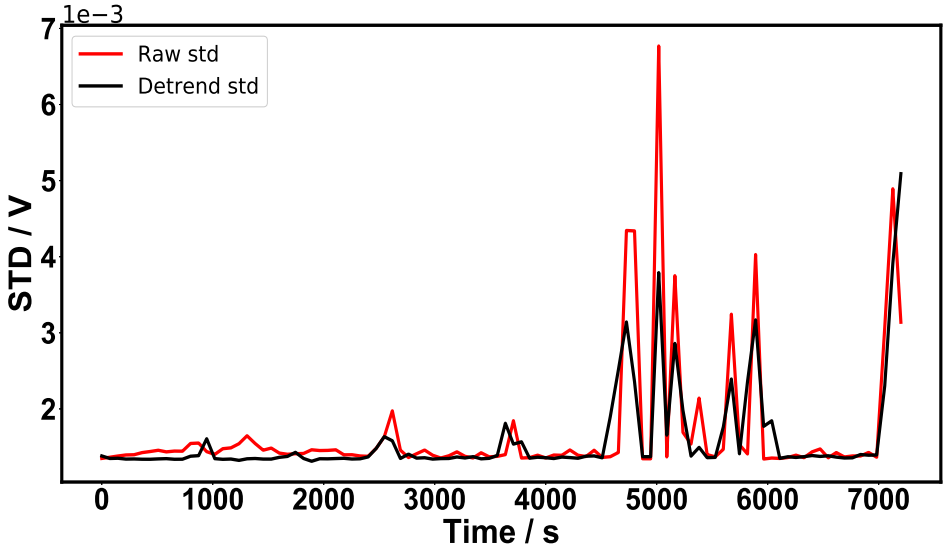

Figure 4.11: Standard deviation on detrend and original signal

4.3.3 Apparatus noise

In order to characterize electrochemical noise of fuel cell, it is important to estimate the intrinsic noise of experimental setup, on the basis of magnitude of energy (intensity) of signals captured Figure 4.13(a). National instrument NI 9234 is used to record signals (Figure 4.12). Hence, in order to differentiate the noise of bench and the electrochemical noise of fuel cell working, measurements have been performed with fuel cell ON and OFF conditions. The data recorded shows peak to peak voltage of 40 mV for the fuel cell ON Figure 4.13(b) and 4 mV for the fuel cell OFF Figure 4.13(c) condition which is roughly 10 times higher. This confirms that the fuel cell noise can be measured by our acquisition system with enough intensity.

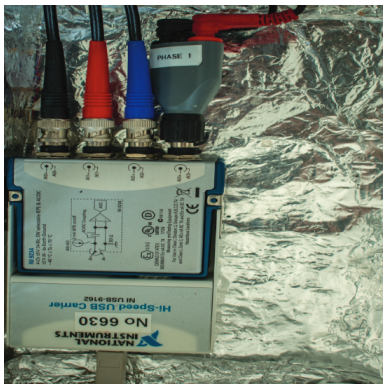

Figure 4.12: National instrument NI box required to record signals.

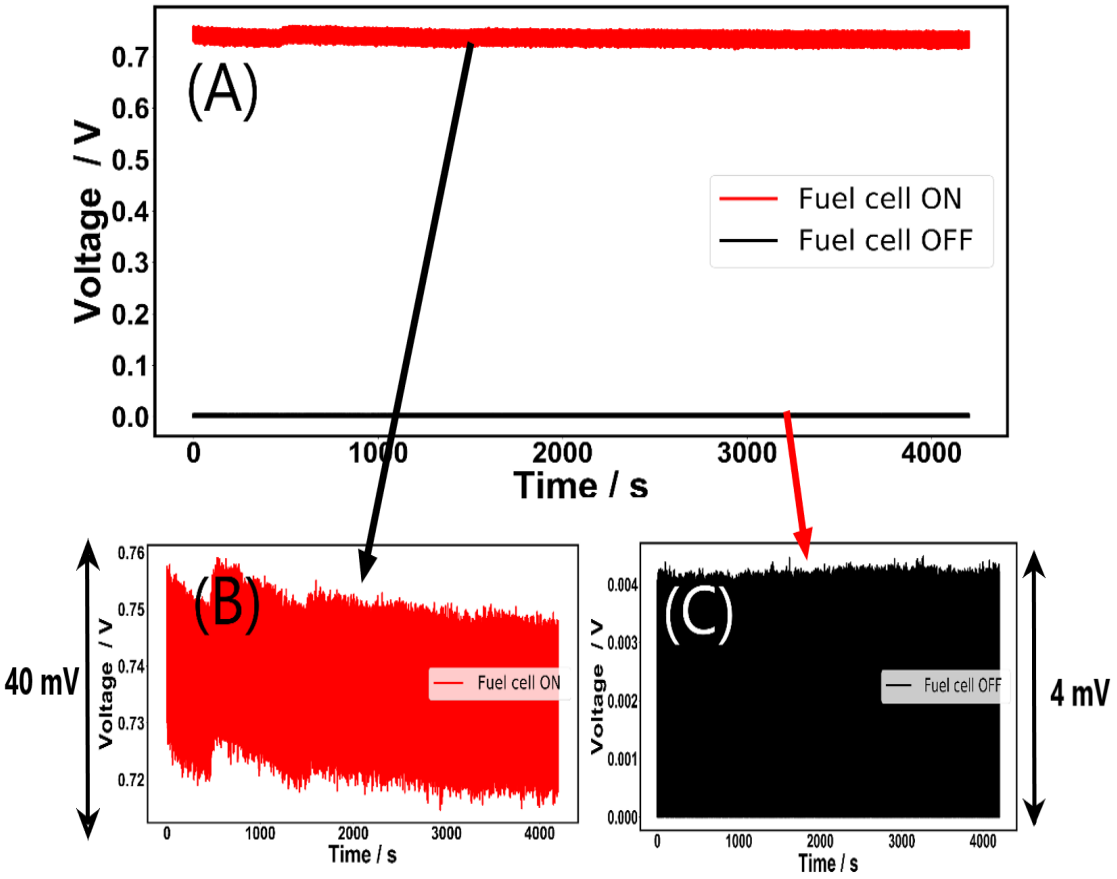

Figure 4.13: (a) Evolution of voltage fluctuation of fuel cell running (ON) and bench noise without any reactants (OFF). Enlarged version and their magnitude of (b) fuel cell voltage at 4 A (0.16 A/cm^2) (c) bench noise.

4.4 Signal characterization using histograms

Apart from short time analysis, checking normal distribution of data can be helpful as statistics test rely on this. However datasets with bigger observations do not pose much risk but still sorting out normality issues can help to identify outliers in the problem. An outlier is an observation that lies at an abnormal distance from

other values in a random sample. How outliers can be helpful in analysis of data set of PEMFC ? Outliers can be values at which the running fuel cell voltage drops to zero. Now such a low voltage stands out in the data distribution and can make errors in the data treatment. But side by side also gives the state of art of the fuel cell and provide strong diagnostic analysis on the fuel cell. In this particular section normal distribution of voltage signal is plotted with normal probability plots. In normal probability plots, data or observations should closely follow the diagonal that represents the normal distribution. In this section, it will be emphasised how the detrending procedure will change the normal distributions in the plot.

4.4.1 Histograms

In the present section histograms of signals are analysed.

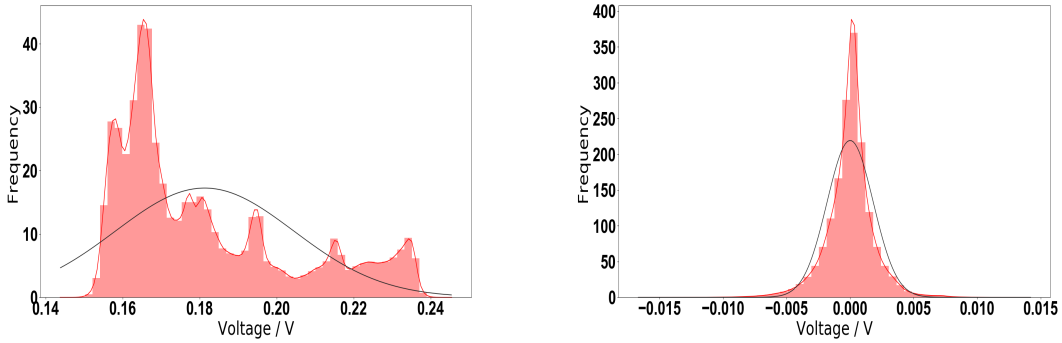

(a) Serpentine 19A without detrend (b) Serpentine 19A with detrend

Figure 4.14: Normal distribution plots (Serpentine) (a) 19A (without detrend) (b) 19A (with detrend)

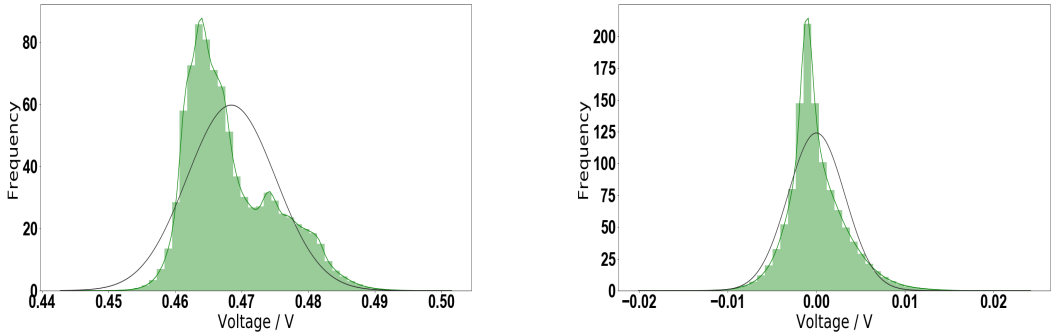

(a) Multi serpentine 19A without detrend (b) Multi serpentine 19A with detrend

Figure 4.15: Normal distribution plots (Multi serpentine) (a) 19A (without detrend) (b) 19A (with detrend)

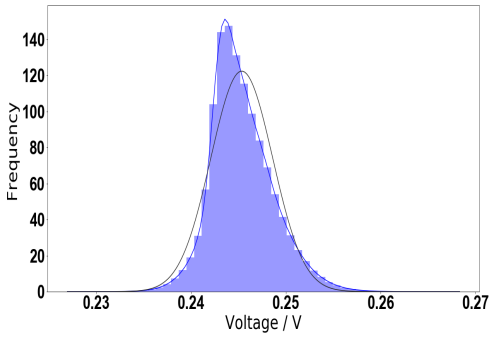

(a) Hybrid 19A without detrend

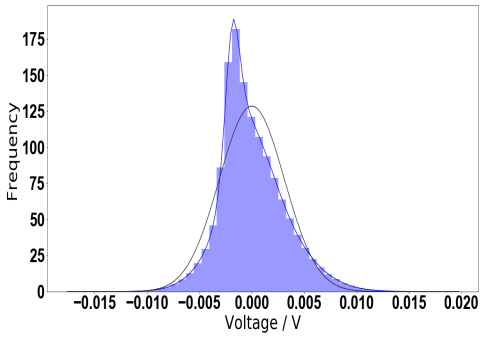

(b) Hybrid 19A with detrend

Figure 4.16: Normal distribution plots (Hybrid) (a) 19A (without detrend) (b) 19A (with detrend)

Section 4.4.1 represents normal distribution plots. Histogram plots helps to visualize distribution of data They show the effect, how detrend procedure effects the data treatment. As it is observed from plots of normal distribution in Figures (4.14(a), 4.15(a) serpentine and multi serpentine data is not only highly skewed but is not normal. After applying detrending, data is normalised (4.14(b), 4.15(b) and 4.16(b).

4.4.2 Probability normal distribution

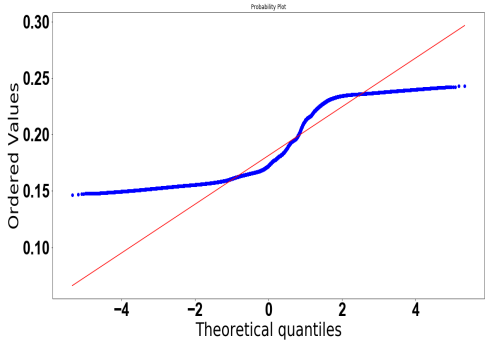

(a) Serpentine 19A without detrend

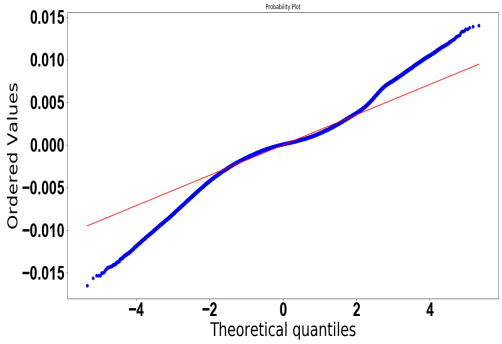

(b) Serpentine 19A with detrend

Figure 4.17: Normal distribution plots (Serpentine) (a) 19A (without detrend) (b) 19A (with detrend)

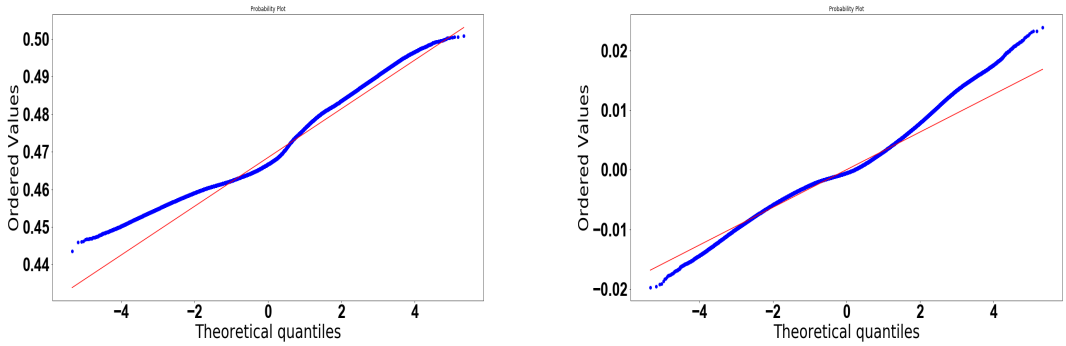

(a) Multi serpentine 19A without detrend (b) Multi serpentine 19A with detrend

Figure 4.18: Normal distribution plots (Multi serpentine) (a) 19A (without detrend) (b) 19A (with detrend)

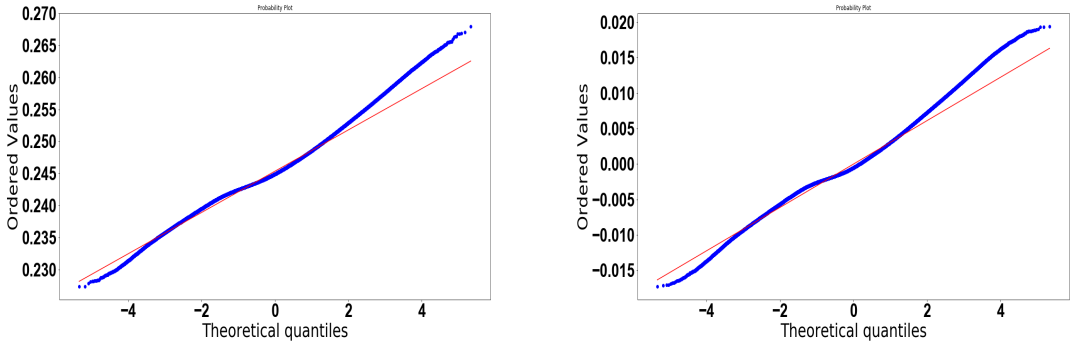

(a) Hybrid 19A without detrend (b) Hybrid 19A with detrend

Figure 4.19: Normal distribution plots (Hybrid) (a) 19A (without detrend) (b) 19A (with detrend)

Section 4.4.2 represents probability normal distributions plots. While histogram plots helps to visualize distribution of data, probability plot calculates a best-fit line for the data and plots the results using Matplotlib. They show the effect, how detrend procedure effects the data treatment. Moreover, a very small window of detrending with a very small time window will make the data perfectly normal and a very large time window will show no effect. From Figures 4.17, 4.18 and 4.19 no noticeable effect of outlier can be observed. and it does not follow the diagonal line in Figures (4.17(a), 4.18(a)). For case in Figures (4.16(a), 4.19(a)) data for hybrid data is normal and most of the points lie on diagonal line both before and after the detrend procedure. Based upon this, it can be explained that the irregularities in serpentine are more compared to multi serpentine and is the least for hybrid design.

4.5 Application of ENA to understanding water management in PEM fuel cells designs

In next paragraphs, ENA will be used to understand water management within PEM fuel cells. For this analysis we do not study all the parameters which can

influence water management. We have put our attention on the parameters which have not yet been studied in the literature, normally on different flow field designs of bipolar plates.

Also, we have studied two operational points I = 4A and I = 19A. The point of I =4A corresponds to kinetic regime and the point of I = 19A reflects mainly the situation where mass transport limitations become important. The influence of humidification has also been studied for serpentine, multi-serpentine and hybrid at 50 % and 100%. For the other two designs mainly spot and circular, operational point of 4A is chosen due to time limitations. In order to use ENA, Raw signal visualization in time domain , descriptors in frequency domain(PSD) are used. The designs are listed in Figure 4.20.

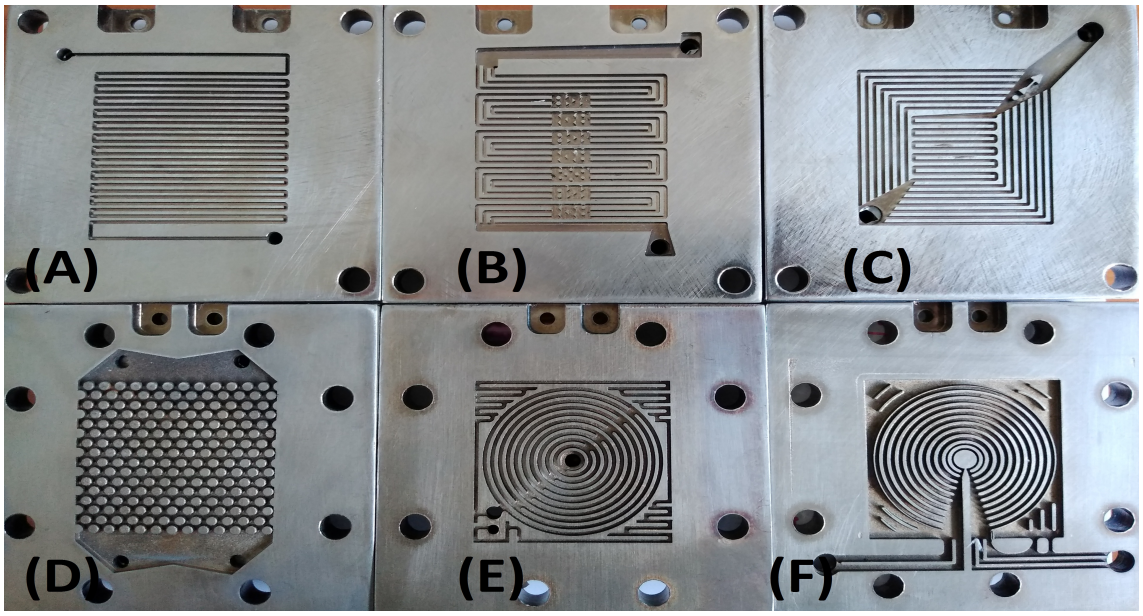

Figure 4.20: (a) Serpentine, (b) Multi-serpentine with slots, (c) Hybrid (d) Spot (e) Circular anode (f) Circular cathode

4.6 Raw signal visualization in time domain

Visualization of signals in time domain helps to understand qualitatively the main signal characteristics. This can give important information considering the trend in the signals, the outliers (Points in signal which behave abnormally, such as a signal of 0.8V, if has a potential drop to 0, has a point 0 as an outlier.) present in the signal. Moreover visualization of signals in time domain helps to estimate the stationarity of the process, thereby opening a way to eliminate irregularities of the measurements.

4.6.1 Signal visualization for serpentine design

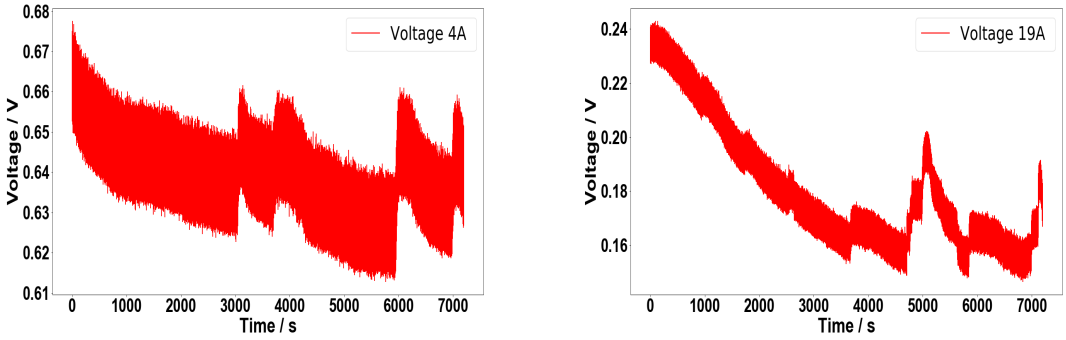

(a) voltage 4A (b) voltage 19A

Figure 4.21: Raw voltage signal(Serpentine) (a) 4A (b) 19A

Figure 4.21(a and b) shows visualization of voltage signals in time domain for serpentine design for two currents. Voltage fluctuations at 4A are recorded for situation where kinetic effects are predominant, Figure 4.21(a). On other hand, at 19A, mass transport effects play an important role. Both the signals lack stationarity through out the time span of 2 hours and it becomes important to use detrending techniques. No critical outlier is observed, however both signals shows drift during major time span.

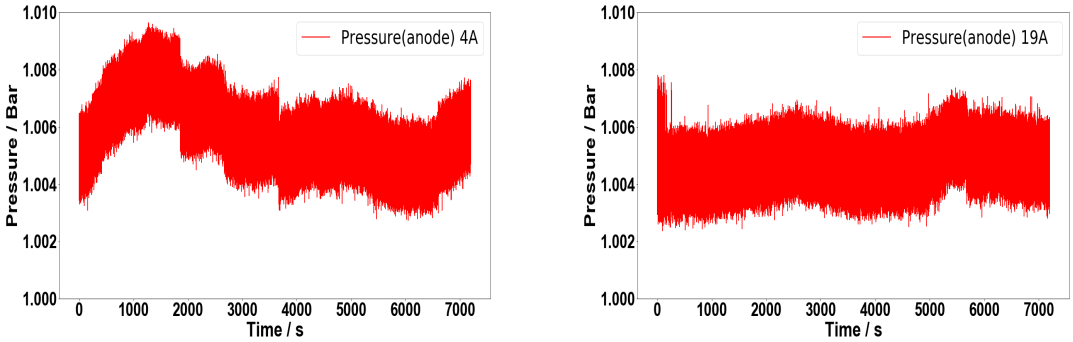

(a) pressure anode 4A (b) pressure anode 19A

Figure 4.22: Raw pressure (anode) signal(Serpentine) (a) 4A (b) 19A

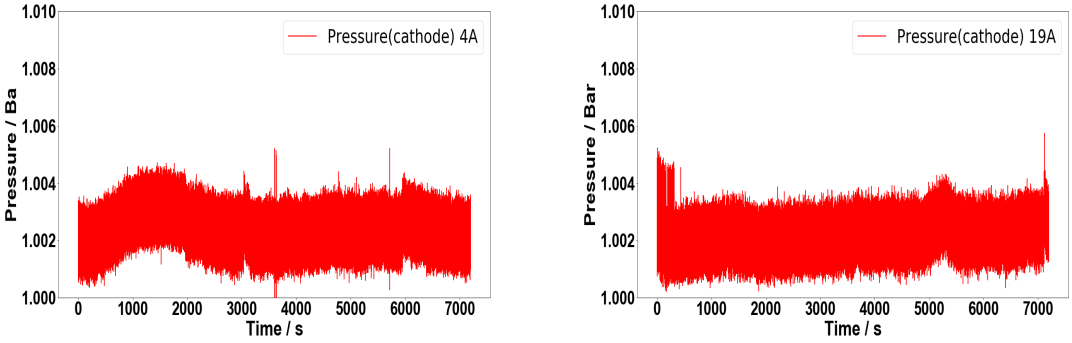

(a) pressure cathode 4A (b) pressure cathode 19A

Figure 4.23: Raw pressure (cathode) signal(Serpentine) (a) 4A (b) 19A

Figure 4.22 and 4.22 presents visualization of pressure signals. Almost all the signals shows stationary behavior, however some irregularities can be observed in 4.23(a) where pressure is found to fluctuate from 1.004 bar to 1.01 bar.

4.6.2 Signal visualization for multi serpentine design

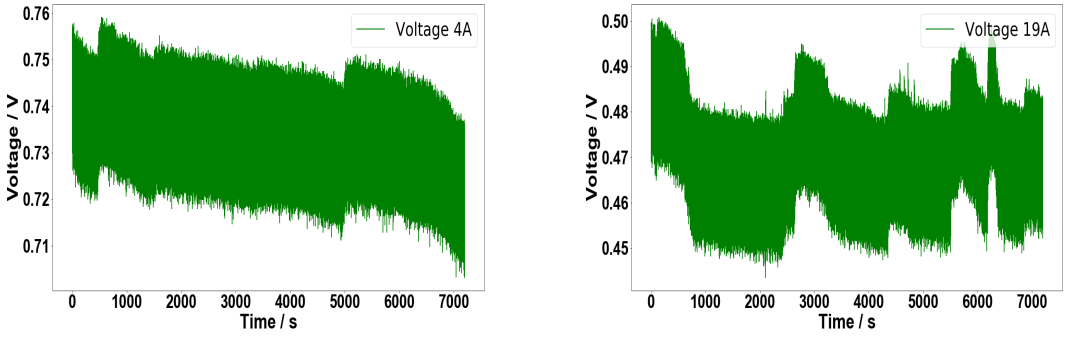

(a) voltage 4A (b) voltage 19A

Figure 4.24: Raw voltage signal(Multi serpentine) (a) 4A (b) 19A

Figure 4.24(a and b) shows visualization of voltage signals in time domain for multi-serpentine design for two currents. Voltage fluctuations at 4A are recorded for situation where kinetic effects are predominant, Figure 4.24(a). On other hand, at 19A, mass transport effects play an important role. Both the signals lack stationarity through out the entire time span of 2 hours and it becomes important to use detrending techniques. No critical outlier is observed, however both signals shows drift during major time span.

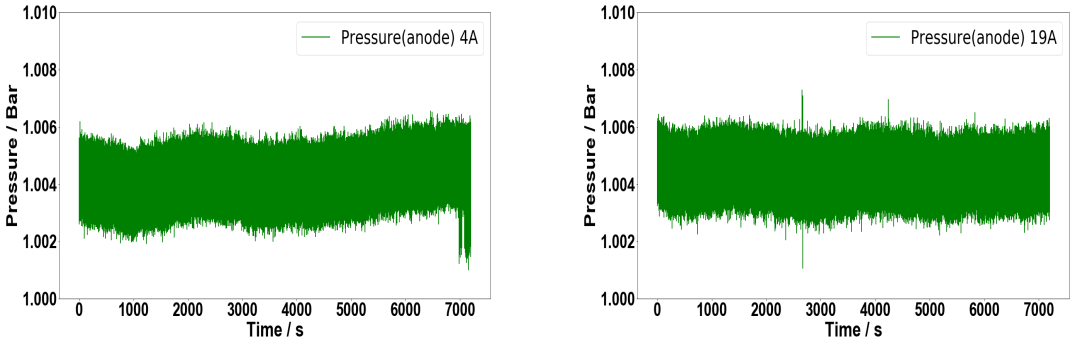

(a) pressure anode 4A (b) pressure anode 19A

Figure 4.25: Raw pressure (anode) signal(Multi serpentine) (a) 4A (b) 19A

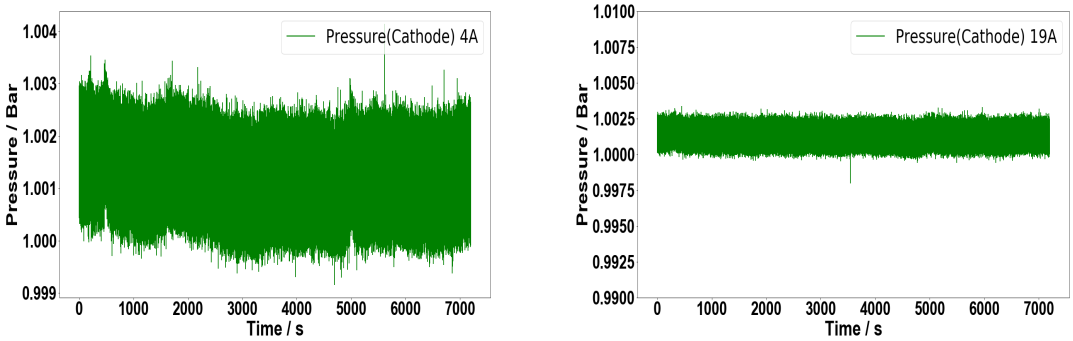

(a) pressure anode 4A (b) pressure anode 19A

Figure 4.26: Raw pressure (cathode) signal(Multi serpentine) (a) 4A (b) 19A

Figure 4.25 and 4.26 presents visualization of pressure signals. Almost all the signals shows stationary behavior, however some irregularities can be observed in 4.26(a) where pressure is found to fluctuate from 1.004 bar to 1.01 bar.

4.6.3 Signal visualization for hybrid design

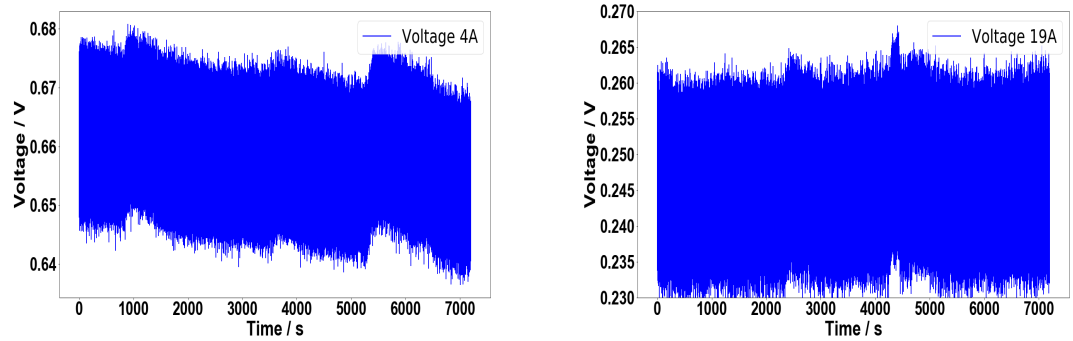

(a) voltage 4A (b) voltage 19A

Figure 4.27: Raw voltage signal(Hybrid) (a) 4A (b) 19A

Figure 4.27(a and b) shows visualization of voltage signals in time domain for multi-serpentine design for two currents. Voltage fluctuations at 4A are recorded for situation where kinetic effects are predominant, Figure 4.24(a). On other hand, at 19A, mass transport effects play an important role. Both the signals shows stationary behavior for most of the time span with little drift in Figure 4.27(a) .

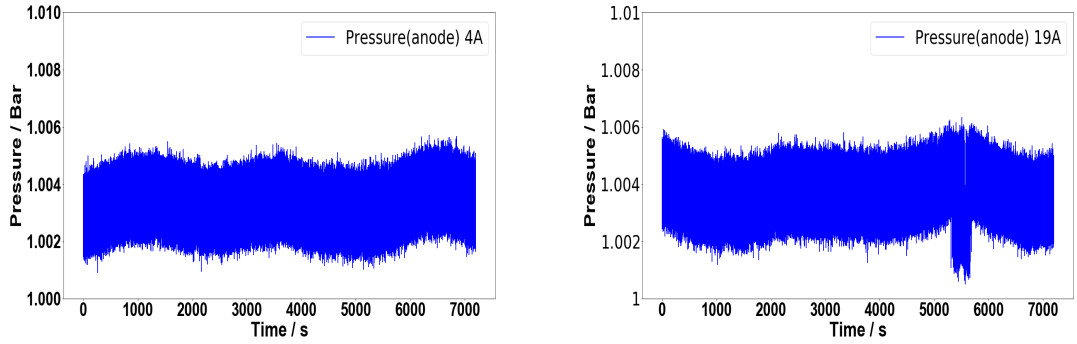

(a) pressure anode 4A (b) pressure anode 19A

Figure 4.28: Raw pressure anode signal(Hybrid) (a) 4A (b) 19A

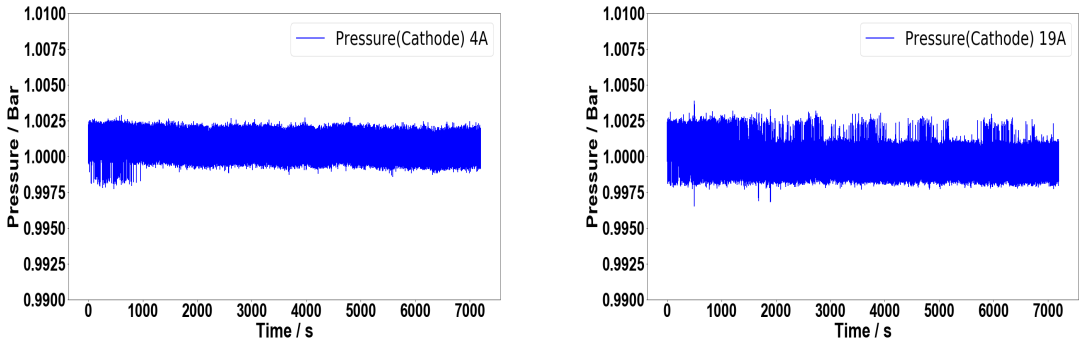

(a) pressure cathode 4A (b) pressure cathode 19A

Figure 4.29: Raw pressure cathode signal(Hybrid) (a) 4A (b) 19A

Based on the qualitative nature of pressure signals observed, almost all the signals shows stationary behavior, the maximum signal fluctuation is (1-2) mbar which is comparatively less. Considering Figure 4.29(a), there are certain abnormality where the data is collected at lower pressures then all other signals observed in previous section. It will be interesting to explore in more details the problems associated with the collection of data through other statistical tools.

Overall in qualitative point of view summing up all the signals, Figure (4.21-4.29) presents the voltage signals for three geometries. Two regime are distinct, at 4A (0.16 A/cm^2 - Figures (4.21a, 4.24a, 4.27a)) where the kinetic effects are predominant and at 19A (0.76 A/cm^2 - Figure (4.21b, 4.24b, 4.27b) where mass transfer effects are predominant. At 4A, low frequency voltage fluctuations are lower in comparison at 19A. That can be due to a higher impact of the water management (due to higher amount of water produced) at 19A. In geometry comparison point of view, serpentine highlights the lowest stability, especially at 19A (Figure 4.21b),

followed by multi-serpentine and hybrid design shows better stability with no low-frequency fluctuations at 19A (Figure 4.27b). The stable evolution of the voltage within hybrid design can be due to a more uniform distribution of gases.

4.6.4 Signal visualization for spot design

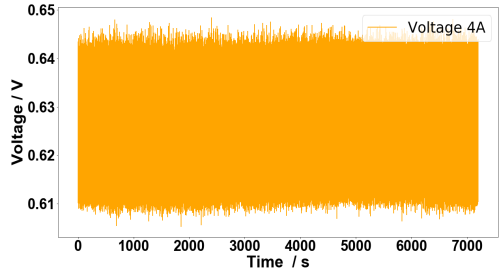

Figure 4.30: Voltage 4A

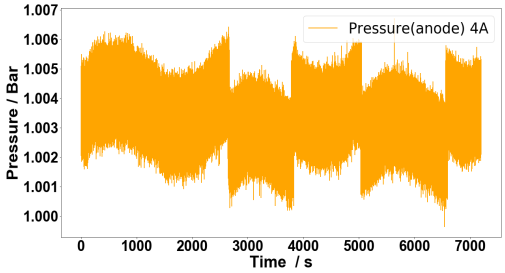

Figure 4.31: Pressure anode 4A

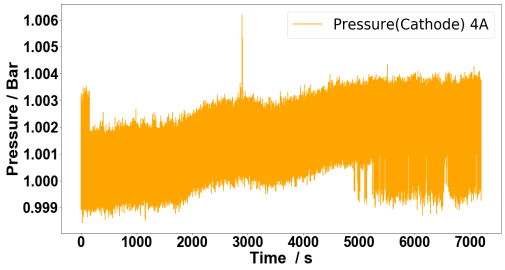

Figure 4.32: Pressure cathode 4A

Considering the figures (4.30, 4.31, 4.32) for spot design, voltage does not show much effect or irregularities but there can be irregularities observed in the pressure side. If we compare with other designs, it is performing better but again due to experimental constraints, further tests of spot designs cannot be continued at higher currents of 19A. Considering the present scenario, at low currents spot design shows good performance but considering the pressure irregularities , it can be inferred that water management is not good for spot designs. However further tests at high currents can open up more in depth analysis of these designs.

4.6.5 Signal visualization for circular design

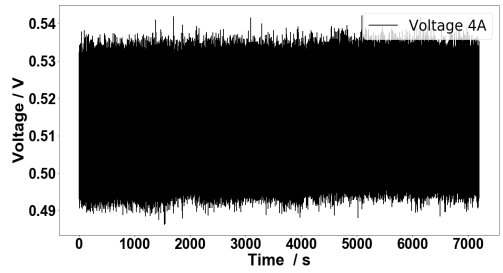

Figure 4.33: Voltage 4A

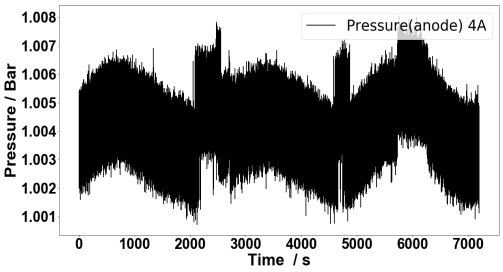

Figure 4.34: Pressure anode 4A

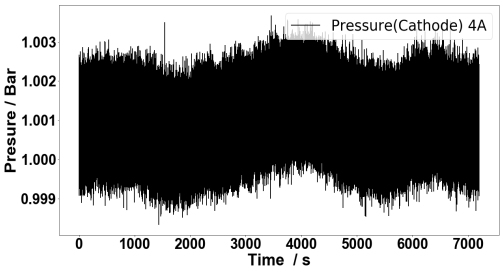

Figure 4.35: Pressure cathode 4A

Considering the figures (4.33, 4.34, 4.35) for circular design voltage signal is stable and irregularities are observed in the pressure side. If we compare with designs, stable signals are observed in voltage but again due to experimental and time issues further tests of spot designs cannot be continued at higher currents of 19A. Considering the present scenario, at low currents circular design shows good performance but considering the pressure irregularities , it can be inferred that water management is not good for circular designs. However further tests at high currents can open up more in depth analysis of these designs. After understanding the figures in time domain it is now important to use statistical tools in order to check the uncertainty of voltage or pressure with respect to different designs.

4.7 Noise descriptors in time domain

Standard deviation (STD) can be a good descriptive tool, describing the intensity of noise signal. As mentioned above, in all the experiments the electrochemical noise is recorded directly without filtering. This allows to understand the influence of detrending on noise descriptors, in particular on STD, to understand the signature and its impact on temporal analysis. For that the 2 hours signal (7200 seconds) is broken down to 200 seconds window (36 parts) and then an individual linear fit is performed for each part of data between two break points. Linear mode calculates the linear least-squares fit to data and subtracts from data in the given time window. Two operating point are used at a current of 4A (0.16 A/cm^2) and at 19A (0.76 A/cm^2) for three geometry: serpentine, multi-serpentine, hybrid. For other geometries (spot and circular design) only 4A (0.16 A/cm^2) is used due to experimental constraints. The three designs initially discussed will be analysed together as the data is available for all current conditions with polarization and spot and circular design will only be limited to 4A (0.16 A/cm^2).

4.7.1 STD of voltage fluctuations

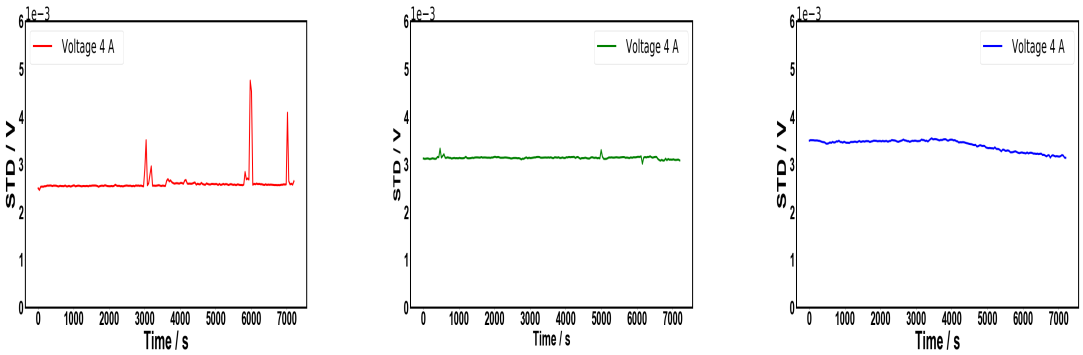

(a) serpentine 4A (b) m-serpentine 4A (c) hybrid 4A

Figure 4.36: STD variation 4A (a) serpentine (b) m-serpentine (c) hybrid

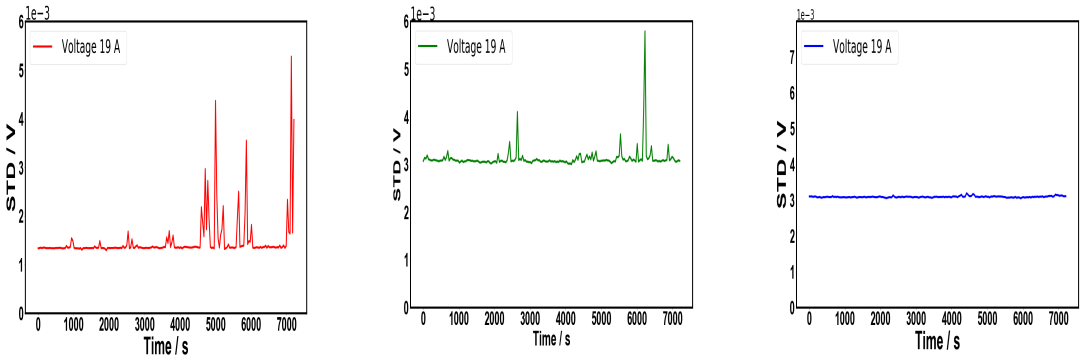

(a) serpentine 19A (b) m-serpentine 19A (c) hybrid 19A

Figure 4.37: STD variation 19A (a) serpentine (b) m-serpentine (c) hybrid

For STD analysis, voltage signals are analysed as for pressure the STD value is far too less for comparison. In a quantitative point of view, Figure (4.36(a)-4.37(c)) shows the STD fluctuations of all signals for the three geometries presented in Figure (4.21-4.29). In overall, STD values of voltage are near the value of 3mV, except at a value of 1.3 mV for the serpentine geometry at 19A. Comparing STD values, traditional serpentine geometry presents the noisiest signature. More peaks and higher standard deviation values at 4A, Figure (4.36a) and 19A are highlighted, which is less for multi-serpentine, some peaks with less intensity are present at 19A, Figure 4.37b. There is no variation or presence of peaks for hybrid design. The appearance of STD peaks and high values is due to a non-optimised water management has shown in our previous work [Dib et al., 2019,].

Serpentine design, signals has high fluctuating behavior. The reason can be explained considering flow only in one channel where water is forced to move in one direction. If slug or plug appears, it will involve more irregularities in voltage signals and STD peaks appears (Figure 4.36a, 4.37a). For multi-serpentine 4A, results shows no fluctuations Figure (4.36b, 4.37b) shows fluctuations but the magnitude is less then traditional serpentine. The reason of this behavior can be attributed to the re-distribution of water in the slots which results in more stable voltage. The stable behavior on voltage signals for hybrid design can be due to an easier removal of water, where it is not forced to follow a fixed trajectory and can distribute at the inlet due to the presence of parallel channel. Also, hydrid combine advantages of parallel and serpentine geometry which further redistribute the water.

[Wu et al., 2018,] has published results using neutron imaging to study water removal in single, double and quad channel serpentine based geometry. They report an ineffective liquid water removal for quad design and in our study based on electrochemical noise analysis, it is seen a stable voltage at lower current and some disturbance at higher currents. This is in agreement with their results, however they found better performance for serpentine compared to quad channel. In the present study, introduction of slots in multi-serpentine channel design can be a reason for better performance and stability compared to serpentine as slots allow more paths for removal of accumulated water. Again, considering neutron imaging results, [Spernjak et al., 2010,] comparing serpentine, parallel and interdigitated, shows that serpentine give better performance considering the removal of accumulated water with time. Since parallel geometry suffers poor water removal hence in our study, hybrid design, combining parallel and serpentine, shows better performance in voltage and STD fluctuations point of view compared to serpentine and multi-serpentine modified with slots.

4.7.2 STD of pressure fluctuations at anode

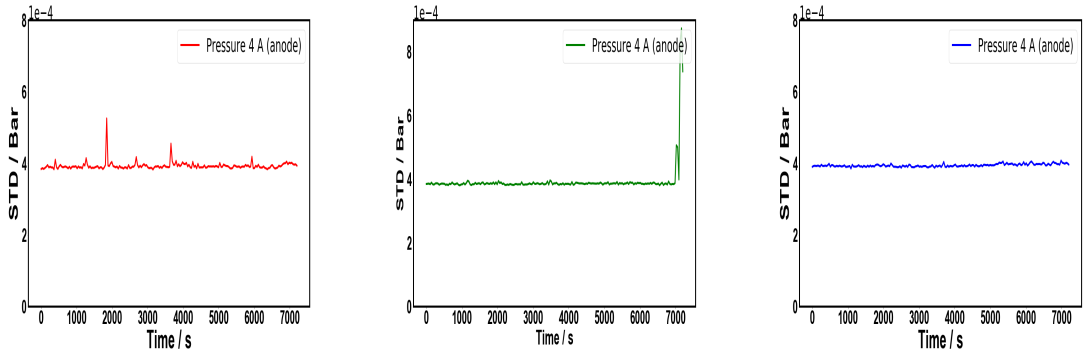

(a) serpentine 4A (b) m-serpentine 4A (c) hybrid 4A

Figure 4.38: STD variation 4A (a) serpentine (b) m-serpentine (c) hybrid

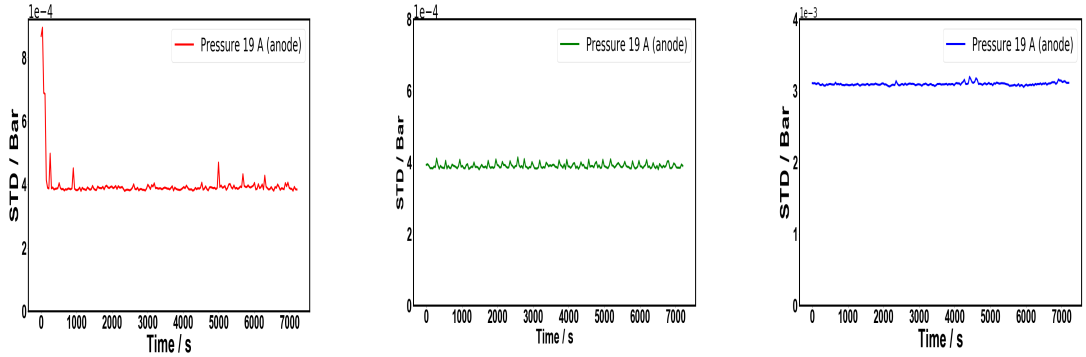

(a) serpentine 19A (b) m-serpentine 19A (c) hybrid 19A

Figure 4.39: STD variation 19A (a) serpentine (b) m-serpentine (c) hybrid

4.7.3 STD of pressure fluctuations at cathode

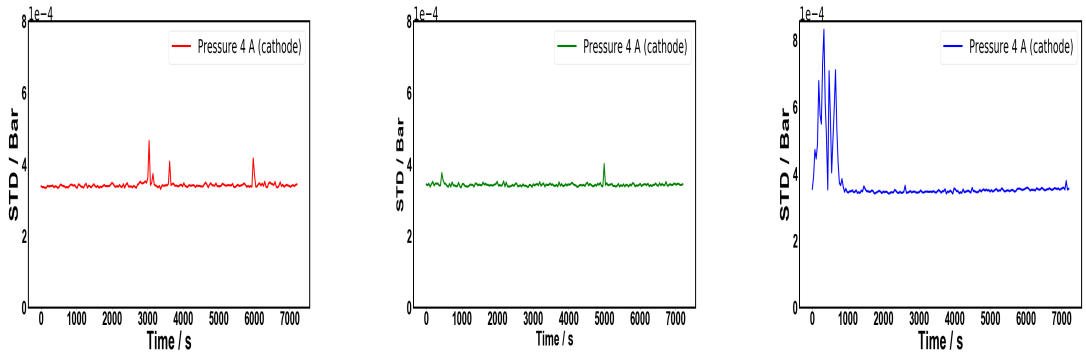

(a) serpentine 4A (b) m-serpentine 4A (c) hybrid 4A

Figure 4.40: STD variation 4A (a) serpentine (b) m-serpentine (c) hybrid

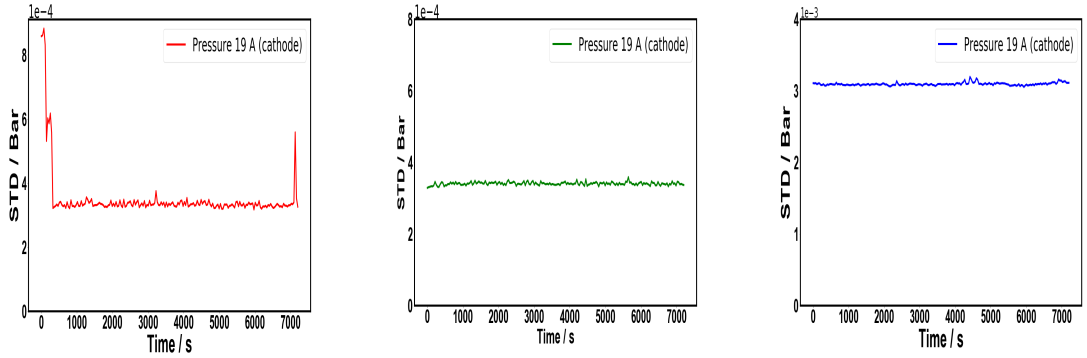

(a) serpentine 19A (b) m-serpentine 19A (c) hybrid 19A

Figure 4.41: STD variation 19A (a) serpentine (b) m-serpentine (c) hybrid

STD plots of pressure at anode and cathode differ from the STD plots of voltage. Again considering the figures of pressure, Figure 4.38a, serpentine 4A and Figure 4.39a and serpentine 19A shows the maximum deviation in the process. Considering the other values, in the anodic side, the signal is stationary with less deviation and hence considering the pressure in the range as measured by the sensor serpentine shows the maximum disturbance followed multi-serpentine and the least is for hybrid geometry. Considering the results, in cathodic pressure side, the fluctuations are more disorganised in the hybrid design at the cathodic side. A close analysis, considering the results in pressure section indicates that for pressure the results can be due to improper measurement by the sensor. For the case of hybrid the value lies in the error limits of the sensors. For the analysis of the pressure at cathode, either more lower value with better accuracy should be used otherwise the results cannot be justified if it lies in the limit of noise.

4.7.4 STD fluctuations for spot and circular design

Spot and circular designs have been separately discussed in this research due to the limited results obtained, at operating conditions of 4A. Based on the preliminary analysis for voltage obtained both the designs shows stability under the operating conditions of 4A. However the pressure fluctuations in cathodic side of circular design based on preliminary observations are unsteady compared to the spot design.

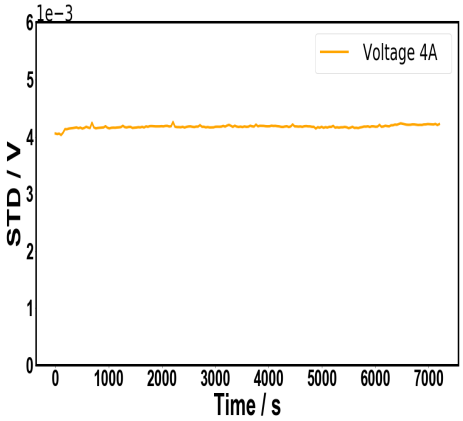

(a) Spot 4A

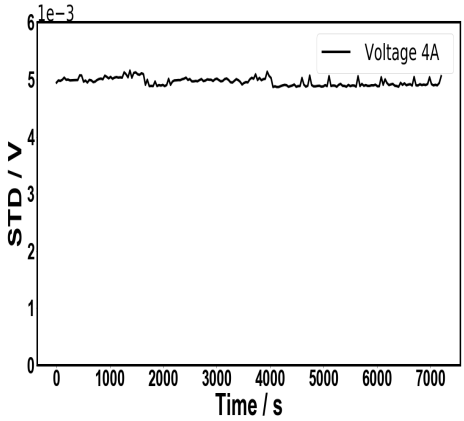

(b) Circular 4A

Figure 4.42: STD variation 4A (a) spot (b) circular , voltage

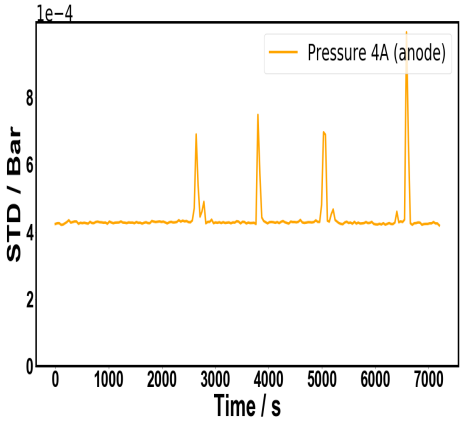

(a) Spot 4A

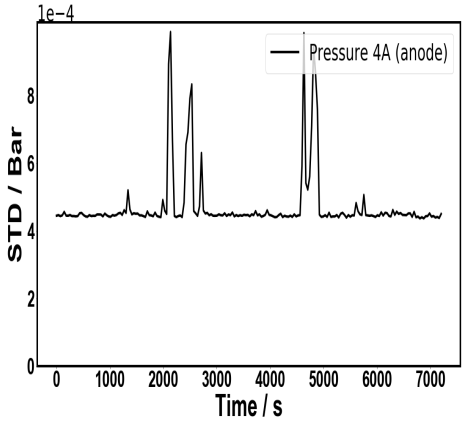

(b) Circular 4A

Figure 4.43: STD variation 4A (a) spot (b) circular , pressure anode

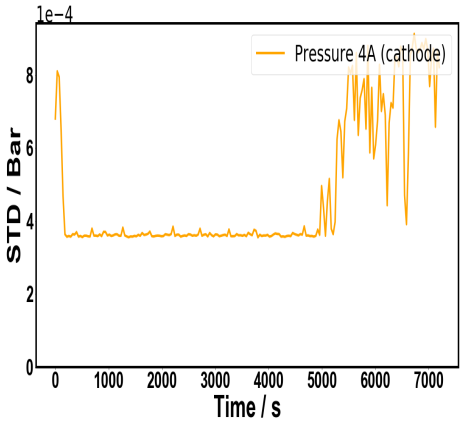

(a) Spot 4A

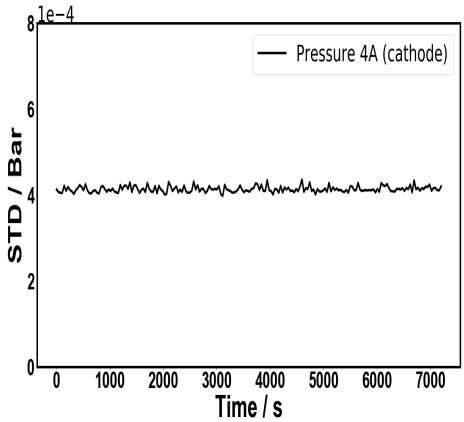

(b) Circular 4A

Figure 4.44: STD variation 4A (a) spot (b) circular, pressure cathode

4.8 Noise methodology in frequency domain

Use of temporal analysis in the previous calculations provides a clear picture of irregularities associated with various systems. Frequency analysis can provide further insights on system behavior. In this modern era, where cost is one of the most important parameter, diagnostic tools which can predict and limit the maintenance required is required.This can be done in several steps, the first step is identification of physical parameters which can be a possible attribute to the problem statement involved. Secondly, to establish techniques and methods in order to measure and record signatures, followed by analysis of recorded signatures which can help to identify pattern or a possible trend and finally to identify the problem in the setup.

In this part of chapter mainly applications with respect to Fast Fourier Transform (FFT) will be discussed in order to analyze the signals. ENA is performed by analyzing and recording the fluctuations generated by fuel cell and similarly is defined as spontaneous fluctuations of potential or current generated by electrochemical processes.

The aim of this research is to compare noise signature of three flow field designs (serpentine, multi-serpentine and hybrid) in frequency domain and to understand how ENA as a tool can be used to differentiate information by various sensors as the pressure sensor is directly in contact with the gases or voltage sensors attached to the body of fuel cell in working. To our best efforts, there is no information in literature considering the comparison of different flow field designs. The noise measurements have been provided for all designs in a 2-hour duration.

4.8.1 Methodology to estimate power spectral density

There are numerous methods in literature to estimate the power spectral density (PSD), Periodogram, Barlett, Welch,[Solomon Jr, 1991,] multi taper and can be extended based on optimization of results based on author's view point. Out of all Welch's method[Welch, 1967,] has widespread use for computing power spectral densities because of its use by Fast Fourier Transform (FFT) and averaging windows, thereby more useful information compared to previous. Welch's method utilizes the concept by dividing the signal into number of smaller segments, and applying an individual Fourier Transform for segments. The individual power spectra results obtained are then averaged to obtain Welch's estimate of PSD. Due to this averaging procedure it is also called as a periodogram averaging method. In order to obtain the best estimate of Welch's in this research further optimization of parameters is done such as number of blocks/segments at which the signal is broken, detrending of signal, windows and overlapping size of windows used. The first optimization starts by fixing window size in the signal.

4.8.2 Estimation of PSD with direct FFT

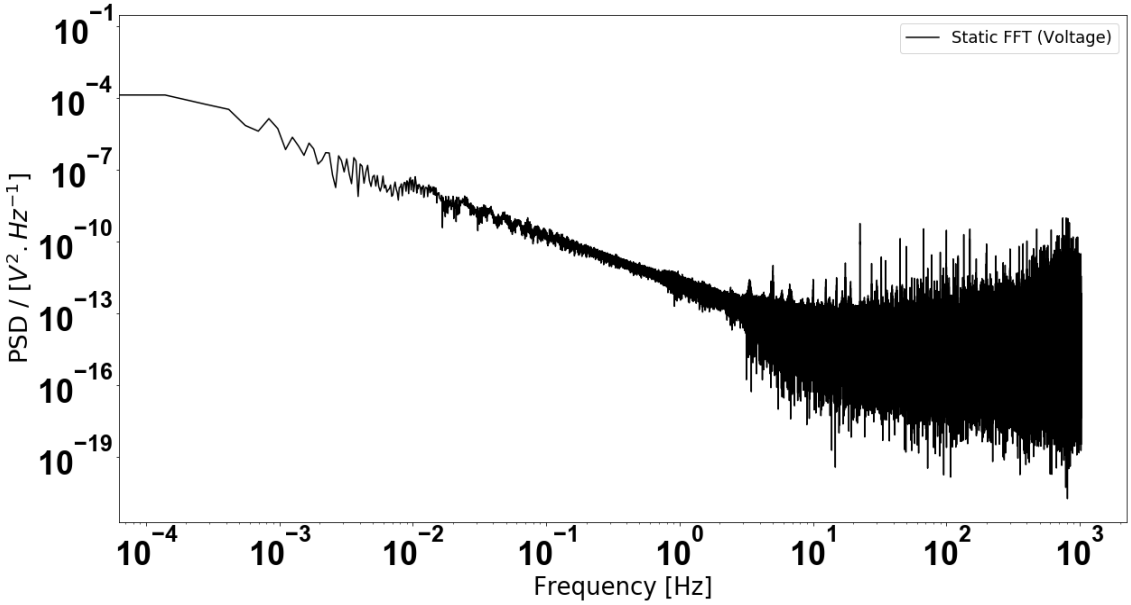

Figure 4.45: PSD estimation by direct FFT method- Voltage

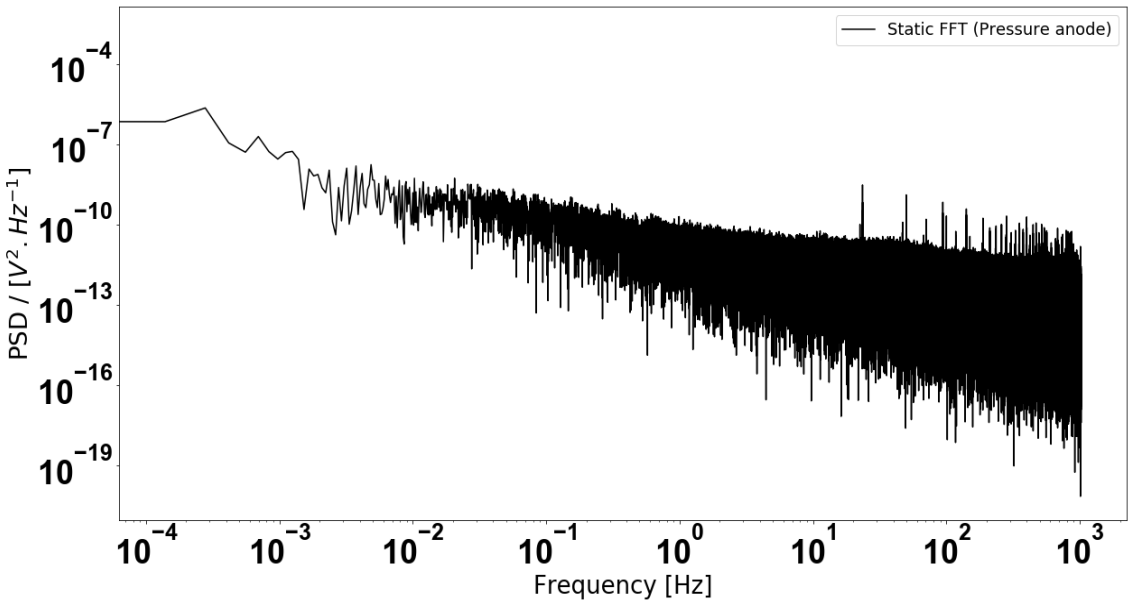

Figure 4.46: PSD estimation by direct FFT method- Pressure

Figure (4.45 and 4.46) shows the PSD estimation as calculated by direct FFT over the length of the signal. Comparing the two figures, PSD resolved like this without averaging does not show any relevant peaks, moreover the noise is comparatively higher and due to this different strategies are required to estimate PSD which can give simplified results, exposing clearly the peaks and reduce noise in the signal.

4.8.3 Parameters involved in estimation of PSD

In this section we will discuss the influence of different parameters on estimation of PSD. Parameters such as detrending type, detrending window size, effect of window size and effect of overlapping are discussed .

Parameters

1. **Effect of window size on the PSD estimation calculations**

   Figure 4.47(a) shows raw signal in time domain and how each signal is divided in blocks and Figure 4.47(b) shows the effect of the window size on the PSD estimations. Because each signals duration is 2 hours, i.e. 7200s, a window of 3600s involves a signal divided in 2 blocks Figure 4.47(a), 360s in 20 blocks, 72s in 100 blocks and 36 in 200 blocks respectively. For each window size calculated, PSD is an average of all spectrum calculated on each block. It can be seen in Figure 4.47(b), that decreasing the window size, impact the first points of the spectrum at low frequency range (f $< 10^{-2}$ Hz), but the slope of the spectrum for 10^{-2} < f< 1 Hz and white noise behavior for f > 1 Hz remains unchanged. Decreasing the size of the windows (or increase the number of blocks) act as a high-pass filter. No changes in spectrum obtained by applying different time windows confirms the stationarity of our recorded signals.

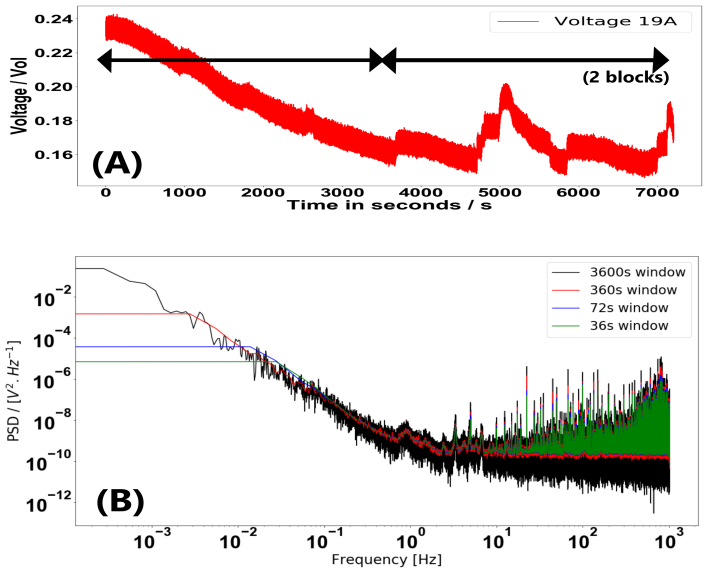

Figure 4.47: Variation of PSD with respect change in number of blocks / time window

2. **Effect of detrending on PSD estimation** Now the number of blocks (time window) for PSD estimation in Figure 4.47 is fixed at 20, i.e with a time window of 360s. After fixing the number of blocks, further window length will involve to detrend the signal. Detrending is again an important parameter while dealing with non-stationary signals in order to apply statistical descriptors. Detrending can be defined as removal of trends in the data. It can be achieved by applying a single window to the entire signal or breaking the

signals into parts in order to achieve stationarity of signals. Detrending the signals at lower time windows will remove the low frequency components and at higher time windows will remove the high frequency components.

Figure 4.48(a) presents the effect of time window size on the linear detrend. It means on each block, the signal is detrended with a linear polynom. As previously (Figure 4.47), the use of lower time windows involves a filtering at low frequency range (f $<$ 0.5 Hz), but the structure of the spectrum is kept same for others frequencies. Figure 4.48(c) represents the effect when there is detrend and no-detrend. It can be seen that detrend has an effect on the PSD calculations. It can be seen in Figure 4.48(b) that PSD signal in low frequency region is richer in information compared to non-detrended signal. Similarly Figure 4.48(c) explains the effect of detrend time window as a smaller window completely removes low frequency components and hence detrend becomes a critical parameter. (Block size for PSD estimation is always fixed to time window of 360s). After this analysis, linear detrend with time windows of 200s on each bock is used to calculate spectra. The choice to use 200s time windows is based on the fact that 200s time window give rich information in lower frequency region during PSD calculations as seen from Figure 4.48(a) and at higher frequency(f>1 Hz) the region is mainly noise.

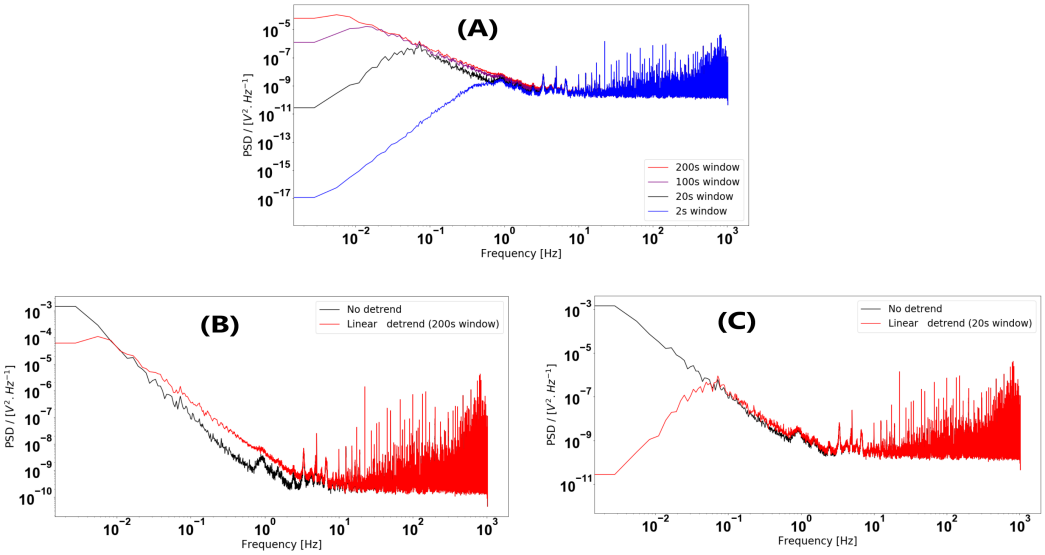

Figure 4.48: PSD estimation with respect to linear detrending procedure (a) represents the effect of window size on detrending, and linear detrend is used (b) represents effect of linear detrend on 200s "detrending window size" (c) represents effect of linear detrend on 200s "window size"

3. **Effect of window and overlapping for PSD estimation**

   Welch's method proceeds by dividing the signal in to blocks, each block has certain artifacts at the end. Based on type of signal for estimation of PSD and in order to limit leakage effects, different windows can be adopted instead of the rectangular such as Hann/Hanning, Blackman, Hamming, Kaiser-Bessel, more detailed regarding choice of windows is presented by [Nuttall, 1981, Harris,

1978]. Hanning and Hamming windows seem particularly suitable because both are characterized by a main lobe width exactly double and side lobe width that is exactly equal compared to those of rectangular windows [Testa et al., 2004] . In this research, Hanning window (Figure 4.49) is chosen. Overlapping is further important tool to remove the errors which can be there due to artifacts created by the windowing effect. Hence, an overlapping feature helps to minimize artifacts errors in the processing of estimation. Below Figure 4.49, represents the effect of overlapping used. The length of overlap window is $1/4^{th}$ the window length to take the maximum effect. Based on results effect of overlapping is not an effective parameter based on above signal.

One of the main properties of signal to discuss standard deviation or PSD, is stationarity of the signal. In this case, stationary signals can be easy to diagnose and drifting / non stationary signals can be a challenge as it effects the main outcomes. The very important parameter is the number of blocks and detrending window length. Out of all the processes applied to understand, linear detrending appears to be quite stable. However, polynomial detrending of higher orders is avoided as this can suppress frequency components of low frequency and thereby resulting only higher frequency components. Another important point considered before presenting results of PSD is Hanning window applied to the signals. In this research, Hanning window is applied at the end of all procedures and before calculation of PSD as Hanning can introduce discontinuities due to artifacts. In order to minimize the effects of artifacts created due to Hanning, it is recommended to use overlapping of windows as this will reduce the effect of artifacts. Based on the above calculations, the final signal obtained is fixed at window size of 360s, the detrending is limited to 'linear', detrending window size is fixed to 200s and overlapping to $1/4^{th}$ of window size in every calculation.

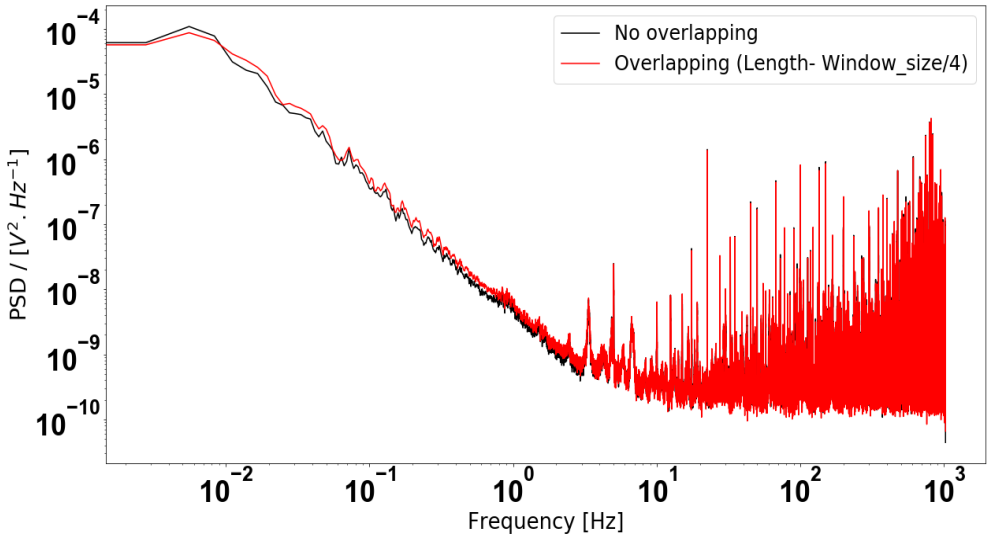

Figure 4.49: Variation of PSD with respect to overlapping of windows

4.8.4 PSD of bench noise and main signal comparison

In order to diffrentiate between the noise of the signal and the main signal it is important to visualize. Based on the results in Figure 4.50(a), the noise of the bench is completely lower then the noise of the actual fuel cell in 'ON' conditions. The data recorded shows a peak to peak voltage of 40 mV for the fuel cell ON (Figure 4.50(a, b)) and 4 mV for the fuel cell OFF (Figure 4.50(a, c)) condition which is roughly 10 times higher. This confirms that the fuel cell noise can be measured by our acquisition system with enough intensity. Figure 4.50(d), also shows that PSD of bench noise is less then the seprentine 19A design signals. Based on the results, the peak to peak PSD value in fuel cell 'ON' conditions is 10^{-4} V^2/Hz and in fuel cell 'OFF' conditions is 10^{-10} V^2/Hz which is roughly 10^6 orders less.

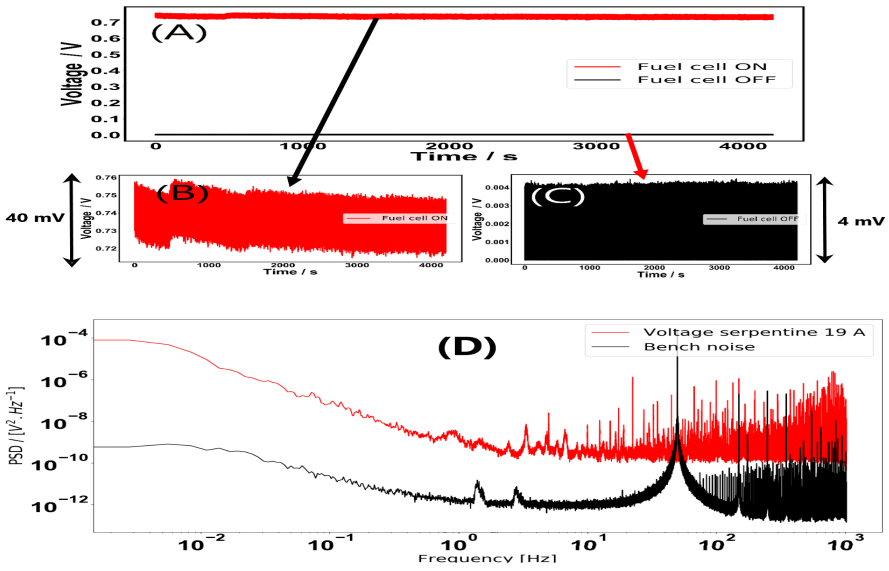

Figure 4.50: Variation of PSD of bench (Fuel cell turned 'OFF' and main signal)

4.9 Noise descriptors in frequency domain

The following section deals with plot of estimated power spectral density for all signals in voltage domain primarily for serpentine, multi-serpentine and hybrid designs. Two other designs of spot and circular have been analysed separately.

4.9.1 Estimated PSD (Voltage)

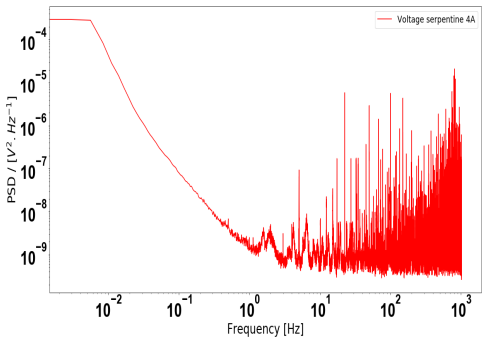

(a) PSD estimation at 4A

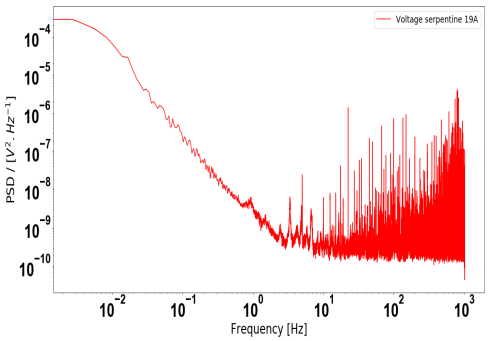

(b) PSD estimation at 19A

Figure 4.51: PSD estimation of serpentine geometry

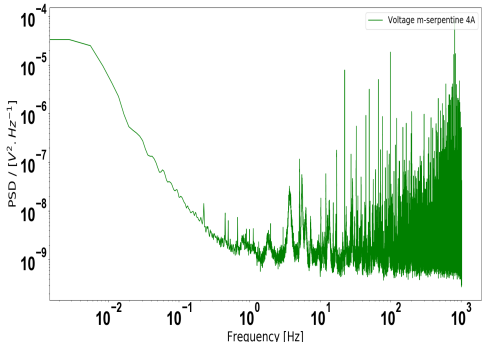

(a) PSD estimation at 4A

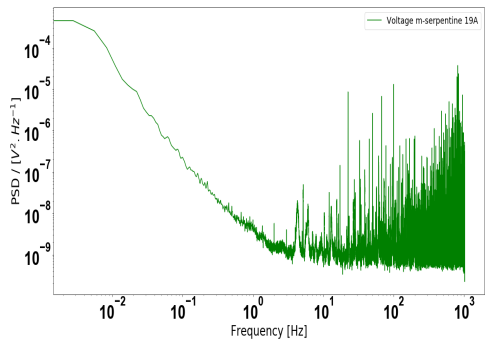

(b) PSD estimation at 19A

Figure 4.52: PSD estimation of multi serpentine geometry

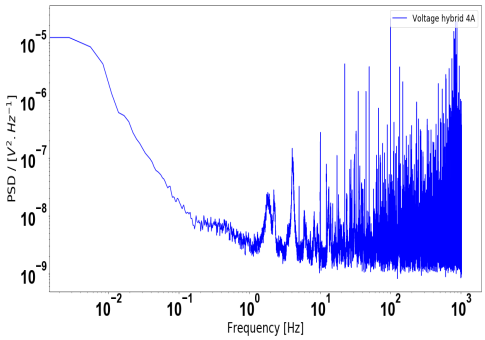

(a) PSD estimation at 4A

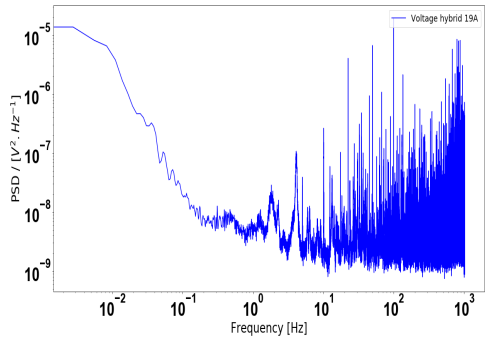

(b) PSD estimation at 19A

Figure 4.53: PSD estimation of hybrid geometry

All observed PSD estimation shows fractional noise at low frequency domain($f 1Hz$) with different slopes and white noise at high frequency domain ($f\ 1Hz$) where some peaks can be observed.

4.9.2 Estimated PSD (Pressure anode)

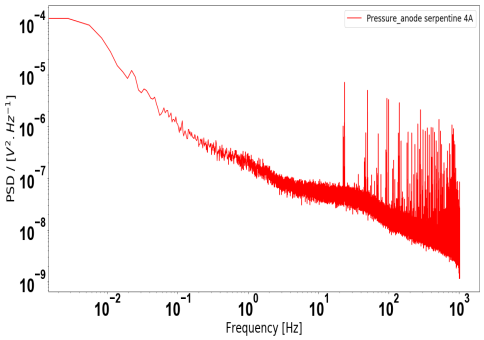

(a) PSD estimation at 4A

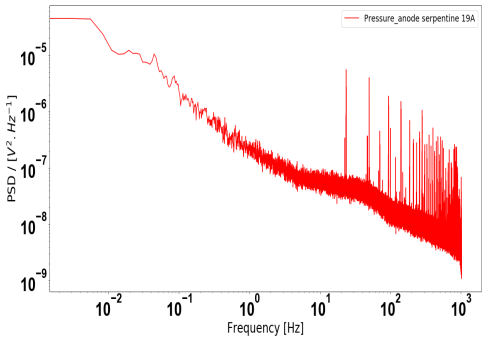

(b) PSD estimation at 19A

Figure 4.54: PSD estimation of multi serpentine geometry (Pressure anode)

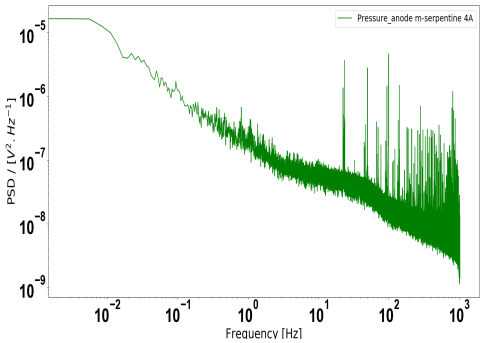

(a) PSD estimation at 4A

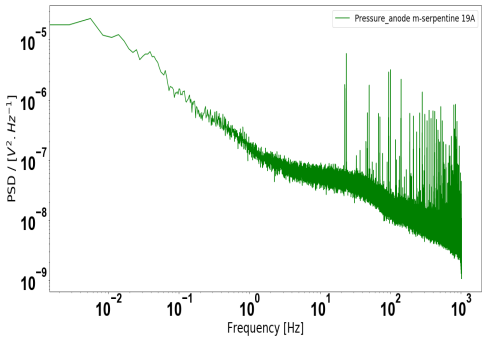

(b) PSD estimation at 19A

Figure 4.55: PSD estimation of multi serpentine geometry(Pressure anode)

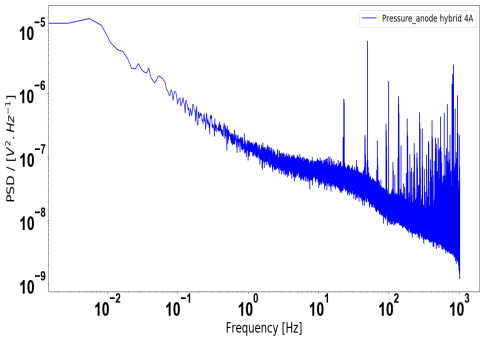

(a) PSD estimation at 4A

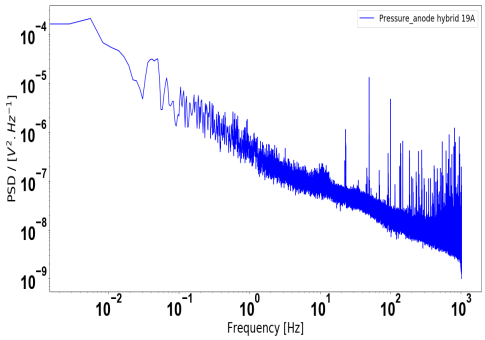

(b) PSD estimation at 19A

Figure 4.56: PSD estimation of hybrid geometry(Pressure anode)

4.9.3 Estimated PSD (Pressure cathode)

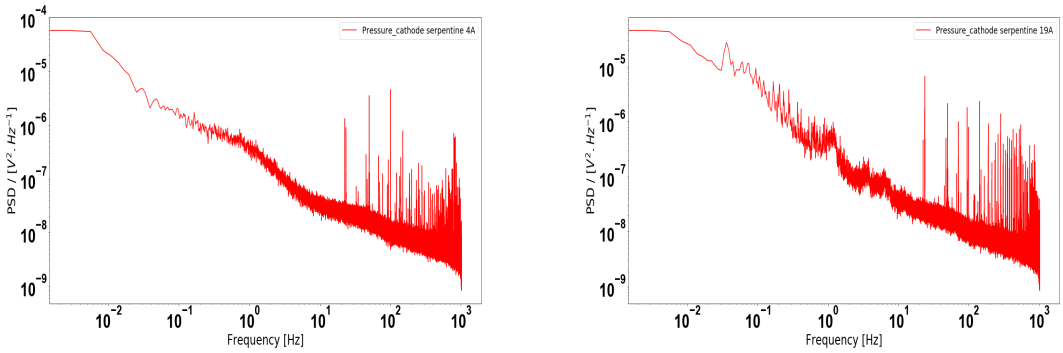

(a) PSD estimation at 4A (b) PSD estimation at 19A

Figure 4.57: PSD estimation of multi serpentine geometry (Pressure cathode)

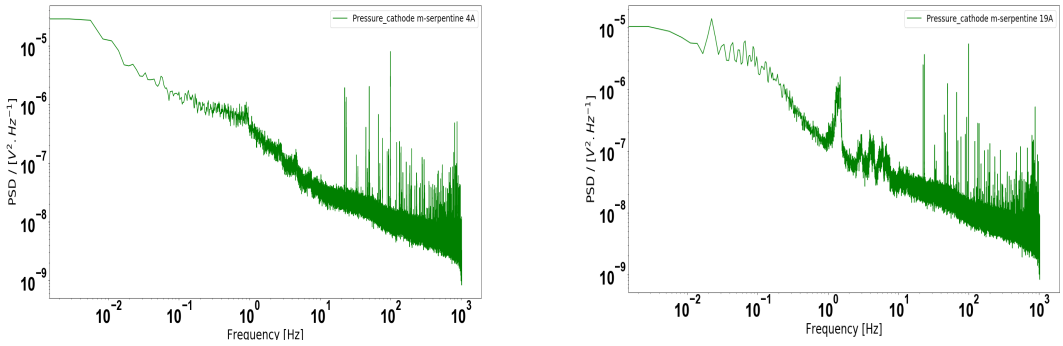

(a) PSD estimation at 4A (b) PSD estimation at 19A

Figure 4.58: PSD estimation of multi serpentine geometry(Pressure cathode)

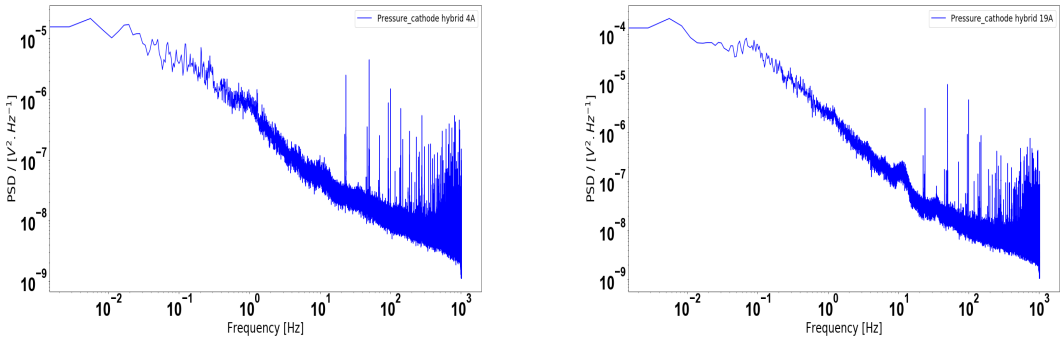

(a) PSD estimation at 4A (b) PSD estimation at 19A

Figure 4.59: PSD estimation of hybrid geometry(Pressure cathode)

Based on the above designs the PSD is more or less same with a very less difference in the energy at lower frequency. In the later sections it will be interesting to explore the necessity to use noise analysis as a tool to explore the details involved.

4.9.4 Estimated PSD (Spot design)

Estimation of spot design is mainly limited to operating conditions of 4A ad results are presented without any comparison.

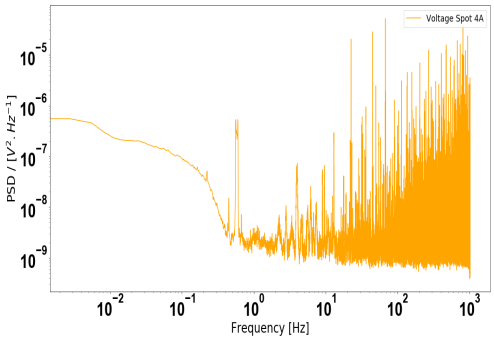

Figure 4.60: PSD estimation 4A

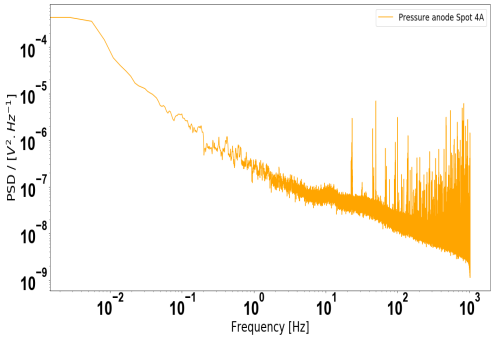

Figure 4.61: Pressure anode 4A

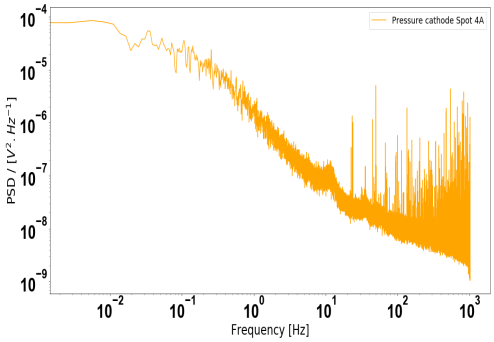

Figure 4.62: Pressure cathode 4A

All observed PSD estimation shows fractional noise at low frequency domain(less then $1Hz$) with different slopes and white noise at high frequency domain (more then $1Hz$) where some peaks can be observed.

4.9.5 Estimated PSD (Circular design)

Estimation of circular design is mainly limited to operating conditions of 4A ad results are presented without any comparison with other geometries.

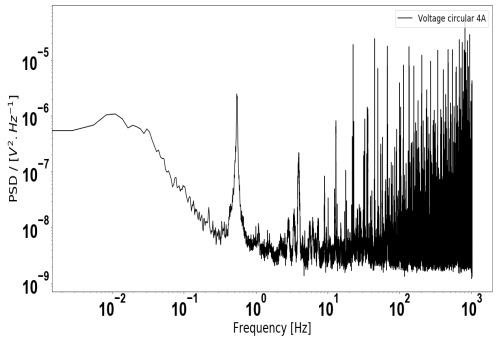

Figure 4.63: Voltage 4A

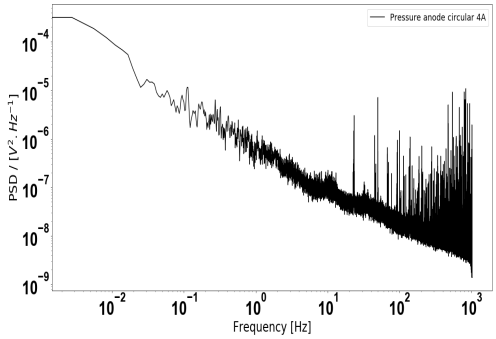

Figure 4.64: Pressure anode 4A

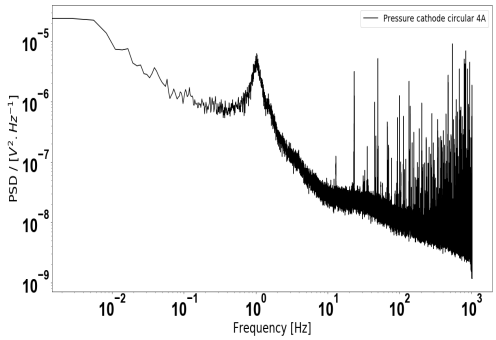

Figure 4.65: Pressure cathode 4A

Based on the results estimated, the peak value of PSD is $7 \times 10^{-7} V^2/Hz$ which is comparatively lower then all the previously obtained results of PSD. Following this a noticeable peak is also observed at frequency of 0.8Hz. Based on the results it is difficult to explain if the present peak is part of white noise or it can be due

to the hydrodynamic fluctuation in the signal. Considering the pressure analysis of the signals pressure at the cathode in Figure 4.65 has a noticeable peak at 1 Hz. Based on the limited operating conditions, the actual estimation is difficult to predict however, a poor water management or noise of instrument can be a reason of this behavior in circular geometry.

4.10 Comparison of noise signature in frequency domain for different flow field design and different operational points

In the subsequent section of 4.10.2, 4.10.1 and 4.10.3, results will be mainly focused on how effective is the ENA tool to predict the performance of the cells and to differentiate between the various operating conditions considering the design, current and relative humidity.

4.10.1 Comparison of PSD for different flow field

In this section, results are analyzed considering three cases(1) comparing the effect of (1) flow field designs (2) current and (3) relative humidity on PSD estimation considering voltage, later PSD for pressure. Considering the flow field designs, 3 geometries based on their performance is evaluated mainly serpentine, multi serpentine and hybrid. In the next part results are categorized based on the current used during calculations (limited to comparison for 4A and 19A) and in the 3rd part it is based in relative humidity of 100 % and 50%. The case of relative humidity at 100 % is applied to 4A conditions only. It is specific at this case only. For rest all results, relative humidity of 50% is chosen. The main results of present work are related using different flow field design. Figure 4.66 represents the noise signatures in frequency domain (PSD), geometries of bipolar plates.

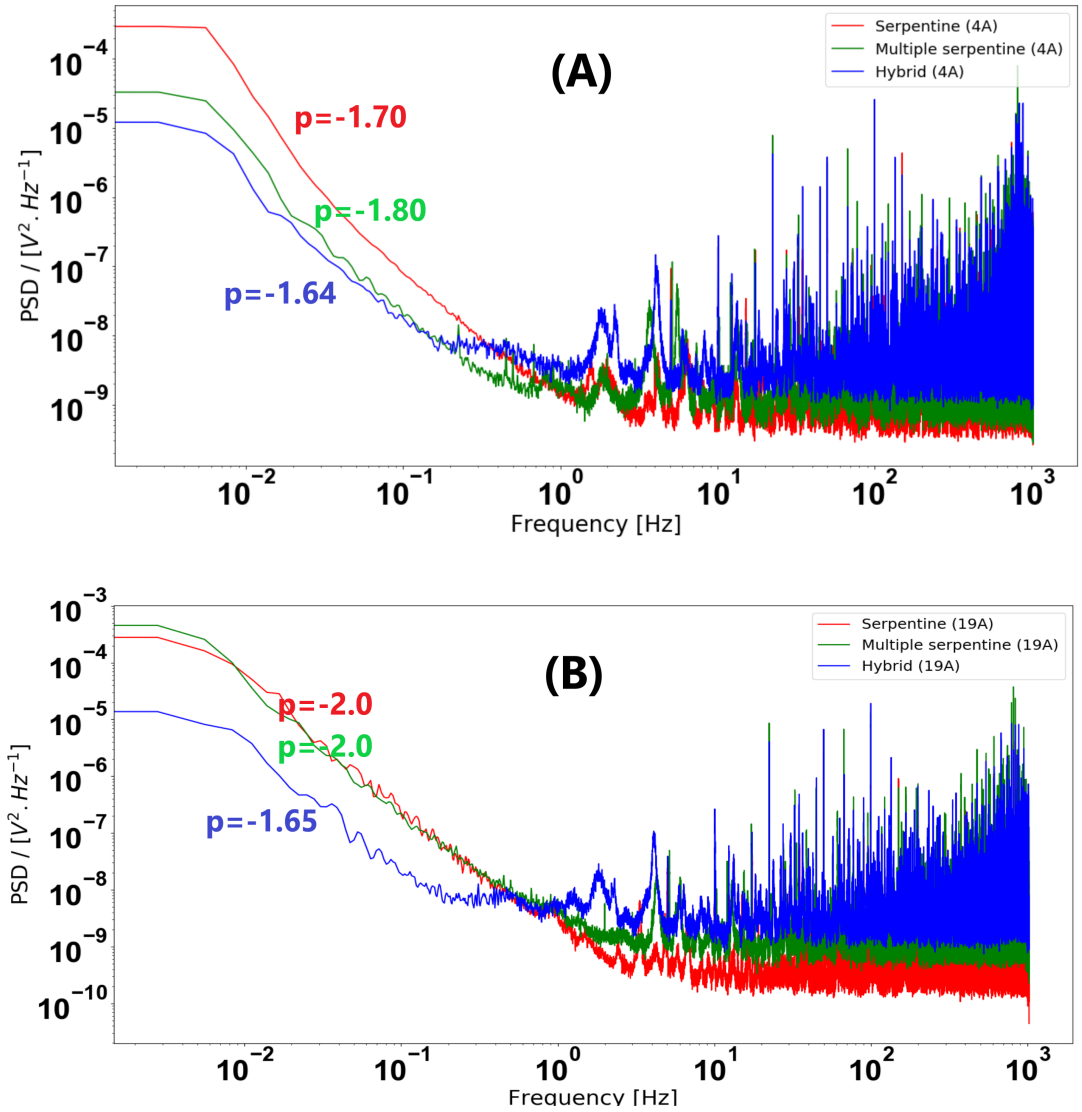

Figure 4.66: PSD estimation by Welch's scheme for three geometries - Voltage

If we consider the PSD values for voltage in Figure 4.66, difference can be observed for all. However still the curve can be divided in to 2 parts, region of low frequency (f $<$ 1 Hz) and region of high frequency (f $>$ 1Hz). For lower frequency region, the PSD area is higher for serpentine, followed by multi serpentine and the minimum area is for hybrid design. For all the different designs, ENA is sensitive, it can bring out a difference considering the slope which varies from -1.70 for serpentine -1.80 for multi-serpentine and is minimum is for hybrid given by -1.60 at current of 4A. At current of 19A, serpentine and multi serpentine have similar slope of -2 followed by hybrid with -1.65. The peak point of PSD value at lower frequency for serpentine at 4A is $8 \times 10^{-5} V^2/Hz$, $5 \times 10^{-6} V^2/Hz$ for multi serpentine and $3 \times 10^{-6} V^2/Hz$ for hybrid design. Similarly, for calculations at 19A, the peak point of PSD value at lower frequency for serpentine is $3 \times 10^{-5} V^2/Hz$, $5 \times 10^{-5} V^2/Hz$ for multi serpentine and $1 \times 10^{-6} V^2/Hz$ for hybrid design. We see an increase in slope with increase in current for all the designs. Slopes at around -2 shows a correct signature of water balance of fuel cell [Maizia et al., 2017,].

Geometry	**PSD value** (V^2/Hz)
Serpentine 4A	1.60×10^{-7}
Serpentine 19 A	4.13×10^{-7}
M serpentine 4A	2.96×10^{-8}
M serpentine 19 A	2.89×10^{-7}
Hybrid 4A	2.94×10^{-8}
Hybrid 19 A	4.39×10^{-8}

Table 4.1: PSD values for voltage

PSD area under the curve gives the uncertainties involved. More the area, higher the uncertainties. Considering the Table 4.1, all PSD values are calculated by Simpson's rule and the end frequency is limited to 5Hz. The reason for end frequency at 5Hz is, after 5Hz it is the white noise and white noise do not contribute in fetching any important information from the signal. Now, considering lower frequency region, a larger area under PSD curve explains higher standard deviation (STD), and which explains that the uncertainties in serpentine design (PSD=$4.13 \times 10^{-7} V^2/Hz$) is higher for serpentine 19A, followed by multi serpentine at 19A (PSD=$2.89 \times 10^{-7} V^2/Hz$) and the minimum is for hybrid at 19A (PSD= $4.39 \times 10^{-8} V^2/Hz$) and it can signify that hybrid performs better in managing hydrodynamic fluctuations or transport of reactants at present operating conditions. Similarly considering the conditions at 4A, uncertainties in serpentine design (PSD=$1.60 \times 10^{-7} V^2/Hz$) is higher for serpentine 4A, followed by multi serpentine at 4A (PSD=$2.96 \times 10^{-8} V^2/Hz$) and the minimum is for hybrid at 4A (PSD= $2.94 \times 10^{-8} V^2/Hz$) and it can signify that hybrid performs better in managing hydrodynamic fluctuations or transport of reactants at present operating conditions. At 4A, both hybrid and serpentine have similar PSD values, however they are 6 times less then serpentine PSD values at 4A.

4.10.2 Comparison based on current

In this section we compare noise signatures with respect to applied current in Figure 4.67.

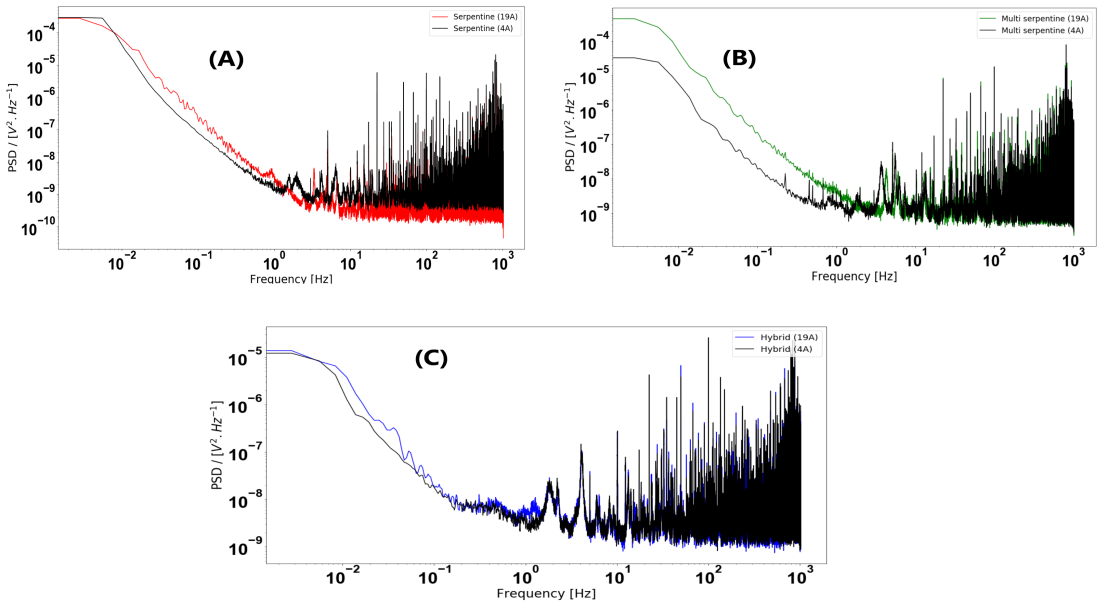

Figure 4.67: Influence of current variation on PSD calculated at (4A and 19A) for (a) serpentine designs, (b) multi serpentine design and (c) hybrid design.

It is seen that noticeable influence of applied current can be seen in multi serpentine geometry only. This geometry leads to significant increase in electrochemical noise. ENA is the most important for multi-serpentine design in comparison to peak values at lower frequency.

4.10.3 Comparison based on relative humidity

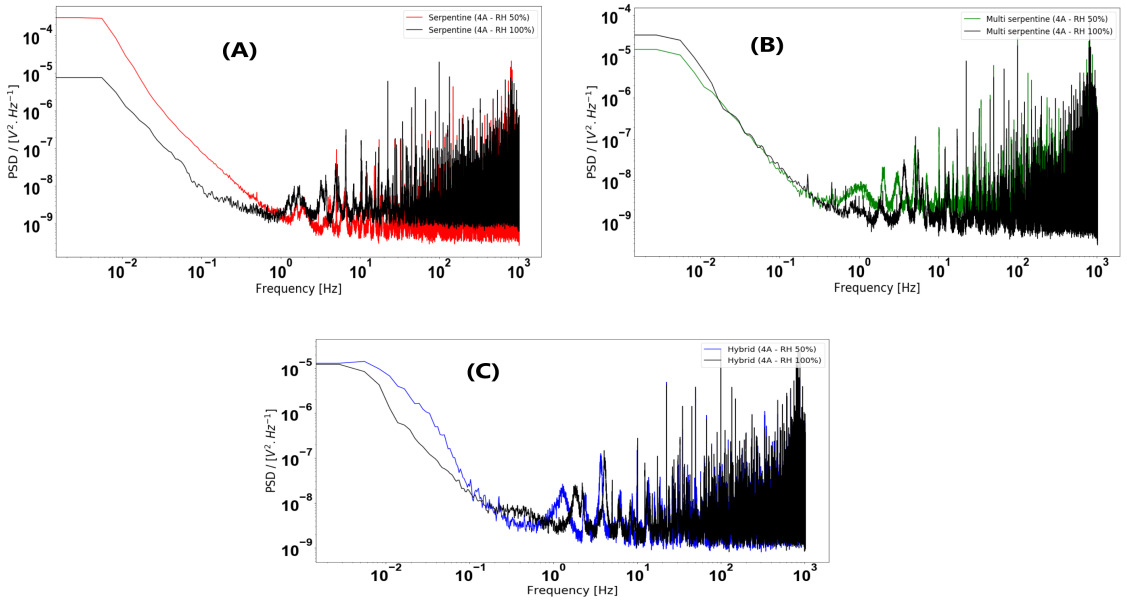

Figure 4.68: Shows effect of relative humidity variation on PSD calculated at (I = 4A) in (a) serpentine designs, (b) multi serpentine design and (c) hybrid design.

The effect of relative humidity is illustrated with Figure 4.69. This effect is important for serpentine geometry and does not effect multi serpentine. It is almost

same for multi serpentine (Figure 4.68b) and again hybrid shows a change. For all the three designs, the PSD curve has the tendency to trend downwards at higher relative humidity. [Maizia et al., 2017,] resulted in similar conclusion based on results of relative humidity.

4.11 Analysing PSD estimation of different signals at pressure

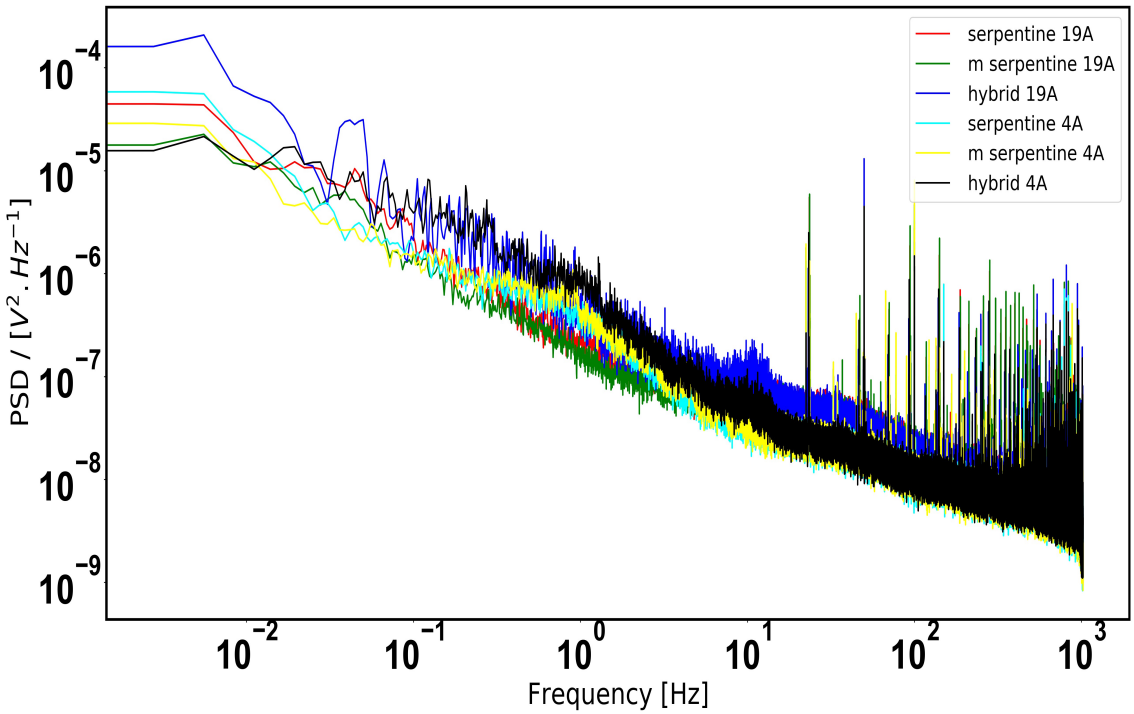

Figure 4.69: PSD estimation by Welch's scheme for three geometries at different currents - Pressure anode

Geometry	**PSD value** (V^2/Hz)
Serpentine 4A	1.36×10^{-6}
Serpentine 19 A	1.30×10^{-6}
M serpentine 4A	1.25×10^{-5}
M serpentine 19 A	1.25×10^{-5}
Hybrid 4A	1.30×10^{-5}
Hybrid 19 A	1.73×10^{-5}

Table 4.2: PSD values for pressure

Figure 4.69 shows results of PSD estimation in case of pressure signals for current at 4A and 19A. Based on the estimations, for all the signals noise signature is approximately same and as depicted by the PSD values in the table above. It shows that the pressure fluctuations do not depend on fuel cell running conditions. It also allows to conclude that voltage and pressure fluctuations are not correlated, atleast for the conditions in present study.

4.12 Conclusions

Considering the application of ENA, it is first study when it is applied in order to compare different flow field designs. All the conditions in our study are limited to normal conditions of 50% RH. The robust noise signature (PSD) of different flow field designs has been obtained in large frequency range ranging from 0.01Hz to 1kHz. The influence of signal duration, treatment of data, the effect of windows and the effect of detrending have been investigated. Three designs namely serpentine, multi serpentine and hybrid have been investigated. Considering the general observations for all designs, at lower frequencies (f< 10 Hz) PSD is inversely proportional to frequency and represent a linear slope ranging from p = (1.6 - 2). This is generally known as fractional noise. ENA allows to differentiate slopes for all designs. ENA is sensitive to current conditions also. We conclude that amplitude of ENA is most important for serpentine design. For this design increase of current from I= 4A to I= 19A does not influence significantly the noise signature. It is not the case of multi-serpentine design where current increase leads to significant increase of ENA. The low signal energy of hybrid design compared to serpentine design is again confirmed from time domain. Considering the case of relative humidity, multi serpentine and hybrid design do not gets effected and only serpentine is affected. Introduction of slots in multi serpentine can be a reason for improved water management. In serpentine, the slope decreases with increase in relative humidity, which based on our study can explain effect of poor water management. Based on the measurements of pressure fluctuations, they are completely de-correlated with voltage fluctuations.

Chapter 5

Modelling approaches to diagnose fuel cell

5.1 Introduction to types of modelling involved in fuel cell applications.

Models have a wide role to play in bringing up the innovations and updates in PEMFC technology as experimental approach is not only sometimes costly but time consuming too. Hence mathematical models play an important role for performance prediction and analysis of fuel cells systems [Shah et al., 2011, Saengrung et al., 2007, Djilali, 2007, Chávez-Ramírez et al., 2010, Napoli et al., 2013,] . Based on the view point of different authors there can be two major approaches, mechanistic and data driven modelling approach [Han and Chung, 2016,].Both of the these approaches have their own advantages and disadvantages based upon the collection of data, physics resolved, parameters available and complexity of end driven results. For example the mechanistic modelling is based on the physics underlying the working in PEMFC and thus it requires a clean study of physico-chemical phenomenon. While dealing with PEMFC, mechanistic approach can be difficult task due to inability to develop an accurate model considering the effect of all parameters and the physics captured. For example in order to develop modelling approach in understanding of transient behavior of PEMFC stack, the knowledge of physico-chemical phenomenon [Mann et al., 2000, Ceraolo et al., 2003,] is important. A model describing transient behavior of PEMFC stack requires the use of important parameters, such as ohmic resistance. It is important as it defines the overall humidity of membrane, drying of electrodes or even flooding conditions. Due to the complexity involved it is difficult to predict the exact value or an in-situ estimation can be difficult so we chose modelling. Here we present 2 modelling approaches a) Analytical model based on calculations of water fluxes 2) Data driven approach use to predict voltage.

5.2 Evolution of effective diffusion coefficient and analysis through water balance modelling under fuel cell operating conditions.

Water balance method, as used in chapter 2 of this research, can provide insights regarding diffusion coefficient when only diffusion is considered. However, electro-osmosis also plays an important role in distribution of water. During experimental campaign, it is difficult to simultaneously estimate accurately the values of water distribution by electro-osmosis, diffusion and thermo-osmosis. Hence, in order to get an idea, analytical modelling can be beneficial to estimate what amount of distribution is governed by various modes of transfers. In this part, 1-d model is developed, considering effect of diffusion and electro-osmosis.

In the literature, multiple numerical simulations and models are developed. Geometric parameters and descriptions are used due to the nature of the system studied. [Siegel, 2008] provides a summary of modelling approach used for the fuel cell modeling. Different approaches can be considered. The model can be analytical (if all theories are known) [Standaert et al., 1998], semi-empirical (empirical equations helps when physics between two parameters cannot be resolved clearly) [Springer et al., 1991], or empirical models. A mechanistic approach with a more or less precise knowledge of the physics and electrochemistry governing the internal phenomena of the system can be considered both at the macroscopic scale and microscopic [Bernardi and Verbrugge, 1991, Bernard et al., 2005]. The system can be modelled considering different regimes [Didierjean et al., 2008]. [Wu et al., 2009] developed a 3D unsteady, non-isothermal model to understand water transport in PEM fuel cells.

5.2.1 Transport of water (1-D model)

There can be multiple water transport mechanism as shown in figure 5.1. The electrochemical reaction produces water which must be drained so as not to clog the reaction sites. This produced water can be transported by diffusion in the membrane or by electro-osmosis (EOD). Other effects can be taken into account within the polymer, such as hydraulic permeation or thermo-osmosis, that is, water transport across the membrane in the presence of a gradient of temperature. In electrodes and porous layers, water can be transported by diffusion, in gaseous form, or by capillarity, in liquid form.

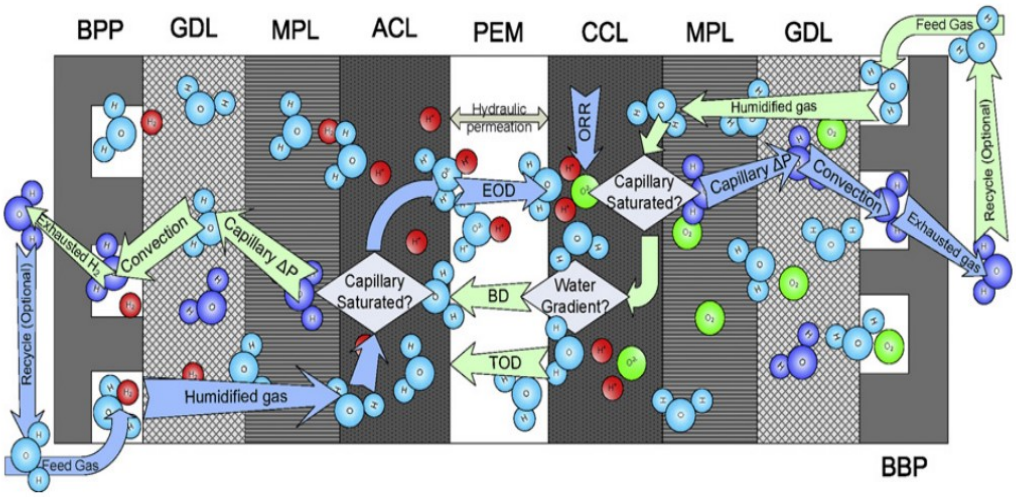

Figure 5.1: Water transport mechanism in PEMFC adopted from [Dai et al., 2009,]

5.2.2 Transport of water by diffusion

In the membrane, the water present in gases is adsorbed on the surface and is found in a liquid state. The total water flux (N_m-$mol/m^2/s$) that passes through the membrane by diffusion can be expressed by Fick's law which is written (equation 5.1) in the direction perpendicular to the plane electrodes:

$$N_m = -D_m \frac{dC(z)}{dz} \tag{5.1}$$

where $D_m(m/s)$ is the effective diffusion coefficient of water in the membrane and C (mol/m^3) the local water concentration in the membrane. In the membranes, the amount of water is generally expressed in water content λ. It is equal to the number of water molecules present by sulfonated site of the polymer chain.

If we consider that the water content at the ends of the membrane on the anode side λ_a and cathode side λ_c is known, then flux of water transported by diffusion [Springer et al., 1991] is -

$$N_m = -D_m \frac{\rho_{dry}}{EW} \frac{d\lambda(z)}{dz} \tag{5.2}$$

At the ends of the membrane, the water content at equilibrium depends on the activity of the water in contact with the polymer. As the sorption mechanisms is complex, water content with water vapor activity can be calculated from sorption curves [Maldonado et al., 2012]. Sorption curves, describe the variation of the content in water as a function of relative humidity. Various works carried out in the literature propose varied sorptions at different relative humidities [Kusoglu and Weber, 2017, Springer et al., 1991]. [Maldonado et al., 2012] gave a detailed view of various drying behavior of membrane and the sorption curves obtained. There is a strong effect of the drying temperature and the experiment on the variation of water content as a function of relative humidity.

In this study, the fuel cell is operating at an average temperature of $60°C$, value of the water content $\lambda_{sat} = 17$ (at saturation) will be taken from the model. The

variation of the water with relative humidity at the ends of the membrane is taken linearly. The water content at the electrodes λ_a and λ_c are therefore expressed by equation 5.3 -

$$\lambda_{(a,c)} = \lambda_{(sat)} \times RH_{(a,c)} \tag{5.3}$$

For an ideal gas we can express relative humidity (RH) as a function of the concentration in water (equation 5.4)-

$$RH_{a,c} = \frac{C_{e,a,c}}{C_{sat}(T_m)} \tag{5.4}$$

where RH is the relative humidity at anode and cathode side of electrode respectively. $C_{e,a}$ is the concentration at anode electrode. $C_{e,c}$ is the concentration at cathode electrode. C_sat is the concentration of water saturated at temperature of membrane (T_m).

From Henry law, (linear approximation of sorption curve) it can be concluded (equation 5.5) -

$$\lambda_a = \lambda_{sat} \frac{C_{ea}}{C_{sat}} \tag{5.5}$$

and concentration can be defined by equation 5.6 -

$$C_{sat}(T_m) = \frac{P_{sat}(T_m)}{RT_m} \tag{5.6}$$

5.2.3 Transport of water by electro-osmosis

Perfluorosulfonic membranes are used as a proton conductor in PEMFC. The protons which cross the polymer membrane from the anode to the cathode are hydrated with one or more water molecules ($H^+(H_2O)^n$). The proton flux therefore induces a water transfer called electro-osmotic flow characterized by its transport coefficient electro-osmotic ξ which gives the number of water molecules transported by a proton (equation 5.7)

$$\xi = \frac{n_{H_2O}}{n_{H^+}} \tag{5.7}$$

The density of the water transported by electro-osmosis is directly proportional to the number of water molecules transported and the current density j (equation 5.8).

$$N_m^{EO} = \xi \frac{j}{F} \tag{5.8}$$

As for the diffusion coefficient, many studies [Springer et al., 1991, Ge et al., 2005, Sellin et al., 2019, Dutta et al., 2001, Fuller and Newman, 1992] worked on electroosmotic coefficient . Several correlations have been developed and in general it has been found that increases with increasing water content [Dutta et al., 2001, Springer et al., 1991, Fuller and Newman, 1992]. [Pivovar, 2006] reviews the different techniques used to measure ξ and describe the advantages and disadvantages of each method. [Luo et al., 2010], use a method based on "the hydrogen pump". For that they use two electrodes separated by the membrane supplied with hydrogen and

impose a voltage between the anode and the cathode. This leads to the oxidation of hydrogen into protons at the anode, the transport of protons through the membrane to the cathode and the reformation of hydrogen at the cathode. Each compartment is controlled by humidified gas flow and pressure. [Luo et al., 2010] found that = [1.1 - 1.9] for = [11 - 18].

Different authors have approached differently for modelling water fluxes in fuel cells, however, in this modelling approach, a different hypothesis is used. Electric equivalent diagram (Figure 5.2) is used, where N represents the water flux, C the water concentration and Z the resistance to material transfer. As seen in figure 5.2, electro-osmosis appears from the anode side and water production term appears at cathode side. The nodes indicated shows the movement of water. These nodes helps to connect the transfer through various modes-

$$N_m = N_a + \xi \frac{j}{F} \tag{5.9}$$

$$(1 + 2\xi)\frac{j}{2F} = N_m + N_c \tag{5.10}$$

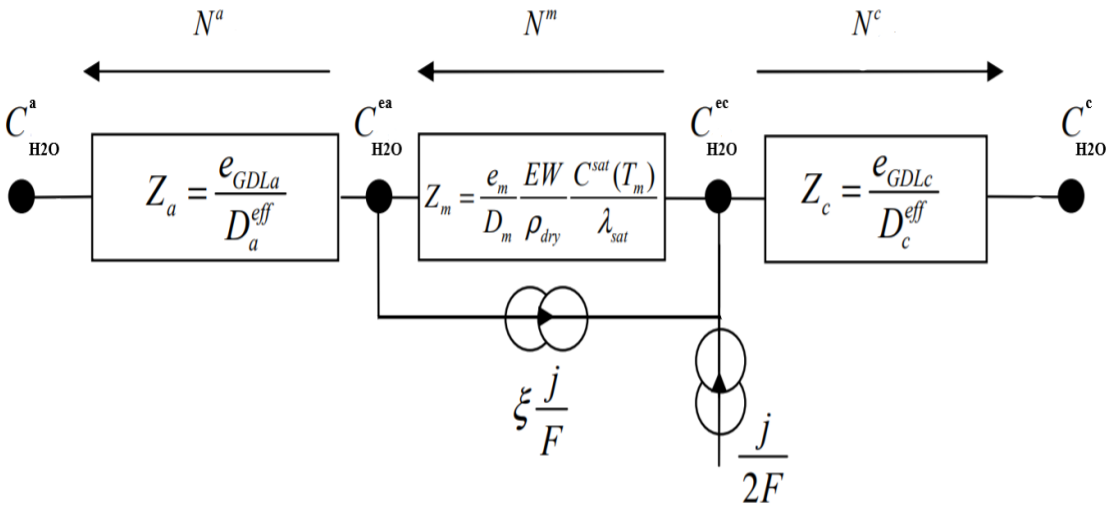

Figure 5.2: Schematic representation of water fluxes in system

As seen in figure 5.2, the symbols have there usual meanings which are as follows- $C^a_{H_2O}$, represents the concentration of water in anode channel. $C^c_{H_2O}$ represents the concentration of water in cathode channel. Similarly, N_a represents the flux for water at anode side, N_c represents the flux of water to cathode side and N_m represents the flux of water from membrane. By convection, water flux is greater than 0, from electrode to channel.

Experimental fluxes of water, within fuel cell running is obtained from [Thomas et al., 2012] (Figure 5.3). As seen in figure, about 80% of the water is collected at cathode side and 20% at anode side. The inputs of model is experimental fluxes and T_m. Relative humidity used is 100 % and temperature of plates is fixed to 60°C. Usually water is transported by four ways, diffusion, electro-osmosis and capillary action and thermo-osmosis. Since we assume that both sides of anode and cathode are fixed to temperature of $60°C$, hence there is no transfer due to thermo-osmosis.

However for the scope of this study some assumptions have been listed in the text below.

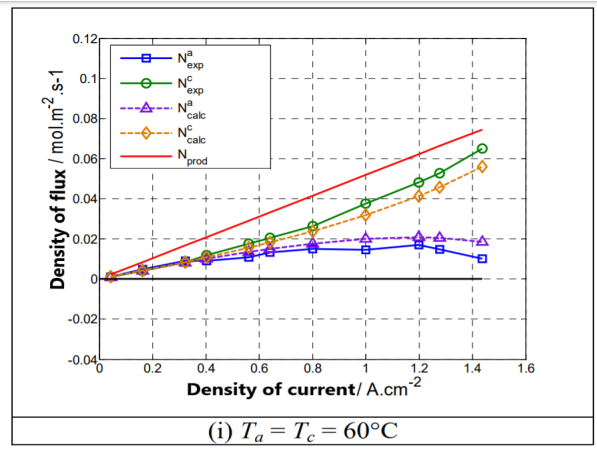

Figure 5.3: Water flux variation from [Thomas et al., 2012]

Non isothermal behavior of fuel cell is taken into account through evolution of membrane temperature with current density. The temperature of membrane has been mesured in real operating conditions, thanks to platinum isolated wires in previous work [Thomas et al., 2014]. Temperature rise of 6.5°C is observed at $j = 1.5A/cm^2$, Figure 5.4. This rise of the temperature of the electrodes therefore causes strong temperature gradients in the GDL ($30K/mm^{-1}$ at most) which result in strong gradients of saturated vapor pressure which will have an influence on the transport of water in the vapor phase within the cell.

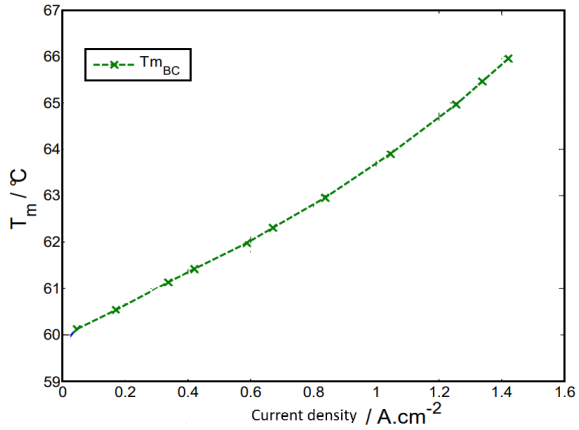

Figure 5.4: Temperature variation from [Thomas et al., 2012]

The assumptions are presented below -

1. 1-d transfer is taken in to system , through plane (along X axis).
2. Water exit in liquid form only and not vapour because channels are saturated at RH = 100%.
3. Water through GDL is transported through vapour form. The condensation occurs only under ribs and channels of bipolar plates.

4. Water is transferred through diffusion and electro-osmosis within the membrane.

5. Temperature of the system is fixed to 60 °C within bipolar plate.

6. Temperature effect with the membrane is taken in to account as seen from the figure 5.4. This implies that the concentration of water at the electrode is always under saturated conditions as seen in figure 5.5.

7. Transport of water through humidified gases is neglected.

8. Water flux is collected at anode side.

5.2.4 Modelling of water fluxes

The model is based on Figure 5.2. $C^a_{H_20}$ represents concentration of water in channel at anode side. $C^c_{H_20}$ at cathode side in channels. $C^{pa}_{H_20}$ represents concentration of water in electrode at anode side. $C^{pc}_{H_20}$ represents concentration of water in the electrode at cathode side.N_a represents the flux of hydrogen at cathode side. N_m represents the water flux passing through membrane. N_{eo} represents the flux due to electro-osmosis.

$$e_{GDLa} = dH^a_2 = 0.00029 \tag{5.11}$$

$$e_{GDLc} = dO^c_2 = 0.00029 \tag{5.12}$$

$$D^{H_2}_{H_20} = 0.00012m^2/s \tag{5.13}$$

$$D^{0_2}_{H_20} = 0.000024m^2/s \tag{5.14}$$

$$P_{total} \times V = n \times R \times T \tag{5.15}$$

where the symbols have their usual meaning. As the humidified gases are 100% in to the channels

$$C^a_{H_20} = \frac{P_{sat}(T_a)}{R \times T_a} \tag{5.16}$$

$$C^c_{H_20} = \frac{P_{sat}(T_c)}{R \times T_c} \tag{5.17}$$

In order to calculate the concentration of hydrogen in the channels, simple mass balance equation can be used. However it is assumed that the water exist in liquid phase only and not vapour. The end result is to calculate the water diffusion coefficient through membrane.

1. **Input parameters**

   For N_a values are obtained from experimental test in Figure 5.3

   For temperature variation over membrane values are obtained from Figure 5.4

   Electro osmosis coefficient is 0.8 [Sellin et al., 2019]

2. **Mechanism of flux transfer**

$$N_c = \frac{i}{2F} - N_a \tag{5.18}$$

$$N_{EO} = \xi \frac{i}{F} \tag{5.19}$$

$$N_m = N_{EO} + N_a \tag{5.20}$$

$$N_m = D_m \frac{\rho_{dry}}{EW} \frac{\lambda_{sat}}{C_{sat(Tm)}} \times \frac{C^{ec}_{H_2O} - C^{ea}_{H_2O}}{e_a} \tag{5.21}$$

D_m = unknown , $\rho_{dry} = 1850\ kg/m^3$, EW = 1.1 kg/mol and $\lambda_{sat} = 17$

$$N_a = \frac{D^{H_2}_{H_2O}}{e_m}(C^{ea}_{H_2O} - C^{a}_{H_2O}) \tag{5.22}$$

$$C^{a}_{H_2O} = \frac{P_{sat}(T_a)}{RT_a} \tag{5.23}$$

$$N_c = \frac{D^{O_2}_{H_2O}}{e_{gdl}}(C^{ec}_{H_2O} - C^{c}_{H_2O}) \tag{5.24}$$

$$C^{C}_{H2O} = RH \times \frac{P_{sat(T_c)}}{RT_c} \tag{5.25}$$

Thanks to this model, D_m will be evaluated by equation 5.21 knowing $C^{ea}_{H_20}$ and $C^{ec}_{H_20}$ from equation 5.22 and equation 5.24.

3. **Results and discussion**

(a) Water concentrations in channel and electrode

Figure 5.5 represents the concentration of water in channel and electrode. There is little variation of water concentration in channels for both anode and cathode at 7.2 mol/m^3 with current density. The concentration changes at electrode in cathodic side as it is also effected by water produced in the system. Water is transported mainly in the vapour form . C_{sat} is always superior to other concentration (figure **??**). This is provided by the fact that, here increase of temperature of membrane with current density is taken into account (non-isothermal). This is also confirmed by previous results [Morin et al., 2017, Thomas et al., 2014].

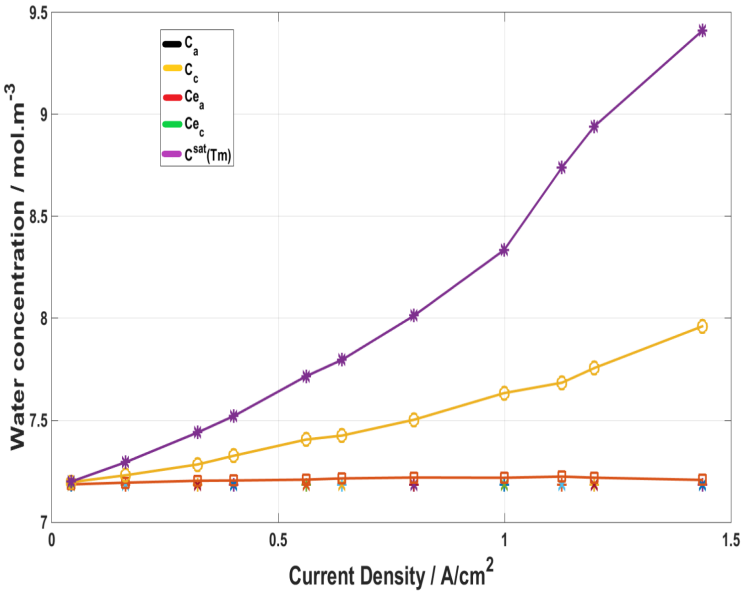

Figure 5.5: Water concentration in channels and electrode

(b) Effect of water content with respect to current density.

Figure 5.6 represents the water content with respect to current density. As observed water content decreases from 17 to 13 at the anode side. Similarly water content reduces from 17 to 14.5 at cathode side.

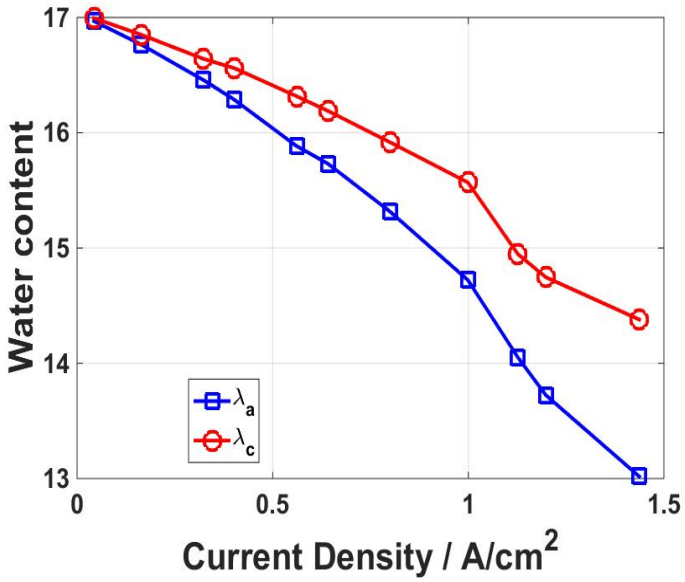

Figure 5.6: Effect of water content with respect to current density

(c) Effect of water diffusion coefficient with respect to average λ.

Figure 5.7 represents the water diffusion coefficient with respect to water content λ and $\xi = 0.8$. It can be observed that with electro-osmosis the diffusion is approximately 3 times higher. In case of electro-osmosis, with respect to average λ, the water diffusion increases from 0.4×10^{-4} to $0.9 \times 10^{-4} m^2/s$. Similarly, without electro osmosis, the diffusion coefficient

increases from 3×10^{-6} to $2 \times 10^{-5} m^2/s$. With increase in current, water diffusion increases and is higher when electro-osmosis is taken in account. In the comparison of chapter 2, the diffusion value found is 2 order higher. The reason can be high humidification in the membrane due to water production in modelling.

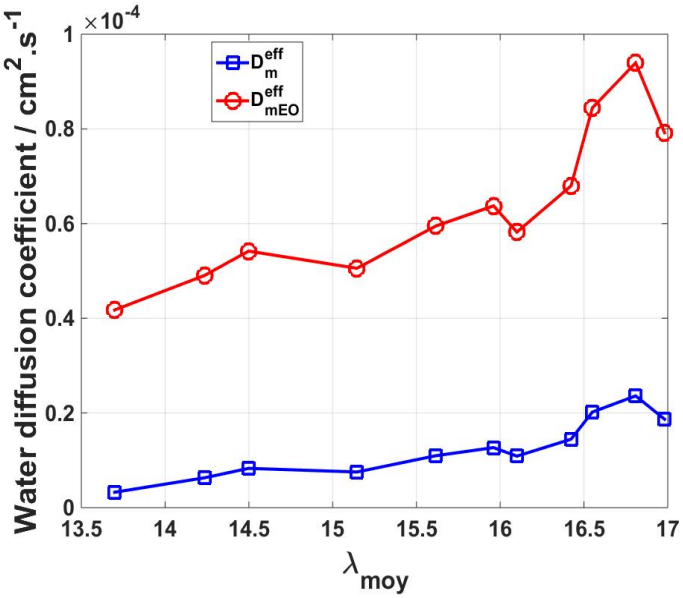

Figure 5.7: Effect of water diffusion coefficient with respect to average λ

(d) Effect of water diffusion coefficient

Figure 5.8 and, figure 5.9 represents the variation of membrane diffusion coefficient of water with respect to factor $\frac{\rho}{EW} \times \Delta\lambda$. The value of minimum and maximum λ is fixed at λ_{min}= 11 and λ_{max}= 17. The value of equivalent weight is varied from 636 - 1100. The value of density varies from 1100 to 2200. Based on the results, effective water diffusion is higher with electro-osmosis by 3-4 times compared to diffusion without electro-osmosis. Considering the diffusion coefficient without electro-osmosis, it lies in order of $0.2 \times 10^{-4} cm^2/s$. This can be due to higher water production due to electro-osmosis. Also, with the increase in λ, the diffusion across the membrane increases. Considering the factor $\frac{\rho}{EW} \times \Delta\lambda$.

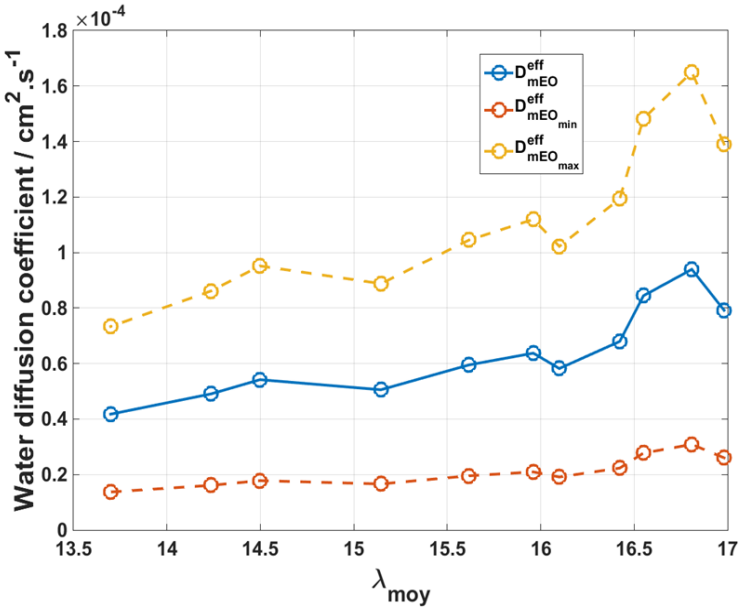

Figure 5.8: Effect of water diffusion coefficient with electro osmosis

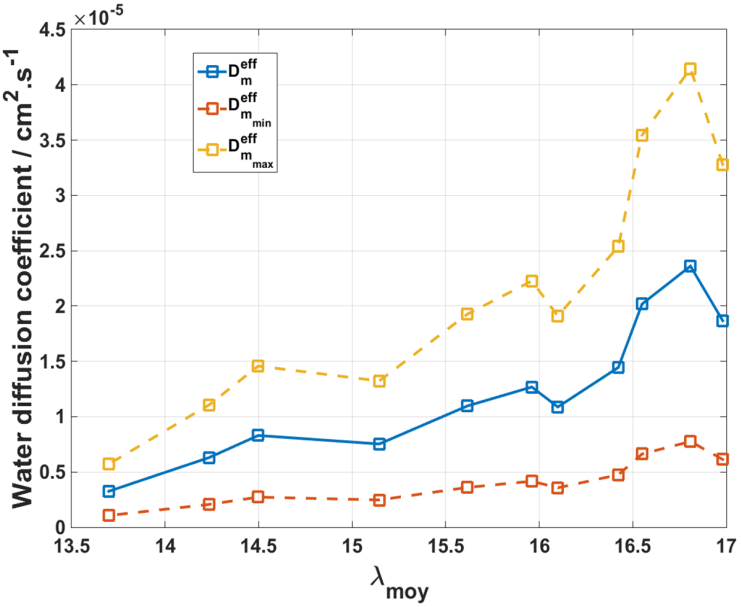

Figure 5.9: Effect of water diffusion coefficient without electro osmosis

Considering the multi-physics involved in PEMFC analysis, modelling remains an important part in order to optimize performance of fuel cells. Need of modelling can help to build up online diagnosis tools which can help in diagnosis and prognosis of fuel cell systems. Modelling can provide details of parameters which cannot be directly calculated or estimated.For present research, it helped to calculate diffusion coefficient through the membrane. The calculated values are 2 order higher than the value calculated from experiments in chapter 2. This behavior can be attributed to water production in modelling data which was not considered during experiments in chapter 2. This can also be explain from cluster based model where isolated cluster dominates in low hydration conditions ($0< \lambda < 2$). With increase of water uptake cluster growth increases. Porosity and cryoporometry calculations show majority of

water in hydrated domain with size distribution> 5nm. High diffusion results can be due to large cluster growth, more water distribution. It was also seen that the diffusion depends on water content λ and it increases with increase in λ.

5.3 Prognosis and importance of data driven modelling

In the previous section, an analytical 1-D model is developed and results are calculated regarding electro-osmosis and diffusion. This type of modelling calculates the transfer results based on certain sets of operating conditions. But what if a new set of data needs to be prognosed for prognosis where emperical relations are not available to create link between all parameters ? In such cases data driven modelling can be useful. This approach does not depends on phisico relations among parameters but creates a link among each other by using certain algorithms. This models comes in machine learning / deep learning analysis.

One of the key features of data driven modelling is that it does not require a deep understanding of the phenomenon involved. There are several types of data driven models available such as Artificial neural network(ANN), Support vector machines (SVMs), partial least squares, regression models, which can be further classified in to linear regression models, logistic regression models, decision tree.

Very limited work considering the use of data driven models is carried out. Linear regression models are very popular because they can be used very easily. These models can provide results accurately based on the complexity involved in the modelling. More the amount of data, linear regression may provide poor results. Hence it is required to use other models such as Ridge regression in order to reduce over-fitting (Training data is a good fit but the test data is poor fit) or Lasso regression. Further data can also be analysed using deep learning. Artificial neural network is a part of deep learning process and deep learning is a sub field of machine learning. Deep learning is a technique that makes computer to do what comes naturally to humans, learning by examples. ANN is a computational model based on the structure and function of biological neural network.

5.3.1 Bibliography and few models used in literature

Ridge regression - Considering the case of linear regression, it imposes higher weights or coefficients on the features which are more important, than the others and produces the problem of over-fitting. In such case, it is not advisable to use regression and the most appropriate choice goes to Ridge regression [Hoerl et al., 1975, Hoerl and Kennard, 1970, Marquardt and Snee, 1975,]. Ridge regression uses a regularization term, which in return penalises the features with higher coefficient with a hyper-parameter λ. Ridge regression introduces a regularization term with squared difference of predicted and true values [Fernández-Delgado et al., 2019,]. The hyper-parameter can be varied from 10^{-5} to 500 in order to get the best fit, in order to optimize the solution or loss function. This is also called as hyper-parameter tuning. If the value of this hyper-parameters is 0, it means that model behaves as linear regression. Ridge regression has been used at many places in order to predict the output where weights of features plays an important role. Every time in case

of regression the choice is to reduce the sum of residuals. The main aim of ridge regression is to reduce over-fitting. [Górski and Jakubowska, 2019,] used ridge regression to predict the voltametric signals.

$$\sum_{i=1}^{n}(y-\bar{y})^2+\lambda(slope)^2 \tag{5.26}$$

where,

1. y = actual values
2. $\bar{y}$ = predicted values
3. λ = hyper parameter
4. m = slope of fitted line

Lasso regression -

Lasso regression is a step ahead of ridge regression which actually takes part into feature selection. In lasso regression, not only the residual sum of square is minimised but it also produces coefficient that are exactly 0 [Tibshirani, 1996,]. The main difference between Ridge and Lasso regression is the slope part, while Ridge shrinks the slope part to zero, Lasso put it to 0. This is important to use when there are number of features used in the selection. Lasso penalized regression is capable of handling linear regression problems where the number of predictors far exceeds the number of cases [Wu et al., 2008,].

For example consider the equation for best fit line

$$y=m_1x_1+m_2x_2+m_3x_3+.....m_nx_n \tag{5.27}$$

where $m_1, m_2...$ are the slopes of the features involved. The equation in Lasso regression is changed to Equation 5.28 where the slope with power raised to 2 is changed to modulus and thereby gives a possibility for the features which are not very important to become 0.

$$\sum_{i=1}^{n}(y-\bar{y})^2+\lambda|(slope)| \tag{5.28}$$

Random forest regressor- Random forest regressor is an improved technique where a small amount of data is sampled from a large set of data. Now multiple decision trees are made and decision is taken. Decision trees is on low bias and high variance so random forest tries to remove high variance. For regression problems mean or median of small data sets is calculated. The main advantage of random forest algorithm is the stability. Since random forest works by dividing the data into small subsets and calculating individual predicted result, hence it is computationally costly. [Morán-Durán et al., 2019] used random forest regressor to predict fuel cell output voltage under transient conditions. [Baker, 2019] used random forest regressor to predict AC optimal power flow by analysing huge amount of data as generated from grid operators.

Artificial neural network-

[Han and Chung, 2016,] worked on predicting the performance of PEMFC stack by use of ANN and SVM models, considering input data of hydrogen and oxygen inlet pressure, stack temperature, relative humidity of gases and predicted the output results with 0.99 coefficient of determination (R^2) for ANN and 0.98 R^2 for SVM model. Also, [Chávez-Ramírez et al., 2010,] worked on prediction of voltage and cathode outlet temperature in a PEM fuel cell stack consisting of seven input variables, and two output variables. A similar work was carried out by [Napoli et al., 2013,] to predict the voltage and cathode outlet temperature. The availability of data can hinder prediction of correct output and based on this [Saengrung et al., 2007,] as they worked on two input variables mainly air flow rate and stack temperature using feed forward neural networks.

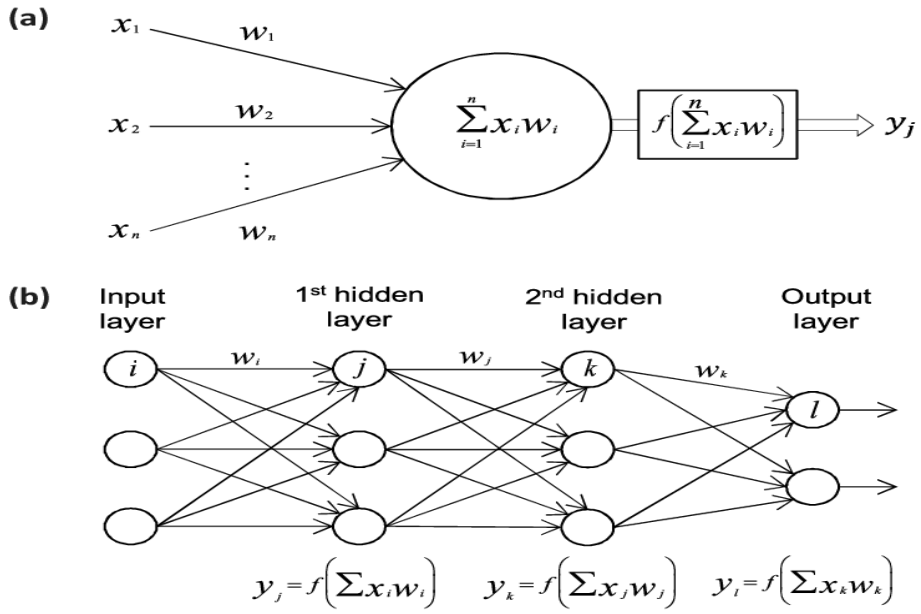

Figure 5.10: Structure of artificial neural network

Figure 5.10 shows a structure of ANN, which consists of input parameters, hidden layers, a set of weights between each layer (w_1, w_2 ...) and a choice of activation function between each layer.

1. **Input parameters** - Input parameters can be also defined as features, which are added as an input to the model.

2. **Hidden layers** - Between input and output of this model, there is a hidden layer. This hidden layer can be single or many depending on the complexity of the model. Hidden layers perform a non linear transformation of inputs applied to data. The size of the hidden layer is normally between the size of the input and output. More the hidden layers, better it will predict the output, but will increase the running time of the calculations.

3. **Weight** - Weight is the parameter within a neural network that transforms input data within the network's hidden layers. Weights are contained within the hidden layer of the network.

4. **Activation function** - Activation functions are mathematical equations that determine the output of a neural network. Being attached to each neuron it determines, if it needs to be fired or not based upon the input neuron relevant to the model prediction. There can be three types of activation function-

   (a) Sigmoid function

   (b) ReLU function

   (c) tanh function

The following steps are performed starting from data cleaning of the data set to preparing the model for the prediction.

5.3.2 Problem statement

The problem statement is prognosis of voltage. The data sets corresponds to voltage change or observed during change in the temperature of fuel cell as presented by [Maizia et al., 2018]. The aim of the research was to observe the flooding and drying trends of PEM fuel cell by varying fuel cell temperature from 10° C to 70° C, current at 12.5A, humidifier temperature was fixed to 46°C. Based on this, there is a humidity change from fully humid conditions to unsaturated. The input variables which govern the target variable (V) are pressure at anode, pressure at cathode, relative humidity,temperature and current. Current values are not taken into account, as it is fixed to 12.5A for all operating conditions. Figure 5.11 explains the voltage variation with respect to the temperature change. Not only temperature but other parameters such as pressure at cathode , pressure at anode , relative humidity which contribute to the overall change are involved in prediction of temperature.

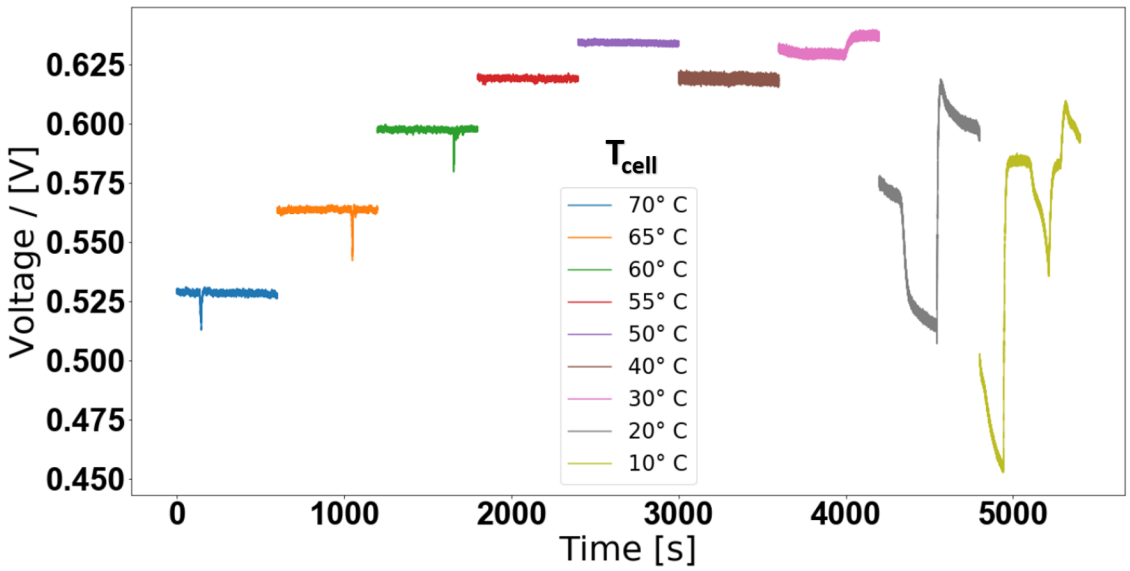

Figure 5.11: Represents the voltage variation with change in temperature

1. **Data cleaning** - Data cleaning is an essential part of the model training and learning as it weeds out the null values, add/remove missing information,

checks for the shape of the columns, duplicate data check as duplicate data can provide errors in the prediction of the output parameter. Based of our data, no outlier is observed. For the analysis, python library pandas and numpy was used for data cleaning. Files have been merged via concat method .

2. **Partition of data**- ANN models utilize the concept of artificial learning and hence learn from data. Each 10 minute signal at particular temperature is merged with other signals to get a 2 hr large signal, showing variation in the temperature, relative humidity, voltage, pressure at cathode and pressure at anode.

3. **Selection of training and testing data** Through the main signal last 20 percent of data is used for testing and initial 80 percent of the data is used for leaning / training the model. Standard-Scalar is used for scaling of features (voltage, pressure at cathode, pressure at anode, relative humidity and temperature)

4. **Correlation matrix** In order to understand how the parameters interact with each other correlation matrix (heat plots) are plotted.. Figure 5.12 shows correlation matrix of parameters involved.

   C - Cathode pressure

   A - Anode pressure

   V - Voltage

   Temp - Temperature

   RH - Relative humidity

   Based on the results of figure 5.12, temperature shows a strong relation, followed by

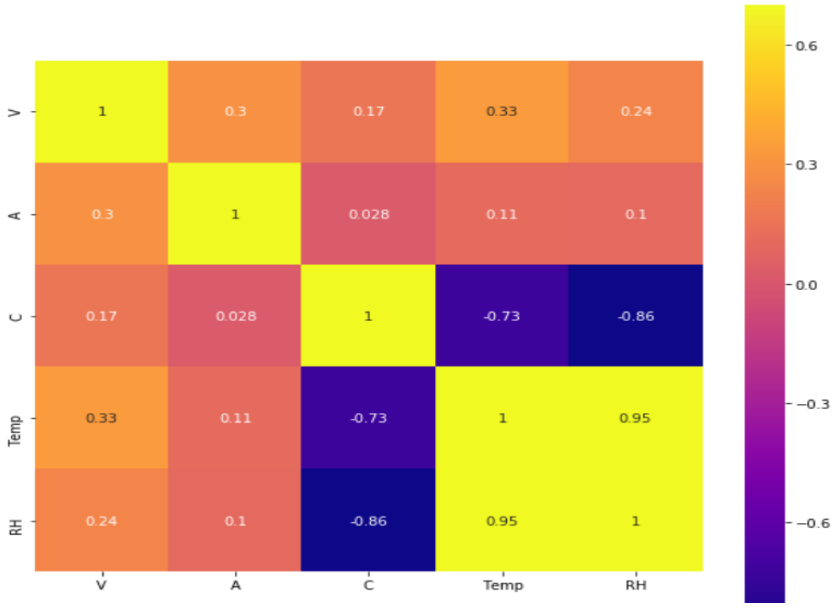

Figure 5.12: Correlation coefficient of various parameters

5. **Model function** The next step is to chose the required model, since the data is continues type so MPL regressor model is chosen here over logistic regression. In case of ANN, ReLU function is used to create a non linear relationship between the parameters.

6. **Minimising objective function** The next step is to minimize the objective function and averaging the mean square errors for the 10 subsets in case of ANN.

5.3.3 Data treatment

Data needs to be treated to avoid further problems of error.

1. Train-Test split and Cross-validation

   In order to check if the model performs good or not, it is mandatory to check the data on unseen data and hence train and test split concept came into practise. Cross validation is a slightly different concept and comes into play when we are interested in finding values or optimising values of various hyper-parameters. An n-fold cross validation simply means dividing the data into n parts and using that part to validate both test and train data. [Varoquaux, 2018,] gave insights about how small sample sizes creates large error bars. [Little et al., 2017,] explained about various cross validation strategies.

2. Standardization and Normalization-

   In a data-set there are many features and these features are arranged in different units. For example a feature can be 10 to 20 orders more then the other. In such cases it becomes difficult to predict the actual results with increased accuracy. Normalization (equation 5.29) scale down the features to (0-1), whereas standardization scales down the features to standard normalised data with mean = 0 and standard deviation = 1.

$$X_{norm} = \frac{X - X_{min}}{X_{max} - X_{min}} \tag{5.29}$$

   Normalization of data also helps to increase the calculation speed as the weights assigned becomes smaller and hence much easier to calculate. For k-nearest algorithm, linear regression problems or Artificial Neural Network (ANN) problems scaling plays a very important role, however for decision trees , logistic regression, boosting techniques data need not to be scaled. For all the calculations performed further, MinMaxScaler imported from sklearn prepossessing is used in python to scale down all features in range of (0-1).

3. Over-fitting and under-fitting data -

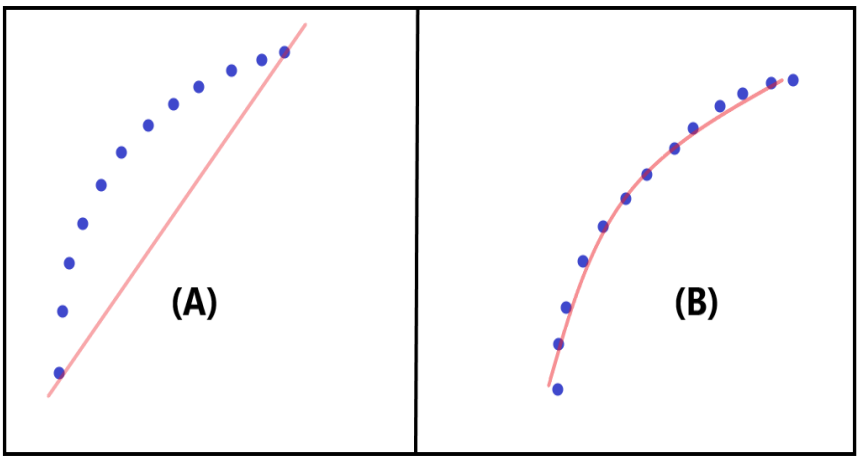

Figure 5.13: (a) represents under-fit data and (b) represents over-fit data

Both under-fitting, Figure 5.13(a) and over-fitting, Figure 5.13(b) problems in data analysis are important while treating data. While under-fitting results in both test and training data poorly fit, over-fitting results in training data to be good fit but the test data is poorly fit. This results in high bias and high variance for under-fitting data and low bias, high variance for over-fitting data. Bias can be defined as error of training data and variance can be defined as error of testing data.[Van der Aalst et al., 2010,] gave method to analyse between under-fitting and over-fitting data.

5.3.4 Results

Considering the fitting by linear regression, the model accuracy involved is 56% when the data is not normalised and the method used to predict is test and split. However, when the normalization is performed the accuracy increased to 62%. The test and training data was divided in the ratio of 20:80. Considering the accuracy there is a stronger need to deploy other models.

Sklearn library is used to use Ridge regression in python. Negative mean square error was used as a scoring parameter with cross validation of 5. Based on the optimization by grid search, value of hyper parameter chosen was 0.0001 and the value of best score was -3.79×10^{-18}. The model accuracy is 59%.

Sklearn library is used to perform Lasso regression in python. Negative mean square error was used as a scoring parameter with cross validation of 5. Based on the optimization by grid search, value of hyper parameter chosen was 0.000109 and the value of best score was -0.00010. The accuracy score is found to be 58%.

Based on the simulation results, accuracy obtained by random forest regressor, came out to be 98.5 %. It is seen boosting techniques perform better than other regression techniques.

In this research, ANN is used and five variables, temperature, relative humidity (RH),pressure at cathode and anode and voltage are considered. The parameter to predict is voltage and the input variables are temperature, relative humidity (RH),pressure at cathode and anode.

(a) With number of layers set to 5, and iteration up to 100, the accuracy score is 0.93.

(b) With number of layers set to 8, and iteration up to 500, the accuracy score is 0.98.

No.	Linear regression	Ridge regression	Lasso regression	Random forest regressor	ANN (5 Layers)	ANN (8 Layers)
1	62%	59%	58%	98.5%	93%	99 %

Table 5.1: Results of accuracy of different models in predicting voltage

Comparing the models in the below Table 5.1, the accuracy involved increases from 59 % (Lasso regression), 62% for linear regression, 98.5 % for random forest regressor to 99 % (8 layers) using ANN. Regression models used perform poorly as the accuracy score is very less. The reason can be poor fit based on parameters involved. Moving further is Random forest regressor, where the accuracy score is 98.5 %. Since Random forest regressor uses the technique of sampling a small amount of data from large dataset and predicting results out of it, hence it shows an increase in accuracy score. Based on the results, ANN performs better, and it is observed more the layers involved better is the result of prediction. Considering the computational time, it is minimum for linear regression, followed by random forest and is highest for artificial neural network modelling. As the number of layers and iterations increases, computational time increases. We have considered only 4 parameters here, however in future research a much more complex model can be developed and hyper-parameter tuning (optimizes the parameters of the model) can be used.

5.4 Conclusions

Considering the multi-physics involved in PEMFC analysis, modelling remains an important part in order to optimize performance of fuel cells. Need of modelling can help to build up online diagnosis tools which can help in diagnosis and prognosis of fuel cell systems. Modelling can provide details of parameters which cannot be directly calculated or estimated. In the present research, we considered two types of modelling, 1) Analytical and 2) Data driven. Considering the first, it helped to calculate diffusion coefficient through the membrane. The calculated values are 2 order higher than the value calculated from experiments in chapter 2. This behavior can be attributed to water production and electro-osmosis in modelling data which

was not considered during experiments in chapter 2. This can also be explained from cluster based model where isolated cluster dominates in low hydration conditions ($0 < \lambda < 2$). With increase of water uptake, cluster growth increases. Porosity and cryoporometry calculations, show majority of water is in hydrated domain with size distribution $>$ 5nm. High diffusion results can be due to large cluster growth, more water distribution. It was also seen that the diffusion depends on water content λ and it increases with increase in λ.

Data driven modelling also plays an important role in order to estimate fuel cell parameters.Not much work has been done in this field considering the applications of PEMFC. The importance arises when it is difficult to link physio-chemical relations among parameters. In such case data generated from experiments can be used to estimate results. In this study based on the experimental dataset used, voltage values were estimated. Five models were employed (regressor based) namely Linear, Ridge, Lasso regression, Random forest and artificial neural network. Random forest and Artificial neural network shows better accuracy , but also with accuracy the computational time and cost increases. Both the modelling approaches, based on our study can be used to further optimize the performance of fuel cells.

Conclusion

The main objective of this research is to improve water management in PEM fuel cells with water balance and Electrochemical Noise Analysis (ENA) techniques. There can be numerous parameters such as temperature, relative humidity, material of GDL, thickness of MEA, which can affect the water management. However, in this study the main attention is focused on the influence of different flow field designs of bipolar plates on water management and fuel cell performance. Another point which have been studied in details in this work is related with in-situ measurement of effective water diffusion coefficient. Indeed, there is a real lack of information concerning this governing parameter responsible for water transport, especially for in-situ conditions. In order to achieve these two goals we have used both traditional experimental techniques, as polarisation curve and pressure losses measurements, as well as more advanced methodologies, namely water balance and ENA. We have finished our study by the demonstration of some analytical approaches allowing to use obtained experimental information for modelling and prognostics of fuel cell performance.

Water diffusion coefficient plays an important role in overall transport of reactants in the fuel cell working but remains difficult to measure by in-situ methods. Traditional gravimetric methods give ex-situ information, only. The methods as neutron are costly and utilize special setups. The above two shortcomings can be overcome (Chapter 2) by using water balance method which can be adapted for the same fuel cell setup and provides result in in-situ condition. We have used this method in our study to calculate values of water diffusion coefficient. Nafion and Anion membranes were used to see the variation of diffusion coefficient. Based on this our values lies in region of transient and steady state ($\approx 10^{-7} cm^2/s$), moreover values with respect to a particular operating condition was calculated. Apart from the analysis, effect of density, equivalent weight and water content was estimated. Results shows that water content plays an important role in variation of diffusion results.

The next Chapter 3 deals with the study of impact of new flow field designs of bipolar plates on water management. Due to high-pressure head losses in traditional serpentine design and less experimental work in this area, there is need to explore flow field designs with improved efficiency and better water management. In this, we have introduced four new designs and compared them experimentally based on polarization curve and pressure head losses. Out of all designs, multi serpentine shows superior electrical performance and hybrid design shows improved water management compared to serpentine design. Both the designs shows reduced pressure head losses compared to traditional serpentine design. Based on our results and study, the two designs can be employed in fuel cell stacks in order to have more uniform water management. This will result increased performance and savings in compres-

sor power cost. Circular and spot designs are still under research and unfortunately complete analysis have not been performed due to limitations in time.

In-situ diagnosis plays a very important role in monitoring and management of fuel cell stacks. For practical applications it is important that a technique is robust, reliable and can provide un-interrupted diagnosis. Unfortunately, most of the traditional techniques cannot be used in this way as they suffer from high costs, cannot provide un-interrupted diagnosis and requires experience. Considering the applications of ENA, it is first study when this method is applied in order to compare different flow field designs, the results are presented in Chapter 4. For our study only two operational points were used which correspond to two values of applied current, namely I = 4A and I = 19 A. and limited variations in humidification conditions (RH=50% and RH=100%). The main attention have been payed to different flow field design. The results of ENA were presented with descriptors in time and frequency domain, special attention have been put on data treatment, in particular on detrending procedure. Below are the detailed results obtained using ENA.

• Traditional serpentine geometry of flow field bipolar plate design has been compared to two novel geometry (multi-serpentine with slots and hybrid geometry). ENA was applied to voltage measurements for two operating point. Based on the signals obtained, qualitative and quantitative analysis was performed in temporal domain thanks to standard deviation variations with short-time analysis. Considering the case of voltage signals, qualitative analysis of three geometries shows a maximum disturbance in serpentine geometry, followed by multi-serpentine geometry set-up with slots and mostly stable fluctuations for hybrid geometry. Hybrid design highlights the higher stability with no presence of large fluctuations or peaks that is a signature of good water management. Serpentine geometry reveals the lowest stability and highest presence of peaks due to worse removal of water. Multi-serpentine design helped with the addition of slots shows a reasonable stability of voltage fluctuations and good performance. The results of ENA in time domain are in a good agreement with previously presented traditional measurements of polarization curve pressure head losses.

• ENA has been used for generation of statistical descriptors in frequency domain also (power spectral density - PSD). The noise signature of a fuel cell in frequency domain (some hertz or less) can be interpreted as a fractal noise with different slopes p varying from p = 1.6 to 2. This noise signature is sensitive to flow field design and current conditions also. We conclude that amplitude of ENA is the most important for serpentine design. For this design increase of current from I= 4A to I= 19A does not influence significantly the noise signature. It is not the case of multi-serpentine design where current increase leads to significant increase of PSD. Thus, for this design ENA allows to separate for two operational points, namely I = 4A and I = 19 A. We want to emphasized, that traditional polarization curve measurements don't allow to separate above mentioned operational points with respect to different flow field design. At the last, the lowest energy of noise has been detected for the hybrid design. It confirms, in accordance with the previously obtained descriptors in time domain, that this design allows to obtain the higher performance with respect to water management.

• Multi serpentine and hybrid design are not affected by the effect of relative humidity, and only serpentine design demonstrates the dependence on this factor

in the frame of provided experiments. In particular, for serpentine design the slope p decreases with increase in relative humidity; in previous study it was shown that it can be explained by poor water management. Introduction of slots in multi serpentine can be a reason for improved water management and all our experiments show that hydride design is the most adapted for water management. Thus, we can suppose that in our experiments for all humidification rates multi serpentine and hydride design work in normal working conditions contrary to traditional serpentine design.

• In order to understand the physical nature of fuel cell electrochemical noise (EN), namely the voltage fluctuations, we have recorded and analysed simultaneously the pressure fluctuations both on the anode and the cathode side. Based on these measurements, it is possible to conclude that pressure fluctuations are completely de-correlated with voltage fluctuations.

• In general, ENA can is a robust and reliable technique to provide is-situ diagnosis of new flow field designs and to understand water management over varying operating conditions. In particular, ENA shows the advantage of multi serpentine and especially hydride design in comparison to traditional serpentine design with respect to water management.

Considering the multi-physics involved in PEMFC analysis, modelling remains an important instrument in order to optimize performance of fuel cells and to develop the methods for its prognosis. Modelling can help to build up online diagnosis tools which can help in diagnosis and prognosis of fuel cell systems. Modelling can provide details of parameters which cannot be directly calculated or estimated. In the present research we considered two types of modelling, namely analytical and data driven (Chapter 5). Using analytical approach, water diffusion coefficient through the membrane have been calculated. The calculated value are 2 order magnitude higher than the value calculated from the experiments in chapter 2. This result can be attributed to water production in modelling data which was not considered during experiments in chapter 2. It was also shown that the diffusion depends on water content λ and it increases with increase in λ. Data driven modelling also plays an important role in estimation of fuel cell parameters. Not a lot of works have been done in this field considering the applications of PEMFC. The difficulties arise when it is necessary to link physio-chemical relations among parameters. In such case data generated from experiments can be used to estimate results. In this study we have demonstrated the possibilities of data driven approach for estimation of voltage values using previously obtained experimental data. Five regressor based models were employed namely: linear, ridge, lasso regression, random forest and artificial neural network. Random forest and artificial neural network show better accuracy, but the computational time and the cost increases with increasing of accuracy. Both proposed in this study modelling approaches can be used to further optimization of fuel cells.

Perspectives

The new flow field geometries of bipolar plated proposed in this work to enhance water management can be considered as a first step for further development in fuel cell stacks area. To go further concomitant measurements and cross-measurements of pressure, impedance and temperature evolution and correlation between different signals for several operating points and relative humidity should be done in a future works. In particular we propose, increasing of data base (different operating set of

experimental conditions) for new flow field bipolar plate designs. Use of pressure sensors with improved accuracy in order to collect pressure drop information for hybrid design. Use of different sensors for ENA and cross-correlation measurements in order to understand the nature of electrochemical noise. Experiments for estimation of diffusion coefficient with electro-osmosis in relation with 2-D modelling of transfer processes through the membrane. Developing numerical models for new flow field designs in order to optimize the performance numerically for different operating conditions and track diphasic behavior within bipolar plate. Testing of new flow field design of bipolar plates for stack conditions. Development of online diagnosis on the basis of ENA and associated prognosis tools in order to evaluate faults in running PEMFC stack.

Bibliography

[Aballe et al., 1999] Aballe, A., Bethencourt, M., Botana, F., and Marcos, M. (1999). Using wavelets transform in the analysis of electrochemical noise data. *Electrochimica Acta*, 44(26):4805–4816.

[Alduchov and Eskridge, 1996] Alduchov, O. A. and Eskridge, R. E. (1996). Improved magnus form approximation of saturation vapor pressure. *Journal of applied meteorology*, 35(4):601–609.

[Álvarez et al., 2012] Álvarez, G., Alcaide, F., Cabot, P. L., Lázaro, M. J., Pastor, E., and Solla-Gullón, J. (2012). Electrochemical performance of low temperature pemfc with surface tailored carbon nanofibers as catalyst support. *International journal of hydrogen energy*, 37(1):393–404.

[Andújar and Segura, 2009] Andújar, J. M. and Segura, F. (2009). Fuel cells: History and updating. a walk along two centuries. *Renewable and sustainable energy reviews*, 13(9):2309–2322.

[Antunes et al., 2011] Antunes, R. A., De Oliveira, M. C., Ett, G., and Ett, V. (2011). Carbon materials in composite bipolar plates for polymer electrolyte membrane fuel cells: A review of the main challenges to improve electrical performance. *Journal of Power Sources*, 196(6):2945–2961.

[Aslam et al., 2018] Aslam, R., Ingham, D., Ismail, M., Hughes, K., Ma, L., and Pourkashanian, M. (2018). Simultaneous direct visualisation of liquid water in the cathode and anode serpentine flow channels of proton exchange membrane (pem) fuel cells. *Journal of the Energy Institute*, 91(6):1057–1070.

[Asri et al., 2017] Asri, N. F., Husaini, T., Sulong, A. B., Majlan, E. H., and Daud, W. R. W. (2017). Coating of stainless steel and titanium bipolar plates for anticorrosion in pemfc: A review. *International Journal of Hydrogen Energy*, 42(14):9135–9148.

[Atiyeh et al., 2007] Atiyeh, H. K., Karan, K., Peppley, B., Phoenix, A., Halliop, E., and Pharoah, J. (2007). Experimental investigation of the role of a microporous layer on the water transport and performance of a pem fuel cell. *Journal of Power Sources*, 170(1):111–121.

[Baert and Vervaet, 2003] Baert, D. and Vervaet, A. (2003). Small bandwidth measurement of the noise voltage of batteries. *Journal of power sources*, 114(2):357–365.

[Bahrami et al., 2014] Bahrami, M., Shahidi, M., and Hosseini, S. (2014). Comparison of electrochemical current noise signals arising from symmetrical and asymmetrical electrodes made of al alloys at different ph values using statistical and wavelet analysis. part i: Neutral and acidic solutions. *Electrochimica Acta*, 148:127–144.

[Bai et al., 2010] Bai, C.-Y., Wen, T.-M., Hou, K.-H., and Ger, M.-D. (2010). The bipolar plate of aisi 1045 steel with chromized coatings prepared by low-temperature pack cementation for proton exchange membrane fuel cell. *Journal of Power Sources*, 195(3):779–786.

[Baker, 2019] Baker, K. (2019). Learning warm-start points for ac optimal power flow. In *2019 IEEE 29th International Workshop on Machine Learning for Signal Processing (MLSP)*, pages 1–6. IEEE.

[Banerjee et al., 2016] Banerjee, R., Hinebaugh, J., Liu, H., Yip, R., Ge, N., and Bazylak, A. (2016). Heterogeneous porosity distributions of polymer electrolyte membrane fuel cell gas diffusion layer materials with rib-channel compression. *International Journal of Hydrogen Energy*, 41(33):14885–14896.

[Barbir, 2012] Barbir, F. (2012). *PEM fuel cells: theory and practice*. Academic press.

[Barbir et al., 2005] Barbir, F., Gorgun, H., and Wang, X. (2005). Relationship between pressure drop and cell resistance as a diagnostic tool for pem fuel cells. *Journal of Power Sources*, 141(1):96–101.

[Barbir and Yazici, 2008] Barbir, F. and Yazici, S. (2008). Status and development of pem fuel cell technology. *International Journal of Energy Research*, 32(5):369–378.

[Behrou et al., 2019] Behrou, R., Pizzolato, A., and Forner-Cuenca, A. (2019). Topology optimization as a powerful tool to design advanced pemfcs flow fields. *International Journal of Heat and Mass Transfer*, 135:72–92.

[Bernard et al., 2005] Bernard, J., Boinet, M., Chatenet, M., and Dalard, F. (2005). Contribution of the acoustic emission technique to study aluminum behavior in aqueous alkaline solution. *Electrochemical and Solid-State Letters*, 8(7):E53–E55.

[Bernardi and Verbrugge, 1991] Bernardi, D. M. and Verbrugge, M. W. (1991). Mathematical model of a gas diffusion electrode bonded to a polymer electrolyte. *AIChE journal*, 37(8):1151–1163.

[Bertocci et al., 1998] Bertocci, U., Frydman, J., Gabrielli, C., Huet, F., and Keddam, M. (1998). Analysis of electrochemical noise by power spectral density applied to corrosion studies: Maximum entropy method or fast fourier transform? *Journal of the Electrochemical Society*, 145(8):2780.

[Bhunia and Dutta, 2018] Bhunia, P. and Dutta, K. (2018). Biochemistry and electrochemistry at the electrodes of microbial fuel cells. *Progress and Recent Trends in Microbial Fuel Cells*, pages 327–345.

[Boinet et al., 2007] Boinet, M., Marlot, D., Lenain, J., Maximovitch, S., Dalard, F., and Nogueira, R. (2007). First results from coupled acousto-ultrasonics and electrochemical noise techniques applied to gas evolving electrodes. *Electrochemistry communications*, 9(9):2174–2178.

[Bouchet and Siebert, 1999] Bouchet, R. and Siebert, E. (1999). Proton conduction in acid doped polybenzimidazole. *Solid state ionics*, 118(3-4):287–299.

[Brett and Brandon, 2007] Brett, D. J. and Brandon, N. P. (2007). Review of materials and characterization methods for polymer electrolyte fuel cell flow-field plates.

[Cano-Andrade et al., 2010] Cano-Andrade, S., Hernandez-Guerrero, A., Von Spakovsky, M., Damian-Ascencio, C., and Rubio-Arana, J. (2010). Current density and polarization curves for radial flow field patterns applied to pemfcs (proton exchange membrane fuel cells). *Energy*, 35(2):920–927.

[Carton and Olabi, 2017] Carton, J. and Olabi, A.-G. (2017). Three-dimensional proton exchange membrane fuel cell model: comparison of double channel and open pore cellular foam flow plates. *Energy*, 136:185–195.

[Ceraolo et al., 2003] Ceraolo, M., Miulli, C., and Pozio, A. (2003). Modelling static and dynamic behaviour of proton exchange membrane fuel cells on the basis of electro-chemical description. *Journal of power sources*, 113(1):131–144.

[Chávez-Ramírez et al., 2010] Chávez-Ramírez, A. U., Muñoz-Guerrero, R., Durón-Torres, S., Ferraro, M., Brunaccini, G., Sergi, F., Antonucci, V., and Arriaga, L. (2010). High power fuel cell simulator based on artificial neural network. *International Journal of Hydrogen Energy*, 35(21):12125–12133.

[Chen et al., 2008] Chen, J., Xu, H., Zhang, H., and Yi, B. (2008). Facilitating mass transport in gas diffusion layer of pemfc by fabricating micro-porous layer with dry layer preparation. *Journal of power sources*, 182(2):531–539.

[Chevalier et al., 2018] Chevalier, S., Josset, C., and Auvity, B. (2018). Analytical solutions and dimensional analysis of pseudo 2d current density distribution model in pem fuel cells. *Renewable energy*, 125:738–746.

[Cho et al., 2020] Cho, J., Marquis, J., Trogadas, P., Neville, T., Brett, D., and Coppens, M.-O. (2020). Optimizing the architecture of lung-inspired fuel cells. *Chemical Engineering Science*, 215:115375.

[Choi et al., 2011] Choi, K.-S., Kim, H.-M., and Moon, S.-M. (2011). Numerical studies on the geometrical characterization of serpentine flow-field for efficient pemfc. *International Journal of Hydrogen Energy*, 36(2):1613–1627.

[Cochet et al., 2018] Cochet, M., Forner-Cuenca, A., Manzi, V., Siegwart, M., Scheuble, D., and Boillat, P. (2018). Novel concept for evaporative cooling of fuel cells: an experimental study based on neutron imaging. *Fuel Cells*, 18(5):619–626.

[Cooper et al., 2016] Cooper, N. J., Smith, T., Santamaria, A. D., and Park, J. W. (2016). Experimental optimization of parallel and interdigitated pemfc flow-field channel geometry. *international journal of hydrogen energy*, 41(2):1213–1223.

[Cunningham et al., 2007] Cunningham, B., Huang, J., and Baird, D. (2007). Review of materials and processing methods used in the production of bipolar plates for fuel cells. *International materials reviews*, 52(1):1–13.

[Dai et al., 2009] Dai, W., Wang, H., Yuan, X.-Z., Martin, J. J., Yang, D., Qiao, J., and Ma, J. (2009). A review on water balance in the membrane electrode assembly of proton exchange membrane fuel cells. *International Journal of Hydrogen Energy*, 34(23):9461–9478.

[Diakite et al., 2014] Diakite, I., Edwards, D., Emerick, B., Raymond, C., Zumbrum, M., Panaggio, M., and Peace, A. (2014). Improving a fuel cell assembly process. *Mathematics-in-Industry Case Studies*, 6:22–47.

[Dib et al., 2019] Dib, A., Maizia, R., Martemianov, S., and Thomas, A. (2019). Statistical short time analysis for proton exchange membrane fuel cell diagnostic-application to water management. *Fuel Cells*, 19(5):539–549.

[Dicks, 2004] Dicks, A. L. (2004). Molten carbonate fuel cells. *Current Opinion in Solid State and Materials Science*, 8(5):379–383.

[Didierjean et al., 2008] Didierjean, S., Lottin, O., Maranzana, G., and Geneston, T. (2008). Pem fuel cell voltage transient response to a thermal perturbation. *Electrochimica Acta*, 53(24):7313–7320.

[Didierjean et al., 2015] Didierjean, S., Perrin, J.-C., Xu, F., Maranzana, G., Klein, M., Mainka, J., and Lottin, O. (2015). Theoretical evidence of the difference in kinetics of water sorption and desorption in nafion® membrane and experimental validation. *Journal of Power Sources*, 300:50–56.

[Dillet et al., 2010] Dillet, J., Lottin, O., Maranzana, G., Didierjean, S., Conteau, D., and Bonnet, C. (2010). Direct observation of the two-phase flow in the air channel of a proton exchange membrane fuel cell and of the effects of a clogging/unclogging sequence on the current density distribution. *Journal of power sources*, 195(9):2795–2799.

[Djilali, 2007] Djilali, N. (2007). Computational modelling of polymer electrolyte membrane (pem) fuel cells: Challenges and opportunities. *Energy*, 32(4):269–280.

[Dong-Hui et al., 2017] Dong-Hui, W., Lin-Zhi, Y., Zhong-Yu, P., Cong-Da, L., Gang, L., and Qiao-Hui, L. (2017). A novel intersectant flow field of metal bipolar plate for proton exchange membrane fuel cell. *International Journal of Energy Research*, 41(14):2184–2193.

[Dorenbos and Suga, 2009] Dorenbos, G. and Suga, Y. (2009). Simulation of equivalent weight dependence of nafion morphologies and predicted trends regarding water diffusion. *Journal of Membrane Science*, 330(1-2):5–20.

[Dutta et al., 2001] Dutta, S., Shimpalee, S., and Van Zee, J. (2001). Numerical prediction of mass-exchange between cathode and anode channels in a pem fuel cell. *International Journal of Heat and Mass Transfer*, 44(11):2029–2042.

[Elfring and Struchtrup, 2008] Elfring, G. J. and Struchtrup, H. (2008). Thermodynamics of pore wetting and swelling in nafion. *Journal of Membrane Science*, 315(1-2):125–132.

[Eriksson et al., 2019] Eriksson, B., Grimler, H., Carlson, A., Ekström, H., Lindström, R. W., Lindbergh, G., and Lagergren, C. (2019). Quantifying water transport in anion exchange membrane fuel cells. *International Journal of Hydrogen Energy*, 44(10):4930–4939.

[Fernández-Delgado et al., 2019] Fernández-Delgado, M., Sirsat, M., Cernadas, E., Alawadi, S., Barro, S., and Febrero-Bande, M. (2019). An extensive experimental survey of regression methods. *Neural Networks*, 111:11–34.

[Fick, 1855] Fick, A. (1855). V. on liquid diffusion. *The London, Edinburgh, and Dublin Philosophical Magazine and Journal of Science*, 10(63):30–39.

[Fishman and Bazylak, 2011] Fishman, Z. and Bazylak, A. (2011). Heterogeneous through-plane porosity distributions for treated pemfc gdls i. ptfe effect. *Journal of The Electrochemical Society*, 158(8):B841.

[Fuller and Newman, 1992] Fuller, T. F. and Newman, J. (1992). Experimental determination of the transport number of water in nafion 117 membrane. *Journal of the Electrochemical Society*, 139(5):1332.

[Gabrielli et al., 1986] Gabrielli, C., Huet, F., and Keddam, M. (1986). Investigation of electrochemical processes by an electrochemical noise analysis. theoretical and experimental aspects in potentiostatic regime. *Electrochimica Acta*, 31(8):1025–1039.

[Gallagher et al., 2009] Gallagher, K. G., Pivovar, B. S., and Fuller, T. F. (2009). Electro-osmosis and water uptake in polymer electrolytes in equilibrium with water vapor at low temperatures. *Journal of the Electrochemical Society*, 156(3):B330–B338.

[Ge et al., 2019] Ge, N., Banerjee, R., Muirhead, D., Lee, J., Liu, H., Shrestha, P., Wong, A., Jankovic, J., Tam, M., Susac, D., et al. (2019). Membrane dehydration with increasing current density at high inlet gas relative humidity in polymer electrolyte membrane fuel cells. *Journal of Power Sources*, 422:163–174.

[Ge et al., 2005] Ge, S., Li, X., Yi, B., and Hsing, I.-M. (2005). Absorption, desorption, and transport of water in polymer electrolyte membranes for fuel cells. *Journal of the Electrochemical Society*, 152(6):A1149–A1157.

[Gebel et al., 1993] Gebel, G., Aldebert, P., and Pineri, M. (1993). Swelling study of perfluorosulphonated ionomer membranes. *Polymer*, 34(2):333–339.

[Gielen et al., 2019] Gielen, D., Boshell, F., Saygin, D., Bazilian, M. D., Wagner, N., and Gorini, R. (2019). The role of renewable energy in the global energy transformation. *Energy Strategy Reviews*, 24:38–50.

[Gierke et al., 1981] Gierke, T. D., Munn, G., and Wilson, F. (1981). The morphology in nafion perfluorinated membrane products, as determined by wide-and

small-angle x-ray studies. *Journal of Polymer Science: Polymer Physics Edition*, 19(11):1687–1704.

[Gong et al., 2001] Gong, X., Bandis, A., Tao, A., Meresi, G., Wang, Y., Inglefield, P., Jones, A., and Wen, W.-Y. (2001). Self-diffusion of water, ethanol and decafluropentane in perfluorosulfonate ionomer by pulse field gradient nmr. *Polymer*, 42(15):6485–6492.

[Górski and Jakubowska, 2019] Górski, Ł. and Jakubowska, M. (2019). Ridge regression with self-paced learning algorithm in interpretation of voltammetric signals. *Chemometrics and Intelligent Laboratory Systems*, 191:73–81.

[Grimm et al., 2012] Grimm, M., See, E. J., and Kandlikar, S. G. (2012). Modeling gas flow in pemfc channels: Part i–flow pattern transitions and pressure drop in a simulated ex situ channel with uniform water injection through the gdl. *international journal of hydrogen energy*, 37(17):12489–12503.

[Gu and Bollen, 2000] Gu, Y. H. and Bollen, M. H. (2000). Time-frequency and time-scale domain analysis of voltage disturbances. *IEEE Transactions on Power Delivery*, 15(4):1279–1284.

[Gurz et al., 2017] Gurz, M., Baltacioglu, E., Hames, Y., and Kaya, K. (2017). The meeting of hydrogen and automotive: a review. *International Journal of Hydrogen Energy*, 42(36):23334–23346.

[Hack et al., 2020] Hack, J., Rasha, L., Cullen, P. L., Bailey, J. J., Neville, T. P., Shearing, P. R., Brandon, N. P., and Brett, D. J. (2020). Use of x-ray computed tomography for understanding localised, along-the-channel degradation of polymer electrolyte fuel cells. *Electrochimica Acta*, page 136464.

[Hallinan Jr and Elabd, 2009] Hallinan Jr, D. T. and Elabd, Y. A. (2009). Diffusion of water in nafion using time-resolved fourier transform infrared- attenuated total reflectance spectroscopy. *The Journal of Physical Chemistry B*, 113(13):4257–4266.

[Han and Chung, 2016] Han, I.-S. and Chung, C.-B. (2016). Performance prediction and analysis of a pem fuel cell operating on pure oxygen using data-driven models: A comparison of artificial neural network and support vector machine. *International Journal of Hydrogen Energy*, 41(24):10202–10211.

[Harris, 1978] Harris, F. J. (1978). On the use of windows for harmonic analysis with the discrete fourier transform. *Proceedings of the IEEE*, 66(1):51–83.

[Haubrock et al., 2006] Haubrock, J., Heideck, G., and Styczynski, Z. (2006). Electrical efficiency losses occurred by the air compressor for pemfc. In *Proceedings of the World Hydrogen Energy Conference WHEC Lyon, France*.

[Healy et al., 2005] Healy, J., Hayden, C., Xie, T., Olson, K., Waldo, R., Brundage, M., Gasteiger, H., and Abbott, J. (2005). Aspects of the chemical degradation of pfsa ionomers used in pem fuel cells. *Fuel cells*, 5(2):302–308.

[Hemmer et al., 2019] Hemmer, S., Walters, M., and Tinz, S. (2019). Scalable fuel cell systems for commercial vehicles. *MTZ worldwide*, 80(7-8):64–71.

[Hensley et al., 2007] Hensley, J. E., Way, J. D., Dec, S. F., and Abney, K. D. (2007). The effects of thermal annealing on commercial nafion® membranes. *Journal of Membrane Science*, 298(1-2):190–201.

[Hickner et al., 2008] Hickner, M. A., Siegel, N., Chen, K., Hussey, D., Jacobson, D., and Arif, M. (2008). In situ high-resolution neutron radiography of cross-sectional liquid water profiles in proton exchange membrane fuel cells. *Journal of The Electrochemical Society*, 155(4):B427–B434.

[Hietala et al., 2000] Hietala, S., Maunu, S. L., and Sundholm, F. (2000). Sorption and diffusion of methanol and water in pvdf-g-pssa and nafion® 117 polymer electrolyte membranes. *Journal of Polymer Science Part B: Polymer Physics*, 38(24):3277–3284.

[Hizir et al., 2010] Hizir, F., Ural, S., Kumbur, E., and Mench, M. (2010). Characterization of interfacial morphology in polymer electrolyte fuel cells: Micro-porous layer and catalyst layer surfaces. *Journal of Power Sources*, 195(11):3463–3471.

[Hladky and Dawson, 1982] Hladky, K. and Dawson, J. (1982). The measurement of corrosion using electrochemical 1f noise. *Corrosion Science*, 22(3):231–237.

[Hoerl et al., 1975] Hoerl, A. E., Kannard, R. W., and Baldwin, K. F. (1975). Ridge regression: some simulations. *Communications in Statistics-Theory and Methods*, 4(2):105–123.

[Hoerl and Kennard, 1970] Hoerl, A. E. and Kennard, R. W. (1970). Ridge regression: Biased estimation for nonorthogonal problems. *Technometrics*, 12(1):55–67.

[Hu et al., 2004] Hu, G., Fan, J., Chen, S., Liu, Y., and Cen, K. (2004). Three-dimensional numerical analysis of proton exchange membrane fuel cells (pem-fcs) with conventional and interdigitated flow fields. *Journal of Power Sources*, 136(1):1–9.

[Huet, 1998] Huet, F. (1998). A review of impedance measurements for determination of the state-of-charge or state-of-health of secondary batteries. *Journal of power sources*, 70(1):59–69.

[Huet et al., 2004] Huet, F., Musiani, M., and Nogueira, R. (2004). Oxygen evolution on electrodes of different roughness: an electrochemical noise study. *Journal of Solid State Electrochemistry*, 8(10):786–793.

[Huet et al., 2006] Huet, F., Nogueira, R., Lailler, P., and Torcheux, L. (2006). Investigation of the high-frequency resistance of a lead-acid battery. *Journal of Power Sources*, 158(2):1012–1018.

[Hung and Lin, 2012] Hung, J.-C. and Lin, C.-C. (2012). Fabrication of micro-flow channels for metallic bipolar plates by a high-pressure hydroforming apparatus. *Journal of Power Sources*, 206:179–184.

[Hung et al., 2011] Hung, J.-C., Yang, T.-C., and Li, K.-c. (2011). Studies on the fabrication of metallic bipolar plates—using micro electrical discharge machining milling. *Journal of Power Sources*, 196(4):2070–2074.

[Hussey et al., 2007] Hussey, D. S., Jacobson, D. L., Arif, M., Owejan, J. P., Gagliardo, J. J., and Trabold, T. (2007). Neutron images of the through-plane water distribution of an operating pem fuel cell. *Journal of Power Sources*, 172(1):225–228.

[Ibrahimoglu et al., 2017] Ibrahimoglu, B., Yilmazoglu, M., and Celenk, S. (2017). Investigation of spiral flow-field design on the performance of a pem fuel cell. *Fuel Cells*, 17(6):786–793.

[Ilie et al., 2016] Ilie, V. R., Martemianov, S., and Thomas, A. (2016). Investigation of the local temperature and overheat inside the membrane electrode assembly of pem fuel cell. *international journal of hydrogen energy*, 41(34):15528–15537.

[Jalani and Datta, 2005] Jalani, N. H. and Datta, R. (2005). The effect of equivalent weight, temperature, cationic forms, sorbates, and nanoinorganic additives on the sorption behavior of nafion®. *Journal of membrane science*, 264(1-2):167–175.

[Jannat et al., 2019] Jannat, S., Rashtchi, H., Atapour, M., Golozar, M. A., Elmkhah, H., and Zhiani, M. (2019). Preparation and performance of nanometric ti/tin multi-layer physical vapor deposited coating on 316l stainless steel as bipolar plate for proton exchange membrane fuel cells. *Journal of Power Sources*, 435:226818.

[Joseph et al., 2016] Joseph, D., Büsselmann, J., Harms, C., Henkensmeier, D., Larsen, M. J., Dyck, A., Jang, J. H., Kim, H.-J., and Nam, S. W. (2016). Porous nafion membranes. *Journal of Membrane Science*, 520:723–730.

[Juarez-Robles et al., 2011] Juarez-Robles, D., Hernandez-Guerrero, A., Ramos-Alvarado, B., Elizalde-Blancas, F., and Damian-Ascencio, C. E. (2011). Multiple concentric spirals for the flow field of a proton exchange membrane fuel cell. *Journal of Power Sources*, 196(19):8019–8030.

[Jung and Nguyen, 1998] Jung, S. Y. and Nguyen, T. V. (1998). An along-the-channel model for proton exchange membrane fuel cells. *Journal of the Electrochemical Society*, 145(4):1149.

[Junzeng et al., 2012] Junzeng, X., Qi, W., Shizhang, P., and Yanmei, Y. (2012). Error of saturation vapor pressure calculated by different formulas and its effect on calculation of reference evapotranspiration in high latitude cold region. *Procedia Engineering*, 28:43–48.

[Kahveci and Taymaz, 2018] Kahveci, E. E. and Taymaz, I. (2018). Assessment of single-serpentine pem fuel cell model developed by computational fluid dynamics. *Fuel*, 217:51–58.

[Karan et al., 2006] Karan, K., Atiyeh, H., Phoenix, A., Halliop, E., Pharoah, J., and Peppley, B. (2006). An experimental investigation of water transport in pemfcs: The role of microporous layers. *Electrochemical and Solid State Letters*, 10(2):B34.

[Karimi et al., 2012] Karimi, S., Fraser, N., Roberts, B., and Foulkes, F. R. (2012). A review of metallic bipolar plates for proton exchange membrane fuel cells: materials and fabrication methods. *Advances in Materials Science and Engineering*, 2012.

[Karthikeyan et al., 2015] Karthikeyan, P., Vasanth, R., and Muthukumar, M. (2015). Experimental investigation on uniform and zigzag positioned porous inserts on the rib surface of cathode flow channel for performance enhancement in pemfc. *International Journal of Hydrogen Energy*, 40(13):4641–4648.

[Kerres, 2001] Kerres, J. A. (2001). Development of ionomer membranes for fuel cells. *Journal of Membrane Science*, 185(1):3–27.

[Kessentini et al., 2019] Kessentini, R., Klinkova, O., Tawfiq, I., and Haddar, M. (2019). Modeling the moisture diffusion and hygroscopic swelling of a textile reinforced conveyor belt. *Polymer Testing*, 75:159–166.

[Khazaee and Ghazikhani, 2011] Khazaee, I. and Ghazikhani, M. (2011). Performance improvement of proton exchange membrane fuel cell by using annular shaped geometry. *Journal of Power Sources*, 196(5):2661–2668.

[Kidena, 2008] Kidena, K. (2008). Anisotropic diffusion of water in perfluorosulfonic acid membrane and hydrocarbon membranes. *Journal of Membrane Science*, 323(1):201–206.

[Kim and Mench, 2009] Kim, S. and Mench, M. (2009). Investigation of temperature-driven water transport in polymer electrolyte fuel cell: phase-change-induced flow. *Journal of The Electrochemical Society*, 156(3):B353–B362.

[Klein et al., 2013] Klein, M., Perrin, J.-C., Leclerc, S., Guendouz, L., Dillet, J., and Lottin, O. (2013). Spatially and temporally resolved measurement of water distribution in nafion using nmr imaging. *ECS Transactions*, 58(1):283.

[Kloess et al., 2009] Kloess, J. P., Wang, X., Liu, J., Shi, Z., and Guessous, L. (2009). Investigation of bio-inspired flow channel designs for bipolar plates in proton exchange membrane fuel cells. *Journal of Power Sources*, 188(1):132–140.

[Kötter et al., 2016] Kötter, E., Schneider, L., Sehnke, F., Ohnmeiss, K., and Schröer, R. (2016). The future electric power system: Impact of power-to-gas by interacting with other renewable energy components. *Journal of Energy Storage*, 5:113–119.

[Kravanja et al., 2018] Kravanja, G., Škerget, M., Knez, Ž., and Hrnčič, M. K. (2018). Diffusion coefficients of water and propylene glycol in supercritical co2 from pendant drop tensiometry. *The Journal of Supercritical Fluids*, 133:1–8.

[Kreuer et al., 2008] Kreuer, K. D., Schuster, M., Obliers, B., Diat, O., Traub, U., Fuchs, A., Klock, U., Paddison, S. J., and Maier, J. (2008). Short-side-chain proton conducting perfluorosulfonic acid ionomers: Why they perform better in pem fuel cells. *Journal of Power Sources*, 178(2):499–509.

[Kumar et al., 2010] Kumar, A., Ricketts, M., and Hirano, S. (2010). Ex situ evaluation of nanometer range gold coating on stainless steel substrate for automotive polymer electrolyte membrane fuel cell bipolar plate. *Journal of Power Sources*, 195(5):1401–1407.

[Kusoglu and Weber, 2017] Kusoglu, A. and Weber, A. Z. (2017). New insights into perfluorinated sulfonic-acid ionomers. *Chemical Reviews*, 117(3):987–1104.

[Lamibrac, 2013] Lamibrac, A. (2013). *Etude des dégradations dans les piles à combustible PEMFC pendant les phases de démarrage/arrêt*. PhD thesis, Université de Lorraine.

[Larminie et al., 2003] Larminie, J., Dicks, A., and McDonald, M. S. (2003). *Fuel cell systems explained*, volume 2. J. Wiley Chichester, UK.

[Le et al., 2010] Le, A. D., Zhou, B., Shiu, H.-R., Lee, C.-I., and Chang, W.-C. (2010). Numerical simulation and experimental validation of liquid water behaviors in a proton exchange membrane fuel cell cathode with serpentine channels. *Journal of Power Sources*, 195(21):7302–7315.

[Lee and Bae, 2012] Lee, D. and Bae, J. (2012). Visualization of flooding in a single cell and stacks by using a newly-designed transparent pemfc. *International Journal of Hydrogen Energy*, 37(1):422–435.

[Lee et al., 2015] Lee, D., Lim, J. W., Nam, S., Choi, I., et al. (2015). Gasket-integrated carbon/silicone elastomer composite bipolar plate for high-temperature pemfc. *Composite Structures*, 128:284–290.

[Lee et al., 2013] Lee, J., Hinebaugh, J., and Bazylak, A. (2013). Synchrotron x-ray radiographic investigations of liquid water transport behavior in a pemfc with mpl-coated gdls. *Journal of power sources*, 227:123–130.

[Lee and Lalk, 1998] Lee, J. and Lalk, T. (1998). Modeling fuel cell stack systems. *Journal of Power Sources*, 73(2):229–241.

[Lee et al., 2011] Lee, S., Kim, T., and Park, H. (2011). Comparison of multi-inlet and serpentine channel design on water production of pemfcs. *Chemical engineering science*, 66(8):1748–1758.

[Lee et al., 2020] Lee, S. Y., Chae, J. E., Choi, J., Park, H. S., Henkensmeier, D., Yoo, S. J., Kim, J. Y., Na, Y., Jang, J. H., and Kim, H.-J. (2020). Dual exchange membrane fuel cell with sequentially aligned cation and anion exchange membranes for non-humidified operation. *Journal of Membrane Science*, 596:117745.

[Li et al., 2013] Li, Y., Nguyen, Q. T., Buquet, C. L., Langevin, D., Legras, M., and Marais, S. (2013). Water sorption in nafion® membranes analyzed with an improved dual-mode sorption model—structure/property relationships. *Journal of membrane science*, 439:1–11.

[Li et al., 2010] Li, Y., Zhao, T., and Yang, W. (2010). Measurements of water uptake and transport properties in anion-exchange membranes. *international journal of hydrogen energy*, 35(11):5656–5665.

[Li et al., 2015] Li, Z., Outbib, R., Giurgea, S., and Hissel, D. (2015). Diagnosis for pemfc systems: A data-driven approach with the capabilities of online adaptation and novel fault detection. *IEEE Transactions on Industrial Electronics*, 62(8):5164–5174.

[Li et al., 2014] Li, Z., Outbib, R., Hissel, D., and Giurgea, S. (2014). Data-driven diagnosis of pem fuel cell: A comparative study. *Control Engineering Practice*, 28:1–12.

[Lin and Tsai, 2012] Lin, C.-H. and Tsai, S.-Y. (2012). An investigation of coated aluminium bipolar plates for pemfc. *Applied energy*, 100:87–92.

[Litster and McLean, 2004] Litster, S. and McLean, G. (2004). Pem fuel cell electrodes. *Journal of power sources*, 130(1-2):61–76.

[Little et al., 2017] Little, M. A., Varoquaux, G., Saeb, S., Lonini, L., Jayaraman, A., Mohr, D. C., and Kording, K. P. (2017). Using and understanding cross-validation strategies. perspectives on saeb et al. *GigaScience*, 6(5):gix020.

[Long et al., 2011] Long, N. V., Hien, T. D., Asaka, T., Ohtaki, M., and Nogami, M. (2011). Synthesis and characterization of pt–pd alloy and core-shell bimetallic nanoparticles for direct methanol fuel cells (dmfcs): Enhanced electrocatalytic properties of well-shaped core-shell morphologies and nanostructures. *international journal of hydrogen energy*, 36(14):8478–8491.

[Lundblad, 2004] Lundblad, A. (2004). Materials characterization of thin film electrodes for pefc-survey of methods and an example. *Journal of New Materials for Electrochemical Systems*, 7(1):21–28.

[Luo et al., 2018] Luo, X., Wright, A., Weissbach, T., and Holdcroft, S. (2018). Water permeation through anion exchange membranes. *Journal of Power Sources*, 375:442–451.

[Luo et al., 2010] Luo, Z., Chang, Z., Zhang, Y., Liu, Z., and Li, J. (2010). Electro-osmotic drag coefficient and proton conductivity in nafion® membrane for pemfc. *International Journal of Hydrogen Energy*, 35(7):3120–3124.

[Ma et al., 2018] Ma, R., Yang, T., Breaz, E., Li, Z., Briois, P., and Gao, F. (2018). Data-driven proton exchange membrane fuel cell degradation predication through deep learning method. *Applied Energy*, 231:102–115.

[Maalouf et al., 2009] Maalouf, M., Pyle, B., Sun, C.-N., Wu, D., Paddison, S. J., Schaberg, M., Emery, M., Lochhaas, K. H., Hamrock, S. J., Ghassemi, H., et al. (2009). Proton exchange membranes for high temperature fuel cells: Equivalent weight and end group effects on conductivity. *Ecs Transactions*, 25(1):1473.

[Maes et al., 2017] Maes, K., Van Nimmen, K., Gillijns, S., and Lombaert, G. (2017). Validation of time-delayed recursive force identification in structural dynamics. *Procedia engineering*, 199:2154–2159.

[Maickel et al., 1968] Maickel, R. P., Cox Jr, R. H., Saillant, J., and Miller, F. P. (1968). A method for the determination of serotonin and norepinephrine in discrete areas of rat brain. *International Journal of Neuropharmacology*, 7(3):275–281.

[Maizia et al., 2017] Maizia, R., Dib, A., Thomas, A., and Martemianov, S. (2017). Proton exchange membrane fuel cell diagnosis by spectral characterization of the electrochemical noise. *Journal of Power Sources*, 342:553–561.

[Maizia et al., 2018] Maizia, R., Dib, A., Thomas, A., and Martemianov, S. (2018). Statistical short-time analysis of electrochemical noise generated within a proton exchange membrane fuel cell. *Journal of Solid State Electrochemistry*, 22(6):1649–1660.

[Majsztrik et al., 2007] Majsztrik, P. W., Satterfield, M. B., Bocarsly, A. B., and Benziger, J. B. (2007). Water sorption, desorption and transport in nafion membranes. *Journal of Membrane Science*, 301(1-2):93–106.

[Maldonado et al., 2012] Maldonado, L., Perrin, J.-C., Dillet, J., and Lottin, O. (2012). Characterization of polymer electrolyte nafion membranes: Influence of temperature, heat treatment and drying protocol on sorption and transport properties. *Journal of Membrane Science*, 389:43–56.

[Malekbala et al., 2015] Malekbala, M. R., Khodadadi, A. R., and Kazempoor, P. (2015). Modeling and control of a proton exchange membrane fuel cell with the air compressor according to requested electrical current. *Thermal Science*, 19(6):2065–2078.

[Malevich et al., 2008] Malevich, D., Halliop, E., Peppley, B. A., Pharoah, J. G., and Karan, K. (2008). Investigation of charge-transfer and mass-transport resistances in pemfcs with microporous layer using electrochemical impedance spectroscopy. *Journal of The Electrochemical Society*, 156(2):B216.

[Mann et al., 2000] Mann, R. F., Amphlett, J. C., Hooper, M. A., Jensen, H. M., Peppley, B. A., and Roberge, P. R. (2000). Development and application of a generalised steady-state electrochemical model for a pem fuel cell. *Journal of power sources*, 86(1-2):173–180.

[Mansfeld and Lee, 1997] Mansfeld, F. and Lee, C. (1997). The frequency dependence of the noise resistance for polymer-coated metals. *Journal of the Electrochemical Society*, 144(6):2068.

[Mansfeld et al., 2001] Mansfeld, F., Sun, Z., and Hsu, C. (2001). Electrochemical noise analysis (ena) for active and passive systems in chloride media. *Electrochimica Acta*, 46(24-25):3651–3664.

[Manso et al., 2012] Manso, A., Marzo, F., Barranco, J., Garikano, X., and Mujika, M. G. (2012). Influence of geometric parameters of the flow fields on the performance of a pem fuel cell. a review. *International journal of hydrogen energy*, 37(20):15256–15287.

[Mao et al., 2017] Mao, L., Jackson, L., and Dunnett, S. (2017). Fault diagnosis of practical polymer electrolyte membrane (pem) fuel cell system with data-driven approaches. *Fuel Cells*, 17(2):247–258.

[Marquardt and Snee, 1975] Marquardt, D. W. and Snee, R. D. (1975). Ridge regression in practice. *The American Statistician*, 29(1):3–20.

[Martemianov et al., 2015] Martemianov, S., Adiutantov, N., Evdokimov, Y. K., Madier, L., Maillard, F., and Thomas, A. (2015). New methodology of electrochemical noise analysis and applications for commercial li-ion batteries. *Journal of Solid State Electrochemistry*, 19(9):2803–2810.

[Martemianov and Danaila, 2003] Martemianov, S. and Danaila, L. (2003). On the study of electrochemical turbulent noise in a stirred vessel. *Fluctuation and Noise Letters*, 3(04):L463–L471.

[Martemianov et al., 2020] Martemianov, S., Thomas, A., Adiutantov, N., Denisov, E., Evdokimov, Y., and Hissel, D. (2020). Electrochemical noise analysis of a pem fuel cell stack under long-time operation: noise signature in the frequency domain. *Journal of Solid State Electrochemistry*, pages 1–13.

[Martinet et al., 1999] Martinet, S., Durand, R., Ozil, P., Leblanc, P., and Blanchard, P. (1999). Application of electrochemical noise analysis to the study of batteries: state-of-charge determination and overcharge detection. *Journal of power sources*, 83(1-2):93–99.

[Martinez et al., 2018] Martinez, N., Morin, A., Berrod, Q., Frick, B., Ollivier, J., Porcar, L., Gebel, G., and Lyonnard, S. (2018). Multiscale water dynamics in a fuel cell by operando quasi elastic neutron scattering. *The Journal of Physical Chemistry C*, 122(2):1103–1108.

[Martinez et al., 2017] Martinez, N., Peng, Z., Morin, A., Porcar, L., Gebel, G., and Lyonnard, S. (2017). Real time monitoring of water distribution in an operando fuel cell during transient states. *Journal of Power Sources*, 365:230–234.

[Mauritz and Moore, 2004] Mauritz, K. A. and Moore, R. B. (2004). Chemical reviews. *State of understanding of Nafion*, 104:4535.

[McLean et al., 2002] McLean, G., Niet, T., Prince-Richard, S., and Djilali, N. (2002). An assessment of alkaline fuel cell technology. *International Journal of Hydrogen Energy*, 27(5):507–526.

[Mench et al., 2003] Mench, M., Dong, Q., and Wang, C. (2003). In situ water distribution measurements in a polymer electrolyte fuel cell. *Journal of Power Sources*, 124(1):90–98.

[Mench, 2008] Mench, M. M. (2008). *Fuel cell engines*. John Wiley & Sons.

[Meresi et al., 1998] Meresi, G., Tao, A., Gong, X., Wen, W., Inglefield, P., and Jones, A. (1998). An nmr study of the diffusion of water in nafion and the associated morphological structure. In *ABSTRACTS OF PAPERS OF THE AMERICAN CHEMICAL SOCIETY*, volume 216, pages U143–U143. AMER CHEMICAL SOC 1155 16TH ST, NW, WASHINGTON, DC 20036 USA.

[Merle et al., 2011] Merle, G., Wessling, M., and Nijmeijer, K. (2011). Anion exchange membranes for alkaline fuel cells: A review. *Journal of Membrane Science*, 377(1-2):1–35.

[Meyer et al., 2016] Meyer, Q., Ashton, S., Boillat, P., Cochet, M., Engebretsen, E., Finegan, D. P., Lu, X., Bailey, J. J., Mansor, N., Abdulaziz, R., et al. (2016). Effect of gas diffusion layer properties on water distribution across air-cooled, open-cathode polymer electrolyte fuel cells: a combined ex-situ x-ray tomography and in-operando neutron imaging study. *Electrochimica Acta*, 211:478–487.

[Meyer et al., 2019] Meyer, Q., Zeng, Y., and Zhao, C. (2019). Electrochemical impedance spectroscopy of catalyst and carbon degradations in proton exchange membrane fuel cells. *Journal of Power Sources*, 437:226922.

[Milburn et al., 1996] Milburn, S. M., Cronin, J. J., and Cohen, B. M. (1996). A variable displacement compressor/expander for vehicular fuel cell air management. Technical report, SAE Technical Paper.

[Mishima and Hibiki, 1996] Mishima, K. and Hibiki, T. (1996). Some characteristics of air-water two-phase flow in small diameter vertical tubes. *International journal of multiphase flow*, 22(4):703–712.

[Mohammadi et al., 2015] Mohammadi, A., Djerdir, A., Steiner, N. Y., and Khaburi, D. (2015). Advanced diagnosis based on temperature and current density distributions in a single pemfc. *International Journal of Hydrogen Energy*, 40(45):15845–15855.

[Mond and Langer, 1890] Mond, L. and Langer, C. (1890). V. a new form of gas battery. *Proceedings of the Royal Society of London*, 46(280-285):296–304.

[Morán-Durán et al., 2019] Morán-Durán, A., Martínez-Sibaja, A., Rodríguez-Jarquin, J. P., Posada-Gómez, R., and González, O. S. (2019). Pem fuel cell voltage neural control based on hydrogen pressure regulation. *Processes*, 7(7):434.

[Moreno et al., 2015] Moreno, N. G., Molina, M. C., Gervasio, D., and Robles, J. F. P. (2015). Approaches to polymer electrolyte membrane fuel cells (pemfcs) and their cost. *Renewable and Sustainable Energy Reviews*, 52:897–906.

[Morin et al., 2017] Morin, A., Gebel, G., Porcar, L., Peng, Z., Martinez, N., Guillermo, A., and Lyonnard, S. (2017). Quantitative multi-scale operando diagnosis of water localization inside a fuel cell. *Journal of The Electrochemical Society*, 164(2):F9–F21.

[Mortazavi et al., 2018] Mortazavi, M., Benner, J., and Santamaria, A. (2018). Evaluation of liquid-gas two-phase flow pressure drop signatures in proton exchange membrane (pem) fuel cell flow channels. In *International Conference on Nanochannels, Microchannels, and Minichannels*, volume 51197, page V001T02A008. American Society of Mechanical Engineers.

[Mortazavi and Tajiri, 2015] Mortazavi, M. and Tajiri, K. (2015). Two-phase flow pressure drop in flow channels of proton exchange membrane fuel cells: Review of experimental approaches. *Renewable and Sustainable Energy Reviews*, 45:296–317.

[Napoli et al., 2013] Napoli, G., Ferraro, M., Sergi, F., Brunaccini, G., and Antonucci, V. (2013). Data driven models for a pem fuel cell stack performance prediction. *International journal of hydrogen energy*, 38(26):11628–11638.

[Naudy et al., 2014] Naudy, S., Collette, F., Thominette, F., Gebel, G., and Espuche, E. (2014). Influence of hygrothermal aging on the gas and water transport properties of nafion® membranes. *Journal of membrane science*, 451:293–304.

[Nguyen, 1996] Nguyen, T. V. (1996). A gas distributor design for proton-exchange-membrane fuel cells. *Journal of the Electrochemical Society*, 143(5):L103.

[Nuttall, 1981] Nuttall, A. (1981). Some windows with very good sidelobe behavior. *IEEE Transactions on Acoustics, Speech, and Signal Processing*, 29(1):84–91.

[Ochi et al., 2009] Ochi, S., Kamishima, O., Mizusaki, J., and Kawamura, J. (2009). Investigation of proton diffusion in nafion® 117 membrane by electrical conductivity and nmr. *Solid State Ionics*, 180(6-8):580–584.

[Okada, 1999] Okada, T. (1999). Theory for water management in membranes for polymer electrolyte fuel cells: Part 1. the effect of impurity ions at the anode side on the membrane performances. *Journal of electroanalytical chemistry*, 465(1):1–17.

[Okel et al., 2008] Okel, E., Schaar, B., and Kanoun, O. (2008). Simultaneous measurement of bulk and contact resistance of conductive materials for fuel cells. In *2008 IEEE Instrumentation and Measurement Technology Conference*, pages 1462–1465. IEEE.

[Owejan et al., 2010] Owejan, J. P., Owejan, J. E., Gu, W., Trabold, T. A., Tighe, T. W., and Mathias, M. F. (2010). Water transport mechanisms in pemfc gas diffusion layers. *Journal of The Electrochemical Society*, 157(10):B1456–B1464.

[Owejan et al., 2007] Owejan, J. P., Trabold, T., Jacobson, D., Arif, M., and Kandlikar, S. (2007). Effects of flow field and diffusion layer properties on water accumulation in a pem fuel cell. *International Journal of Hydrogen Energy*, 32(17):4489–4502.

[Park et al., 2000] Park, S., Vohs, J. M., and Gorte, R. J. (2000). Direct oxidation of hydrocarbons in a solid-oxide fuel cell. *Nature*, 404(6775):265–267.

[Pei et al., 2016] Pei, P., Li, Y., Xu, H., and Wu, Z. (2016). A review on water fault diagnosis of pemfc associated with the pressure drop. *Applied energy*, 173:366–385.

[Peng et al., 2017] Peng, Z., Badets, V., Huguet, P., Morin, A., Schott, P., Tran, T. B. H., Porozhnyy, M., Nikonenko, V., and Deabate, S. (2017). Operando μ-raman study of the actual water content of perfluorosulfonic acid membranes in the fuel cell. *Journal of Power Sources*, 356:200–211.

[Perrin et al., 2016] Perrin, J.-C., El Kaddouri, A., Klein, M., Leclerc, S., Dillet, J., Guendouz, L., and Lottin, O. (2016). Water transport in nafion membranes under various conditions studied by nmr. In *MRPM 13*.

[Perry and Fuller, 2002] Perry, M. L. and Fuller, T. F. (2002). A historical perspective of fuel cell technology in the 20th century. *Journal of the electrochemical society*, 149(7):S59.

[Petrone et al., 2013] Petrone, R., Zheng, Z., Hissel, D., Péra, M.-C., Pianese, C., Sorrentino, M., Becherif, M., and Yousfi-Steiner, N. (2013). A review on model-based diagnosis methodologies for pemfcs. *International Journal of Hydrogen Energy*, 38(17):7077–7091.

[Piringer, 2020] Piringer, O. G. (2020). A predictive power sequence equation for vapor pressures of pure organic fluids and partial pressures in multicomponent systems in equilibrium. *Fluid Phase Equilibria*, 506:112409.

[Pivovar, 2006] Pivovar, B. S. (2006). An overview of electro-osmosis in fuel cell polymer electrolytes. *Polymer*, 47(11):4194–4202.

[Planes et al., 2012] Planes, E., Flandin, L., and Alberola, N. (2012). Polymer composites bipolar plates for pemfcs. *Energy Procedia*, 20:311–323.

[Pozio et al., 2003] Pozio, A., Silva, R., De Francesco, M., and Giorgi, L. (2003). Nafion degradation in pefcs from end plate iron contamination. *Electrochimica acta*, 48(11):1543–1549.

[Prater, 1996] Prater, K. B. (1996). Solid polymer fuel cells for transport and stationary applications. *Journal of power sources*, 61(1-2):105–109.

[Rahimnejad et al., 2015] Rahimnejad, M., Adhami, A., Darvari, S., Zirepour, A., and Oh, S.-E. (2015). Microbial fuel cell as new technology for bioelectricity generation: a review. *Alexandria Engineering Journal*, 54(3):745–756.

[Ren et al., 2020] Ren, X., Lv, Q., Liu, L., Liu, B., Wang, Y., Liu, A., and Wu, G. (2020). Current progress of pt and pt-based electrocatalysts used for fuel cells. *Sustainable Energy & Fuels*, 4(1):15–30.

[Richards et al., 2012] Richards, J., Cremers, C., Fischer, P., and Schmidt, K. (2012). Corrosion studies on electro polished stainless steels for the use as metallic bipolar plates in pemfc applications. *Energy Procedia*, 20:324–333.

[Rubio et al., 2016] Rubio, M., Bethune, K., Urquia, A., and St-Pierre, J. (2016). Proton exchange membrane fuel cell failure mode early diagnosis with wavelet analysis of electrochemical noise. *International Journal of Hydrogen Energy*, 41(33):14991–15001.

[Saebea et al., 2019] Saebea, D., Chaiburi, C., and Authayanun, S. (2019). Model based evaluation of alkaline anion exchange membrane fuel cells with water management. *Chemical Engineering Journal*, 374:721–729.

[Saengrung et al., 2007] Saengrung, A., Abtahi, A., and Zilouchian, A. (2007). Neural network model for a commercial pem fuel cell system. *Journal of Power Sources*, 172(2):749–759.

[Satija et al., 2004] Satija, R., Jacobson, D. L., Arif, M., and Werner, S. (2004). In situ neutron imaging technique for evaluation of water management systems in operating pem fuel cells. *Journal of Power Sources*, 129(2):238–245.

[Scholta et al., 1999] Scholta, J., Rohland, B., Trapp, V., and Focken, U. (1999). Investigations on novel low-cost graphite composite bipolar plates. *Journal of Power Sources*, 84(2):231–234.

[Schoo and Knoll, 2015] Schoo, C. and Knoll, M. (2015). New simple electrochemical method for measuring the water vapor transmission rate and diffusion coefficient of polymer membranes. *Sensors and Actuators A: Physical*, 225:20–24.

[Searson and Dawson, 1988] Searson, P. and Dawson, J. (1988). Analysis of electrochemical noise generated by corroding electrodes under open-circuit conditions. *Journal of the electrochemical society*, 135(8):1908.

[Sellin et al., 2019] Sellin, R., Mozet, K., Ménage, A., Dillet, J., Didierjean, S., and Maranzana, G. (2019). Measuring electro-osmotic drag coefficients in pfsa membranes without any diffusion assumption. *International Journal of Hydrogen Energy*, 44(45):24905–24912.

[Shah et al., 2011] Shah, A., Luo, K., Ralph, T., and Walsh, F. (2011). Recent trends and developments in polymer electrolyte membrane fuel cell modelling. *Electrochimica Acta*, 56(11):3731–3757.

[Shahsavari et al., 2012] Shahsavari, S., Desouza, A., Bahrami, M., and Kjeang, E. (2012). Thermal analysis of air-cooled pem fuel cells. *international journal of hydrogen energy*, 37(23):18261–18271.

[Shiau et al., 2017] Shiau, H.-S., Zenyuk, I. V., and Weber, A. Z. (2017). Elucidating performance limitations in alkaline-exchange-membrane fuel cells. *Journal of The Electrochemical Society*, 164(11):E3583–E3591.

[Shimpalee et al., 2006] Shimpalee, S., Lee, W.-K., Van Zee, J., and Naseri-Neshat, H. (2006). Predicting the transient response of a serpentine flow-field pemfc: I. excess to normal fuel and air. *Journal of Power Sources*, 156(2):355–368.

[Siegel, 2008] Siegel, C. (2008). Review of computational heat and mass transfer modeling in polymer-electrolyte-membrane (pem) fuel cells. *Energy*, 33(9):1331–1352.

[Smith et al., 2014] Smith, T. L., Santamaria, A. D., Park, J. W., and Yamazaki, K. (2014). Alloy selection and die design for stamped proton exchange membrane fuel cell (pemfc) bipolar plates. *Procedia CIRP*, 14:275–280.

[Smulko et al., 2019] Smulko, J. et al. (2019). Methods of trend removal in electrochemical noise data–overview. *Measurement*, 131:569–581.

[Solomon Jr, 1991] Solomon Jr, O. (1991). Psd computations using welch's method. *STIN*, 92:23584.

[Song et al., 2019] Song, Y., Zhang, C., Ling, C.-Y., Han, M., Yong, R.-Y., Sun, D., and Chen, J. (2019). Review on current research of materials, fabrication and application for bipolar plate in proton exchange membrane fuel cell. *International Journal of Hydrogen Energy*.

[Spernjak et al., 2010] Spernjak, D., Prasad, A. K., and Advani, S. G. (2010). In situ comparison of water content and dynamics in parallel, single-serpentine, and interdigitated flow fields of polymer electrolyte membrane fuel cells. *Journal of Power Sources*, 195(11):3553–3568.

[Springer et al., 1991] Springer, T. E., Zawodzinski, T., and Gottesfeld, S. (1991). Polymer electrolyte fuel cell model. *Journal of the electrochemical society*, 138(8):2334.

[Standaert et al., 1998] Standaert, F., Hemmes, K., and Woudstra, N. (1998). Analytical fuel cell modeling; non-isothermal fuel cells. *Journal of Power Sources*, 70(2):181–199.

[Stone and Morrison, 2002] Stone, C. and Morrison, A. E. (2002). From curiosity to "power to change the world®". *Solid State Ionics*, 152:1–13.

[Sudhakar et al., 2018] Sudhakar, Y., Selvakumar, M., and Bhat, D. (2018). Biopolymer electrolytes for fuel cell applications. *Biopolymer Electrolytes*, pages 151–166.

[Sulek et al., 2011] Sulek, M., Adams, J., Kaberline, S., Ricketts, M., and Waldecker, J. R. (2011). In situ metal ion contamination and the effects on proton exchange membrane fuel cell performance. *Journal of Power Sources*, 196(21):8967–8972.

[Sundén and Faghri, 2005] Sundén, B. and Faghri, M. (2005). *Transport phenomena in fuel cells*, volume 19. WIT press.

[Suresh et al., 2006] Suresh, G., Pandey, A., and Goswami, A. (2006). Self-diffusion coefficients of water in nafion-117 membrane with multivalent counterions. *Journal of membrane science*, 284(1-2):193–197.

[Suseendiran et al., 2017] Suseendiran, S., Pearn-Rowe, S., and Rengaswamy, R. (2017). Strategies for effective utilization of hydrogen in cylindrical pem fuel cells. *ECS Transactions*, 80(8):485.

[Swamy et al., 2011] Swamy, T., Kumbur, E., and Mench, M. (2011). Investigation of bipolar plate and diffusion media interfacial structure in pefcs: A fractal geometry approach. *Electrochimica acta*, 56(8):3060–3070.

[Taherian, 2014] Taherian, R. (2014). A review of composite and metallic bipolar plates in proton exchange membrane fuel cell: Materials, fabrication, and material selection. *Journal of Power Sources*, 265:370–390.

[Tasaka et al., 1992] Tasaka, M., Hirai, T., Kiyono, R., and Aki, Y. (1992). Solvent transoport across cation-exchange membranes under a temperature difference and under an osmotic pressure difference. *Journal of membrane science*, 71(1-2):151–159.

[Tasaka et al., 1990] Tasaka, M., Mizuta, T., and Sekiguchi, O. (1990). Mass transfer through polymer membranes due to a temperature gradient. *Journal of membrane science*, 54(1-2):191–204.

[Tawfik et al., 2007] Tawfik, H., Hung, Y., and Mahajan, D. (2007). Metal bipolar plates for pem fuel cell—a review. *Journal of power sources*, 163(2):755–767.

[Testa et al., 2004] Testa, A., Gallo, D., and Langella, R. (2004). On the processing of harmonics and interharmonics: Using hanning window in standard framework. *IEEE Transactions on Power Delivery*, 19(1):28–34.

[Thampan et al., 2000] Thampan, T., Malhotra, S., Tang, H., and Datta, R. (2000). Modeling of conductive transport in proton-exchange membranes for fuel cells. *Journal of the Electrochemical Society*, 147(9):3242.

[Thomas et al., 2012] Thomas, A., Maranzana, G., Didierjean, S., Dillet, J., and Lottin, O. (2012). Thermal effect on water transport in proton exchange membrane fuel cell. *Fuel Cells*, 12(2):212–224.

[Thomas et al., 2014] Thomas, A., Maranzana, G., Didierjean, S., Dillet, J., and Lottin, O. (2014). Thermal and water transfer in pemfcs: investigating the role of the microporous layer. *International Journal of Hydrogen Energy*, 39(6):2649–2658.

[Tibshirani, 1996] Tibshirani, R. (1996). Regression shrinkage and selection via the lasso. *Journal of the Royal Statistical Society: Series B (Methodological)*, 58(1):267–288.

[Trebino et al., 1997] Trebino, R., DeLong, K. W., Fittinghoff, D. N., Sweetser, J. N., Krumbügel, M. A., Richman, B. A., and Kane, D. J. (1997). Measuring ultrashort laser pulses in the time-frequency domain using frequency-resolved optical gating. *Review of Scientific Instruments*, 68(9):3277–3295.

[Tsushima et al., 2005] Tsushima, S., Teranishi, K., Hirai, and S (2005). Water diffusion measurement in fuel-cell spe membrane by nmr. *Energy*, 30(2-4):235–245.

[Tüber et al., 2003] Tüber, K., Pócza, D., and Hebling, C. (2003). Visualization of water buildup in the cathode of a transparent pem fuel cell. *Journal of Power Sources*, 124(2):403–414.

[Vachtsevanos and Vachtsevanos, 2006] Vachtsevanos, G. J. and Vachtsevanos, G. J. (2006). *Intelligent fault diagnosis and prognosis for engineering systems*, volume 456. Wiley Hoboken.

[Van der Aalst et al., 2010] Van der Aalst, W. M., Rubin, V., Verbeek, H., van Dongen, B. F., Kindler, E., and Günther, C. W. (2010). Process mining: a two-step approach to balance between underfitting and overfitting. *Software & Systems Modeling*, 9(1):87.

[Varoquaux, 2018] Varoquaux, G. (2018). Cross-validation failure: small sample sizes lead to large error bars. *Neuroimage*, 180:68–77.

[Verhagen et al., 2019] Verhagen, R., O'Malley, E., Smedes, F., Mueller, J. F., and Kaserzon, S. (2019). Calibration parameters for the passive sampling of organic uv filters by silicone; diffusion coefficients and silicone–water partition coefficients. *Chemosphere*, 223:731–737.

[Villaluenga et al., 2006] Villaluenga, J., Barragan, V., Seoane, B., and Ruiz-Bauzá, C. (2006). Sorption and permeation of solutions of chloride salts, water and methanol in a nafion membrane. *Electrochimica acta*, 51(28):6297–6303.

[Wang and Liu, 2004] Wang, L. and Liu, H. (2004). Performance studies of pem fuel cells with interdigitated flow fields. *Journal of Power Sources*, 134(2):185–196.

[Wang et al., 2006] Wang, S.-H., Peng, J., Lui, W.-B., and Zhang, J.-S. (2006). Performance of the gold-plated titanium bipolar plates for the light weight pem fuel cells. *Journal of Power Sources*, 162(1):486–491.

[Wang et al., 2019] Wang, Y., Zhang, S., Wang, P., Lu, Z., Chen, S., and Wang, L. (2019). Synthesis and corrosion protection of nb doped tio2 nanopowders modified polyaniline coating on 316 stainless steel bipolar plates for proton-exchange membrane fuel cells. *Progress in Organic Coatings*, 137:105327.

[Wasmus and Küver, 1999] Wasmus, S. and Küver, A. (1999). Methanol oxidation and direct methanol fuel cells: a selective review. *Journal of Electroanalytical Chemistry*, 461(1-2):14–31.

[Weber and Newman, 2004] Weber, A. Z. and Newman, J. (2004). Modeling transport in polymer-electrolyte fuel cells. *Chemical reviews*, 104(10):4679–4726.

[Welch, 1967] Welch, P. (1967). The use of fast fourier transform for the estimation of power spectra: a method based on time averaging over short, modified periodograms. *IEEE Transactions on audio and electroacoustics*, 15(2):70–73.

[Wilberforce et al., 2019] Wilberforce, T., El Hassan, Z., Ogungbemi, E., Ijaodola, O., Khatib, F., Durrant, A., Thompson, J., Baroutaji, A., and Olabi, A. (2019). A comprehensive study of the effect of bipolar plate (bp) geometry design on the performance of proton exchange membrane (pem) fuel cells. *Renewable and Sustainable Energy Reviews*, 111:236–260.

[Wiley and Weihs, 2016] Wiley, D. and Weihs, G. F. (2016). *Electro-osmosis, Overview of*, pages 1–3. Springer Berlin Heidelberg, Berlin, Heidelberg.

[Wind et al., 2002] Wind, J., Späh, R., Kaiser, W., and Böhm, G. (2002). Metallic bipolar plates for pem fuel cells. *Journal of Power Sources*, 105(2):256–260.

[Wu et al., 2009] Wu, H., Li, X., and Berg, P. (2009). On the modeling of water transport in polymer electrolyte membrane fuel cells. *Electrochimica Acta*, 54(27):6913–6927.

[Wu et al., 2008] Wu, J., Yuan, X. Z., Martin, J. J., Wang, H., Zhang, J., Shen, J., Wu, S., and Merida, W. (2008). A review of pem fuel cell durability: Degradation mechanisms and mitigation strategies. *Journal of Power Sources*, 184(1):104–119.

[Wu et al., 2018] Wu, Y., Cho, J., Neville, T., Meyer, Q., Ziesche, R., Boillat, P., Cochet, M., Shearing, P., and Brett, D. (2018). Effect of serpentine flow-field design on the water management of polymer electrolyte fuel cells: an in-operando neutron radiography study. *Journal of Power Sources*, 399:254–263.

[Wu et al., 2020] Wu, Y., Cho, J., Whiteley, M., Rasha, L., Neville, T., Ziesche, R., Xu, R., Owen, R., Kulkarni, N., Hack, J., et al. (2020). Characterization of water management in metal foam flow-field based polymer electrolyte fuel cells using in-operando neutron radiography. *International Journal of Hydrogen Energy*, 45(3):2195–2205.

[Wu et al., 2019] Wu, Y., Meyer, Q., Liu, F., Rasha, L., Cho, J., Neville, T., Millichamp, J., Ziesche, R., Kardjilov, N., Boillat, P., et al. (2019). Investigation of water generation and accumulation in polymer electrolyte fuel cells using hydro-electrochemical impedance imaging. *Journal of Power Sources*, 414:272–277.

[Xia and Behnamian, 2015] Xia, D.-H. and Behnamian, Y. (2015). Electrochemical noise: a review of experimental setup, instrumentation and dc removal. *Russian Journal of Electrochemistry*, 51(7):593–601.

[Yan et al., 2010] Yan, W.-M., Wu, D.-K., Wang, X.-D., Ong, A.-L., Lee, D.-J., and Su, A. (2010). Optimal microporous layer for proton exchange membrane fuel cell. *Journal of Power Sources*, 195(17):5731–5734.

[Yan et al., 2006] Yan, X., Hou, M., Zhang, H., Jing, F., Ming, P., and Yi, B. (2006). Performance of pemfc stack using expanded graphite bipolar plates. *Journal of power sources*, 160(1):252–257.

[Yang et al., 2010] Yang, L., Yu, H., Jiang, L., Zhu, L., Jian, X., and Wang, Z. (2010). Improved anticorrosion properties and electrical conductivity of 316l stainless steel as bipolar plate for proton exchange membrane fuel cell by lower temperature chromizing treatment. *Journal of Power Sources*, 195(9):2810–2814.

[Yang et al., 2005] Yang, X.-G., Burke, N., Wang, C.-Y., Tajiri, K., and Shinohara, K. (2005). Simultaneous measurements of species and current distributions in a pefc under low-humidity operation. *Journal of The Electrochemical Society*, 152(4):A759–A766.

[Ye and LeVan, 2003] Ye, X. and LeVan, M. D. (2003). Water transport properties of nafion membranes: Part i. single-tube membrane module for air drying. *Journal of Membrane Science*, 221(1-2):147–161.

[Yi et al., 2013] Yi, P., Peng, L., Zhou, T., Wu, H., and Lai, X. (2013). Development and characterization of multilayered cr–c/ac: Cr film on 316l stainless steel as bipolar plates for proton exchange membrane fuel cells. *Journal of power sources*, 230:25–31.

[Yuan et al., 2005] Yuan, X. Z., Wang, H., Zhang, J., and Wilkinson, D. P. (2005). Bipolar plates for pem fuel cells-from materials to processing. *Journal of New Materials for Electrochemical Systems*, 8(4):257.

[Yun, 2010] Yun, Y.-H. (2010). Deposition of gold–titanium and gold–nickel coatings on electropolished 316l stainless steel bipolar plates for proton exchange membrane fuel cells. *international journal of hydrogen energy*, 35(4):1713–1718.

[Zaffou et al., 2006] Zaffou, R., Jung, S. Y., Kunz, H. R., and Fenton, J. M. (2006). Temperature-driven water transport through membrane electrode assembly of proton exchange membrane fuel cells. *Electrochemical and Solid State Letters*, 9(9):A418.

[Zawodzinski Jr et al., 1993] Zawodzinski Jr, T. A., Derouin, C., Radzinski, S., Sherman, R. J., Smith, V. T., Springer, T. E., and Gottesfeld, S. (1993). Water uptake by and transport through nafion® 117 membranes. *Journal of the electrochemical society*, 140(4):1041.

[Zawodzinski Jr et al., 1991] Zawodzinski Jr, T. A., Neeman, M., Sillerud, L. O., and Gottesfeld, S. (1991). Determination of water diffusion coefficients in perfluorosulfonate ionomeric membranes. *The Journal of Physical Chemistry*, 95(15):6040–6044.

[Zelsmann et al., 1990] Zelsmann, H., Pineri, M., Thomas, M., and Escoubes, M. (1990). Water self-diffusion coefficient determination in an ion exchange membrane by optical measurement. *Journal of applied polymer science*, 41(7-8):1673–1684.

[Zhang, 2008] Zhang, J. (2008). *PEM fuel cell electrocatalysts and catalyst layers: fundamentals and applications*. Springer Science & Business Media.

[Zhang et al., 2006] Zhang, J., Xie, Z., Zhang, J., Tang, Y., Song, C., Navessin, T., Shi, Z., Song, D., Wang, H., Wilkinson, D. P., et al. (2006). High temperature pem fuel cells. *Journal of power Sources*, 160(2):872–891.

[Zhuang et al., 2012] Zhuang, L., Zheng, Y., Zhou, S., Yuan, Y., Yuan, H., and Chen, Y. (2012). Scalable microbial fuel cell (mfc) stack for continuous real wastewater treatment. *Bioresource technology*, 106:82–88.

[Zook and Leddy, 1996] Zook, L. A. and Leddy, J. (1996). Density and solubility of nafion: recast, annealed, and commercial films. *Analytical chemistry*, 68(21):3793–3796.

Préambule

Aujourd'hui la demande énergétique est fortement dévolue aux hydrocarbures et, avec l'augmentation de la population, la nécessité d'en extraire davantage pose un grave problème sur la biocapacité de la planète. Avec une forte dépendance aux énergies fossiles, il existe un besoin de trouver de nouvelles sources plus propre et l'hydrogène peut jouer un rôle rôle important en termes de vecteur énergétique. En effet, l'hydrogène est une solution énergétique propre et durable (si celui-ci est produit de façon la plus décarbonée possible) et peut être stocké efficacement sous forme gazeuse, liquide ou solide, mais les problèmes de coûts et durabilité empêche un développement plus important de ce vecteur. L'hydrogène (H2) est l'élément le plus abondant de l'univers et est principalement dans l'eau et les composés organiques. Actuellement, l'hydrogène gris (issue des énergies fossiles) contribue à la majeure partie de la production d'hydrogène (96%) et un passage à une production d'hydrogène plus « vert » utilisant le flux solaire et le vent ou les combustibles issus de la biomasse serait opportun.

Les piles à combustible ont gagné en importance en tant que dispositif électrochimique ces dernières années, utilisant l'hydrogène comme carburant. Dans la pile à combustible, l'hydrogène se combine à l'oxygène pour produire de l'eau, de l'électricité et de la chaleur. Certains des avantages tels qu'une bonne densité énergétique et une large plage de fonctionnement de température en fait un choix intéressant. Encore une fois le coût du chargement en platine, le poids de l'empilement dû aux plaques bipolaires, et le coût des métaux nobles pour le revêtement joue un rôle majeur sur le prix d'un stack de pile à combustible Une pile à combustible typique de 135 kW peut peser jusqu'à 44, hors auxiliaires (compresseur, stockage de l'hydrogène). En termes de géométrie des plaques d'alimentation, la conception des canaux est souvent en forme de serpentin dans les piles à combustible commerciales. Cependant, ces géométries traditionnelles souffrent de pertes de charge importantes et la formation de bouchons d'eau liquide est possible dans les canaux. Plus la formation de bouchons sera élevée, plus la puissance requise par le compresseur sera élevée pour faire fonctionner le stack de pile à combustible. Ainsi, la recherche et le développement sont nécessaires pour une répartition efficace des espèces réactives et de l'évacuation de l'eau et de la chaleur produite. Cela passe donc par des conceptions nouvelles en termes de géométrie et matériaux pour les plaques d'alimentation des piles à combustibles. C'est donc l'un des objectifs de ce travail de thèse.

Afin de favoriser la commercialisation des piles à combustible, le développement d'outils de diagnostic et d'analyse des défauts jouent un rôle important. Il existe de nombreuses techniques utilisées telles que les mesures de perte de charge dans les canaux, la tomographie aux rayons X pour connaitre la répartition de l'eau au sein de la cellule, ou encore la visualisation directe par voie optique [Cochet et al., 2018, Meyer et al., 2016]. Ces techniques peuvent être coûteuses et nécessitent l'utilisation de prototypes particuliers pour la mesure. Les techniques d'analyse électrochimique tel que le bruit (enregistrement de la fluctuation d'un signal) peuvent être plus favorable par rapport à la robustesse des informations enregistrées. Les bruits électrochimiques ont déjà été utilisés pour comprendre l'analyse et la dégradation des revêtements [Huet, 1998, Huet et al., 2004], et appliqués dans les piles à combustible [Martemianov et Danaila, 2003, Maizia et al., 2018, Lee et Bae, 2012]. La technique des bruits électrochimiques peut être utilisé pour analyser des signaux ininterrompus sur de longue durée et ces résultats peuvent être interprétés par la visualisation dans le domaine temporel, mais aussi être caractérisés dans le domaine fréquentiel (densité spectrale de

puissance) ou encore par une analyse dans le domaine temps-fréquence. Des outils basés sur le bruit électrochimique ont donc été développés dans ce travail pour le diagnostic piles à combustible et permettant de caractériser l'impact des nouvelles géométries développés sur la performance et la répartition de l'eau au sein d'une cellule de pile à combustible de type PEMFC (Polymer Electrolyte Membrane Fuel Cell).

Les expériences fournissent toujours un moyen clair pour examiner les performances, mais le développement d'une pile à combustible est un processus coûteux. De plus, ce n'est pas toujours possible de déployer des capteurs sur mesure et capturer le diagnostic in situ du système étudié. Afin de prédire ces informations la modélisation [Chevalier et al., 2018, Morin et al., 2017] peut jouer un rôle important. Les modèles développés de manière analytique ou numérique peuvent donner beaucoup d'informations et peuvent aider pour faciliter le processus de développement d'une pile à combustible. Outre la modélisation analytique, il peut y avoir une approche de modélisation basée sur les données utilisant une boîte noire complète et utilisant données expérimentales pour prédire les performances. Dans tous les cas, une approche conjointe de la modélisation pouvant aider à l'interprétation des résultats expérimentaux peuvent faciliter le développement et la commercialisation des piles à combustible. Deux modèles ont donc été développé dans ce travail un consacré à l'évaluation du coefficient de diffusion effective de l'eau au sein de la membrane d'une pile à combustible en fonctionnement et l'autre, basé sur le « machine and deep learning » permettant le pronostique du système étudié.

Cette recherche est donc principalement axée sur le développement de nouvelles conceptions de plaques d'alimentation et l'amélioration de la gestion de l'eau au sein d'une pile à combustible. L'objectif principal est d'étudier l'impact des différentes géométries de plaques avec des techniques électrochimiques classiques (courbe de polarisation, mesure de pression) et moins classiques (bruit électrochimique), et à travers le bilan d'eau d'obtenir la valeur du coefficient de diffusion effectif de l'eau au sein de la membrane d'une PEMFC, valeur alimentant la modélisation de la gestion de l'eau au sein de spiles à combustibles.

Chapitre 1

Le premier chapitre est une présentation du contexte général et une classification des différents types de technologies de pile à combustibles ainsi que des différentes plaques bipolaires utilisées au niveau de la technologie PEMFC. Les mécanismes de transferts des réactifs gazeux, d'eau et de chaleur au sein des différents composants d'une cellule PEMFC, comme par exemple, la membrane, les couches poreuses et les plaques alimentation, sont détaillés et discutés. Une bibliographie riche permet de bien poser la problématique et dans quel contexte se place ce travail de thèse.

Le chapitre commence avec une présentation des composants d'une la pile à combustible à savoir, la membrane, les plaques d'alimentation, les électrodes et les couches poreuses. Au sein d'un PEMFC trois type de gaz sont utilisés, l'hydrogène, l'oxygène et l'air (azote + oxygène). Le principe général d'une pile à combustible (Figure 1) se base sur deux demi-réactions, l'oxydation de l'hydrogène à l'anode et la réduction de l'oxygène à la cathode produisant de l'énergie électrique (50% -60%), de l'eau et de la chaleur.

L'équation globale de ces deux demi réactions est

$$H2 + 1/2\ O2 \rightarrow H2O + \text{Chaleur} + \text{Electricité}$$

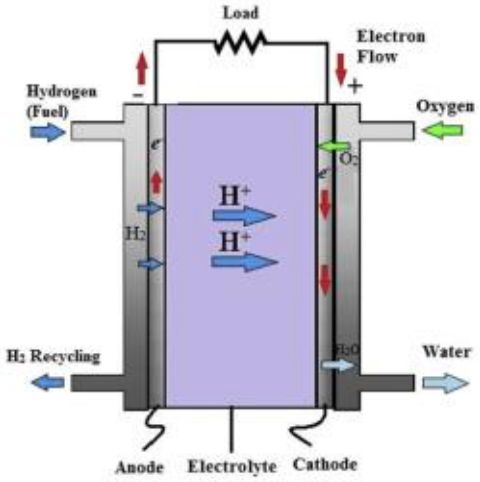

Figure 1 : Principe de fonctionnement d'une pile PEMFC [Gurz et al., 2017]

On voit donc que seul de l'eau et de la chaleur sont présent comme sous-produits de réaction et comme aucun atome de carbone n'est présent, à l'utilisation une pile à combustible produit de l'énergie électrique décarbonée (à l'oxydation du carbone de l'électrode près mais qui reste en des quantités très faibles).

Ensuite, le chapitre discute des techniques directes et indirectes permettant l'analyse des cellules de pile à combustible comme l'imagerie à neutron rapide, la technique d'interruption de courant, la tomographie aux rayons X, les mesures électrochimiques (polarisation, voltampérométrie cyclique, l'impédancemétrie), l'analyse des bruits électrochimiques dans le domaine temporel et fréquentiel.

Le chapitre se termine par la présentation de l'objectif principal de cette recherche qui est l'amélioration de la gestion de l'eau par l'introduction de nouvelles conceptions de géométries de plaques d'alimentation pouvant améliorer le mécanisme de transfert d'eau et l'efficacité de la pile à combustible. Deux outils de métrologie sont utilisés, le bilan hydrique et l'analyse des bruits électrochimiques.

Une fois le contexte introduit, une présentation des différents chapitres à suivre est faite. Le deuxième chapitre traite principalement des calculs du coefficient de diffusion effectif de l'eau à l'aide d'un bilan hydrique pour deux types de membranes : une membrane Nafion (cationique) et une membrane anionique. Étant donné que le coefficient de diffusion est un paramètre critique au niveau des modélisation et que sa valeur dans la littérature est très variable entre 10^{-5} - 10^{-8} cm²/s, il est donc nécessaire d'obtenir une valeur effective de ce coefficient pour la modélisation du transport d'eau au sein des piles à combustibles. La nécessité de la méthode du bilan d'eau, de l'expérimentation utilisée, des calculs et de l'analyse des erreurs sont tous discutés dans le but d'une meilleure compréhension des résultats. Le chapitre 3 traite principalement de l'introduction de nouvelles géométries de plaques d'alimentation. La conception traditionnelle en forme de serpentin a été largement utilisée mais souffre de pertes de charge importantes et de problèmes liés à la gestion de l'eau. À la fin de ce chapitre, la performance électrique de la pile avec les nouvelles conceptions de plaques bipolaires et la diminution de la puissance du compresseur engendré par ces nouvelles géométries sont discutées. Le chapitre 4 est dédié principalement à l'analyse du bruit électrochimique (Electrochemical Noise Analysis - ENA) et son application au niveau des signaux des piles à combustible, tel que la tension et la pression mesurées, sont discutées et analysées. Le développement d'outils et de descripteurs robustes et efficaces étant nécessaire pour diagnostiquer les performances des piles à combustible, une présentation de ceux-ci est faite et sont basés sur la variation de l'écart type dans l'espace

temporel et des spectres de puissance dans l'espace fréquentiel. L'objectif principal est de comprendre l'implication de l'ENA comme un outil de diagnostic pour une meilleure compréhension de la gestion de l'eau. Dans la dernière section du chapitre, les résultats sont analysés en regard des différentes géométries de plaques d'alimentation, pour deux conditions opératoires : influence de l'humidité relative et du courant appliqué. Le chapitre 5 traite lui de la partie modélisation. Deux modélisations sont proposées. Une analytique permettant d'obtenir le coefficient de diffusion effectif de l'eau au sein d'une pile à combustible et comparé aux résultats de diffusion de l'eau calculés expérimentalement au chapitre 2. Une autre ouvre le champ d'outils développés par apprentissage automatisé (« machine and deep learning ») pour le pronostic des piles à combustible.

Chapitre 2

Ce chapitre traite de la mesure du coefficient de diffusion effectif de l'eau dans une configuration de cellule qui ressemble à une configuration de pile à combustible mais sans réaction chimique et donc production d'eau. Seul de l'air est utilisé comme gaz pour cette expérience. Au début de ce chapitre l'idée principale est d'expliquer la méthode du bilan d'eau et d'explorer la faisabilité de cette procédure pour expliquer divers résultats sur l'estimation du coefficient de diffusion en fonction de l'humidité relative et donc de la teneur en eau dans la membrane. L'un des paramètres clés de la modélisation des piles à combustible étant le coefficient de diffusion et la prise en compte de sa variation avec les conditions opératoires. Par conséquent, ce chapitre traite de la méthode du bilan hydrique en tant que procédure simple et rapide pour estimer le coefficient de diffusion effectif de l'eau (Figure 2). Dans la littérature, il existe une grande variation des valeurs du coefficient de diffusion en fonction de divers points d'intérêt des différents auteurs et, par conséquent, il est nécessaire d'obtenir une valeur effective réaliste. La recherche est encore élargie pour comprendre comment la méthode du bilan hydrique est efficace pour prendre en compte la variation du gradient d'humidité relative imposé de chaque côté de la membrane et les variations des résultats en ce qui concerne le changement de température à travers la cellule (60°C et 70°C). Il est décrit de façon détaillée comment la méthode du bilan hydrique est sujet à des erreurs et quelles étapes sont nécessaires pour maintenir les résultats dans les limites d'erreur admissibles.

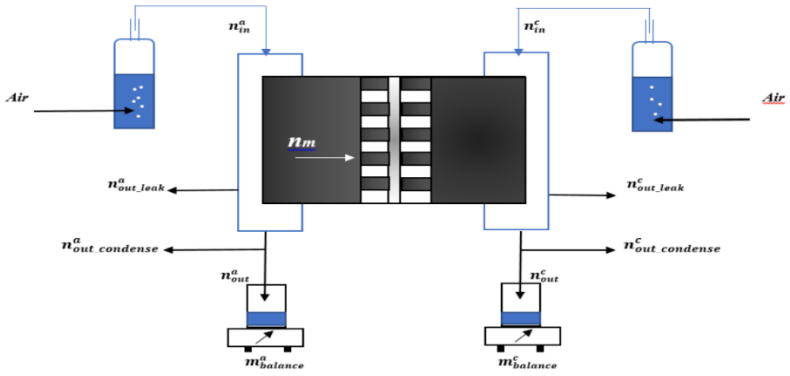

Figure 2 : Bilan hydrique au sein d'une cellule de pile à combustible

La deuxième moitié de ce chapitre traite de la variation des paramètres utilisés pour calculer le coefficient de diffusion et prenant en compte la sorption de l'eau sur la membrane. L'impact de ces facteurs est généralement peu étudié et peut expliquer les larges variations sur les valeurs du coefficient de diffusion de l'eau au sein de la membrane. Ces facteurs sont la densité volumique d'une membrane sèche, le poids équivalent de la membrane et la teneur en eau au sien de celle-ci et

notamment la différence de teneur en eau de chaque côté de la membrane qui impacte grandement les résultats du coefficient de diffusion (Figure 4). Ceci peut expliquer en détail l'effet du gonflement de la membrane et la variation de la diffusivité de Fick (différence de concentration) par rapport à la diffusivité de la membrane (différence de teneur en eau) compte tenu de la sorption de l'eau au niveau de la membrane.

Au niveau du transport de l'eau dans une cellule de pile à combustible, il existe quatre manières importantes de transporter l'eau à travers la membrane pendant le fonctionnement de la pile à combustible (Figure 3) : l'électro-osmose, la diffusion, la thermo-osmose et la convection

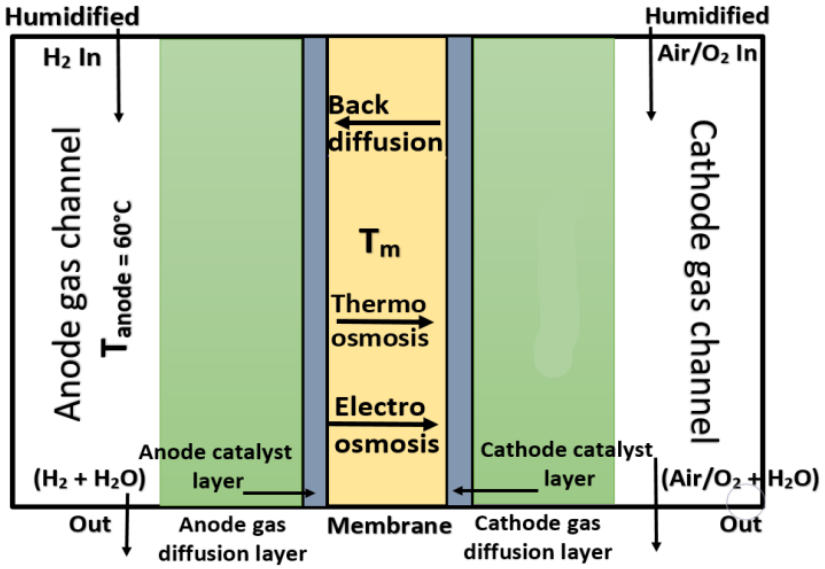

Figure 3 : Vue générale de la distribution de l'eau au sein d'une PEMFC

Dans ce travail, nous nous concentrerons principalement sur le transport par diffusion et notamment via la loi de Fick. Cette loi exprime une relation entre le flux de matière et le gradient de concentration dans l'hypothèse d'un régime stationnaire. La loi explique que le flux est dirigé de la région où la concentration est la plus élevée vers la concentration la plus faible afin d'atteindre un équilibre.

Dans une cellule de pile à combustible, la loi de Fick doit être modifiée pour prendre en compte la sorption de l'eau au niveau de la membrane. Il existe de nombreuses méthodes expérimentales pour comprendre la sorption et le transport de l'eau dans Nafion®. Majsztrik2007 a donné une description des diverses méthodes utilisées jusqu'à présent pour comprendre et analyser le transport et la sorption de l'eau, qui comprend : les techniques de mesure de la sorption et desorption de l'eau, la résonance magnétique nucléaire (RMN), les mesures de variation de masse de la membrane et le bilan d'eau. Dans ce travail de recherche nous avons utilisé la méthode du bilan d'eau pour évaluer le coefficient de diffusion effectif de l'eau dans la membrane.

Dans nos expériences, le système est maintenu à une température de 60°C ou 70°C. Afin de modifier l'humidité relative, la température des humidificateurs est modifiée et l'humidité relative varie entre 20% et 100% . Une circulation d'eau froide, dans des tubes en spirale à condensation, est utilisé pour maintenir la température à 2°C afin de condenser l'eau contenue dans l'air en sortie. Pour les expériences, la membrane utilisée est une NRE-211 (épaisseur - 29µm) fournie par Ion power et une membrane Anion fournie par TokuyamaA-201.

Dans cette section, les résultats liés à l'effet du coefficient de diffusion sur la différence d'humidité relative et la température sont discutés en fonction de l'humidité relative et de la température.

Le tableau 1 présente les résultats de variation du coefficient de diffusion à une température de pile à combustible de 60°C et 70°C.

Anode section and cathode section relative humidity	Cell Temperature temperature – 60°C Diffusion diffusion coefficient $(D_\lambda) cm^2/s$	Cell Temperature temperature – 70°C Diffusion diffusion coefficient $(D_\lambda) cm^2/s$
A20%-C40%	$1.42 \pm 0.21 \times 10^{-7}$	$1.58 \pm 0.40 \times 10^{-7}$
A20%-C60%	$1.26 \pm 1.34 \times 10^{-8}$	$3.28 \pm 0.52 \times 10^{-7}$
A20%-C80%	$2.92 \pm 0.43 \times 10^{-7}$	$2.35 \pm 0.40 \times 10^{-7}$
A20%-C100%	$1.37 \pm 0.20 \times 10^{-7}$	$1.60 \pm 0.33 \times 10^{-7}$
A40%-C60%	$9.45 \pm 1.41 \times 10^{-7}$	$4.31 \pm 0.71 \times 10^{-7}$
A40%-C80%	$2.56 \pm 0.38 \times 10^{-7}$	$1.79 \pm 0.26 \times 10^{-7}$
A40%-C100%	$1.17 \pm 0.17 \times 10^{-7}$	$1.26 \pm 0.22 \times 10^{-7}$
A60%-C80%	$1.16 \pm 0.17 \times 10^{-7}$	$3.78 \pm 0.64 \times 10^{-7}$
A80%-C100%	$4.41 \pm 0.73 \times 10^{-8}$	$8.62 \pm 1.24 \times 10^{-8}$

Tableau 1 : Comparaison des coefficients de diffusion effectifs obtenus en fonction de la température de la cellule

Sur la base des résultats, une légère augmentation du coefficient de diffusion est observée avec l'augmentation de la température. Majsztrik2007 a trouvé une augmentation similaire de la diffusivité de l'eau avec l'augmentation de la température.

La prise en compte de la sorption de l'eau au niveau de la membrane peut être prise à travers trois coefficients : la densité volumique de la membrane sèche ρ, le poids équivalent de la membrane EW et la teneur en eau λ (à saturation λsat). Il est possible d'obtenir une relation entre le coefficient de diffusion de l'eau via la loi de Fick (D_f) et le coefficient de l'eau dans la membrane (D_λ) à partir de ces trois coefficients et en supposant que la courbe de sorption de la membrane (variation de la teneur en eau en fonction de l'humidité relative) est linéaire (ce qui en réalité n'est pas le cas).

$$D_f = \frac{\rho}{EW} \times D_\lambda \times \frac{\lambda_{sat}}{C_{sat}}$$

Etudier donc l'impact de ces trois coefficients sur la valeur de D_λ est important car ce coefficient varie en fonction des membranes et conditions expérimentales étudiées dans la littérature. Nous proposons un encadrement minimal et maximal des valeurs trouvées dans la littérature du produit. Ces valeurs rapportées ici sont juste pour expliquer la variation du coefficient de diffusion qui est la plupart du temps négligée, mais si elle est prise en compte, il peut y avoir un changement de 10 à 15 fois dans les valeurs obtenues. Ces deux limites sont reportées sur la Figure 4.

$$(\frac{\rho}{EW} \times \Delta\lambda)_{minimum} = 1136$$

$$(\frac{\rho}{EW} \times \Delta\lambda)_{maximum} = 20454$$

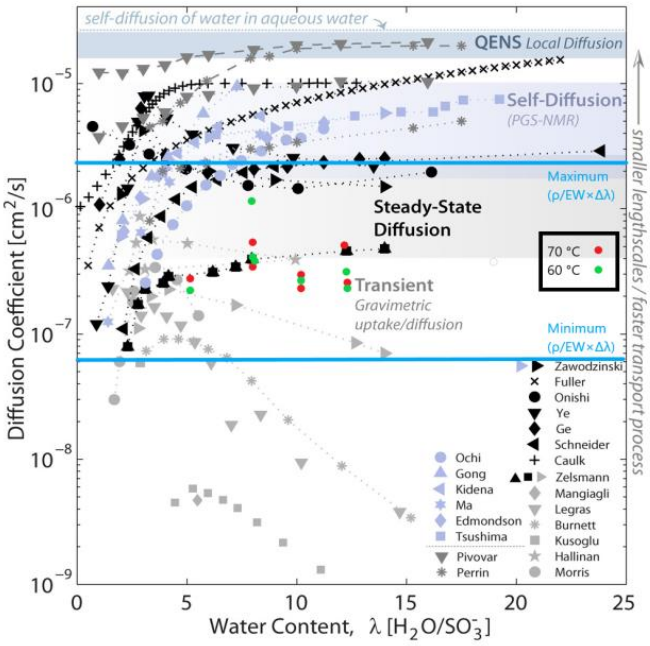

Figure 4 : Comparaison des valeurs expérimentales du coefficient de diffusion de l'eau mesurés dans ce travail aux valeurs de la littérature [Kusoglu2017]

Dans ce travail, nous avons calculé le coefficient de diffusion effectif à l'aide de la méthode du bilan hydrique. Le coefficient de diffusion peut avoir un grand nombre de valeurs en fonction du point de vue des auteurs et de la méthode utilisée et il devient difficile de fixer une valeur en fonction de conditions de fonctionnement données. Nous trouvons une valeur comprise entre 5 10^{-8} et 5 10^{-7} cm²/s ce qui correspond à des valeurs entre le domaine transitoire et le régime permanent, ce qui correspond à nos conditions opératoires. Dans la littérature, il existe des méthodes telles que la gravimétrie qui ne peuvent pas fournir de résultats in-situ, ou des méthodes in-situ telles que l'imagerie neutronique, mais qui sont coûteuses. En cela, nous avons choisi une méthode peu couteuse, efficace et permettant d'obtenir de façon in situ la mesure du coefficient de diffusion. La méthode du bilan hydrique peut donc être très utile pour fournir la valeur du coefficient de diffusion in situ en fonction des conditions de fonctionnement et utilise la même configuration de travail que celle d'une pile à combustible. Cela peut être fait dans n'importe quelle configuration de pile à combustible avec de l'azote ou de l'air (lorsque la pile à combustible ne fonctionne pas) ou quand la pile est en fonctionnement (voir chapitre 5). Cette méthode a été utilisée pour voir un effet sur l'humidité relative et la température. Pour la température, on observe une augmentation du coefficient de diffusion avec la température de la cellule. Les résultats du coefficient de diffusion ont également été calculés pour une membrane anionique donnant des valeurs similaires à celle du Nafion. Ces résultats montrent que la méthode du bilan hydrique, non seulement donne des informations sur la production et la distribution d'eau dans une pile à combustible en fonctionnement,

mais peut également être appliquée facilement pour mesurer un coefficient de diffusion de l'eau membranaire en fonction de nos conditions de fonctionnement souhaitées. De plus, à la fin de ce chapitre, des résultats tenant compte de l'effet de la densité, du poids équivalent et de la différence de la teneur en eau de chaque côté de la membrane (Δλ) sur le coefficient de diffusion ont été reportés. Δλ est le coefficient qui montre un impact maximal sur les résultats du coefficient de diffusion effective suivi de la densité et du poids équivalent.

Chapitre 3

Ce chapitre traite des nouveaux développements dans le domaine de la conception de nouvelles géométries des plaques d'alimentation en gaz (bipolaire) et l'analyse de leurs impacts basées sur les performances électriques globales de la cellule par mesure électrochimiques. Au début de ce chapitre, l'idée principale est d'expliquer le besoin de conceptions innovantes de géométrie de plaque d'alimentation et la raison de cela. Pourquoi est-il nécessaire d'améliorer la conception de ces plaques? Comment cela peut avoir un impact sur la durabilité à long terme, les performances globales, les pertes de charge.

Dans cette recherche, quatre nouvelles conceptions de plaque bipolaire sont comparées à la géométrie "serpentine" traditionnelle. La figure 5 représente les cinq géométries utilisées : A - la géométrie serpentine traditionnelle,) B - la géométrie en serpentin multiple (multi-serpentine) avec des plots supplémentaires, C la conception "hybrid" (serpentine + parallèle). Le choix de cette conception est expliqué ci-dessous. La figure 5D représente la géométrie en plot "spot" et la figure 5E représente le géométrie circulaire "circular" coté anodique et 5F coté cathodique. Malheureusement, en raison d'un problème de temps et des manips, la conception "circular" et "spot" est conservée pour une analyse ultérieure.

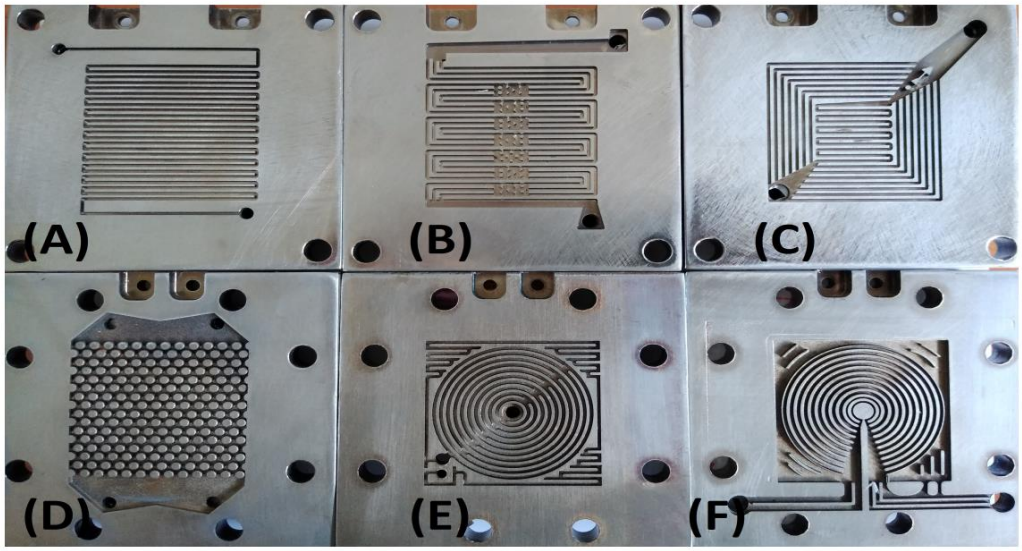

Figure 5 : A – Serpentin, B – Multi-serpentin avec plots, C- Hybride, D – Plots, E & F - Circulaire

La géométrie traditionnelle en serpentin souffre de divers problèmes d'inondation (bouchons des canaux) et d'assèchement de la membrane (répartition non homogène de l'eau). Le2010 a présenté des résultats concernant les comportements de l'eau liquide dans la plaque cathodique de pile à combustible à membrane échangeuse de protons avec des canaux serpentins. Lee2011, Lee2013, a effectué des recherches radiographiques sur le comportement du transport de l'eau liquide dans le PEMFC. Aslam2018 a simulé de la même manière pour la visualisation directe de l'eau liquide dans le PEMFC. Des recherches approfondies ont été publiées jusqu'à présent concernant l'utilisation de ces

plaques avec les deux performances, modifications et inconvénients (Choi2011, Kahveci2018, Shimpalee2006).

Une géométrie en serpentin multiple avec des plots supplémentaires a été développée pour permettre une distribution plus homogène de l'eau et éviter la présence de bouchon. Les conceptions multi-serpentines ont déjà analysé dans la littérature (Shimpalee2006) en analysant la longueur optimale du canal pour l'écoulement mais pas avec l'ajout de fentes.

La géométrie hybride, permettant de réduire les pertes de charge et de favoriser l'homogénéité et faciliter l'élimination de l'eau a été développée. L'idée derrière l'utilisation de cette géométrie est de réduire la longueur des canaux en serpentin et de les remplacer également par des canaux en parallèle extérieurs pour favoriser l'élimination de l'eau et une distribution de gaz plus rapides et réduire les pertes de charge. La partie suivante de ce chapitre traite de la caractérisation électrochimique par des mesures de courbe de polarisation et de perte de charge.

Pour ces trois géométries deux points de fonctionnement 4A et 19A sont étudiés pour deux humidités relatives 50% et 100%.

Deux conceptions supplémentaires ont été lancées dans cette recherche, à savoir la conception d'une géométrie par plots qui ont déjà été étudiées dans la littérature et la conception circulaire qui elle est complétement nouvelle d'un point de vue expérimentale. Pour ces deux conceptions, les données disponibles sont mesurées à un courant de 4 A pour des signaux de 2 heures et les pertes de charge sont calculées. En raison des limites de temps pour la portée de cette recherche, seules les pertes de charge sont calculées. Pour le chapitre 4, l'accent sera mis sur l'analyse des bruits électrochimique.

Les courbes de polarisation sont généralement utilisées pour décrire le phénomène des réactions électrochimiques et pour caractériser les performances électriques de la pile à combustible. Cela peut être un outil très important pour comprendre la cinétique, la résistance et le transfert de masse d'une pile à combustible. Sur cette base, des observations importantes peuvent être retirées expliquant qu'elles peuvent être la source des pertes de performances globales dans le fonctionnement de la pile à combustible. La courbe de polarisation des trois plans est présentée sur la figure 6.

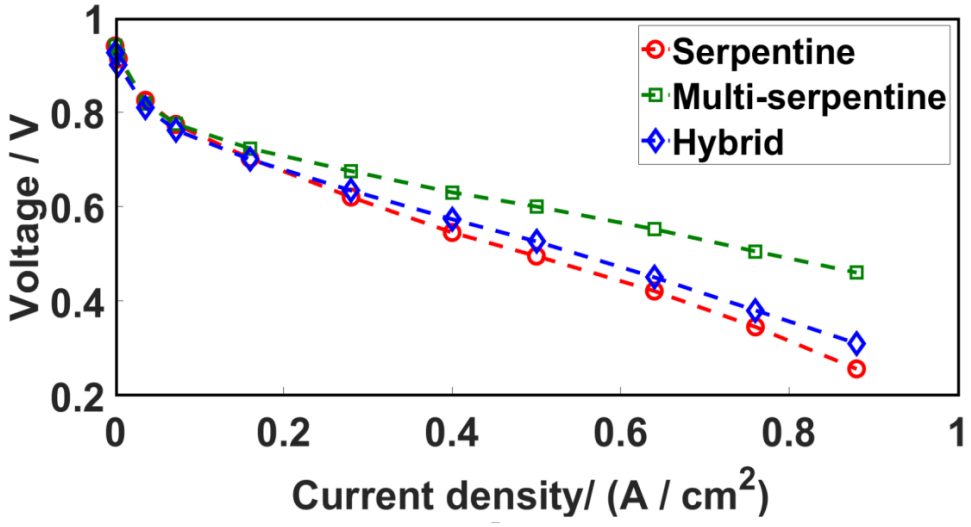

Figure 6 : Courbe de polarisation pour la comparaison de trois géométries (serpentin, multi-serpentin et hybride)

Les pertes d'activation, qui se produisent à de faibles densités de courant j < 0,2 A / cm², sont similaires pour les trois designs sauf que la géométrie multi-serpentine montre une perte moins importante pour commencer la réaction. Une différence majeure concernant les performances de la pile à combustible, entre les trois géométries, peut être observée dans la partie ohmique (partie linéaire). La figure 6 met en évidence que la géométrie multi-serpentine donne les meilleures performances électriques. La conception multi-serpentine démontre une tension de 0,65 V contre 0,6 V par rapport à l'hybride et 0,58 V par rapport à la cellule en serpentin à 0,4 A/cm², et de 0,5 V comparé à 0,3 V et 0,25 V à 0,9 A/cm², respectivement. La perte ohmique est principalement significative pour le cas de la géométrie en serpentin qui est suivie par l'hybride par rapport à la multi-serpentine principalement en raison d'une résistance de membrane plus élevée.

La masure de la chute de pression peut fournir diverses informations sur le fonctionnement et la gestion de l'eau des plaques bipolaires. Un signal stable avec des chutes de pression réduites signifie de meilleures performances par rapport à des chutes de pression plus élevées pendant le travail. De plus, les capteurs de pression aident à collecter les données in situ en ce qui concerne la surveillance des performances de la pile à combustible. La Figure 7A montre les valeurs moyennes de perte de charge du côté anode et 7B du côté cathode.

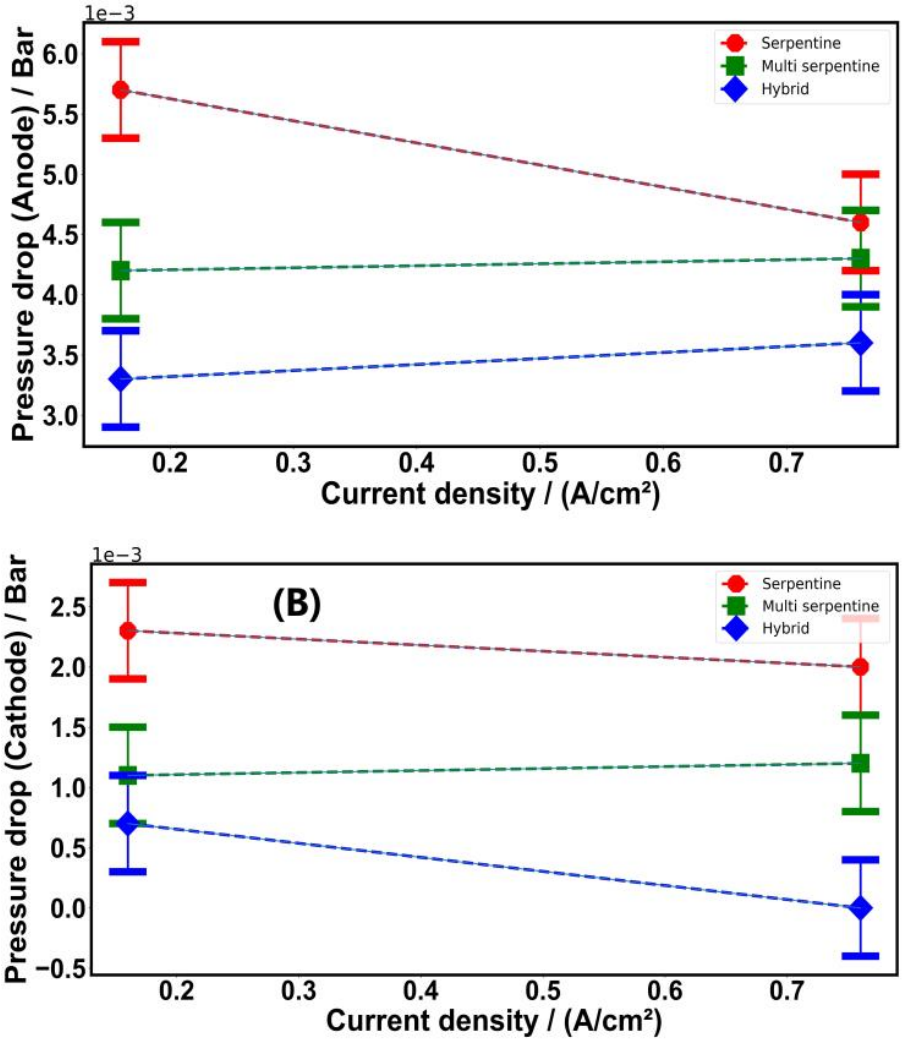

Figure 7 : A- Pertes de pression coté anode, B – Pertes de pression coté cathode

Pour les deux côtés, la géométrie en serpentin présente la perte de charge la plus élevée avec une variation entre 4,7 et 5,7 mbar côté anode et une variation entre 2 et 2,4 mbar côté cathode. A des courants plus élevés (19A), une diminution de la perte de charge est observée côté anode. La géométrie multi-serpentine donne des pertes de charge stables et inférieures de près de 4,2 mbar côté anode et 1,2 mbar côté cathode. La géométrie hybride met en évidence la perte de charge la plus faible avec une valeur stable proche de 3,3 mbar côté anode. Côté cathode, une valeur de 0,7 mbar à 4A et 0 mbar est mesurée (mauvais fonctionnement du capteur).

En considérant la Figure 6, pour une seule cellule, la performance électrique la plus élevée est observée pour la multi-serpentine, suivie d'une efficacité similaire pour la conception hybride et serpentine. Coté pression, la multi-serpentine montre de meilleures performances avec une augmentation de 1% pour une configuration à cellule unique aux conditions actuelles de 4A. Le compresseur dans ce cas ne représente que 2% de la puissance totale consommée et les calculs basés ici reposent sur l'hypothèse que le compresseur comprime le gaz de l'atmosphère à 1,013 bar aux conditions de fonctionnement à 3,0 bar en entrée et à 1,0 bar en sortie. Encore une fois, compte tenu de la puissance globale consommée par la pile, à 19A, la géométrie multi serpentine montre des performances supérieures à la géométrie en serpentine de 9% et 6% pour la conception hybride. Cependant, compte tenu des conditions à un courant inférieur de 4A, les résultats sont plus ou moins les mêmes avec seulement 1% d'augmentation de l'efficacité totale pour la conception multi-serpentine au niveau du compresseur.

En considérant à nouveau la Figure 7, dans le cas des cellules individuelles, on ne peut pas observer de différence notable dans la puissance du compresseur, cependant dans un système stack de pile à combustible, la puissance requise par le compresseur pour la conception hybride sera la plus faible et le plus élevé pour la conception serpentine. Seulement quelques dizaines de W de gain en puissance ont été observé pour le calcul dans un stack. Les présents calculs ayant uniquement été soumis à l'augmentation de la pression du gaz de la pression atmosphérique à 1,013 bar à 3 bar et à la compensation de la perte de charge entre les cellules, comme il est nécessaire de le maintenir dans un stack. Par conséquent, du point de vue du compresseur, il y a très peu de changement dans les économies d'énergie, mais du point de vue de la conception, compte tenu de la puissance électrique, il y a une augmentation de l'efficacité de 6-8%.

En résumé, ce chapitre a traité principalement des nouvelles conceptions de plaques et de son diagnostic par des tests de polarisation et des pertes de charge. En raison des pertes de charge à haute pression dans la conception des géométries en serpentin traditionnelles, il y a toujours un besoin d'une nouvelle géométrie de plaques d'alimentation. La recherche liée à la conception de nouvelles géométries se limite principalement aux études numériques avec très peu d'expériences. Par conséquent, il est nécessaire de développer davantage d'études expérimentales en fonction de la réduction des pertes de charge et de l'amélioration des performances. En cela, nous avons introduit quatre nouveaux modèles et les avons comparés expérimentalement sur la base de la courbe de polarisation et de la mesure des pertes de charge. Parmi toutes les conceptions, la géométrie multi-serpentine présente des performances électriques supérieures, la conception hybride montre une gestion de l'eau améliorée par rapport à la géométrie traditionnelle en serpentin. Du point de vue d'un empilement en stack de 100 plaques, notre étude estime 8% d'énergie électrique supplémentaire par rapport à la serpentine traditionnelle. Dans l'ensemble, il y a une réduction des pertes de charge, mais pour les 3 conceptions, mais cela ne crée pas un grand effet car la puissance du compresseur représente beaucoup moins par rapport à la puissance totale du stack. Les géométries circulaires et en plots sont encore en cours de recherche et malheureusement, peu d'analyses peuvent être effectuées en raison des limitation de temps.

Chapitre 4

Ce chapitre se consacre principalement à l'analyse du bruit électrochimique (ENA) et son application dans les signaux des piles à combustible seront discutées et analysées. L'objectif principal est de comprendre l'application de l'ENA comme un outil de diagnostic pour comprendre la gestion de l'eau. Dans les prochaines sections, les résultats de l'ENA sont analysés en ce qui concerne les conceptions des plaques d'alimentation aux regards de l'impact de l'humidité relative (50 et 100%) et du courant appliqué (4A et 19A).

Traditionnellement, les études électrochimiques sont orientées vers le diagnostic ou le pronostic des piles à combustible et l'utilisation des techniques électrochimiques conventionnelles, telles que la courbe de polarisation, la technique d'interruption de courant et les mesures d'impédance. Ces études permettent de caractériser les performances et la durabilité et les impacts de conception sur les piles à combustible en fonctionnement.

Le but du présent travail est d'utiliser l'ENA pour étudier l'impact des nouvelles géométries développées et la gestion de l'eau au sein de celles-ci. L'ENA sera réalisée en utilisant un descripteur temporel comme l'évolution de l'écart type (STD) dans le domaine temporel, ainsi que des descripteurs dans le domaine fréquentiel (densité spectrale de puissance). Cela aidera, qualitativement et quantitativement, à comprendre les impacts de la conception en ce qui concerne l'élimination de l'eau.

Sur la base des résultats de l'évolution du STD en tension (Figure 8), la conception en serpentin présente un comportement fluctuant élevé. La raison peut être expliquée en considérant le débit dans un seul canal, l'eau est forcée de se déplacer dans une direction et si un bouchon apparaît, cela implique plus d'irrégularités dans les signaux de tension et des pics STD apparaissent. Pour les résultats multi-serpentine à 4A, les résultats ne montrent aucune fluctuation. La multi-serpentine à 19A montre des fluctuations mais la magnitude est inférieure à la géométrie en serpentin traditionnelle. La raison de ce comportement peut être attribuée à une meilleure redistribution de l'eau dans les plots qui se traduit par une tension plus stable. Concernant la géométrie hybride, un comportement stable des signaux de tension est observé et peut être dû à une élimination plus facile de l'eau, où elle n'est pas obligée de suivre une trajectoire fixe et peut se distribuer à l'entrée en raison de la présence d'un canal en parallèle. En outre, la géométrie hydrid combine les avantages de la géométrie parallèle et serpentine qui gèrent de manière avantageuse la distribution de l'eau.

Wu2018 a publié des résultats utilisant l'imagerie neutronique pour étudier l'élimination de l'eau dans une géométrie à base de serpentine à un, deux et quatre canaux. Ils rapportent une élimination inefficace de l'eau liquide pour la conception à quatres canaux et dans notre étude basée sur l'analyse du bruit électrochimique, on observe une tension stable à faible courant et une certaine perturbation à des courants plus élevés pour la géométrie en multi-serpentin. Ceci est en accord avec leurs résultats, mais ils ont établi de meilleures performances pour la serpentine par rapport au quadruple canal. Dans la présente étude, l'introduction des plots dans la conception de canaux multi-serpentins peut être une raison pour une meilleure performance et stabilité par rapport à la serpentine, car la présence de plots permet une meilleure élimination de l'eau accumulée par une accélération de la vitesse du fluide. Encore une fois, en considérant les résultats d'imagerie neutronique, Spernjak2010 en comparant les géométries e, serpentin, parallèle et interdigitée, montre que la géométrie en serpentin donne de meilleures performances compte tenu de l'élimination de l'eau accumulée avec le temps. Étant donné que la géométrie parallèle souffre d'une mauvaise élimination de l'eau, par conséquent, dans notre étude, la conception hybride, combinant le parallèle et la serpentine, montre de meilleures performances en termes de tension et de fluctuations.

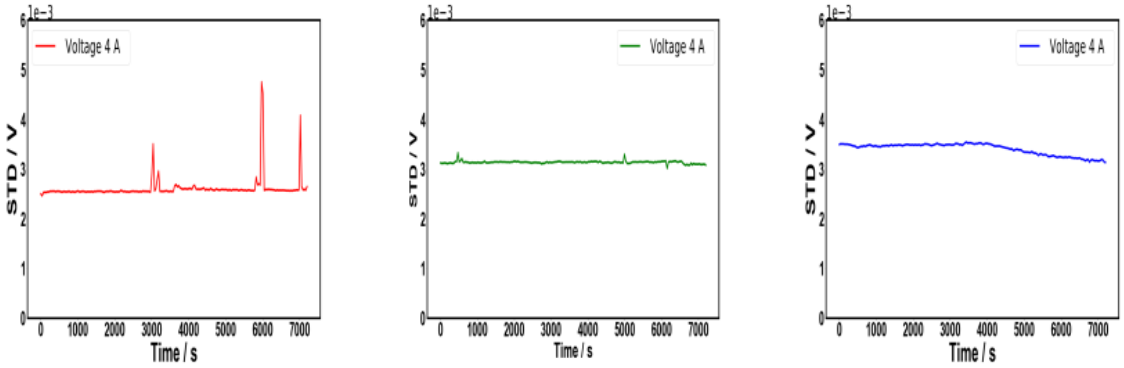

(a) serpentine 4A (b) m-serpentine 4A (c) hybrid 4A

Figure 4.35: STD variation 4A (a) serpentine (b) m-serpentine (c) hybrid

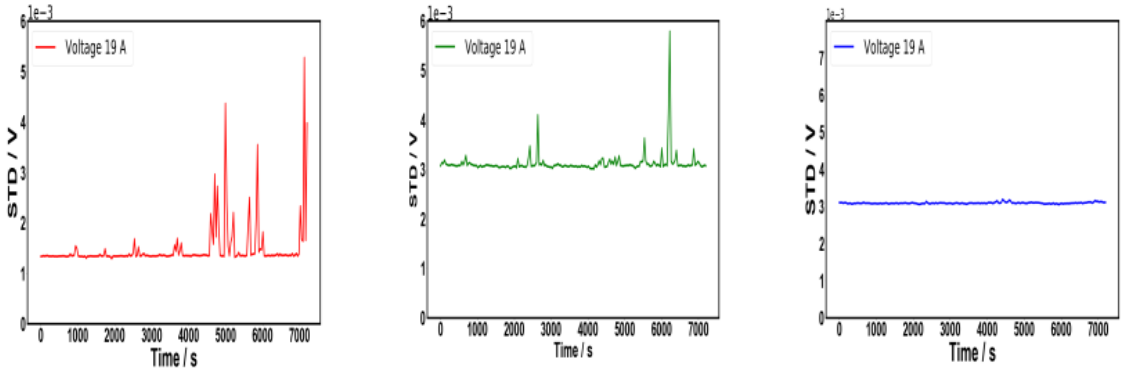

(a) serpentine 19A (b) m-serpentine 19A (c) hybrid 19A

Figure 8 : Evolution du STD de tension en fonction du temps pour trois géométries (serpentin, multi-serpentin et hybride)

Les conceptions en plots et circulaires ont été discutées séparément dans cette recherche en raison des résultats limités obtenus dans des conditions de fonctionnement de 4A. Sur la base de l'analyse préliminaire de la tension obtenue, les deux conceptions montrent une stabilité dans les conditions de fonctionnement de 4A. Cependant, les fluctuations de pression du côté cathodique de la conception circulaire basées sur des observations préliminaires sont instables par rapport à la conception ponctuelle (Figure 9).

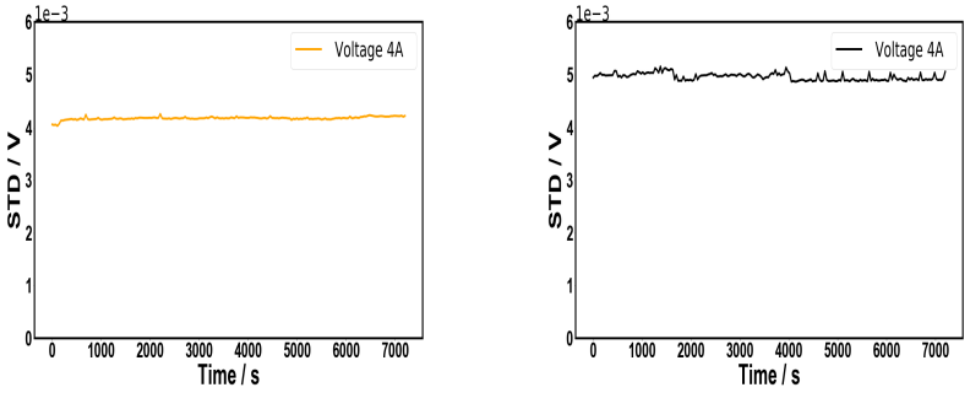

(a) Spot 4A (b) Circular 4A

Figure 9 : Evolution du STD de tension en fonction du temps pour le géométrie en plots (a) et circulaire (b)

La deuxième partie traite des résultats axés sur l'efficacité de l'ENA en tant qu'outil pour prédire les performances des cellules et pour différencier les différentes conditions de fonctionnement en tenant compte de la conception, du courant et de l'humidité relative dans le domaine fréquentiel.

Compte tenu de l'application de l'ENA, il s'agit d'une première étude lors de son application afin de comparer différentes conceptions de plaque d'alimentation. La signature robuste (PSD) du bruit électrochimique de différentes conceptions de plaques d'alimentations a été obtenue dans une large gamme de fréquences allant de 0,01 Hz à 1 kHz (Figure 10).

L'influence de la durée du signal, le traitement des données, l'effet des fenêtres et l'effet de la dépréciation ont été étudiés. Trois modèles, à savoir serpentin, multi-serpentin et hybride, ont été étudiés. Compte tenu des observations générales, à des fréquences inférieures f < 10 Hz), la PSD est inversement proportionnelle à la fréquence et représente une pente linéaire allant de p = (1,6 - 2). Ceci est généralement connu sous le nom de bruit fractionnaire. ENA permet de différencier les pentes pour toutes les conceptions. L'ENA est également sensible aux conditions actuelles. Nous concluons que l'amplitude de l'ENA est la plus importante pour la géométrie en serpentin. Pour cette géométrie, l'augmentation du courant de I = 4A à I = 19A n'influence pas de manière significative la signature du bruit. Ce n'est pas le cas pour la conception multi-serpentin où l'augmentation du courant conduit à une augmentation significative de l'ENA. La faible énergie du signal de la conception hybride par rapport à la conception serpentine est à nouveau confirmée dans le domaine fréquence comme observé dans le domaine temporel (faible fluctuation du STD).

Compte tenu du cas de la variation de l'humidité relative entre 50% et 100% (Figure 11), la conception multi-serpentine et hybride n'est pas affectée et seule la géométrie en serpentin est affectée. L'introduction de plots dans la géométrie en multi serpentin peut être une raison pour une meilleure gestion de l'eau. Pour la géométrie en serpentin, la pente diminue avec l'augmentation de l'humidité relative, ce qui, d'après notre étude, peut expliquer l'effet d'une mauvaise gestion de l'eau. Sur la base des mesures des fluctuations de pression, elles sont complètement décorrélées des fluctuations de tension avec une pente de 1 ce qui correspond à un bruit d'appareillage électronique et non à un bruit lié à la mesure de pression.

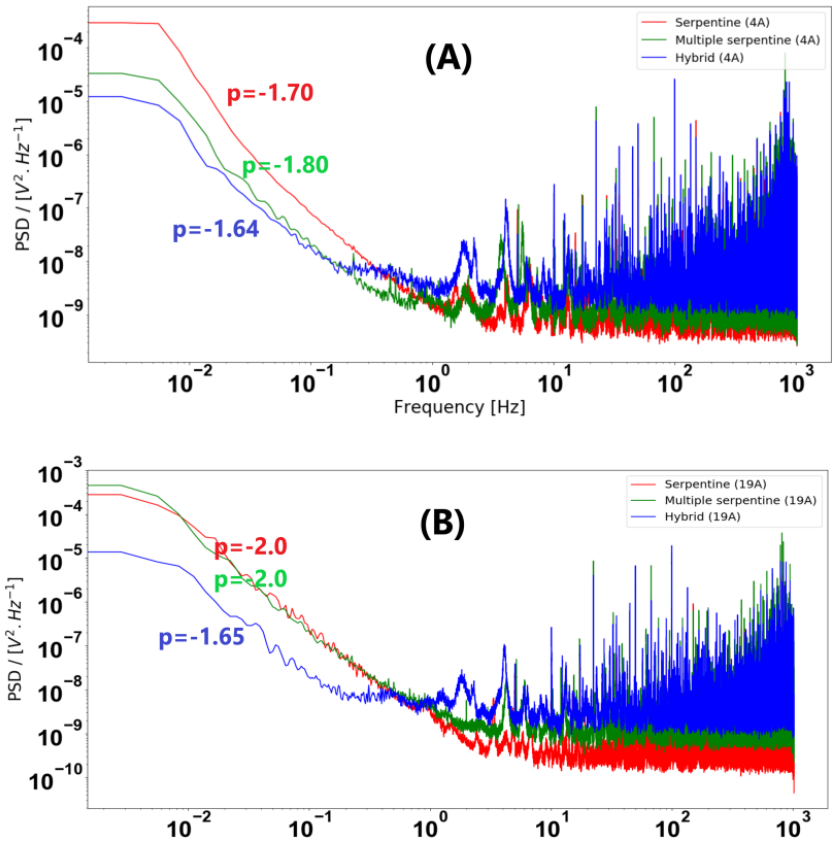

Figure 10 : Estimation du spectre de puissance (PSD)pour trois géométries (serpentin, multi-serpentin et hybride) et deux courants (4A et 19A)

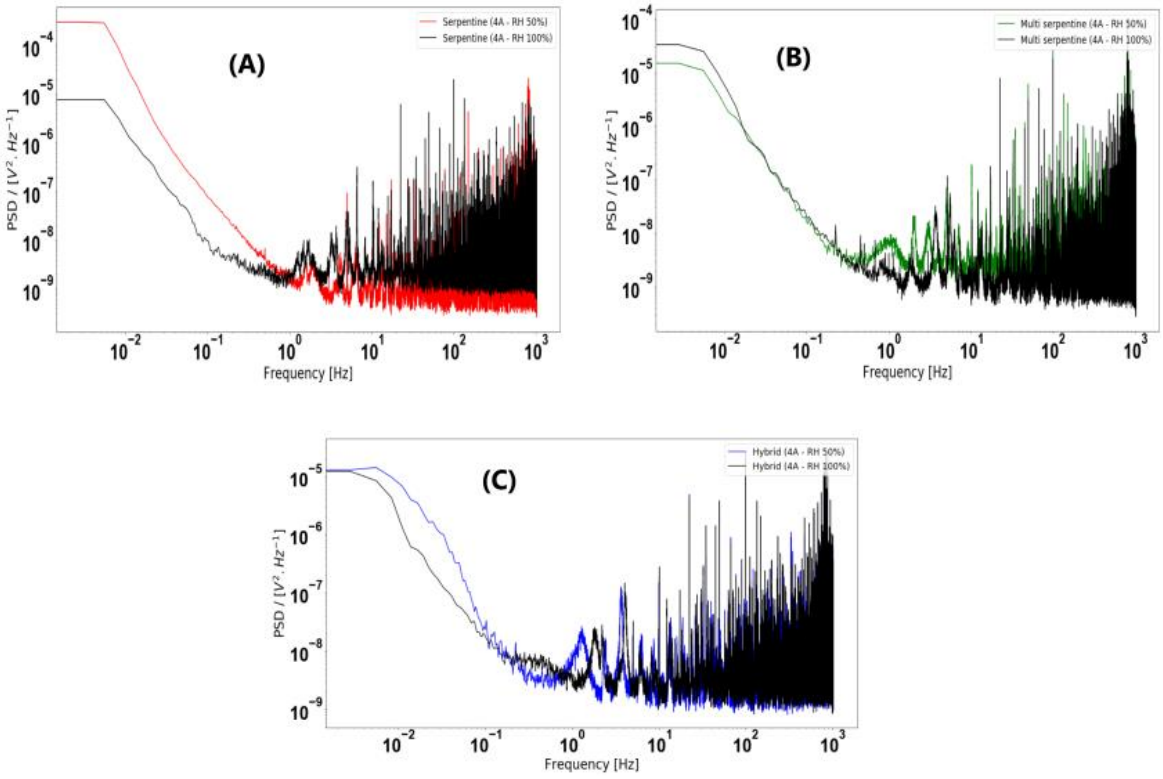

Figure 11 : Estimation du spectre de puissance (PSD) pour trois géométries (serpentin, multi-serpentin et hybride) et deux humidités relatives (50% et 100%) à 4A

Chapitre 5

Compte tenu de caractère multi-physique impliquée dans l'analyse PEMFC, la modélisation reste un élément important pour optimiser les performances des piles à combustible. Le besoin de modélisation peut aider à créer des outils de diagnostic en ligne qui peuvent aider au diagnostic et au pronostic des systèmes de piles à combustible. La modélisation peut fournir des détails sur des paramètres qui ne peuvent être directement calculés ou estimés. Dans la présente recherche, nous avons considéré deux types de modélisation, 1) analytique et 2) axée sur les données. Considérant le premier, il a permis de calculer le coefficient de diffusion à travers la membrane. Les valeurs calculées ont des ordres de grandeurs 2 fois supérieures à la valeur calculée (6 10^{-5} avec electro-osmose et 1 10^{-5} cm^2/s) à partir des expériences du chapitre 2 (Figure 12).

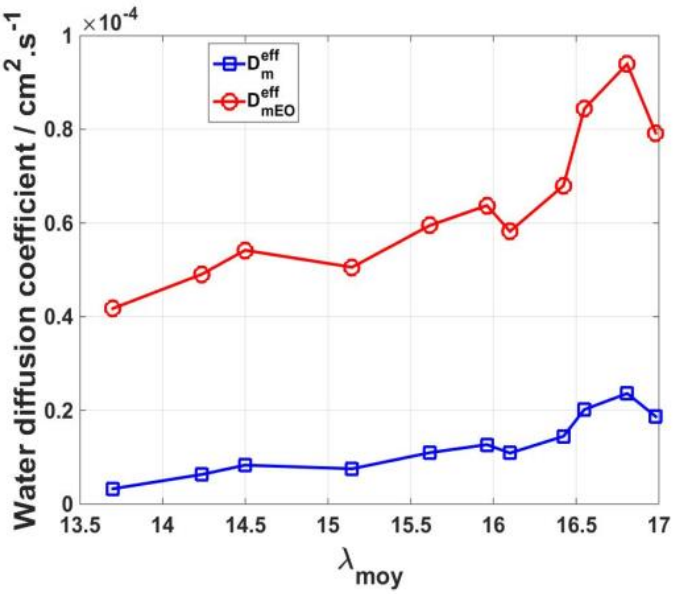

Figure 12 : Evolution du coefficient de diffusion effectif au sein d'une pile en fonctionnement en fonction de la teneur en eau moyenne si l'on prend en compte l'électro-osmose (EO) ou non.

Ce comportement peut être attribué à la production d'eau au sein d 'une pile en fonctionnement qui n'a pas été prise en compte lors des expériences du chapitre 2. Cette production amène à une meilleure hydratation de la membrane (λ >13). Cela peut également être expliqué à partir du modèle basé sur des clusters où les clusters isolés domine dans des conditions de faible hydratation (0 < λ <2) et pour des fortes hydratations (λ >13), la quantité d'eau liquide augmentant, les clusters percolent et créé des « voies de passage » pour la diffusion de l'eau. En effet, avec l'augmentation de l'absorption d'eau, la croissance des grappes augmente. Des résultats de diffusion élevés peuvent être dus à une croissance importante des grappes, à une plus grande distribution d'eau. On se retrouve donc avec des valeurs de diffusion de l'eau correspond à une diffusion des ions hydratés (HXO+ X>3) dans de l'eau liquide (> 10^{-5} cm^2/s – self diffusion). On a également vu que la diffusion dépend de la teneur en eau λ et qu'elle augmente avec l'augmentation de λ (Figure 4).

La seconde modélisation, utilisant l'apprentissage avancée (machine and deep learning), est basée sur des données riches (variation de température, tension, pression, …) jouant un rôle important pour estimer les paramètres des piles à combustible (pronostique). L'importance survient lorsqu'il est difficile de lier les relations physico-chimiques entre les paramètres. Dans ce cas, les données générées par les expériences peuvent être utilisées pour estimer les résultats. Dans cette étude basée sur l'ensemble expérimental utilisé, les valeurs de tension ont été estimées à partir des données de

température, pression et courant. Cinq modèles ont été utilisés (basés sur des régresseurs) à savoir la régression linéaire, crête, lasso, forêt aléatoire et réseau neuronal artificiel. La forêt aléatoire et le réseau de neurones artificiels montrent une meilleure précision des résultats éstimés, mais aussi avec une précision et un temps de calcul et de coût qui augmentent. Les deux approches de modélisation, basées sur notre étude, peuvent être utilisées pour optimiser davantage les performances des piles à combustible et réaliser le pronostique de ce système.

Conclusions et perspectives

L'objectif principal de cette recherche était d'améliorer la gestion de l'eau dans les PEMFC à l'aide du bilan hydrique et de la technique d'analyse du bruit électrochimique (ENA). Il peut y avoir de nombreux paramètres tels que la température, l'humidité relative, le matériau de GDL, épaisseur de MEA, qui peut affecter la gestion de l'eau. Cependant, cette étude s'est concentrée principalement sur l'influence des différentes géométries de plaques d'alimentation sur la gestion de l'eau et les performances des piles à combustible. Un autre point qui ont été étudiés en détail dans ce travail est lié à la mesure in-situ du coefficient effectif de diffusion de l'eau. En effet, il y a un réel manque d'information concernant ce paramètre directeur responsable du transport par eau, en particulier pour des mesures in situ. Afin d'atteindre ces deux objectifs, nous avons utilisé à la fois les techniques expérimentales, comme la courbe de polarisation et les mesures de pertes de charge, ainsi que des méthodologies plus avancées, à savoir le bilan hydrique et l'ENA. On a terminé notre étude par la démonstration de quelques approches analytiques permettant de utiliser les informations expérimentales obtenues pour la modélisation et les pronostics de la pile à combustible performance.

D'un point de vue des perspectives, les nouvelles géométries de plaques d'alimentation proposées dans ce travail pour améliorer la gestion de l'eau peut être considérée comme une première étape pour un développement ultérieur dans les stacks de pile à combustible. Pour aller plus loin des mesures concomitantes et des mesures croisées de l'évolution de pression, d'impédance et de température et de corrélation entre différents signaux pour plusieurs points de fonctionnement et humidité relative devraient être effectués dans des travaux futurs. En particulier, nous proposons, l'augmentation de la base de données (ensemble d'exploitation des différents de conditions expérimentales notamment dans des conditions d'engorgement) pour les nouvelles conceptions de plaques bipolaires (multi-serpentin, hybride, circulaires et plots). L'utilisation des capteurs avec une précision améliorée afin de collecter des informations de perte de charge pour la conception hybride et circulaire devront être améliorer. L'utilisation de différents capteurs pour les mesures ENA et de corrélation croisée dans afin de comprendre la nature du bruit électrochimique doit être poursuivi. Coté modélisation, l'estimation du coefficient de diffusion avec ou sans électro-osmose devra passer par un modèle 2D prenant en compte la non-homogénéisation de la teneur en eau, le long de la membrane. Des développements de modèles numériques prenant en compte le comportement diphasique de l'eau dans les canaux des plaques d'alimentation (effet dent et canal) permettra d'optimiser les performances des piles à combustibles pour différentes conditions de fonctionnement. Elargir l'étude de l'impact des nouvelles géométries dans un stack de pile à combustible est aussi une voie à envisager. Enfin le développement d'un modèle de diagnostic en ligne sur base du bruit électrochimique et des outils de pronostic associés pour évaluer les défauts de fonctionnement des stacks de pile à combustible serait opportun pour le développement commercial des piles à combustibles.

A Poitiers, le 18 décembre 2020

Monsieur THOMAS ANTHONY

Monsieur,

Par décision en date du 13 novembre 2020, le Président de l'Université de Poitiers vous a désigné pour participer au jury devant examiner les travaux de M. KUSH CHADHA en vue de l'obtention du diplôme :

Doctorat en Energétique, Thermique, Combustion

Le titre des travaux est : Amélioration de la gestion de l'eau dans les piles à combustible PEM à l'aide du bilan hydrique et de l'analyse des bruits électrochimique.

Les travaux sont dirigés par M. ANTHONY THOMAS et M. SERGUEI MARTEMIANOV

La soutenance aura lieu le 07 janvier 2021 à 9h30 à l'adresse suivante :

Bâtiment B 17 6 rue Marcel Doré Salle Visioconférence 86073 POITIERS CEDEX

La soutenance sera publique.

Je vous prie d'agréer, Monsieur, l'expression de mes salutations distinguées.

Directeur des Etudes

Patrick MASPEYROT

Le début de la soutenance initialement prévu à 9h30 est avancé à 9 heures

Les membres du jury qui ont demandé à participer en visioconférence recevront les adresses de connexion par Monsieur Anthony THOMAS, directeur de thèse

Conferences

1) **A vision for hydrogen & Fuel cells in UK**. H2FC SUPERGEN 2019 Conference. (30 Jan – 01 Feb 2019), University of Warwick Coventry, England

2) **Presented Poster - "Estimation of various parameters in fuel cell system." 8th International Conference on Fundamentals and Development of Fuel Cells** - FDFC 2019 (12-14 march 2019) La Cité Nantes Congress Center – Nantes, France

3) Presented work on – "In-situ diffusion coefficient for Nafion membranes." 6th CARISMA International Conference on Medium and High Temperature Proton Exchange Membrane Fuel Cells (27-30th August 2019) Duisburg, Germany.

4) Presented work on - "Electrochemical noise analysis on water management and diffusion coefficient estimation" GdR 3652 HySPàC, Réunion plénière Le Croisic (11-13 juin 2019), Le Croisic, France

Publications

1) **"Estimation of the Effective Nafion® Membrane Water Diffusion Coefficient by Water Balance Measurements"**. Kush CHADHA, Serguei Martemianov, Thomas Anthony, Journal: *Fuel cells*

2) **"Study of new flow field geometries to enhance water redistribution and pressure head losses reduction within PEM Fuel Cell."** Kush CHADHA, Serguei Martemianov, Thomas Anthony, Journal: *International journal of hydrogen energy* (IJHE)

Résumé

Cette thèse s'inscrit dans une démarche d'optimisation des performances des PEMFC, à travers le développement de nouveaux designs de plaque d'alimentation. Des outils tel que le bilan hydrique et l'analyse des bruits électrochimiques ont été utilisés pour diagnostiquer la gestion de l'eau au sein d'une mono-cellule. Une gestion optimale du transport d'eau permet une augmentation des performances et de la durée de vie de ce système. Le bilan hydrique a permis de mesurer la valeur du coefficient de diffusion effectif de l'eau au sein des membranes. De nouvelles géométries de plaque d'alimentation ont été développées et caractériser par des mesures de courbes de polarisation et de pression. L'analyse des bruits électrochimiques a permis de détecter des phénomènes liés au comportement de l'eau lors du fonctionnement de la pile pour chaque géométrie développée. Ces bruits ont été associés à des mécanismes sources grâce à une démarche expérimentale et à un traitement de signal approprié basé sur l'analyse fréquentielle et temporelle. Les résultats des descripteurs obtenus ont permis d'obtenir la signature dans un fonctionnement normal de pile à combustible utilisant une géométrie de canaux en serpentin. Cette signature a été comparée aux nouvelles géométries permettant de caractériser l'influence de celles-ci sur le transport d'eau. Enfin, pour compléter l'approche expérimentale, une modélisation permettant l'estimation du coefficient de diffusion au sein d'une pile en fonctionnement a été développé. L'impact des nouvelles géométries a été étendu à leur utilisation en stack et un modèle de pronostique basé sur l'apprentissage automatisé a été proposé.

Mots clés : Design des plaques d'alimentation, Bilan hydrique, Modélisation, Machine and deep learning, Traitement du signal, Bruit électrochimique, Analyse statistique, Gestion de l'eau, Diagnostic, Pronostique, PEMFC.

Abstract

This thesis deals to optimize the performance of PEMFC, through the development of new flow-field plate designs. Tools such as water balance and electrochemical noise analysis have been used to diagnose water management within a PEMFC single cell. Optimal management of the water transport enables an increase of the performance and durability of fuel cells. Water balance method was used to measure and frame the value of the effective water diffusion coefficient within the membranes of fuel cells. New flow-flied plate geometries have been developed and characterized by conventional polarization curve and pressure measurements. The electrochemical noise technique was used to detect phenomena related to the behavior of water within fuel cell for each geometry developed. These noises have been associated with source mechanisms through an experimental approach and an appropriate signal processing based on frequency and time analysis. The descriptors obtained by time and frequency analysis shows that it possible to obtain the signature in normal operation of a fuel cell using a classical serpentine design. This signature was compared to the new designs allowing to characterize the influence of these new geometries on the water transport. Finally, to complete the experimental approach, a model allowing the estimation of the water diffusion coefficient within an operating fuel cell has been developed. In perspective, the impact of the new geometries has been extended in a stack utilization and a prognostic model based on machine and deep learning model has been proposed.

Keywords: Flow field designs, Water balance, Modelling, Machine and deep learning, Signal processing, Electrochemical noise, Statistical analysis, Water management, Diagnosis, Prognosis, PEMFC.